MODELING THE DYNAMICS OF QUASIPARTICLES IN SUPERCONDUCTING DEVICES AT LOW TEMPERATURES

Von der Fakultät für Mathematik und Naturwissenschaften der RWTH Aachen University zur Erlangung des akademischen Grades eines Doktors der Naturwissenschaften genehmigte Dissertation

vorgelegt von

Paul Benedikt Fischer

aus

Witten

Berichter*:* *Univ.-Prof. Dr. David DiVincenzo*

Univ.-Prof. Dr. Fabian Hassler

Tag der mündlichen Prüfung*:* *02.10.2025*

Diese Dissertation ist auf den Internetseiten der Universitätsbibliothek verfügbar.

Eidesstattliche Erklärung

Paul Benedikt Fischer erklärt hiermit, dass diese Dissertation und die darin dargelegten Inhalte die eigenen sind und selbstständig, als Ergebnis der eigenen originären Forschung, generiert wurden. Hiermit erkläre ich an Eides statt

- Diese Arbeit wurde vollständig oder größtenteils in der Phase als Promovierender dieser Fakultät und Universität angefertigt;
- Sofern irgendein Bestandteil dieser Dissertation zuvor für einen akademischen Abschluss oder eine andere Qualifikation an dieser oder einer anderen Institution verwendet wurde, wurde dies klar angezeigt;
- Wenn immer andere eigene- oder Veröffentlichungen Dritter herangezogen wurden, wurden diese klar benannt;
- Wenn aus anderen eigenen- oder Veröffentlichungen Dritter zitiert wurde, wurde stets die Quelle hierfür angegeben. Diese Dissertation ist vollständig meine eigene Arbeit, mit der Ausnahme solcher Zitate;
- Alle wesentlichen Quellen von Unterstützung wurden benannt;
- Wenn immer ein Teil dieser Dissertation auf der Zusammenarbeit mit anderen basiert, wurde von mir klar gekennzeichnet, was von anderen und was von mir selbst erarbeitet wurde;
- Teile dieser Arbeit wurden zuvor veröffentlicht und zwar in:
  - P.B. Fischer and G. Catelani. "Nonequilibrium Quasiparticle Distribution in Superconducting Resonators: An Analytical Approach". In: *Phys. Rev. Appl.* 19 (5 May 2023), p. 054087. DOI: 10.1103/PhysRevApplied.19.054087
  - Paul B. Fischer and Gianluigi Catelani. "Nonequilibrium quasiparticle distribution in superconducting resonators: Effect of pair-breaking photons". In: *SciPost Phys.* 17 (2024), p. 070. DOI: 10.21468/SciPostPhys.17.3.070
  - Paul B. Fischer and Gianluigi Catelani. "Excess quasiparticles and their dynamics in the presence of subgap states". In: *arXiv:2507.06902* (2025). DOI: https://doi.org/10.48550/arXiv.2507.06902

Aachen, 14.10.2025

Acknowledgements

I would especially like to thank Dr. Gianluigi Catelani for his support in writing this thesis. Not only did he introduce me to the topic of quasiparticles in superconductors, but also co-authored all papers I published during the research for this thesis, offered helpful discussions whenever I ran out of ideas and proofread this thesis. I am also very grateful to Prof. Dr. David DiVincenzo for giving me the opportunity to do my research in his group. I would also like to thank all members of the defense committee for taking the time to review this work.

While most of the challenges I encountered were of academic nature, there were also bureaucratic hurdles to overcome. Fortunately, I could always count on Luise Snyder's help to overcome them before they could turn into real problems.

Finally, I would like to thank the German Federal Ministry of Education and Research (BMBF) for providing funds for my research within the funding program "Quantum technologies – from basic research to market", project QSolid (Grant No. 13N16149).

Superconducting materials are useful for a large variety of applications, ranging from particle detectors to quantum computation. The presence of excitations (quasiparticles) in the superconductor can be a resource in some superconducting devices and a disturbance in others - in kinetic inductance detectors the production of quasiparticles by an incoming photon can be read out and used to estimate the photon's energy, while tunneling of quasiparticles provides a source for decoherence in quantum computation.

While early research was focused on superconductors close to the critical temperature, current applications frequently use temperatures far below the critical temperatures. At these low temperatures exchange of energy between quasiparticles and phonons becomes slow, and even small perturbations may drive the quasiparticle distribution out of thermal equilibrium. Indeed, experiments reveal a residual number of quasiparticles even at milikelvin (fridge-) temperatures, for which the thermal density of quasiparticles should be negligible. Thus, an accurate modelling of the quasiparticle distribution function in the presence of non-equilibrium processes is of great importance for applications.

This thesis consists of two parts: In the first part we model the quasiparticle energy distribution in superconducting resonators. Quasiparticles are driven out of equilibrium by the interaction with the photons used to probe the resonator and relax towards equilibrium by exchange of energy with the phonons. As the resonator's quality factor and resonance frequency are affected by the density of quasiparticles and their distribution in energy, this allows for a straightforward comparison of our understanding of the quasiparticle's dynamics to experiments. Moreover, as resonators are an important component of many superconducting devices, it is a relevant topic on its own. In the second part of this thesis, we investigate the effect of spatial fluctuations of the superconducting energy gap on the dynamics of quasiparticles. Recently, such fluctuations have been suggested to lead to quasiparticle localization in sub-gap states, which may cause a finite quasiparticle density even at very low temperatures. We extend existing models by accounting for the dynamics of both localized and mobile states, and derive new limits on the quasiparticle density depending on the fluctuation's strength.

In chapter 1 we give an introduction to superconductivity and superconducting devices. We discuss the relevance of elementary excitations (quasiparticles) for qubits and resonators based on BCS theory. In chapter 2 we use the quasiclassical Keldysh Green's function formalism to derive the (Keldysh-)Usadel equation describing both the retarded/advanced Green's functions and the quasiparticle distribution function, including collision integrals due to photons and phonons. In chapter 3 we calculate the quasiparticle energy distribution in superconducting resonators and compare the predicted shifts in resonance frequency and quality factor to experiments. Chapter 4 contains our calculations regarding the effect of localization on the dynamics of quasiparticles.

Contents

1. Introduction **1**
- 1.1. Phenomoneolgical theories . . . 2
- 1.2. BCS theory . . . 4
- 1.3. Superconductor in electromagnetic fields . . . 7
- 1.4. Coplanar waveguide resonators . . . 8
  - 1.4.1. Impedance . . . 8
  - 1.4.2. Quality factor and resonance frequency . . . 9
- 1.5. Qubits . . . 11
- 1.6. Superconducting detectors . . . 14
- 1.7. Conclusion . . . 15

2. Green's functions in superconductors **17**
- 2.1. Keldysh Green's functions . . . 17
  - 2.1.1. Notation . . . 17
  - 2.1.2. Green's functions . . . 18
  - 2.1.3. Keldysh contour and Keldysh Green's functions . . . 20
  - 2.1.4. Hamiltonians . . . 22
  - 2.1.5. Feynman rules and Gorkov-Keldysh equation . . . 23
- 2.2. Quasiclassical Green's functions . . . 25
  - 2.2.1. Wigner transform and Keldysh-Eilenberger equation . . . 26
  - 2.2.2. The dirty limit and Usadel equation . . . 31
- 2.3. Distribution function . . . 32
- 2.4. Current-field relation and complex conductivity . . . 36
  - 2.4.1. BCS Limit . . . 38

3. Quasiparticle energy distribution in resonators **39**
- 3.1. Rate equations . . . 40
  - 3.1.0.1. Interaction with phonons . . . 41
  - 3.1.0.2. Interaction with photons . . . 42
  - 3.1.1. Phonon rates . . . 43
- 3.2. Numerics . . . 44
- 3.3. Relevant timescales . . . 46
- 3.4. Photons below the pair-breaking threshold . . . 47
  - 3.4.1. Shape of the quasiparticle distribution function . . . 47
    - 3.4.1.1. Phonons in equilibrium at $T_B = 0$ . . . 49
    - 3.4.1.2. Equilibrium phonons, $T_B > 0$ . . . 51
    - 3.4.1.3. Finite thermalization time . . . 52

3.4.2. Quasiparticle density . . . 53
3.4.2.1. Generalized Rothwarf-Taylor model . . . 54
3.4.3. Gap suppression . . . 57
3.4.4. Comparison to numerics . . . 57
3.5. Photons above the pair-breaking threshold . . . 60
3.5.1. Generation by pair-breaking photons . . . 63
3.5.1.1. Validity of assumptions . . . 68
3.5.2. Perturbative regime . . . 72
3.5.3. Heating regime . . . 74
3.5.4. Quasiparticle density and its fluctuations . . . 77
3.6. Comparison to experiments . . . 78
3.6.1. No pair-breaking photons . . . 82
3.6.2. Pair-breaking photons . . . 83

4. Quasiparticle dynamics in the presence of magnetic impurities 90
4.1. Introduction . . . 90
4.2. Density of states and coherence factors . . . 91
4.2.1. Abkrikosov-Gorkov theory of paramagnetic impurities . . . 91
4.2.1.1. Mean field theory . . . 92
4.2.1.2. Perturbative regime . . . 93
4.2.1.3. Optimal fluctuations . . . 94
4.3. Quasiparticle rates . . . 95
4.3.1. Rates . . . 96
4.3.1.1. Zero temperature . . . 96
4.3.1.2. Finite temperature . . . 97
4.4. Quasiparticle dynamics . . . 98
4.5. Experimental consequences . . . 100

5. Conclusion 103

A. Thin film coplanar waveguides A 1
A.1. Transverse electromagnetic modes . . . A 1
A.2. Impedance . . . A 1

B. Feynman rules B 5

C. Quasiparticle and phonon lifetimes C 7

D. Non-pair-breaking photons D 10
D.1. Finite phonon temperature . . . D 10
D.2. Nonequilibrium phonon distribution . . . D 13
D.3. Normalization equation . . . D 16
D.4. Photon-number dependent corrections in the generalized RT model . . . D 18

E. Parameters for comparison to experiment **E 20**
E.1. Kinetic inductance fraction and order parameter . . . . . E 20
E.2. Coupling constant . . . . . E 20

F. Pair breaking photons **F 23**
F.1. Neumann series . . . . . F 23
F.2. Power spectral density . . . . . F 24

G. Fluctuations **G 26**
G.1. Two dimensional fluctuations . . . . . G 26
G.2. Disorder averaging . . . . . G 28
G.3. Rates . . . . . G 30
G.3.1. Localization rate . . . . . G 30
G.3.2. Excitation rates . . . . . G 30
G.3.3. Mobile-mobile transitions . . . . . G 31
G.3.4. Recombination rates . . . . . G 32
G.3.5. Pair-breaking rates . . . . . G 32
G.4. Generation-recombination Noise . . . . . G 33
G.5. Self consistency equation . . . . . G 36

H. List of symbols **H 38**

Bibliography **i**

List of Figures

1.1. Internal quality factor and resonance frequency of a resonator 11
1.2. Transition rates of a Transmon 14
1.3. Operating principle of superconducting detectors 16

2.1. Contours used to rewrite the Green's function 19
2.2. Matsubara, zero temperature and Keldysh contours 22
2.3. Electron self energy 28

3.1. Model of a thin film resonator 44
3.2. Schematic depiction of the collision processes 48
3.3. Different regimes of the quasiparticle density 56
3.4. Quasiparticle energy distribution in the absence of pair-breaking photons 59
3.5. Phonon energy distribution in the absence of pair-breaking photons . . 59
3.6. Quasiparticle density in the absence of pair-breaking photons 60
3.7. Order parameter shift in the absence of pair-breaking photons 61
3.8. Numerically calculated γ_* 67
3.9. Low energy expansion coefficients 68
3.10. Quasiparticle energy distribution for only pair breaking photons 69
3.11. Quasiparticle energy distribution for pair breaking and few non-pair-breaking photons 75
3.12. Quasiparticle energy distribution for pair breaking and many non-pair-breaking photons 76
3.13. Quasiparticle density including only pair breaking photons 79
3.14. Internal quality factor and resonance frequency without pair-breaking photons 84
3.15. Low temperature quality factor 86
3.16. Internal quality factor with pair-breaking photons 86
3.17. Resonance frequency shift including pair breaking photons 89
3.18. Resonance frequency shift as function of quasiparticle density 89

4.1. Depiction of the processes affecting the quasiparticle density in a superconductor containing localized states 91
4.2. Regimes determining the quasiparticle density in a superconductor containing localized states 100

A.1. Thin film coplanar waveguide geometry . . . . . A 4

D.1. Distribution averaged recombination coefficient . . . . . D 19

G.1. Analytically and numerically calculated optimal fluctuation in two dimensions . . . . . G 27

1. Introduction

Superconductivity has been one of the most active areas of physics for more than a century. It was first discovered by Onnes in 1911 [Onn11] who noticed a sharp drop in the resistance of mercury at temperatures below a critical temperature $T_c \simeq 4.2K$. For more than twenty years the possibility of a dissipationless (dc) current was believed to be the defining feature of a superconductor until Meissner and Ochsenfeld discovered an even more striking effect, the expulsion of magnetic fields from the inside of a superconductor upon cooling below the transition temperature [MO33].[1] After the discovery of superconductivity for a long time only phenomenological theories were available, most famously the London theory [LL35a; LL35b] and the Ginzburg-Landau theory [GL50].[2] Ginzburg-Landau theory is a theory that describes superconductors in the vicinity of the transition temperature and is not applicable to the effects far below T_c investigated in this thesis. Although London theory provides a reasonable description of electromagnetic properties of a superconductor at low temperatures, including the Meissner effect, it has some limitations; most importantly for this thesis it does not account for the existence of quasiparticles, i.e. it assumes all current to be superconducting. As quasiparticles induce losses, they are important for a proper modelling and optimization of a wide range of superconducting devices. To properly account for quasiparticles, one must go beyond phenomenological theories and use microscopic theories. The first fully microscopic theory of superconductivity was famously published in 1957 by Bardeen, Cooper, and Schrieffer (BCS) [BCS57]. The main insight of their theory is that a finite attractive interaction between electrons leads to the formation of pairs of electrons that – in close analogy to Bose Einstein Condensation – condense into a ground state with macroscopic occupation number. This ground state can carry a current and is separated from a continuum of single-particle excitations (the quasiparticles) by a finite gap in energy Δ. Thus, as long as the frequency of the current is far below the energy gap, it cannot create new quasiparticles, and – if there are no quasiparticles in the system – current is dissipationless. Moreover, for a system in thermal equilibrium at temperatures far below the gap the number of quasiparticles is suppressed exponentially in Δ/T and one would expect a negligible number of quasiparticles at the milikelvin temperatures accessible nowadays. It turns out however, that in experiments various non-equilibrium processes become important that create a non-negligible number of quasiparticles.

[1] It is in fact possible to create superconductors without a gap in the excitation spectrum that do not support a dissipationless current but do exhibt the Meissner effect [AG61]. Thus, nowadays the Meissner effect and not the dissipationless current is considered the defining experimentally accessible porperty of a superconductor.

[2] The original paper is in Russian, a translation is given e.g. in [Gin09].

Various techniques have been developed to mitigate the influence of quasiparticles – e.g. shielding the device from stray light [Bas+12], trapping of quasiparticles in normal metals [Riw+16; RCP09] and vortices [UFN98; Tau+16] away from critical components, shielding against cosmic radiation [Car+21], and trapping of phonons [Kar+19; Val+19] – and yet the influence of quasiparticles on the performance of superconducting devices is generally non-negligible. In the remainder of this chapter we therefore give a short introduction to superconductivity based on BCS theory and discuss the influence of quasiparticles on different applications. In the next chapter, we use a different approach based on Green's functions to describe superconductors. Although more complicated, this will enable us to investigate inhomogeneous superconductors and superconductors containing magnetic impurities, which will be the topic of chapter 4.

Throughout this thesis units with $\hbar = k_B = c = 1$ are used.

1.1. Phenomoneolgical theories

Before the development of a microscopic theory of superconductivity by Bardeen, Cooper, and Schrieffer in 1957 [BCS57] phenomenological theories have been used to model the (macroscopic) electromagnetic and thermodynamic properties of a superconductor. It is instructive to motivate one of these theories, known as London theory, in analogy with a superfluid [L P08]: A superfluid is characterized by a macroscopic number of (bosonic) particles in the zero-momentum state. Its momentum distribution thus contains a delta function

$$N(\vec{p}) = (2\pi)^3 n_0 \delta(\vec{p}) + n'(\vec{p}) \tag{1.1}$$

It can be evaluated from the one body density matrix [for simplicity we assume a time independent and spatially homogeneous system]

$$\rho^{(1)}(\vec{r}) \equiv \rho^{(1)}(\vec{r}_1 - \vec{r}_2) = \langle \psi^\dagger(\vec{r}_1)\psi(\vec{r}_2)\rangle \tag{1.2}$$

Its Fourier transform is

$$\int d^3 r e^{i\vec{r}\vec{p}} \rho^{(1)}(\vec{r}) \tag{1.3}$$

Because of the delta function in (1.1) the density matrix approaches a non-zero constant at infinite distance $\rho^{(1)}(\vec{r}) \to n_0$ for $|\vec{r}| \to \infty$. This off-diagonal long-range order is the defining property of a superfluid. For $|\vec{r}| \to \infty$ there is no correlation between both positions and we obtain $\langle \psi^\dagger \rangle \approx \langle \psi \rangle = \sqrt{n_0}$ aside from an arbitrary phase. Here, we denoted $\langle \psi \rangle = \langle N-1|\psi|N\rangle$. Allowing for a time dependence gives

$$\psi_0 \equiv \langle N-1|\psi(t)|N\rangle \propto e^{-i\mu t} \tag{1.4}$$

with chemical potential μ. ψ_0 can be interpreted as wavefunction, and we can write

$$\psi_0(\vec{r},t) = \sqrt{n_0} e^{i\chi(\vec{r},t)} \text{ with } \frac{\partial \chi}{\partial t} = -\mu \tag{1.5}$$

The superfluid current thus becomes

$$\vec{j} = \frac{i}{2m}(\psi_0 \vec{\nabla}\psi_0^* - \psi_0^* \vec{\nabla}\psi_0) = \frac{n_0}{m}\vec{\nabla}\chi \tag{1.6}$$

which can be non-zero even in the ground state. Thus, a superfluid permits a lossless flow of a particle current with velocity $v_{sf} = \frac{\vec{\nabla}\chi}{m}$. A phenomenological model for a superconductor can be motivated in an analogous way to the superfluid: As will be shown in chapter 2, electron-phonon interaction leads to an attractive interaction between pairs of electrons.[3] In the presence of an attractive interaction electrons form bound pairs of zero total momentum, that play a similar role as bosons in a superfluid. Thus, in analogy to the superfluid, we are led to introduce off-diagonal long range order by considering the two-particle density matrix

$$\rho_{\sigma_1,\sigma_1',\sigma_2,\sigma_2'}(\vec{r}_1,\vec{r}_1',\vec{r}_2,\vec{r}_2') = \langle \psi_{\sigma_1}^\dagger(r_1)\psi_{\sigma_1'}^\dagger(r_1')\psi_{\sigma_2}(r_2)\psi_{\sigma_2'}(r_2')\rangle \tag{1.7}$$

Considering the density matrix at $\vec{r}_1 = \vec{r}_1'; \vec{r}_2 = \vec{r}_2'$ we get

$$\rho_{\sigma_1,\sigma_1',\sigma_2,\sigma_2'}(\vec{r}_1,\vec{r}_1,\vec{r}_2,\vec{r}_2) \to \Lambda_{\sigma_1,\sigma_1'}^*(\vec{r}_1)\Lambda_{\sigma_2,\sigma_2'}(\vec{r}_2) \text{ for } |\vec{r}_1 - \vec{r}_2| \to \infty \tag{1.8}$$

with $\Lambda_{\sigma_2,\sigma_2'}(\vec{r}_2) = \langle N-2|\psi_{\sigma_2}(r_2)\psi_{\sigma_2'}(r_2)|N\rangle$. Typically, pairing is between electrons of opposite spin and we can write $\Lambda_{\sigma_2,\sigma_2'}(\vec{r}_2) = (i\sigma_2)_{\sigma_2,\sigma_2'}\Lambda(\vec{r}_2)$ with Pauli matrix σ_2, where the order parameter is given by $\Lambda(\vec{r}_2) = |\Lambda|e^{i\chi}$. The square of its amplitude is the density of superconducting electrons. If one were to ignore the charge of the electron pairs forming the superconducting condensate, the velocity of the current of pairs would be $v_s = \frac{\vec{\nabla}\chi}{2m_e}$ with electron mass m_e. For a charged superfluid – as encountered in superconductors – this is however not correct, as it is not gauge invariant: a transformation of the vector potential $\vec{A} \to \vec{A} + \vec{\nabla}\gamma$ leaves all physical quantities invariant but introduces an additional phase $\chi \to \chi + 2e\gamma$. Thus, the pair velocity is instead given by $\vec{v}_s = -\frac{1}{2m_e}\vec{P}$ with gauge invariant potential $\vec{P} = \left(\vec{A} - \frac{1}{2e}\vec{\nabla}\chi\right)$. The supercurrent is thus given by

$$\vec{j} = -\frac{e^2 n_s}{m_e}\vec{P} \tag{1.9}$$

with density of superconducting electrons n_s. Approximating it as constant in both space and time and neglecting terms of higher order in the supercurrent, the energy-phase relation

$$\frac{\partial\chi}{\partial t} = -2\mu(\vec{r}) \tag{1.10}$$

follows from the Schrödinger equation of a charged particle, where the chemical potential includes the electric potential. The time derivative of (1.9) is, using (1.10) with chemical potential $\mu(\vec{r}) = \mu + e\phi_{el}(\vec{r})$ with a constant μ and electrical potential ϕ_{el} ,

$$\vec{E} = \frac{m_e}{e^2 n_s}\frac{\partial}{\partial t}\vec{j} \tag{1.11}$$

[3] In principle other causes for the attractive interaction are possible as well, we however restrict the discussion in this work to conventional superconductors, in which the electron-phonon interaction causes the attractive interaction.

and the curl of (1.9) is

$$\nabla \times \vec{j} = -\frac{e^2 n_s}{m_e}\vec{B} \tag{1.12}$$

Equations (1.11) and (1.12) are the famous London equations [LL35a; LL35b]. Together with Maxwell's equation they provide a description of the macroscopic properties of a superconductor that accounts for the Meissner effect [MO33] as well as for the dissipationless currents. It however fails to properly account for fields varying over distances short compared to the superconducting coherence length. Thus, it in particular does not properly describe the field distribution in superconductors whose coherence length exceeds the penetration depth of a magnetic field (this type of superconductors is commonly refereed to as 'Pippard Superconductor'). Moreover, implicitly the whole current was assumed to be superconducting. At finite temperature, or in non-equilibrium situations, there is a non-zero density of quasiparticle excitations that are not properly accounted for in London theory. As quasiparticles, in contrast to pairs, dissipate energy, it is crucial to include them in a realistic description of superconducting devices. Thus, we need to go beyond phenomenological theories and consider a microscopic theory of superconductivity.

1.2. BCS theory

The first complete microscopic theory of superconductivity was developed in 1957 by Bardeen, Cooper and Schrieffer (BCS) [BCS57]. It assumes a (net) attractive interaction between pairs of electrons, as can be shown to arise for example due to electron-phonon interaction for electrons close to the Fermi surface. Let us assume an attractive interaction between electrons of the form

$$H'_{int} = V_{BCS} \sum_{\vec{k},\vec{k}',\vec{\kappa},\sigma,\sigma'}{}' c^\dagger_{\vec{k}'-\vec{\kappa},\sigma'} c_{\vec{k}',\sigma'} c^\dagger_{\vec{k}+\vec{\kappa},\sigma} c_{\vec{k},\sigma} \tag{1.13}$$

with positive V_{BCS}. Here, $\sum'$ is to be understood to only include states between which the attractive interaction exists and dominates over the repulsive Coulomb interaction.[4] When forming matrix elements from the operators in (1.13) between different, arbitrary, many-electron states, their sign alternate. Thus, if the probability for each configuration was roughly the same in the ground state, the interaction contributions to the ground state energy would approximately cancel. It is however possible to find a set of configurations for which the sign of the matrix elements is the same. Such a set is given by the configurations in which single electron states are occupied in pairs $(\vec{k}_1, \vec{k}_2)$ with fixed momentum $\vec{k}_1 + \vec{k}_2 = \vec{q}$. For a ground state, the most important contribution comes from $\vec{q} = 0$, and the main effects of superconductivity can be understood by considering only the reduced interaction Hamiltonian

$$H'_{int} = -V_{BCS} \sum_{\vec{k},\vec{k}'}{}' c^\dagger_{-\vec{k}',\sigma'} c^\dagger_{\vec{k}',-\sigma'} c_{-\vec{k},\sigma} c_{\vec{k},-\sigma} \tag{1.14}$$

[4] For electron-phonon interaction this includes states within an energy shell of size of the Debye energy around the Fermi surface.

Here, the spin of the pairs was chosen to be zero because of exchange interaction.[5] One immediately recognizes the importance of the pairs $c^\dagger_{-\vec{k}',\sigma'}c^\dagger_{\vec{k}',-\sigma'}$ postulated for phenomenological reasons in the previous section. In the original paper by BCS, variational methods were used to calculate properties of the superconductor from the interaction Hamiltonian (1.14). We instead follow [Ric69] and use a transformation proposed by [Bog58], as it allows for a more transparent discussion of quasiparticles. First, we rewrite

$$c^\dagger_{-\vec{k}',\sigma'}c^\dagger_{\vec{k}',-\sigma'} = \langle c^\dagger_{-\vec{k}',\sigma'}c^\dagger_{\vec{k}',-\sigma'}\rangle + \left(c^\dagger_{-\vec{k}',\sigma'}c^\dagger_{\vec{k}',-\sigma'} - \langle c^\dagger_{-\vec{k}',\sigma'}c^\dagger_{\vec{k}',-\sigma'}\rangle\right) \tag{1.16}$$

and note that, for a large number of pairs, the term in the parenthesis in equation (1.16) are small. Thus, we can insert (1.16) in equation (1.14) and neglect terms of second order in the term in parenthesis to get

$$H = \sum_{\vec{k}} \epsilon_{\vec{k}} c^\dagger_{\vec{k}} c_{\vec{k}} - \sum_{\vec{k}}{}' \left(c^\dagger_{-\vec{k},\sigma'}c^\dagger_{\vec{k},-\sigma'}\Delta - \Delta^* c_{-\vec{k},\sigma}c_{\vec{k},-\sigma}\right) + \frac{|\Delta|^2}{V_{BCS}} \tag{1.17}$$

with $\epsilon_{\vec{k}}$ the single electron energy in the absence of the interaction measured from the chemical potential. The order parameter Δ was introduced as

$$\Delta = V_{BCS} \sum_{\vec{k}'}{}' \langle c_{-\vec{k},\sigma}c_{\vec{k},-\sigma}\rangle \tag{1.18}$$

Hamiltonian (1.17) can be rewritten by introducing new fermionic operators [Bog58] $\gamma_{\vec{k},0}$ and $\gamma_{\vec{k},1}$ as

$$\begin{pmatrix} c_{\vec{k},\uparrow} \\ c^\dagger_{-\vec{k},\downarrow} \end{pmatrix} = \begin{pmatrix} u_{\vec{k}} & v^*_{\vec{k}} \\ -v_{\vec{k}} & u^*_{\vec{k}} \end{pmatrix} \begin{pmatrix} \gamma_{\vec{k},0} \\ \gamma_{\vec{k},1} \end{pmatrix} \tag{1.19}$$

where $|u_{\vec{k}}|^2 + |v_{\vec{k}}|^2 = 1$ ensures fermionic commutation relations for the γ operators. A particularly useful choice is

$$|u_{\vec{k}}|^2 = \frac{1}{2}\left(1 + \frac{\epsilon_{\vec{k}}}{E_{\vec{k}}}\right) \tag{1.20}$$

$$|v_{\vec{k}}|^2 = \frac{1}{2}\left(1 - \frac{\epsilon_{\vec{k}}}{E_{\vec{k}}}\right) \tag{1.21}$$

$$\arg\left(\frac{u}{v}\right) = \arg(\Delta) \tag{1.22}$$

[5] This can be motivated by considering a two particle wavefunction as [Tin96]

$$\phi(\vec{r}_1, \vec{r}_2) = \sum_{\vec{k}} g_{\vec{k}} e^{i\vec{k}\vec{r}_1} e^{-i\vec{k}\vec{r}_2} \tag{1.15}$$

Due to the Pauli principle this results in sums of products of $\cos(\vec{k}(\vec{r}_1 - \vec{r}_2))$ for singlet, and sums of products of $\sin(\vec{k}(\vec{r}_1 - \vec{r}_2))$ for triplet states. As the interaction is attractive, singlet states can usually be expected to have a lower energy. Superconductors for which the Cooper pairs form a triplet state exist [Ish+98], but are beyond the scope of this thesis.

with

$$E_{\vec{k}} = \sqrt{\epsilon_{\vec{k}}^2 + |\Delta|^2} \tag{1.23}$$

as it diagonalizes the Hamiltonian (1.17) to

$$H = \sum_{\vec{k}} (\epsilon_{\vec{k}} - E_{\vec{k}}) + \frac{|\Delta|^2}{V_{BCS}} + \sum_{\vec{k}} E_{\vec{k}} \left(\gamma_{\vec{k},0}^\dagger \gamma_{\vec{k},0} + \gamma_{\vec{k},1}^\dagger \gamma_{\vec{k},1} \right) \tag{1.24}$$

The self consistency equation for the order parameter becomes

$$\Delta = V_{BCS} \sum_{\vec{k}} u_{\vec{k}} v_{\vec{k}}^* (1 - 2f(E_{\vec{k}})) \tag{1.25}$$

with quasiparticle distribution $f(\vec{k}) = \langle \gamma_{\vec{k},0}^\dagger \gamma_{\vec{k},0} \rangle$ where we for simplicity assumed an equal population of both quasiparticle types $\langle \gamma_{\vec{k},0}^\dagger \gamma_{\vec{k},0} \rangle = \langle \gamma_{\vec{k},1}^\dagger \gamma_{\vec{k},1} \rangle$. Thus, the presence of quasiparticles increases the systems energy by decreasing the order parameter Δ and by introducing excitations of energy $E_{\vec{k}} \geq |\Delta|$. In the ground state $|0\rangle$ the system contains no quasiparticles, and one can determine the order parameter from (1.25) with $f(E) = 0$. In the normal state the order parameter is zero and $E_{\vec{k}} = |\epsilon_{\vec{k}}|$. Therefore, the energy difference between superconducting and normal state in the absence of quasiparticles is

$$\delta E = 2 \sum_{\vec{k} > k_F} (\epsilon_{\vec{k}} - E_{\vec{k}}) + \frac{|\Delta|^2}{V_{BCS}} \tag{1.26}$$

Converting the sum to an integral and making use of the self consistency equation (1.25) to rewrite the integral in terms of the order parameter gives $\delta E = -\frac{|\Delta|^2 \rho_F}{2} < 0$ with (normal state) density of states per spin per energy close to the Fermi surface ρ_F. Since the energy of the superconducting state is lower than that of the normal state, one should choose the solution of the self consistency equation with finite order parameter and discard the trivial solution $\Delta = 0$. The ground state of the system is

$$|\psi_\phi\rangle = \prod_{\vec{k}}{}' (u_{\vec{k}}^* + v_{\vec{k}}^* c_{\vec{k},\uparrow}^\dagger c_{-\vec{k}\downarrow}^\dagger)|0\rangle \tag{1.27}$$

where $|0\rangle$ is the vacuum state, as can be verified from $\gamma_{\vec{k}}|\psi_\phi\rangle = 0$. From (1.24) one immediately recognizes the importance of quasiparticles for superconducting devices: In the ground state, an energy of 2Δ is required to break a pair and to create new quasiparticles. Therefore, in the absence of quasiparticles, an external perturbation of frequency $\omega_0 < 2\Delta$ cannot be absorbed by the superconductor and conduction is without losses. If instead the superconductor contains a finite number of quasiparticles, these quasiparticles can absorb perturbations of any frequencies, and lead to losses even for $\omega_0 \ll 2\Delta$.

So far we have assumed for concreteness plane waves as Eigenstates of the electrons in the absence of the interaction. The procedure outlined above can however be generalized straightforwardly to general Eigenstates, provided time reversal symmetry is not broken [this especially excludes effects of magnetic fields]. In that case, Kramer's

theorem ensures all electron Eigenstates to be doubly degenerate, allowing electrons to occupy a state and its time reversed state with both of the same energy. This pair of a state and its time reversed state plays the same role as the pair of opposite momentum states used above, and one can immediately generalize above discussion by interpreting $\vec{k}$ as an arbitrary label for an unperturbed one electron state and $-\vec{k}$ as its time reversed state instead of momentum. Such a procedure has been first proposed by Anderson [And59] to explain the insensitivity of superconductors with regards to (non-magnetic) disorder, but it also applies e.g. to superconducting islands if the level spacing is small compared to the superconducting gap [GC21].

1.3. Superconductor in electromagnetic fields

For a superconductor in an electromagnetic field, described by a vector potential $\vec{A}(\omega)$, the response of the superconductor to the field can be calculated to linear order in the field as derived in [MB58].[6] Let us consider the dirty limit,[7] in which $l \ll \lambda, \xi_0$, with (clean limit) coherence length $\xi_0 = v_f/\Delta$ with Fermi velocity v_f, penetration depth of the electromagnetic field λ (defined below), and mean free path against impurity scattering l. In that case the current field relation

$$\vec{j}(\vec{R},\omega) = -K(\omega)\vec{P}(\vec{R},\omega) \tag{1.28}$$

can be expressed in terms of the complex conductivity σ

$$\sigma = \sigma_1 + i\sigma_2 = \frac{iK(\omega)}{\omega} \tag{1.29}$$

with

$$\frac{\sigma_1(\omega)}{\sigma_N} = \frac{2}{\omega}\int_0^\infty dE(f(E) - f(E+\omega))\rho(E)U^+(E,E+\omega) \tag{1.30}$$

$$+ \frac{1}{\omega}\int_0^\omega dE(1-2f(\omega-E))\rho(E)U^-(E,\omega-E) \tag{1.31}$$

and

$$\frac{\sigma_2}{\sigma_N} = \frac{1}{\omega}\int_{\max(\Delta-\omega,-\Delta)}^{\Delta} dE\,[1-2f(E+\omega)]\,\frac{U^+(E,E+\omega)E}{\sqrt{\Delta^2-E^2}} \tag{1.32}$$

with the shorthand notation

$$U^\pm(E,E') = \rho(E')K^\pm(E,E') \tag{1.33}$$

[6] We postpone a derivation of the current-field relation to chapter 2.4 where it is obtained from Green's function theory.

[7] In a more general case the current-field relation becomes non-local, see [Pip53; MB58].

and the BCS density of states (normalized to four times the normal state density of states)

$$\rho(E) = \frac{E}{\sqrt{E^2 - \Delta^2}}\Theta(E - \Delta) \tag{1.34}$$

and coherence factor

$$K^{\pm}(E_1, E_2) = 1 \pm \frac{\Delta^2}{E_1 E_2} \tag{1.35}$$

At low quasiparticle densities and photon energies below the pair breaking threshold, the imaginary part of the conductivity is much larger than the real part. Ampere's law[8] $\vec{j} = \vec{\nabla} \times \vec{H}$, the current field relation (1.28), and the definition of the vector potential $\vec{H} = \vec{\nabla} \times \vec{A}$ result in

$$\nabla^2 \vec{A} = \frac{1}{\lambda^2}\vec{P} \quad \text{with} \quad \frac{1}{\lambda^2} = -i\mu_0\sigma\omega \tag{1.36}$$

For $\Delta \gg \omega$ we have

$$\lambda \simeq \frac{1}{\sqrt{\mu_0\omega\sigma_2}} \simeq \frac{1}{\sqrt{\mu_0\pi\Delta\sigma_N}} = \lambda_L\sqrt{\frac{\xi_0}{l}} \tag{1.37}$$

with the London depth λ_L. Thus, the penetration depth λ for a magnetic field incident on a superconductor is dominated by the imaginary part of the complex conductivity. The real part of the conductivity accounts for losses due to photon absorption processes by quasiparticles, the effect of these absorption processes on the quasiparticles is discussed in chapters 2 and 3. Note that, while the current-field relation in the low-quasiparticle limit has a similar form as postulated in section 1.1, the value of the factor differs from the one in equation (1.9) due to the diffusive motion of electrons in disordered superconductors.

The current-field relation (1.28), energy-phase relation (1.10), and Ampere's law result in the (linearized) first London equation

$$\vec{j}(\omega) = -\sigma\vec{E}(\omega) \tag{1.38}$$

1.4. Coplanar waveguide resonators

1.4.1. Impedance

A commonly used superconducting device are coplanar waveguide resonators. They are devices manufactured from a thin superconducting film on a dielectric substrate. They consist of a long, narrow, superconducting strip that is separated by two gaps (one to each side) from the superconducting ground planes. An alternating current runs through the central strip and returns to the ground planes. Due to (1.38), the average energy density of an alternating current of frequency ω_0 inside the superconductor is $w_k \simeq |\vec{j}|^2\sigma_2/4\omega_0|\sigma|^2$ where $\vec{j}$ is the amplitude of the current. It is convenient

[8] Here, the displacement current was neglected as it is small in good conductors

to describe superconducting transmission lines and resonators using the kinetic inductance per unit length L_k, relating the energy per unit length inside the superconductor to the amplitude of the total current $\vec{I}$ as

$$L_k \vec{I}^2 = \frac{\sigma_2}{\omega_0 |\sigma|^2} \int dS |\vec{j}|^2 \tag{1.39}$$

where the integral is over the area of the conductor. In addition to the kinetic inductance L_k the line has a geometric inductance L_m accounting for the energy stored in the magnetic field induced by the current

$$L_m \vec{I}^2 = \frac{1}{\mu_0} \int dS B^2 \tag{1.40}$$

Here, the transmission line was approximated as infinite in the direction perpendicular to the plane S and the integral extends over the whole plane. The resistance per unit length R can be defined using the power loss per unit length P_l as [Poz12]

$$R = \frac{2}{I_z^2} P_l = \frac{1}{I_z^2} \frac{\sigma_1}{|\sigma|^2} \int dS j^2 = \frac{L_k \omega_0 \sigma_1}{|\sigma|^2} \tag{1.41}$$

where the first London equation and the definition of the kinetic inductance were used. For a film much thinner than the penetration depth $d \ll \lambda$ the two dimensional screening length $\Lambda = 2\lambda^2/d$ gives the lengthscale on which fields penetrate the central strip of the CPW from the gaps. If that length is much smaller than the width of the central conductor w and the slot width s, penetration of flux in the superconductor adjacent to the slots can be neglected and the electromagnetic fields can be obtained approximating the resonator as perfect conductor. This allows to calculate the impedance of the transmission line as done by [Cle13]. For completeness we summarize the calculation in appendix A. The geometric inductance per unit length is [WYK94; Cle13]

$$L_m = \frac{\mu_0 K(k')}{4K(k)} \tag{1.42}$$

and the kinetic inductance per unit length

$$L_k \approx \frac{\mu_0 \Lambda}{w} \frac{\ln\left(\frac{2(1-k)}{\epsilon(1+k)}\right)}{2(1-k)K^2(k)} \tag{1.43}$$

with cutoff $\epsilon \sim \Lambda/w$, $k = w/(w+2s)$, $k' = \sqrt{1-k^2}$ and the Legendre elliptic integral K.

1.4.2. Quality factor and resonance frequency

According to transmission line theory [Poz12], a capacitively coupled half wavelength resonator can be modelled as a lumped element parallel RLC-circuit with effective resistance

$$R' \simeq \frac{2\omega_0}{\pi} \sqrt{\frac{L}{C}} \frac{L}{R} \tag{1.44}$$

capacitance

$$C' = \frac{\pi}{2\omega_0}\sqrt{\frac{C}{L}} \tag{1.45}$$

and inductance

$$L' = \frac{1}{\omega_0^2 C'} \tag{1.46}$$

where $R \ll \omega_0 L$ was used. The quality factor is thus given by

$$Q = \omega_0 R' C' = \frac{\omega_0 L}{R} = \frac{\sigma_2}{\alpha\sigma_1} \tag{1.47}$$

with kinetic inductance fraction

$$\alpha = \frac{L_k}{L_k + L_m} \tag{1.48}$$

The resonance frequency is

$$\omega_0 = \frac{\pi}{l\sqrt{LC}} \tag{1.49}$$

with length of resonator l. Thus, a change $\delta\sigma$ in the complex conductivity leads to a shift in resonance frequency

$$\frac{\delta\omega_0}{\omega_0} = -\frac{1}{2}\frac{\alpha\delta\sigma_2}{\sigma_2} \tag{1.50}$$

Both resonance frequency and quality factor depend on the complex conductivity, Eqs. (1.30) and (1.32), and thus on both the quasiparticle density and their distribution in energy. Applications relying on the quality factor and resonance frequency of a resonator thus require understanding of the quasiparticle energy distribution within the resonator, which is investigated in chapter 3. Furthermore, measuring quality factor and resonance frequency allows to obtain information about the presence and energy distribution of quasiparticles [Gao08; Gao+08]. Moreover, it is possible to independently measure the recombination time of quasiparticles, using either noise measurements or the time for relaxation to equilibrium after an optical pulse, and thus obtain additional information on the quasiparticle dynamics using resonators [WP04; Vis+11]. A recent measurement [Vis+14] of the quality factor and resonance frequency for different fridge temperatures T_B and readout powers (i.e. different numbers of photons in the resonator) is shown in figure 1.1. There, it was suggested that the dependence on the readout power for $T_B \gtrsim 200\,\mathrm{mK}$ could be explained by a redistribution of quasiparticles in energy, while the plateau at low temperatures would arise from quasiparticle creation by the readout signal. We discuss this interpretation in detail in chapter 3, where we indeed find re-distribution of quasiparticles to be a satisfying explanation of the $T_B \gtrsim 200\,\mathrm{mK}$ measurement, but creation of new quasiparticles through the readout signal to be insufficient to explain the $T_B \lesssim 200\,\mathrm{mK}$ measurement. Instead, we show that it could be explained by assuming a small number of photons above the pair breaking threshold 2Δ.

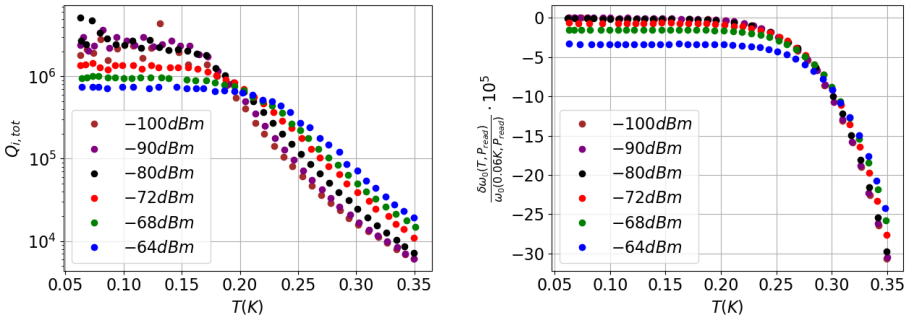

Figure 1.1.: Internal quality factor and resonance frequency of a resonator as function of readout power and temperature. Data is taken from [Vis+14].

1.5. Qubits

In this subsection we give a short introduction to the Josephson effect and superconducting qubits and discuss the relevance of quasiparticle tunneling. A more complete discussion can be found in [GC21] and references therein. So far, we only considered superconductors of infinite size. Now consider a single superconducting island instead. The mean field Hamiltonian (1.24) can be set up analogous to the infinite size case by using one electron states on the island instead of plane wave states, as argue in the end of section 1.2.[9] The ground state $|\psi_\phi\rangle$ has a well defined phase ϕ but is not an Eigenstate of the Cooper pair number operator $N_c = \sum_{\vec{k}} c^\dagger_{k\uparrow} c^\dagger_{-k\downarrow} c_{k\uparrow} c_{-k\downarrow}$. It is however possible to form a linear combination of $|\psi_\phi\rangle$ that is an Eigenstate of the pair number operator

$$|N\rangle = \int_0^{2\pi} \frac{d\phi}{2\pi} e^{-iN_c\phi} |\psi_\phi\rangle \tag{1.51}$$

The set of $|\psi_\phi\rangle$ and $|N\rangle$ form two sets of bases for the ground state of the superconducting island, one in which the phase is arbitrary and the pair number fixed, and one with arbitrary number of pairs but fixed phase. In the ϕ representation, the pair number operator is given by $N_c = -i\frac{\partial}{\partial\phi}$. The operator $T = \sum_N |N+1\rangle\langle N|$ raising the number of pairs by one is given by $T = e^{i\phi}$. Independent of basis, we can thus interpret the phase and pair number as operators obeying the commutation relation $[N_c, e^{-i\phi}] = e^{-i\phi}$. Now, consider an island connected to another island by a thin tunneling barrier. In the absence of quasiparticles, tunneling processes of energy below 2Δ only involve tunneling of pairs. A phenomenological Hamiltonian accounting for pair tunneling is

$$H_J = \text{const} \cdot \left(T_L^\dagger T_R + T_R^\dagger T_L\right) \tag{1.52}$$

where the first term accounts for tunneling of a pair from the right to the left island and the second term for the opposite process. Here, only lowest order processes (i.e.

[9] This implicitly assumes a level spacing that is small compared to the superconducting gap.

tunneling of one pair) are included, as the transmission amplitude usually is small, and an additional irrelevant constant was omitted. In the phase basis we get

$$H_J = -E_J \cos(\phi) \tag{1.53}$$

where ϕ is the phase difference between the two islands. E_J is the Josephson energy, usually $E_J > 0$ as the presence of the tunneling barrier leads to a less restricted movement of electrons. Aside from a phase difference, tunneling of pairs leads to charge transfer between both islands corresponding to

$$H_c = \frac{2e^2}{C}(N_c - n_g)^2 \tag{1.54}$$

where the capacitance C accounts for the junction's capacitance as well as a shunting capacitance and n_g is a static charge induced by a biasing gate, background charges and unpaired electrons. n_g is difficult to control in experiments, and different strategies have been developed to mitigate its harmful influence on the qubit operation; in a Transmon this is done by choosing the Josephson energy much larger than the charging energy, $E_J \gg E_c$. This allows to separate the quantum dynamics of the phase difference in small fluctuations around the minima in the Josephson Hamiltonian $\phi = 2\pi k$ and discrete phase slips by $\pm 2\pi$. The latter can be shown to be suppressed exponentially in $\sqrt{8E_J/E_c}$ [Koc+07]. Neglecting phase slips, one could completely eliminate n_g from the stationary Schrödinger equation by a gauge transformation. As the phase remains close to the minima, one can Taylor expand the Josephson Hamiltonian to obtain the Hamiltonian of a weakly anharmonic oscillator, whose lowest two Eigenstates can be used as qubit states.

The above introduction to the Josephson effect and Transmons does not allow for the inclusion of quasiparticles as it only accounts for pair tunneling. To include quasiparticles, we should instead start by considering a single electron tunneling Hamiltonian

$$H_T = \sum_{k_L,k_R} t_{k_L,k_R} c^\dagger_{k_L,\sigma} c_{k_R,\sigma} + h.c. \tag{1.55}$$

Using the Bogulioubov transform it can be written in terms of the quasiparticle operators as $H_T = H_T^{qp} + H_p^{qp}$ with

$$H_T^{qp} = \sum_{k_L,k_R,\sigma} t_{k_L,k_R} \left(u^*_{k_L} u_{k_R} - v^*_{k_L} v_{k_R}\right) \gamma^\dagger_{k_L,\pm} \gamma_{k_R,\pm} + h.c. \tag{1.56}$$

$$H_p^{qp} = \sum_{k_L,k_R,\pm} \pm t_{k_L,k_R} \left(u^*_{k_L} u^*_{k_R} + v^*_{k_L} v^*_{k_R}\right) \gamma^\dagger_{k_R,\pm} \gamma^\dagger_{k_L,\mp} + h.c. \tag{1.57}$$

The effect of H_p on the ground state energy can be evaluated using second order perturbation theory, it leads to $\delta E_{GS} = -\cos(\phi) E_J$ which is of the same form as the Josephson Hamiltonian H_J. The Josephson energy is $E_J = \pi^2 |\Delta||t|^2/\delta\epsilon^2$ where we approximated the tunneling element t as energy independent, assumed for simplicity a symmetric junction $|\Delta_L| = |\Delta_R|$ and introduced the level spacing $\delta\epsilon$. Thus, we replace $H_p^{qp} \to H_J$ in the following. This is a good approximation if the frequency of

the electromagnetic field biasing the junction is far below the pair breaking threshold $\omega_0 \ll 2\Delta$. In that case, the field cannot break any pairs and thus H_p^{qp} only modifies the ground state energy and supercurrent, but does not lead to transitions between excited states. To understand qubit-quasiparticle interactions we thus consider an effective Hamiltonian

$$H = H_0 + H_T^{qp} + H_{qp} \tag{1.58}$$

with the unperturbed Hamiltonian $H_0 = H_J + H_C$ and H_{qp} is the Hamiltonian of quasiparticles in the absence of tunneling. Treating H_T^{qp} as small perturbation, qubit transition rates from initial state $|i,\eta\rangle$ to final state $|f,\lambda\rangle$ can be calculated from Fermi's golden rule

$$\Gamma_{|i\rangle\to|f\rangle} = 2\pi \sum_{\lambda} \langle\!\langle |\langle f,\lambda|H_T^{qp}|i,\eta\rangle|^2 \rangle\!\rangle_\eta \delta(E_\lambda - E_\eta - \omega_{if}) \tag{1.59}$$

where f/i denotes the qubit state and η/λ the quasiparticle state, E_η and E_λ are respectively the (total) energy of the quasiparticles in initial and final state and $\omega_{i,f}$ is the energy difference between initial and final qubit state. The double angular bracket denotes averaging over all initial quasiparticle states. Note that H_T^{qp} depends on the phase difference (through the Bogoliubov amplitudes u, v) and tunneling of quasiparticles can change the state of a qubit. Changing the sum over quasiparticle states to an integral over energies, Eq. (1.59) gives

$$\begin{aligned}\Gamma_{|i\rangle\to|f\rangle} = \frac{16E_J}{\pi\Delta} \int_\Delta dE\rho(E)f(E)\left(1-f(E+\omega_{if})\right)\Big[&U^+(E,E+\omega_{if})|\langle f|\sin(\phi)|i\rangle|^2 \\ &+ U^-(E,E+\omega_{if})|\langle f|\cos(\phi)|i\rangle|^2\Big]\end{aligned} \tag{1.60}$$

with BCS density of states (1.34), coherence factors (1.35) and quasiparticle energy distribution function f. As in resonators, quasiparticles in qubits induce losses that depend both on the density and energy of the quasiparticles; these losses limit the T_1 time of superconducting qubits. Further experimental insight in the nature of a Transmon's losses can be obtained by including phase slips in above discussion. In that case one finds the Transmon's energy levels to not be completely independent of the gate charge n_g, but to exhibit small oscillations of period 1 as a function of n_g [Koc+07]. As a quasiparticle tunneling event changes the background charge by 1/2, quasiparticle induced transitions are accompanied by a (small but measurable) shift in the energy levels (this is commonly referred to as 'parity switching'). Experiments with Transmon qubits thus enable a distinction between quasiparticle induced transitions and other noise sources by correlating transitions with parity switching events [Ser+18; Ris+13; Cat14]. A typical measurement of the qubit transition rates as function of the fridge temperature is shown in figure 1.2. While at temperatures above 150 mK the transition rates decrease exponentially upon lowering the temperature, they saturate at a constant value $\Gamma_{|0\rangle\to|1\rangle} \approx 400\,\mu$s. The ratio $\frac{\Gamma_{|1\rangle\to|0\rangle}}{\Gamma_{|0\rangle\to|1\rangle}} \approx 1$ at these low temperatures indicates a quasiparticle energy distribution that is broad compared

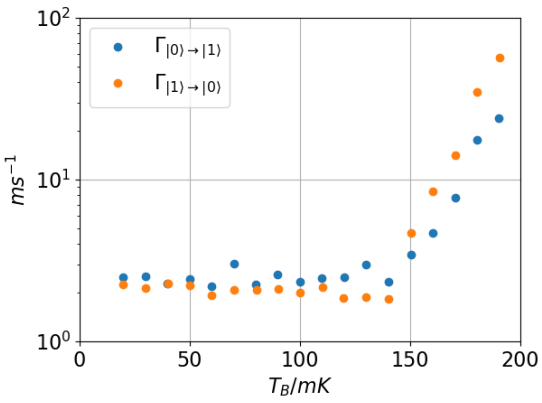

Figure 1.2.: Transition rates of a Transmon that are accompanied by parity switching. Data is taken from [Ser+18]

to the qubit frequency. As this is incompatible with a thermal distribution, one must include non-equilibrium processes to properly model that qubit [Ser+18]. [10] Alternatively, this ratio could be explained by transitions induced by stray photons of energy above the pair breaking threshold 2Δ [Hou+19].

1.6. Superconducting detectors

Superconductors can be used to build photon detectors with a high energy resolution for a broad range of wavelengths ranging from X-rays [Kur00] up to millimeters wavelengths [K H+12]. A large variety of detectors have been developed with quite different properties: Some detectors [e.g. transition edge sensors (TES)] operate at temperatures close to the transition temperature while others [e.g. kinetic inductance detectors (KID), superconducting nanowire single photon detectors (SNSPDs) or superconducting tunneling detectors (STD)] are operated at very low temperatures. We exemplify some of the detectors in figure 1.3. Depending on the detector design different physical processes can dominate the detector's noise. For instance, in SNSPDs vortices crossing the nanowire lead to dark counts [Bul+11; Bar+10] while thermal noise is important for TESs[Low+14] . In KIDs and STDs quasiparticles are particular important as they provide the signal. Compared to semiconductor detectors that are based on quasiparticles (i.e. electrons and holes in semiconductors), their sensitivity is increased due to the lower gap: While semiconductors typically have gaps in the energy spectrum on the order of eV, typical energies of the superconducting gap are of order of a meV. Thus, the same signal creates about a factor 10^3 more quasiparticles N_{sup} than electron-hole pairs in semiconductors. As the statistics

[10] Although quasiparticles that absorb energy from the qubit get heated, such an effect is insufficient to produce a hot distribution [CB19]. A possible explanation could be that quasiparticles get created at a high energy and only lose a part of that energy through phonon emission before recombining, we will discuss a similar situation in resonators in chapter 3.5.1.

of quasiparticle generation provides a limit on the energy resolution of a detector scaling with $\delta E \propto 1/\sqrt{N_{sup}}$ one can expect a better performance of superconducting detectors compared to semiconductors [Gv95]. Moreover, the lower gap allows detection of photons of wavelengths up to millimeters. However, as discussed in the previous sections, usually experiments find a non-negligible number of quasiparticles even at low temperatures without a signal. As these quasiparticles contribute generation-recombination noise, they limit the detector's sensitivity and identifying and mitigating their source will be important to further improve these detector types. Moreover, as the complex conductivity not only depends on the number of quasiparticles but also on their distribution in energy, precise knowledge of the quasiparticle energy distribution may help calibrating KIDs.

1.7. Conclusion

In this chapter we discussed the influence of quasiparticles on several superconducting devices. Experiments at low temperatures usually find a residual quasiparticle density attributed to various non-equilibrium processes that often harms the operation of the device, e.g. by limiting a resonator's quality factor, introducing decoherence in qubits, or contributing generation-recombination noise in KIDs. Thus, identifying and mitigating sources of residual quasiparticles is highly desirable and requires a detailed understanding of the quasiparticle dynamics.

To further understand the behaviour of the quasiparticle distribution function and identify possible causes of the residual quasiparticle density experiments can be done measuring the transition rates of a qubit or resonance frequency and quality factor of a resonator. Distinguishing quasiparticles from other loss sources can be done by measuring the parity (of qubit states) or the recombination time (e.g. through noise measurements in resonators). For concreteness, we will focus on resonators in the remainder of this work.

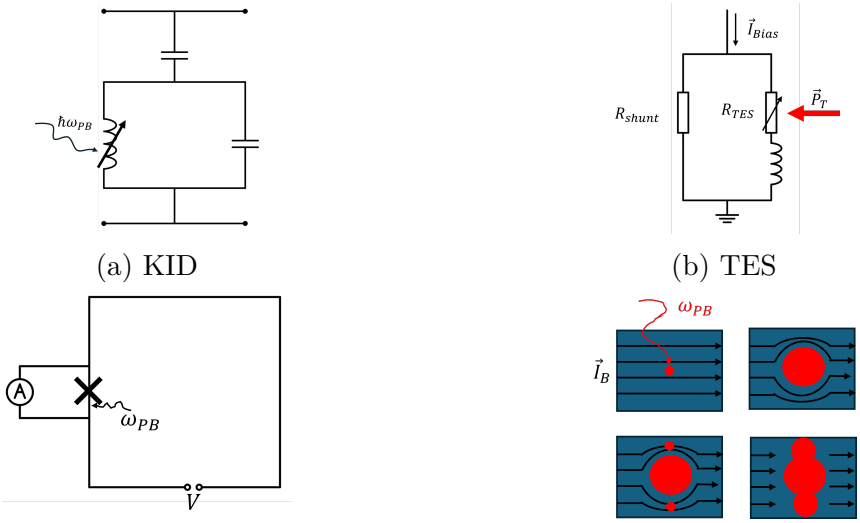

(a) KID (b) TES

(c) STD (d) SNSPD

Figure 1.3.: Fundamental operating principle of a): Kinetic inductance detectors, b) Transition edge sensors, c) Superconducting tunneling detectors, d) superconducting nanowire single photon detectors. a): An incoming photon creates quasiparticles in a superconducting resonator. This changes kinetic inductance and resistance, which can be read out by a coupled feedline [Day+03]. b) A transition edge sensor consists of a superconductor cooled to a temperature slightly below T_c that is thermally connected to an absorber and biased with a constant voltage due to $R_{shunt} \ll R_{TES}$. An incoming photon can be absorbed by the absorber deposing a thermal power $\vec{P}_T$ into the superconductor, increasing its temperature and thus resistance. This decreases the current, which can be read out by coupling to a SQUID (not shown here). Moreover, as the current decreases the power absorbed in the superconductor decreases as well, and the temperature resets to the initial temperature [Mau18]. c) Incoming radiation breaks pairs on one electrode of a voltage biased junction. If the voltage bias is too small to break pairs $eV < 2\Delta$ one naively expects only currents due to quasiparticles to show in the junction's I-V curve (apart from the constant current at $V = 0$), and measuring the current allows calculation of the number of quasiparticles created. More accurately, the pair current can also affect the junction's I-V curve through effects such as inelastic pair tunneling [IGE94; Hol+94]. In practice one mitigates this by suppressing the DC-Josephson current by applying an external magnetic field [Twe88; Teu08]. d) A superconductor is current biased close to the critical current. An incoming photon creates many quasiparticles leading to a normal conducting hotspot. The hotspots expands and the current close to the edge of the hotspot increases as well, eventually switching the whole width of the nanowire to the normal state [Gol+01].

2. Green's functions in superconductors

In the previous chapter superconductivity was discussed based on BCS theory. While BCS theory explains many properties of superconductors [e.g. Meissner and Josephson effects] and can even be used for the description of non-equilibrium situations [CS77; CS78], it is not well-suited to deal with spatial inhomogeneous superconductors and superconductors containing magnetic impurities. As both will be considered in chapter 4 we now introduce superconductivity based on quasiclassical non-equilibrium Green's functions. Reviews of this approach can be found in [LO86; RS86a; Kop01].

2.1. Keldysh Green's functions

2.1.1. Notation

Throughout this thesis the formalism of second quantization is used. It relies on the definition of field operators according to

$$\begin{aligned}\psi(\vec{x},t) &= \sum_i \phi_i(\vec{x},t)a_i \\ \psi^\dagger(\vec{x},t) &= \sum_i \phi_i^*(\vec{x},t)a_i^\dagger\end{aligned} \tag{2.1}$$

Here ϕ_i is the wavefunction of state i, the operators $\psi^{(\dagger)}(\vec{x},t)$ destroy (create) a quasiparticle at position $\boldsymbol{x}$, the operators $a_i^{(\dagger)}$ destroy (create) a quasiparticle in state i and obey the (anti-)commutation relations

$$[\psi(\vec{x}_i,t_i),\psi^\dagger(\vec{x}_j,t_j)]_\pm = \delta(\vec{x}_i-\vec{x}_j)\delta(t_i-t_j) \tag{2.2}$$

$$[\psi^\dagger(\boldsymbol{x_i}),\psi^\dagger(\boldsymbol{x_j})]_\pm = 0 \tag{2.3}$$

$$[\psi(\boldsymbol{x_i}),\psi(\boldsymbol{x_j})]_\pm = 0 \tag{2.4}$$

with the upper (lower) sign for fermions (bosons) and the same relations for $\hat{a}^{(\dagger)}$ when replacing the delta distribution by the Kronecker delta $\delta_{i,j}$. It is convenient to introduce the Nambu [Nam60] pseudospinor fields $\boldsymbol{\psi} = (\psi_\uparrow, \psi_\downarrow^\dagger)^T$ and to define the product of a spinor and a conjugate

$$(\boldsymbol{\psi}^\dagger(1)\boldsymbol{\psi}(2))_{i,j} = \boldsymbol{\psi}_i^\dagger(1)\boldsymbol{\psi}_j(2) \tag{2.5}$$

$$(\boldsymbol{\psi}(1)\boldsymbol{\psi}^\dagger(2))_{i,j} = \boldsymbol{\psi}_i(1)\boldsymbol{\psi}_j^\dagger(2) \tag{2.6}$$

where the arguments include coordinates and times. In the following bold operators and functions denote operators and functions containing matrix or vector structure in Nambu space. Below we will also introduce an additional index specifying components in the so called 'Keldysh' space, operators and functions that have both Keldysh and Nambu indices are denoted with a hat.

2.1.2. Green's functions

Green's function's methods are widely used in condensed matter theory. Different approaches have been developed that are valid within different approximations, the most used are the zero temperature, the Matsubara and the Keldysh technique. Loosely following [vS13] we introduce these different techniques as different limits of the method pioneered by Konstantinov and Perel [KP61]. In subsequent sections the discussion is restricted to the Keldysh formalism, which corresponds to the Konstantinov-Perel formalism within the adiabatic limit (see below).

We start by defining the time ordered n-particle Nambu Green's function

$$\boldsymbol{G}_n(1...n,1'...n') = (-i)^n \mathrm{Tr}\left(\rho \mathcal{T}((\boldsymbol{\tau}_3\boldsymbol{\psi}_H(1))...(\boldsymbol{\tau}_3\boldsymbol{\psi}_H(n))\boldsymbol{\psi}_H^\dagger(1')...\boldsymbol{\psi}_H^\dagger(n'))\right) \tag{2.7}$$

where the field operators are Nambu spinors evolving according to the Heisenberg equation of motion, each index $1,...,n$ includes spatial and temporal coordinates and ρ is the density matrix at time t_0. The product between the spinors is to be understood as a direct product, i.e. it can be written component wise

$$\begin{aligned} &G_n(1..n,1'..n')_{i_1..i_n,j_1,..j_n} \\ &= (-i)^n \mathrm{Tr}\left(\rho \mathcal{T}((\boldsymbol{\tau}_3\boldsymbol{\psi}_H(1))_{i_1}..(\boldsymbol{\tau}_3\boldsymbol{\psi}_H(n))_{i_n}\boldsymbol{\psi}_H^\dagger(1')_{j_1}..\boldsymbol{\psi}_H^\dagger(n')_{j_n})\right) \end{aligned} \tag{2.8}$$

and the time ordering operator is to be understood as acting on each component, i.e. it does not exchange the indices when swapping spinors. Furthermore, the trace is not taken over Nambu indices but separately for each matrix index over all single particle states. The τ_3 matrices acting on the spinors have been introduced to ensure consistency of the definition of the single particle Green's function with literature. It can be conveniently rewritten to

$$\begin{aligned} &\boldsymbol{G}_n(1...n,1'...n') \\ &= (-i)^n \mathrm{Tr}\left(\rho \mathcal{T}_{c_1}\left(\exp\left(-i\int_{c_1} dz H(z)\right)(\boldsymbol{\tau}_3\boldsymbol{\psi}(1))...(\boldsymbol{\tau}_3\boldsymbol{\psi}(n))\boldsymbol{\psi}^\dagger(1')...\boldsymbol{\psi}^\dagger(n')\right)\right) \end{aligned} \tag{2.9}$$

with the operators in the Schrödinger picture and time integration and time ordering along the contour c_1 displayed in Fig. 2.1. Now we allow for complex times z and extend the Hamiltonian to complex times to include the density matrix in the contour integral

$$\boldsymbol{G}_n(1...n,1'...n') \tag{2.10}$$

$$= (-i)^n \frac{\mathrm{Tr}\left(\mathcal{T}_{c_2}\left(\exp\left(-i\int_{c_2} dz H(z)\right)(\boldsymbol{\tau}_3\boldsymbol{\psi}(1))...(\boldsymbol{\tau}_3\boldsymbol{\psi}(n))\boldsymbol{\psi}^\dagger(1')...\boldsymbol{\psi}^\dagger(n')\right)\right)}{\mathrm{Tr}\left(\mathcal{T}_{c_2}\left(\exp\left(-i\int_{c_2} dz H(z)\right)\right)\right)}$$

Here, the contour integral is over c_2 of figure 2.1 and the Hamiltonian was extended to the complex plane such that the initial density matrix becomes

$$\rho = \frac{e^{-\beta H(t_0+i\tau)}}{\mathrm{Tr}\left(e^{-\beta H(t_0+i\tau)}\right)} \tag{2.11}$$

for a real number β that, for equilibrium systems, corresponds to the inverse temperature and $H(t_0 + i\tau_1) = H(t_0 + i\tau_2) \equiv H^M$ for all real $\tau_1, \tau_2 \neq 0$. If the system initially was in equilibrium, the extension of the Hamiltonian to complex times can be done with the obvious definition $H(t_0 + i\tau) = H(t_0)$. For general initial correlations the choice of a proper extension of the Hamiltonian is not trivial, and it may be more convenient to directly work with a perturbation expansion using the initial density matrix [vS13]. I do not dwell on the problem any further, as the Keldysh formalism used in the rest of this thesis neglects the effect of initial correlations anyway.

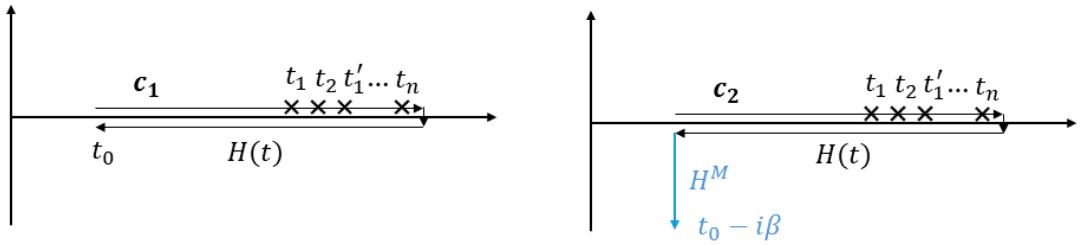

Figure 2.1.: Contours used to rewrite the Green's function, assuming the largest time t_n. Furthermore, the Hamiltonian used on the parts of the contour is given.

To derive Wick's theorem, one assumes a single particle Hamiltonian of the form

$$H_0(z) = \int d^3r \sum_{\sigma=\uparrow,\downarrow} \psi_\sigma^\dagger(\vec{r}) h(\vec{r}, z) \psi_\sigma(\vec{r}) \tag{2.12}$$

Now one can use the Heisenberg equation of motion for the spinors

$$i\boldsymbol{\tau}_3 \frac{d}{dz}\boldsymbol{\psi}(r, z) = \boldsymbol{\tau_3}[\boldsymbol{\psi}(r, z), H_0] = h(r, z)\boldsymbol{\psi}(r, z) \tag{2.13}$$

to obtain the Martin-Schwinger-Kadanoff [KM61] hierarchy for the bare Green's functions

$$\begin{aligned}\left[i\frac{d}{dz_k}\boldsymbol{\tau}_3 - h(k)\right]\boldsymbol{G}^0_n(1...n,1'...n') &= \sum_{j'=1}^{n}(\pm)^{k+j'}\delta(k-j')\boldsymbol{G}^0_{n-1}(1...\not{k}...n,1'...\not{j'}...n')\\ \boldsymbol{G}^0_n(1...n,1'...n')\left[-i\frac{d}{dz_{k'}}\boldsymbol{\tau}_3 - h(k)\right] &= \sum_{j=1}^{n}(\pm)^{k+j}\delta(j-k')\boldsymbol{G}^0_{n-1}(1...\not{j}...n,1'...\not{k'}...n')\end{aligned} \tag{2.14}$$

where the derivative in the second line acts to the left, z_k denotes the complex time of annihilation operator k, the arguments of the Green's functions and Delta distributions include both spatial and temporal terms and the matrix τ_3 acts on term k (k') in the direct product. The unity matrix in components k, j is implied on the RHS. Furthermore, the Green's functions are (anti-) periodic in each time argument for bosons (fermions) along the KP contour c_2 [MS59], i.e. $\boldsymbol{G}^0_n(t_1...t_j = t_{0,+}...t_n, t'_1...t) = \pm\boldsymbol{G}^0_n(t_1...t_j = t_{0,-}...t_n, t'_1...t)$ where $t_{0,\pm}$ symbolizes times on the start or end of the contour. This boundary condition immediately follows from the definition of the contour ordered Green's function, as the time ordering operator sorts the corresponding operator either to the left or right in the trace; the number of permutations required to shift it to the left or right differs by an odd number. A solution of the MSK hierarchy obeying the (anti-) periodic boundary conditions is given by Wick's theorem for a general contour[vS13]

$$\boldsymbol{G}^0_n(1...n,1'...n') = \begin{vmatrix}\boldsymbol{G}^0(1,1') & ... & \boldsymbol{G}^0(1,n')\\ . & & .\\ . & & .\\ . & & .\\ \boldsymbol{G}^0(n,1') & ... & \boldsymbol{G}^0(n,n')\end{vmatrix}_{\pm}$$

with the single particle Green's function $\boldsymbol{G}^0 \equiv \boldsymbol{G}^0_1$ determined by Eq. (2.14) when inserting the trivial zero-particle function $\boldsymbol{G}^0_0 = \mathbf{1}$; which can be straightforwardly checked by inserting into Eq. (2.14). $\|_{\pm}$ denotes the permanent for bosons and the determinant for fermions.

2.1.3. Keldysh contour and Keldysh Green's functions

In principle, Wick's theorem derived in the previous section allows setting up perturbation theory using the contour c_2, i.e. accounting for initial correlations as well as non-equilibrium situations. This is however quite complicated, and in many cases calculations can be considerably simplified by further deforming the integration contour and making use of cancellations of parts of the contour. Some of the most commonly used contours are given in figure 2.2; in the following only the Keldysh Contour [L V65] will be discussed. To obtain it, one needs to make the adiabatic assumption

$$\rho = U_\eta(t_0,-\infty)\rho_0 U_\eta(-\infty,t_0) \tag{2.15}$$

with the time evolution operator U_η for the Hamiltonian

$$H_\eta(t) = H_0^M + e^{-\eta|t_0-t|}\theta(t_0-t)H_{int}^M \tag{2.16}$$

where $\eta \to 0^+$, H_0^M a single particle and H_{int}^M the interaction part of the imaginary time Hamiltonian. If the adiabatic assumption holds, the system is equivalent to a system that was in equilibrium with a non-interacting Hamiltonian at $t \to -\infty$, after which the interactions leading to the initial state are turned on adiabatically. It corresponds to the contour c_K in figure 2.2. In the contour sketched in figure 2.2 the field operators were assumed to be on the positive track of the contour. Although this assumption is intuitive to motivate by rewriting the time ordered Green's function (2.7) in terms of the contour ordered Green's function (2.9), the subsequent calculations made no assumptions on the position of the field operators on the contour. Indeed, it turns out to be advantageous for the calculation of expectation values of operators that are not time ordered to allow the field operators in (2.9) to reside on both branches of the contour [L V65]. As Wick's Theorem applies irrespective of the position on the contour, arbitrary n-particle Green's functions can be decomposed into combinations of the following bare single particle Green's functions: The time ordered Green's function (also called 'causal Green's function') with both operators on the forward branch

$$\boldsymbol{G}_0^c(r,r',t,t') = -i\boldsymbol{\tau}_3 Tr\mathcal{T}_{c_K}\left(\exp\left(-i\int_{c_K} dz H_0(z)\right)\boldsymbol{\psi}(r,t_+)\boldsymbol{\psi}^\dagger(r',t'_+)\right) \tag{2.17}$$

the anti-ordered function with both operators on the return branch

$$\tilde{\boldsymbol{G}}_0^c(r,r',t,t') = -\boldsymbol{\tau}_3 iTr\mathcal{T}_{c_K}\left(\exp\left(-i\int_{c_K} dz H_0(z)\right)\boldsymbol{\psi}(r,t_-)\boldsymbol{\psi}^\dagger(r',t'_-)\right) \tag{2.18}$$

a Green's function with creation operator on the forward and annihilation operator on the return branch

$$\boldsymbol{G}_0^-(r,r',t,t') = -i\boldsymbol{\tau}_3 Tr\mathcal{T}_{c_K}\left(\exp\left(-i\int_{c_K} dz H_0(z)\right)\boldsymbol{\psi}(r,t_-)\boldsymbol{\psi}^\dagger(r',t'_+)\right) \tag{2.19}$$

and a Green's function with creation operator on the return and annihilation operator on the forward branch

$$\boldsymbol{G}_0^+(r,r',t,t') = -i\boldsymbol{\tau}_3 Tr\mathcal{T}_{c_K}\left(\exp\left(-i\int_{c_K} dz H_0(z)\right)\boldsymbol{\psi}(r,t_+)\boldsymbol{\psi}^\dagger(r',t'_-)\right) \tag{2.20}$$

One can identify the greater (lesser) Green's functions $\boldsymbol{G}^{>(<)} = \boldsymbol{G}^{-(+)}$. The full Green's functions are defined similarly, with the full Hamiltonian replacing H_0. A perturbation expansion of the full single particle Green's function on the Keldysh contour can now be obtained by using the Keldysh contour in Eq. (2.10), writing the interaction part of the Hamiltonian in the exponential as an infinite sum and applying Wick's theorem to the bare Green's functions in that expression.

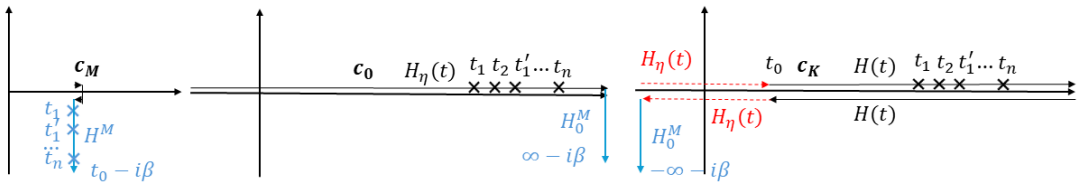

Figure 2.2.: Contours corresponding to Matsubara (c_M), zero temperature (c_0) and Keldysh (c_K) formalisms. Matsubara formalism assumes the field operators to be located on the vertical part of the contour; due to unitarity of the evolution operator the horizontal parts can be shrunk to zero. Keldysh theory uses the adiabatic assumption (2.15) to replace ρ by ρ_0 (and thus H^M by H_0^M on the vertical part) by extending the contour to $-\infty$; and the unitarity of the evolution operator to extend it to $+\infty$. The zero temperature contour uses that the evolution operator between ∞ and $-\infty$ acting on a non-degenerate ground state results in a phase factor that is the same for nominator and denominator, and the returning tracks in (2.10) cancel and can be dropped from the contour. It furthermore assumes a time independent Hamiltonian to replace H by H_η and to shift the vertical part of the contour to $+\infty$.

2.1.4. Hamiltonians

To set up Feynman rules, it is necessary to specify the Hamiltonian. In the remainder of this work, perturbations due to phonons and external electromagnetic fields are considered as well as potential impurities (preserving time reversal symmetry) and magnetic impurities (violating time reversal symmetry). The electromagnetic fields are included in the bare Green's function, while interactions with phonons and impurities are included as a self energy.

The unperturbed part of the Hamiltonian consists of the single particle Hamiltonian

$$H_0 = H_{el,0} + H_{ph,0} \tag{2.21}$$

with the energy measured from the fermi surface

$$H_{el,0} = \int d^3r \psi_\sigma(\vec{r})^\dagger \left(\frac{1}{2m}(i\nabla + \vec{A})^2 - \mu \right) \psi_\sigma \tag{2.22}$$

and

$$H_{ph,0} = \sum_{\aleph} \int d^3\vec{r} u_{\aleph}^\dagger(\vec{r}) u_{\aleph}(\vec{r}) \tag{2.23}$$

where the phonon field operator $u_{\vec{q},\aleph} = (b_{\vec{q}\aleph} + b_{-\vec{q},\aleph}^\dagger)\sqrt{\frac{\omega_{\vec{q},\aleph}^0}{2}}$ does not include screening effects from the electron-electron interaction yet, and the sum $\aleph$ is over the phonon

polarizations, i.e. a longitudinal mode with frequency equal to the plasma frequency $\omega^0_{\vec{q},l} \approx \Omega_p$, and two transversal modes with $\omega^0_{\vec{q},t} \approx qv_t$.

For the bare electron-phonon interaction, we assume a Hamiltonian of the form

$$H_{el-pn,c} = \frac{1}{V} \sum_{\vec{p},\sigma,\vec{k}\neq 0} g_k u^l_{\vec{k}} c^\dagger_{\vec{p}+\vec{k},\sigma} c_{\vec{p},\sigma} \tag{2.24}$$

Here, the coupling strength $g_k = \sqrt{\frac{N}{M}} \frac{kV(k)}{\omega^l_0(k)}$ was introduced for a system with N ions of mass M. $V(k)$ is the fourier transform of the potential describing the interaction between electrons and ions, $c_{\vec{k}}$ is the creation operator for an electron in the plane wave state with momentum $\vec{k}$. The electron-electron interaction can be included in the random phase approximation [BF04]: Screening turns the dispersion of the longitudinal phonons into a linear dispersion and the electron-ion interaction potential (in the long wavelength limit) independent of the wavevector. Thus, the coupling strength g_k becomes independent of the momentum and we can write

$$H^{eff}_{el-pn,c} = g \int d^3\vec{r}_1 u^l(1)\psi^\dagger(1)\psi(1) \tag{2.25}$$

The effective Hamiltonian in Eq. (2.25) is valid for $ql > 1$ for typical phonon wavevectors q and electronic mean free path l. In the opposite limit $ql \ll 1$ and $\omega\tau^{el} \ll 1$ electrons scatter at many impurities during the phonon emission process, and it becomes necessary to renormalize the electron phonon vertex to account for the resulting interference effects. Furthermore, in that limit one should include processes in which phonons are emitted at impurities [GS74]. A discussion of this limit can be found in [SM00; RS86b], in the following only the case of moderate disorder $ql > 1$ is considered.

2.1.5. Feynman rules and Gorkov-Keldysh equation

The linked cluster theorem can be derived exactly in the same way as for systems in equilibrium (e.g. [BF04]) as it does not rely on a specific choice of contour. In passing we note that, because of the unitarity of the time evolution operator along the real time axis, the denominator in Eq. (2.10) evaluates to unity, and cancellation of disconnected diagrams is already implied in the contour in the numerator (i.e. the sum over all vacuum diagrams is unity).[1] The Feynman rules are obtained by expressing the perturbative part of the Hamiltonian in Eq. (2.10) as a Dyson series, expressing the resulting expression in terms of the $n-$particle Nambu Green's function and applying Wicks theorem to the Green's function. They are easiest stated when defining a matrix Green's function

$$\hat{G}^{\pm} \equiv \begin{pmatrix} \boldsymbol{G}^c & \boldsymbol{G}^- \\ \boldsymbol{G}^+ & \bar{\boldsymbol{G}}^c \end{pmatrix} \tag{2.26}$$

[1] This property is sometimes used in the construction of effective field theories for disordered systems to avoid the use of the replica trick [AS10].

The components of $\hat{G}^{\pm}$ are not linearly independent, and one of its components can be set to zero by a properly chosen linear transformation. A particularly convenient form has been suggested by [LO75] by defining the matrix Green's function as $\hat{G} = \hat{L}_{LO}\hat{\tau}_3\hat{G}^{\pm}\hat{L}_{LO}^{\dagger}$ with $\hat{L}_{LO} = 1/\sqrt{2}(\hat{1} - i\hat{\tau}_2)$, where $\hat{\tau}$ are pauli matrices in Keldysh and unit matrices in Nambu space. In the appendix we derive the rules in some detail, here we only state the results, also derived in [RS86a]:

- The electron self energy $\hat{\Sigma}^{LO}$ consists of all topologically different, one line irreducible, connected diagrams containing two external electron lines
- The bare electron Green's function $\hat{G}_1^{(0)}$ is a matrix in Nambu and in Keldysh space, the phonon Green's function $\hat{D}_0$ is a matrix in Keldysh space.
- Interaction vertices with external fields are given by $\boldsymbol{V}(1)\boldsymbol{\tau}_3$ with a unit matrix in Keldysh space, electron phonon interaction vertices by $g\hat{\gamma}$ for absorption and by $g\hat{\tilde{\gamma}}$ for emission, with $\hat{\gamma}^1_{i,j} = \hat{\tilde{\gamma}}^2_{i,j} = \frac{1}{\sqrt{2}}\delta_{i,j}$, and $\hat{\gamma}^2_{i,j} = \hat{\tilde{\gamma}}^1_{i,j} = \frac{1}{\sqrt{2}}(\hat{\tau}_1)_{i,j}$. Here the upper index is the (Keldysh) index of the phonon Green's function while the lower ones give the (Keldysh) indices of the incoming and outgoing electron Green's function. Phonon lines correspond to $i\hat{D}_0$.
- Each Fermion loop is multiplied by -1
- Integrate over internal variables and sum over internal indices, with the time integrals from $-\infty$ to ∞

The structure of the Green's functions and self energies in Keldysh space after the transformation are

$$\hat{G} = \begin{pmatrix} \boldsymbol{G}^R & \boldsymbol{G}^K \\ 0 & \boldsymbol{G}^A \end{pmatrix} \qquad \hat{\Sigma} = \begin{pmatrix} \boldsymbol{\Sigma}^R & \boldsymbol{\Sigma}^K \\ 0 & \boldsymbol{\Sigma}^A \end{pmatrix} \tag{2.27}$$

With

$$\boldsymbol{G}^K = \boldsymbol{G}^+ + \boldsymbol{G}^- = \boldsymbol{G}^c + \tilde{\boldsymbol{G}}^c \tag{2.28}$$

$$\boldsymbol{G}^R = \boldsymbol{G}^c - \boldsymbol{G}^- = \boldsymbol{G}^+ - \tilde{\boldsymbol{G}}^c \tag{2.29}$$

$$\boldsymbol{G}^A = \boldsymbol{G}^c - \boldsymbol{G}^+ = \boldsymbol{G}^- - \tilde{\boldsymbol{G}}^c \tag{2.30}$$

$$\tag{2.31}$$

Furthermore, using the general identity

$$\lim_{t_1 \to t_2} \left[\boldsymbol{G}^{>}_{\alpha,\beta}(1,2) - \boldsymbol{G}^{<}_{\alpha,\beta}(1,2) \right] = i\delta(\vec{r}_1 - \vec{r}_2)\delta_{\alpha,\beta} \tag{2.32}$$

one obtains for the lesser Green's function [Kop01]

$$\lim_{t_1 \to t_2} \boldsymbol{G}^{<}_{\alpha,\beta}(1,2) = \frac{1}{2} \lim_{t_1 \to t_2} \boldsymbol{G}^K_{\alpha,\beta}(1,2) - i\delta(\vec{r}_1 - \vec{r}_2)\delta_{\alpha,\beta} \tag{2.33}$$

which can be used to express observables in terms of Green's functions. In the following Green's functions in Nambu space are denoted

$$\boldsymbol{G}^{R/A} = \begin{pmatrix} G^{R/A} & F^{R/A} \\ -F^{\dagger R/A} & \bar{G}^{R/A} \end{pmatrix} \tag{2.34}$$

The self energy is connected to the electron Green's function by the Gorkov equation

$$(\mathcal{G}^{-1} - \hat{\Sigma}) \otimes \hat{G}(\vec{r}, \vec{r}', t, t') = \delta(\vec{r} - \vec{r}')\delta(t - t') \tag{2.35}$$

where the operator $\mathcal{G}^{-1}(\vec{r}, \vec{r}', t, t') = \left(i\boldsymbol{\tau_3}\partial_t + \frac{1}{2m}\partial_r^2 - e\phi_{el}(\vec{r}, t) + \mu\right)\delta(\vec{r} - \vec{r}')\delta(t - t')$ and its conjugate

$$\hat{G} \otimes (\mathcal{G}^{-1} - \hat{\Sigma})(\vec{r}, \vec{r}', t, t') = \delta(\vec{r} - \vec{r}')\delta(t - t') \tag{2.36}$$

$\hat{G}$ is the electron Green's function in Nambu and Keldysh space, the derivative $\partial_r = \vec{\nabla}_{\vec{r}} - ie\tau_3\vec{A}(\vec{r}, t)$, ϕ_{el} and μ respectively electrical and chemical potential and $\otimes$ denotes multiplication with integration over internal times and positions. The Gorkov equations can be obtained from the Dyson equation $\hat{G} = \hat{G}^{(0)} + \hat{G}^{(0)} \otimes \hat{\Sigma} \otimes \hat{G}$ by multiplying the Dyson equation with $\mathcal{G}^{-1}$ and using $\delta(1 - 1') = \mathcal{G}^{-1} \otimes \hat{G}^{(0)}$, immediately following from Eq. (2.14).

2.2. Quasiclassical Green's functions

While the Gorkov equations in principle allow for an exact description of superconductors, they are too complicated to be solved in most spatially inhomogeneous cases without further simplification. A widely used approximation scheme has first been developed by Eilenberger [Eil68] for systems in equilibrium, and by Eliashberg [GM 72] for systems out of equilibrium. A further simplification has been introduced by Usadel [Usa70] using the smallness of anisotropies of the Green's function for disordered superconductors. Assuming all fields and superconducting properties to vary on length-scales much larger than the Fermi wavelength, the spatial dependence of the Green's function can be split into a dependence on the relative position and on the average position, with the Fourier transform of the relative position resulting in the momentum. Modifications of the Green's function due to superconductivity are relevant only in a small momentum shell of order of the inverse (clean) coherence length $\xi_0^{-1} \sim \Delta/v_F \ll p_F$ around the fermi surface. Most observables can be calculated as products of some power of the momentum with the Green's function, integrated over momentum.[2] As the difference of the Green's function from the unperturbed normal state Green's function is sharply peaked close to the Fermi surface, knowledge of the integral of the Green's function over the absolute value of the momentum is usually sufficient for the calculation of these observables. In the next section thus an equation (known as 'Eilenberger Equation') determining the momentum integrated Green's function (also known as 'quasiclassical Green's function') is derived.

[2] For example the current of a homogeneous superconductor in equilibrium is given by [Kop01] $\vec{j} = -\frac{Ne^2}{mc}\vec{A} - \frac{2e}{m}\int_{-\infty}^{\infty}\frac{d\epsilon}{4\pi i}\int\frac{d^3p}{(2\pi)^3}\tanh\left(\frac{\epsilon}{2T}\right)\vec{p}\left(G^R(\epsilon, \vec{p}) - G^A(\epsilon, \vec{p})\right)$.

2.2.1. Wigner transform and Keldysh-Eilenberger equation

Starting point of the quasiclassical approximation are the Gorkov equations (2.35) and (2.36) with the spatial coordinates replaced by the relative and average coordinates

$$\vec{x} = \frac{\vec{r} - \vec{r}'}{2} \qquad \vec{X} = \frac{\vec{r} + \vec{r}'}{2} \tag{2.37}$$

Sometimes it is useful to perform a similar transformation in the temporal coordinates as well. This is in particular the case if $(\partial_T \vec{A}(T))(\partial_E \hat{G}(E,T)) \ll \vec{A}(T)\hat{G}(E,T)$, with average time T and transform of relative times E, i.e. if the external electromagnetic field's variation in time is sufficiently slow compared to the energy scale over which the Green's function $\omega \ll \Delta$ varies. In that case convolutions can be replaced by a gradient expansion [RS86a]. In order to keep the discussion more general to include also external fields of larger frequency,[3] only the spatial coordinates are changed to an average/relative basis here. The average position accounts for long range inhomogeneities while the dependence of the Green's function on the relative position is only weakly affected by inhomogeneities. It is therefore useful to perform a Fourier transform with respect to the relative coordinates

$$\hat{G}(\vec{X},\vec{p},t,t') = \int d\vec{x} e^{i\vec{p}\vec{x}} \hat{G}(\vec{X} + \frac{\vec{x}}{2}, \vec{X} - \frac{\vec{x}}{2}, t, t') \tag{2.38}$$

Convolutions can be written in the new basis as

$$(\hat{A} \otimes \hat{B})(\vec{X},\vec{p},t,t') = \int dt'' \exp\left[\frac{i}{2}\left(\vec{\nabla}^A_{\vec{X}} \cdot \vec{\nabla}^B_{\vec{p}} - \vec{\nabla}^A_{\vec{p}} \cdot \vec{\nabla}^B_{\vec{X}}\right)\right] \hat{A}(\vec{X},\vec{p},t,t'')\hat{B}(\vec{X},\vec{p},t'',t') \tag{2.39}$$

with derivatives $\partial^{A(B)}$ acting only on A(B). The Gorkov equations (2.35) and (2.36) vary quickly as a function of E and $\vec{p}$, complicating the use of approximations allowing for the calculation of the quasiclassical Green's functions. Therefore, it is useful to remove this strong dependence by considering the difference between the two Gorkov equations

$$[\mathcal{G}^{-1} - \Sigma \overset{\otimes}{,} \hat{G}] = 0 \tag{2.40}$$

where $[\overset{\otimes}{,}]$ denotes a commutator using the $\otimes$ product. The spatial derivative term in $\mathcal{G}^{-1}$ transforms as $\partial_r^2 \delta(\vec{r} - \vec{r}') \to -\frac{\vec{p}^2}{2m} + e\boldsymbol{\tau}_3 \vec{A}(\vec{R},t) \cdot \frac{\vec{p}}{m} - \frac{e^2}{2m}\vec{A}^2(\vec{R},t)$. To lowest order in the quasiclassical parameter $(p_F\xi)^{-1}$ it is sufficient to keep terms up to linear order in the expansion of the exponential in Eq. (2.39) to rewrite the difference of the Gorkov equations as

$$0 = [\mathcal{G}^{-1} + i\Sigma \overset{\otimes}{,} \hat{G}] \simeq [\mathcal{G}^{-1} + i\Sigma \overset{\circ}{,} \hat{G}] + \frac{i}{2}\left[\vec{\nabla}^{\mathcal{G}^{-1}+i\Sigma}_{\vec{R}} \cdot \vec{\nabla}^{\hat{G}}_{\vec{p}} - \vec{\nabla}^{\mathcal{G}^{-1}+i\Sigma}_{\vec{p}} \cdot \vec{\nabla}^{\hat{G}}_{\vec{R}}\right][\mathcal{G}^{-1} + i\Sigma \overset{\circ}{,} \hat{G}] \tag{2.41}$$

where $[\overset{\circ}{,}]$ denotes a commutator with integration over the internal times. In the second commutator it is sufficient to keep the $\vec{p}^2$ term in its first argument, as all other

[3] e.g. microwaves in resonators

contributions are of a higher order in the quasiclassical parameter than a corresponding term in the first commutator. Thus

$$0 \simeq [g^{-1} + i\Sigma \overset{\circ}{,} \hat{G}] \tag{2.42}$$

with $g^{-1}(\vec{R},\vec{p},t_1,t') = (\boldsymbol{\tau_3}\partial_{t_1} + \frac{\vec{p}}{m}\cdot[\nabla_{\vec{R}} - ie\vec{A}\boldsymbol{\tau_3}] + ie\phi_{el}(t_1) - \frac{e^2}{2m}\vec{A}^2(\vec{R},t_1))\delta(t_1 - t')$. Neglecting the dependency of the self energy on the absolute value of the momentum, equation (2.42) is integrated over $|\vec{p}|$ and the quasiclassical Green's function is introduced as

$$\hat{g}(\vec{e}_{\vec{p}},\vec{R},t,t') = \frac{i}{\pi}\int_{-E_c}^{E_c} d\xi_p \hat{G}(\vec{p},\vec{R},t,t') \tag{2.43}$$

to obtain the Eilenberger equation [Eil68] extended to systems out of equilibrium

$$[g^{-1} + i\hat{\Sigma} \overset{\circ}{,} \hat{g}] = 0 \tag{2.44}$$

Note that the integral in Eq. (2.43) involves a cutoff below the Fermi energy $E_c \ll \epsilon_F$, to avoid high energy divergences arising from the normal state Green's function. The precise value of the cutoff is not important [JD83]. The quasiclassical Green's functions obey the normalization condition

$$(\hat{g}\circ\hat{g})(\vec{R},\vec{e}_{\vec{p}},t,t') = \delta(t-t') \tag{2.45}$$

as discussed by [Eil68] and [LO69] for systems in equilibrium, and [LO75] and [She85] for the general case. Intuitively, this normalization condition can be understood by noting that the Eilenberger equation (2.44) is solved by $\hat{g}\circ\hat{g}$ as well, for any solution $\hat{g}$. This implies $\hat{g}\circ\hat{g} = \delta(t-t')\times const$ with some arbitrary constant. In the spatially homogeneous case in equilibrium, it can be directly calculated to unity, which can thus be used without contradiction in general.

For Eq. (2.44) to provide a closed equation the self energy must be expressed in terms of the quasiclassical Green's functions. For the interaction with non-magnetic impurities we assume a potential of the form $V(\vec{r}) = \sum_{i=1}^{N_{imp,non}} V_{imp}(\vec{r} - \vec{R}_i)$. If the properties of the superconductor and external fields change slowly over length-scales set by the coherence length, the system is in the *self-averaging* limit: One can think of the system as several coherent subsystems of size of the coherence length. Observables can be obtained using incoherent averages over the collection of subsystems. If the number of these subsystems is sufficiently large, the Green's function averaged over position coincides with the impurity averaged Green's function, and one can replace the Green's function with the impurity averaged Green's function [KL57]

$$\langle\hat{G}\rangle_{\vec{R}} \simeq \langle\hat{G}\rangle_{imp} = \frac{1}{\mathcal{V}^{N_{imp}}}\int d\vec{R}_1 ... d\vec{R}_{N_{imp}} \hat{G}(\vec{p},\vec{R}_1,...,\vec{R}_{N_{imp}},t,t') \tag{2.46}$$

where the Green's function on the right-hand side implicitly depends on the impurity positions. Here the position average on the left side is to be understood as average over lengthscales on which the external fields and parameters of the superconductor do not change significantly.

For a homogeneous system whose size is much larger than the coherence length, we can take the average over the impurity positions in the standard way [BF04], recovering momentum conservation at each impurity vertex. To lowest order in V_{imp}/ϵ_F it is sufficient to include diagrams with two lines per impurity vertex. Neglecting diagrams with intersecting lines, that are suppressed by a factor $1/p_F l \ll 1$ with mean free path l, leads to the self consistent Born approximation for the self energy [Kop01]

$$\Sigma^V(\vec{p}) = n_{imp} \int \frac{d^3\vec{q}}{(2\pi)^3} |V_{imp}(\vec{p}-\vec{q})|^2 \hat{G}(\vec{q}) \tag{2.47}$$

corresponding to the left diagram in figure 2.3. As both $\vec{p}$ and $\vec{q}$ are close to the Fermi surface, V_{imp} only depends on the angle between them. Assuming isotropic scattering, this angular dependence is neglected. The self energy can then be written in terms of the elastic scattering lifetime $1/\tau_{el} = 2\pi\rho_F n_{imp}|V_{imp}|^2$ as

$$\Sigma^V(\vec{p}) = \frac{i}{2\tau} \int \frac{d\vec{e}_{\vec{q}}}{(2\pi)^3} \hat{g}(\vec{q}) \tag{2.48}$$

If the impurities have a magnetic moment, exchange interaction causes the interaction to have a component proportional to $\boldsymbol{\tau}_3$. Including this component in a similar way as for the non-magnetic impurities leads to a self energy

$$\Sigma^{sf}(\vec{p}) = \frac{i}{2\tau_{sf}} \int \frac{d\vec{e}_{\vec{q}}}{(2\pi)^3} \boldsymbol{\tau}_3 \hat{g}(\vec{q}) \boldsymbol{\tau}_3 \tag{2.49}$$

with spin flip time $1/\tau_{sf} = 2\pi\rho_F n_{imp,sf}|V_{sf}|^2 S(S+1)$ [RS86a] with spin S of the impurity. In rewriting the self energy in terms of the quasiclassical Green's functions contributions from momenta outside the cutoff in Eq. (2.43) have been included in the chemical potential.

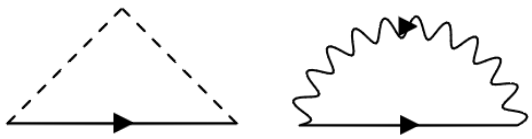

Figure 2.3.: Contribution of impurity and electron-phonon scattering to the electron self energy. Full lines correspond to the full Green's function, dotted lines to impurity scattering, wavy lines to the phonon Green's function.

The self energy (2.49) was first derived by Abrikosov and Gorkov (AG) [AG61]. It can also be obtained by replacing the random distribution of the impurities by their averaged density. Thus, it corresponds to a mean field theory that neglects effects arising from spatial fluctuations in the impurity concentration. As was already realized long ago [KI68], these fluctuations are particularly important in the case of magnetic impurities, as they directly affect the properties of the superconductor –

in fact, assuming a Poisson distribution of the impurities it was argued that every superconductor with magnetic impurities would contain (extremely rare) regions in space with sufficient impurity density to turn the superconductor gapless [BT97].[4] As the impurities are randomly distributed, the number of impurities in a finite volume is Poisson distributed, and fluctuates with the variance equal to its mean. This observation led [SI05] to include spatial fluctuations of the spin flip time in the model of a disordered superconductor by assuming $\tau_{sf}^{-1}(\vec{R}) = \tau_{sf,0}^{-1} + \delta\tau_{sf}^{-1}(\vec{R})$ with the Gaussian distributed random variable $\delta\tau_{sf}^{-1}(\vec{R})$

$$\langle \delta\tau_{sf}^{-1}(\vec{R})\delta\tau_{sf}^{-1}(\vec{R}')\rangle = \frac{\tau_{sf,0}^{-2}}{n_{imp}}\delta(\vec{R}-\vec{R}') \tag{2.50}$$

where the central limit theorem was used to replace the Poisson distribution of the impurity densities by a Gaussian distribution. Due to the proximity effect, only fluctuations of size of the order of the coherence length and larger are relevant for the modification of the superconductor's properties and the replacement with a Gaussian distribution is justified if the number of impurities in such a volume is large. As magnetic impurities suppress the gap in the energy spectrum, the fluctuations (2.50) lead to regions in space in which the gap in the energy spectrum is lowered compared to the bulk, i.e. regions in space that can trap quasiparticles. The effect of this trapping on the dynamics of quasiparticles is discussed in chapter 4.

The contribution of phonons to the electronic self energy is given by the Fock diagram (see figure 2.3)

$$\Sigma_{j,n}^{pn} = i\int \frac{d^3\vec{p}}{(2\pi)^3}|g|^2\tilde{\gamma}_{j,k}^{i}\hat{G}_{k,m}(\vec{R},\vec{p}+\vec{q},t,t')\gamma_{m,n}^{l}\hat{D}_{i,l}(\vec{p},t,t') \tag{2.51}$$

where summation over repeated indices is implied and the indices refer to indices in Keldysh space. We do not need to consider the Hartree diagram for the self energy as it contains a phonon propagator of zero momentum, which is zero for acoustic phonons. As the Debye energy is much smaller than the Fermi energy, due to Migdal's theorem [Mig58], vertex corrections do not need to be included. It is instructive to write the retarded and advanced parts of the self energy as

$$\begin{aligned}\boldsymbol{\Sigma}_{R(A)}^{ph}(\vec{R},\vec{e}_{\vec{p}},t_1,t_2) = {} & \frac{\lambda}{8}\int d_{\vec{e}_{\vec{p}}}\boldsymbol{g}^{R(A)}(\vec{R},\vec{e}_{\vec{p}'},t_1,t_2)D^{K}(\vec{R},\vec{e}_{\vec{p}'}-\vec{e}_{\vec{p}},t_1,t_2)\\ \overset{(+)}{(-)} & \frac{\lambda}{16}\int d_{\vec{e}_{\vec{p}}}\left[D^{R}-D^{A}\right](\vec{R},\vec{e}_{\vec{p}'}-\vec{e}_{\vec{p}},t_1,t_2)\boldsymbol{g}^{K}(\vec{R},\vec{e}_{\vec{p}'},t_1,t_2)\\ & +\frac{\lambda}{16}\int d_{\vec{e}_{\vec{p}}}\left[D^{R}+D^{A}\right](\vec{R},\vec{e}_{\vec{p}'}-\vec{e}_{\vec{p}},t_1,t_2)\boldsymbol{g}^{K}(\vec{R},\vec{e}_{\vec{p}'},t_1,t_2)\end{aligned} \tag{2.52}$$

[4] For weak disorder these regions are of course too rare to be of practical relevance (as will be shown in chapter 4 the probability to find a region in which the gap is suppressed by δE_g decreases exponentially in δE_g) but even small fluctuations in the superconducting properties may lead to significant modifications to observables

with dimensionless coupling strength $\lambda = |g|^2 \rho_F$. In thermal equilibrium the retarded and advanced phonon functions are given by

$$D_0^{R(A)}(\vec{q},\omega) = \omega_q^2 \left[\frac{1}{\omega^2 - \omega_{\vec{q}}^2} \overset{(+)}{(-)} i\pi\delta\left(\omega^2 - \omega_{\vec{q}}^2\right) \right] \tag{2.53}$$

with frequency ω and momentum $\vec{q}$, and by zero for $\omega_q = \omega = 0$. Processes in the first two lines of Eq. (2.52) correspond to real emission/absorption processes and result in inelastic quasiparticle scattering. In rewriting the self energy in terms of the quasiclassical Green's function, the electron Green's function was assumed to be a faster function of momentum than the phonon Green's function. For very low temperatures and strong disorder this can be violated: The electron Green's function changes for momenta varying on the scale set by the inverse mean free path, while the Keldysh part of the phonon function varies over a scale set by $q_T = T/u_{l,t}$ with the longitudinal/transversal speed of sound $u_{l,t}$. We restrict the discussion to the limit $l^{-1} \ll q_T$, transition rates in the opposite limit are discussed in [RS86b].

Now employ the BCS approximation by defining the gap using the off-diagonal components of the term in the third line of (2.52)

$$\mathbf{\Delta} = \begin{pmatrix} 0 & \Delta \\ \Delta^* & 0 \end{pmatrix} \tag{2.54}$$

and – using the static approximation for the phonon function – the gap becomes frequency independent

$$\begin{aligned} \Delta(\vec{R},\vec{e}_{\vec{p}},E,T) &= \frac{\lambda}{16} \int d_{\vec{e}_{\vec{p}'}} \int dE' f^K(\vec{R},\vec{e}_{\vec{p}'},E',T)(D^R + D^A)(\vec{R},\vec{e}_{\vec{p}'} - \vec{e}_{\vec{p}},E'-E) \\ &\simeq \frac{-\lambda}{8} \int d_{\vec{e}_{\vec{p}'}} \int_{-\Omega_D}^{\Omega_D} dE' f^K(\vec{R},\vec{e}_{\vec{p}'},E',T) \equiv \Delta(\vec{R},T) \end{aligned} \tag{2.55}$$

where it was used that f^K decreases over energy-scale $E' \sim \Delta \ll \Omega_D$ much smaller than the Debye frequency,[5] allowing to set $D^{R(A)} \approx -1$. For a homogeneous superconductor without external fields, equation (2.55) gives the BCS self consistency equation[BCS57]. In a weak-coupling superconductor with $\lambda \ll 1$, the terms in the retarded/advanced phonon self energies of the form $g^K(D^R + D^A)$ can be included in the normal state chemical potential and are neglected in the following [Kop01]. The remaining terms result in processes in which quasiparticles absorb and emit phonons, as discussed in the next sections.

Note that in our discussion we disregarded self energies arising from direct electron-electron (Coulomb-)interaction. It is possible extend the preceding discussion by also including a Fock-diagram for the direct electron-electron interaction, which should be included in calculations of superconducting properties from first principle within the

[5] This condition defines a weak-coupling superconductor; we do not explore strongly-coupled superconductors in which gap and Debye frequency are of a similar magnitude in this thesis.

well known Migdal-Eliashberg theory [Eli60; SSW66].[6] For a weak-coupling superconductor, the repulsive Coulomb interaction can be included as an effective reduction of the pairing constant. As we do not attempt a first-principle calculation of the zero temperature-gap in the following, but rather use its experimental value, we disregard this effect. Moreover, at finite quasiparticle density electron-electron interaction leads to additional collision integrals for the interaction between quasiparticles. These are however of higher order in the quasiparticle density than corresponding collision integrals arising from electron-phonon interaction and can be disregarded in the limit of small quasiparticle density considered in this thesis [GM 72].

2.2.2. The dirty limit and Usadel equation

In the limit of strong disorder[7] $\tau_{el}T_c \ll 1$, the Green's functions become approximately isotropic. This allows to expand self energies and Green's functions to linear order in spherical harmonics [Usa70]

$$\hat{\sigma}(\vec{R},\vec{e}_{\vec{p}}) = \hat{\sigma}_s(\vec{R}) + \vec{e}_{\vec{p}}\cdot\vec{\hat{\sigma}}_p(\vec{R}) \tag{2.56}$$

$$\hat{g}(\vec{R},\vec{e}_{\vec{p}}) = \hat{g}_s(\vec{R}) + \vec{e}_{\vec{p}}\cdot\vec{\hat{g}}_p(\vec{R}) \tag{2.57}$$

Here, and in the following, the self energy is denoted by σ instead of Σ to emphasize its dependence on $\hat{g}$ instead of $\hat{G}$. The part of the g^{-1} operator containing the spatial derivative and electromagnetic field is proportional to momentum direction, while the remaining part is independent of it. Thus, by averaging over momentum directions we can obtain an s-wave part of the kinetic equation

$$0 = \left[\left(\partial_{t_1}\boldsymbol{\tau_3} + ie\phi\right)\delta(t-t') + i\hat{\sigma}_s \circ \hat{g}_s\right] + \frac{1}{3}v_F[\partial_{\vec{R}}\circ\vec{\hat{g}}_p] \tag{2.58}$$

where $\partial_{\vec{R}} = [\nabla_{\vec{R}} - ie\vec{A}\boldsymbol{\tau_3}]\delta(t-t')$ and the scalar product in the last term is implied. By multiplying with $\vec{e}_{\vec{v}_F}$ before averaging, the p- wave part of the equation of motion is

$$0 = i[\hat{\sigma}_s\circ\vec{\hat{g}}_p] + i[\vec{\hat{\sigma}}_p\circ\hat{g}_s] + v_F[\partial_{\vec{R}}\circ\hat{g}_s] + [\partial_{t_1}\boldsymbol{\tau_3}\delta(t-t')\circ\vec{\hat{g}}_p] \tag{2.59}$$

If the non-spin flip scattering is dominant, the self energies can be written as

$$\hat{\sigma}_s = -\frac{i}{2}\tau^{-1}\hat{g}_s + \hat{\sigma}'_s \tag{2.60}$$

$$\hat{\sigma}'_s = -\frac{i}{2}\tau_{sf}^{-1}(\vec{R})\tau_3\hat{g}_s\tau_3 + \sigma_s^{ph} \tag{2.61}$$

$$\vec{\hat{\sigma}}_p = -\frac{i}{2}(\tau^{-1} - \tau_{tr}^{-1})\vec{\hat{g}}_p \tag{2.62}$$

[6] Note that even apart from the inclusion of the Coulomb interaction, Migdal-Eliashberg theory is more general, as it allows for general values of the phonon propagator as well as anisotropies, making it an appropriate theory also in the description of strong-coupling superconductors.

[7] Note that this assumption is not in contradiction with the assumption of 'weak' disorder $ql \gtrsim 1$ that was required for rewriting the phonon self energy in terms of the quasiclassical Green's function, as the two requirements differ by a factor $v_F/u_l \gg 1$.

with spin-flip time $\tau_{sf}(\vec{R})$ and transport time

$$\tau_{tr} = 2\pi n_{imp}\nu_F \int \frac{d\vec{e}_{\vec{q}}}{4\pi}|V_{imp}(\vec{p}-\vec{q})|^2(1-\vec{e}_{\vec{p}}\cdot\vec{e}_{\vec{q}}) \tag{2.63}$$

Neglecting the last term in Eq.(2.59) compared to the first, using the dirty limit to neglect the phonon part of the self energy σ_s' and using the normalization condition (2.45) split in p- and s-wave parts by the same averaging procedure as for the Green's function, the p-wave part of the equation can be solved for, giving

$$\hat{g}_p = -l\hat{g}_s \circ [\partial_{\vec{R}}, \circ\hat{g}_s] \tag{2.64}$$

with mean free path $l = \tau_{tr}v_F$. Inserted in the s-wave equation one obtains the Keldysh-Usadel equation

$$[(\partial_{t_1}\boldsymbol{\tau_3} + ie\phi_{el})\,\delta(t_1-t') + i\hat{\sigma}_s' + D\partial_{\vec{R}}\circ\hat{g}_s\circ\partial_{\vec{R}}\circ\hat{g}_s] = 0 \tag{2.65}$$

with diffusion coefficient $D = \frac{1}{3}v_F l$. The diagonal elements (in Keldysh space) of Eq. (2.65) allow the calculation of the retarded/advanced Green's functions, the off-diagonal the calculation of the quasiparticle distribution function. Green's functions change on a characteristic lengthscale $\xi = \sqrt{D/2\Delta}$ known as the coherence length characterizing the size of a Cooper pair. Note that it is reduced compared to the clean limit coherence length $\xi_0 = v_F/\Delta$, i.e. $\xi \approx \sqrt{l\xi_0}$.

In the absence of electromagnetic fields, the components of Eq. (2.65) that are diagonal in Keldysh and off-diagonal in Nambu space result in the retarded part of the Usadel equation,[8] neglecting inelastic electron-phonon collisions,

$$0 = \frac{D}{2}\left(g^R\nabla^2 f^R - f^R\nabla^2 g^R\right) - iEf^R - ig^R\Delta + \frac{1}{\tau_{sf}(\vec{R})}g^R f^R \tag{2.66}$$

and a second equation, which can be solved by $f^R = (f^R)^\dagger$, $\bar{g}^R = -g^R$ and $\Delta = \Delta^*$. We do not consider the retarded/advanced components of Eq. (2.65) in its full generality, in chapter 3 we instead use the BCS limit and neglect spatial inhomogeneities and electromagnetic fields, while in chapter 4 we consider spatial inhomogeneities but neglect electromagnetic fields by using equation (2.66). We however include the effect of electromagnetic fields on the distribution function as shown in the next subsection.

2.3. Distribution function

To obtain an equation of motion for the quasiparticle distribution function, consider the Keldysh component of Eq. (2.65). We will derive the electron-photon collision

[8] If we assume the electromagnetic field to be time independent and Green's functions and electromagnetic fields to be spatially homogeneous, an electromagnetic field can be easily included by replacing $\tau_{sf}^{-1} \to \tau_{sf}^{-1} + 2De^2A^2$. Accounting for the effect of a high-frequency field (in the microwave range) on the density of states is much more complicated, as terms containing a time derivative must be kept. In that case equation Eq. (2.65) can be used to derive the regular Green's functions, but it is not possible anymore to include the field in a trivial way in Eq. (2.66) [Sem+16].

integral only for the spatial homogeneous case, while the electron-phonon integral derived below remains valid also for inhomogeneous systems. Decomposing the Keldysh function as $\boldsymbol{g}^K = \boldsymbol{g}^R \circ \boldsymbol{h} - \boldsymbol{h} \circ \boldsymbol{g}^A$ automatically fulfills the Keldysh part of the normalization condition (2.45). Only two independent components of $\boldsymbol{h}$ are relevant for the calculation of $\boldsymbol{g}^K$ [Sch80; Kop01], these can be chosen as $\boldsymbol{h} = h_L\mathbf{1} + h_T\boldsymbol{\tau_3}$ where h_L is an odd and h_T an even function in energy. The retarded/advanced parts of the Usadel equation can be used to rewrite the Keldysh part as [RS86a]

$$\boldsymbol{g}_R \circ \boldsymbol{B} - \boldsymbol{B} \circ \boldsymbol{g}_A = 0 \tag{2.67}$$

with

$$\boldsymbol{B} = \left(\boldsymbol{g}_0^R\right)^{-1} \circ \boldsymbol{h} - \boldsymbol{h} \circ \left(\boldsymbol{g}_0^A\right)^{-1} - i\boldsymbol{\sigma}^K - D\partial_{\vec{R}} \circ \boldsymbol{g}^R \circ [\partial_{\vec{R}}, \boldsymbol{h}] - D[\partial_{\vec{R}}, \boldsymbol{h}] \circ \boldsymbol{g}^A \circ \partial_{\vec{R}} \tag{2.68}$$

and $\left(\boldsymbol{g}_0^{R(A)}\right)^{-1}(t_1,t_2) = \left(\partial_{t_1}\boldsymbol{\tau}_3 + ie\phi_{el} - i\boldsymbol{\Delta}\right)\delta(t_1 - t_2) + i\boldsymbol{\sigma}_s^{R(A)}$. Here, the gap was written explicitly and is not included in the self energy anymore. In the following, we assume an even distribution in energy $\boldsymbol{h} = h_L\mathbf{1}$ and thus neglect branch imbalances that could e.g. arise in tunneling experiments [TC72; Cla72]. Consider first the term of the form

$$\boldsymbol{g}_R \circ \left[\left(\boldsymbol{g}_0^R\right)^{-1} - i\boldsymbol{\sigma}_s^R\right] \circ \boldsymbol{h} - \boldsymbol{g}_R \circ \boldsymbol{h} \circ \left[\left(\boldsymbol{g}_0^A\right)^{-1} - i\boldsymbol{\sigma}_s^A\right] = \int dt' \boldsymbol{g}_R(t_1,t')(\partial_{t'} + \partial_{t_2})h_L(t',t_2) \tag{2.69}$$

Here, we assumed a time independent Δ and dropped ϕ_{el} as it can be removed by a gauge transformation for a spatially homogenous system. To lowest order in ∂_T this transforms to $2\boldsymbol{g}_R(T,\omega)\partial_T h_L(T,\omega)$. Tracing over Nambu space, collecting all terms containing a self energy in a phonon collision integral, and all terms containing an electromagnetic field in a photon collision integral results in the diffusion equation

$$\rho(\omega)\frac{\partial f(\omega,t,\vec{R})}{\partial t} - D\vec{\nabla}\cdot\left(\rho(\omega)^2 K^-(\omega,\omega)\vec{\nabla} f(\omega,t,\vec{R})\right) = I^{pt}(\omega,\vec{R},t) + I^{pn}(\omega,\vec{R},t) \tag{2.70}$$

where we replaced $h_L \to 1 - 2f$ and defined the density of states (normalized by four times the normal state density of states per spin)

$$\rho(\omega) = \Re(g_R)(\omega) \tag{2.71}$$

and the coherence factors

$$K^{\pm}(E,E') = 1 \pm \Re(f_R)(E)\Re(f_R)(E')[\Re(g_R)(E)\Re(g_R)(E')]^{-1} \tag{2.72}$$

To get an expression for the electron-photon collision integral, it is useful to perform a Fourier transform in both time arguments as

$$g(E,E-\omega) = \int dt'dt'' \exp(iEt' - i(E-\omega)t'')g(t',t'') \tag{2.73}$$

In the Fourier-transformed expression, we encounter terms of the form

$$(A\circ g\circ A\circ g\circ h)(E,E-\omega)=\int d\omega_1 d\omega_2 d\omega' d\omega'' A(\omega_1)g(E-\omega_1,E-\omega') \times A(\omega_2)g(E-\omega'-\omega_2,E-\omega-\omega'')h(E-\omega-\omega'',E-\omega) \tag{2.74}$$

Rewriting the Green's functions and distribution using

$$g(E,E-\omega)=g_\omega(E-\frac{\omega}{2}) \tag{2.75}$$

with Fourier transform ω of the sum of the times and E of the difference of times[9] the RHS of equation (2.74) becomes

$$\int d\omega_1 d\omega_2 d\omega' d\omega'' A(\omega_1)g_{\omega_1-\omega'}(E-\frac{3}{2}\omega_1+\frac{\omega'}{2})A(\omega_2) \times g_{\omega_2+\omega'-\omega-\omega''}(E-\frac{3\omega'+3\omega_2-\omega-\omega''}{2})h_{-\omega''}(E-\omega-\frac{\omega''}{2}) \tag{2.76}$$

We now assume a monochromatic field of frequency ω_0

$$\vec{A}(\omega)=\left[\delta(\omega-\omega_0)+\delta(\omega+\omega_0)\right]\vec{A}_{\omega_0} \tag{2.77}$$

and take the quasi-static limit, in which distribution and Green's functions are assumed to be a much faster function of $\tau=t_1-t_2$ than $T=t_1+t_2$ to set $g_x(y+x)\approx g_x(y)$ and simplify (2.76) to

$$\int d\omega' d\omega'' \vec{A}^2_{\omega_0} g_{\omega_0-\omega'}(E-\omega_0)g_{\omega'-\omega_0-\omega-\omega''}(E)h_{-\omega''}(E) + \int d\omega' d\omega'' \vec{A}^2_{\omega_0} g_{-\omega_0-\omega'}(E+\omega_0)g_{\omega_0+\omega'-\omega-\omega''}(E)h_{-\omega''}(E) \tag{2.78}$$

for small frequencies $\omega\ll E,\omega_0$. Transforming to a mixed representation with E,T gives

$$(A\circ g\circ A\circ g\circ h)(E,T)\approx\sum_{\pm}A^2_{\omega_0}g(T,E\pm\omega_0)g(T,E)h(T,E) \tag{2.79}$$

The other terms containing the electromagnetic field in equation (2.67) can be simplified in a similar manner, leading to the electron-photon collision integral

$$I^{pt}(E,t)=-\frac{De^2}{8}\sum_{\pm}\vec{A}^2_{\omega_0}\Big(h(E\pm\omega_0)-h(E)\Big) \times Tr\Big(\left[\boldsymbol{g}_R(E\pm\omega_0)-\boldsymbol{g}_A(E\pm\omega_0)\right]\boldsymbol{\tau_3}\left[\boldsymbol{g}_R(E)-\boldsymbol{g}_A(E)\right]\boldsymbol{\tau_3}\Big) \tag{2.80}$$

Here, we assumed spatial homogeneity to drop terms containing only a single $\vec{A}_{\omega_0}$. To further simplify the photon integral, we make use of the symmetries

$$\Re(f_R(-E))=\Re(f_R(E)) \qquad \Re(g_R(-E))=-\Re(g_R(E)) \tag{2.81}$$

[9] In the following ω is called frequency, E energy.

implied by Eq. (2.66) to restrict the energies to values $E > 0$. For the static case, assuming $f^R(E) = (f^R)^\dagger(E)$, one can obtain the general relation $\boldsymbol{g}^R(E) = -\boldsymbol{g}_A^*(E)$ from the definition of the Green's functions and introduce the quasiparticle distribution $f(E)$ as $h_L(E) = 1 - 2f(E) = -h_L(-E)$ to obtain

$$\begin{aligned} I^{pt}(E,t) = 2De^2 \sum_{\pm} \vec{A}^2_{\omega_0} \Big(f(E \pm \omega_0) - f(E) \Big) K^+(E, E \pm \omega_0) \rho(E) \rho(E \pm \omega_0) \\ + 2De^2 \vec{A}^2_{\omega_0} \Big(1 - f(\omega_0 - E) - f(E) \Big) K^-(E, \omega_0 - E) \rho(E) \rho(\omega_0 - E) \end{aligned} \tag{2.82}$$

Here, terms in which the second argument of the coherence factor is negative must be set to zero. The photon integral (2.82) was first derived by Eliashberg [GM 72], here it was written in a form that is also directly applicable to a superconductor containing magnetic impurities. We can also relate the prefactor to the normal state (Drude-) conductivity σ_N and density of states per spin at Fermi energy ρ_F as

$$e^2 D = \sigma_N / 2\rho_F \tag{2.83}$$

The phonon collision integral is

$$\begin{aligned} I^{ph} = -\frac{i}{16} Tr \Big(- \boldsymbol{g}_R \circ \boldsymbol{\sigma}^{ph}_K + \boldsymbol{\sigma}^{ph}_K \circ \boldsymbol{g}_A + \boldsymbol{g}_R \circ \boldsymbol{\sigma}^{,R}_s \circ \boldsymbol{h} \\ - \boldsymbol{g}_R \circ \boldsymbol{h} \circ \boldsymbol{\sigma}^{,A}_s - \boldsymbol{\sigma}^{,R}_s \circ \boldsymbol{h} \circ \boldsymbol{g}_A + \boldsymbol{h} \circ \boldsymbol{\sigma}^{,A}_s \circ \boldsymbol{g}_A \Big) \end{aligned} \tag{2.84}$$

For (nearly) isotropic Green's functions considered here the contribution from the spin-flip collision integral is negligible and dropped in the following. The electron-phonon collision integral becomes [again taking the static limit, i.e. neglecting terms with a ∂_T]

$$\begin{aligned} I^{ph}(\omega, \vec{R}, T) &= -\frac{i}{16} Tr \left((\boldsymbol{g}^R_\omega - \boldsymbol{g}^A_\omega)(\boldsymbol{\sigma}^{R,ph}_\omega - \boldsymbol{\sigma}^{A,ph}_\omega) h_{L,\omega} - (\boldsymbol{g}^R_\omega - \boldsymbol{g}^A_\omega) \boldsymbol{\sigma}^{K,ph}_\omega \right) \\ &= -\frac{i\lambda}{16} Tr \int d_{\vec{e}_{\vec{p}}} \int dE \Re(\boldsymbol{g}^R(\omega)) \Re(\boldsymbol{g}^R(E)) (D^R - D^A)(\omega - E, \vec{e}_{\vec{p}} - \vec{e}_{\vec{p}'}) \\ &\times \left[h_E h_\omega - 1 + N_{\omega - E}(h_\omega - h_E) \right] \end{aligned} \tag{2.85}$$

which was already given in [LO77]. Here the phonon functions are to be understood to have momentum $p_F(\vec{e}_{\vec{p}} - \vec{e}_{\vec{p}'})$ for some arbitrary unit vector $\vec{e}_{\vec{p}'}$ To further simplify it, we make use of the symmetries (2.81), use $\int d_{\vec{e}_{\vec{p}}} (D^R - D^A)(\omega, \vec{e}_{\vec{p}} - \vec{e}_{\vec{p}'}) = i2\pi^2 \frac{\omega^2}{\omega_D^2} \mathrm{sgn}(\omega)$ for $\omega_{\vec{q}} \approx \frac{\omega_D}{k_F} |\vec{q}| \ll \omega_D$, introduce the quasiparticle distribution as $h_L(E) = 1 - 2f(E)$ and the phonon distribution $N(E) = 1 + 2n(E)$ to bring it in the form

$$\begin{aligned} I^{ph}(E, \vec{R}, t) = \frac{1}{\tau_0 T_c^3} \int_0^E d\omega \rho(E) \rho(E - \omega) K^-(E, E - \omega) \omega^2 \\ \times \left(n(\omega) \left[f(E - \omega) - f(E) \right] - f(E) \left[1 - f(E - \omega) \right] \right) \end{aligned}$$

$$
\begin{aligned}
&+ \frac{1}{\tau_0 T_c^3} \int_0^\infty d\omega \rho(E)\rho(E+\omega) K^-(E, \omega+E)\omega^2 \\
&\times \left(n(\omega)\left[f(\omega+E) - f(E)\right] + f(\omega+E)\left[1 - f(E)\right]\right) \\
&+ \frac{1}{\tau_0 T_c^3} \int_E^\infty d\omega K^+(E, \omega-E)\rho(E)\rho(\omega-E)\omega^2 \\
&\times \left[n(\omega)\left(1 - f(\omega-E) - f(E)\right) - f(E)f(\omega-E)\right] \qquad (2.86)
\end{aligned}
$$

Here, the constants were written in terms of a lifetime τ_0, in accordance with [Kap+76]. The first two integrals correspond to transitions in which a quasiparticle absorbs or emits a phonon and conserve the total number of quasiparticles. The last integral describes processes in which a phonon breaks a pair, or two quasiparticles recombine while emitting a phonon.

The diffusion equation (2.70), together with the Usadel equation (2.66), normalization (2.45), self consistency equation (2.55), collision integrals (2.82) and (2.86), allows for the calculation of the quasiparticle distribution in space and energy in a dirty, weak-coupling superconductor under microwave irradiation, containing magnetic impurities. In deriving the photon collision integral spatial homogeneity was assumed, the phonon integral is valid also in the spatial inhomogeneous case. In the absence of magnetic impurities[10] and spatial inhomogeneities, the collision integrals can also be obtained from Fermi's golden rule [CS78].

2.4. Current-field relation and complex conductivity

To close the system of equations for the calculation of properties of superconducting resonators, we need to relate the current to the electromagnetic field using the Keldysh Green's function. In the following, we derive the current-field relation by perturbation theory to linear order in the electromagnetic field. In this section we neglect spatial inhomogeneities inside the superconductor in the absence of electromagnetic fields.[11] The electrical current density

$$
\vec{j} = -\frac{e}{2m}(\vec{\nabla}_1 - \vec{\nabla}_{1'}) G^K(1, 1')\Big|_{1'=1} - \frac{ne^2}{m}\vec{A} \qquad (2.87)
$$

can be rewritten in terms of the quasiclassical Green's functions as

$$
\vec{j}(t) = \lim_{t_2 \to t} \frac{e\rho_F}{4} \int d\vec{e}_{\vec{p}}\, \vec{v}_F g^K(\vec{p_F}, t, t_2) \qquad (2.88)
$$

The diamagnetic term was canceled by the normal state contribution [GM 72].

[10] i.e. assuming BCS coherence factors and densities of states.

[11] This excludes for example situations in which the superconductor is in contact with a normal metal as well as situations with magnetic impurities treated beyond mean field theory.

Now, we seek a solution to the Eilenberger equation in terms of a perturbative expansion in powers of the gauge invariant potential $\vec{P} = \left(\vec{A} - \frac{1}{2e}\vec{\nabla}\theta\right)$

$$\hat{g} = \hat{g}^{(0)} + \hat{g}^{(1)} + ... \qquad \text{and} \qquad \hat{\Delta} = \hat{\Delta}^{(0)} + \hat{\Delta}^{(1)} ... \tag{2.89}$$

and assume the unperturbed part $g^{(0)}$ to be isotropic and homogeneous within the superconductor apart from a position dependent phase $\theta(\vec{R}, T)$, which we assume to be independent of energy, i.e. $\hat{g}^{(0)}(\vec{R}, T) = e^{i\theta\tau_3/2}\hat{g}^{\cdot,(0)}e^{-i\theta\tau_3/2}$ with $\hat{g}^{\cdot,(0)}$ position and time independent. Using the expansion in s- and p-wave parts used in section 2.2.2, we can replace the Green's function in (2.88) by g_p^K of Eq. (2.64), as the s-wave part vanishes upon averaging over momentum directions. To obtain the current-field relation to linear order in $\vec{P}$, the Green's functions $\hat{g}_s$ in that equation can be replaced by the unperturbed Green's function $g^{(0)}$. This results in the current phase relation

$$\vec{j}(\vec{R}, t) = -\pi i \sigma_N \lim_{t_2 \to t} \left(g^R \circ \vec{P} \circ g^K + f^R \circ \vec{P} \circ f^K + g^K \circ \vec{P} \circ g^A + f^K \circ \vec{P} \circ f^A\right)(t, t_2) \tag{2.90}$$

where we dropped the superscript (0). Fourier transforming gives the field-current relation (1.28) with Kernel

$$K(\omega) = \frac{i\sigma_N}{2} \int dE \Big(g^R(E) g^K(E-\omega) + f^R(E) f^K(E-\omega) \tag{2.91}$$

$$+ g^K(E) g^A(E-\omega) + f^K(E) f^A(E-\omega) \Big) \tag{2.92}$$

The current-field relation, energy-phase relation (1.10) and Ampere's law result in the (linearized) first London equation (1.38) with complex conductivity [Tin96; MB58]

$$\sigma = \sigma_1 + i\sigma_2 = \frac{iK}{\omega} \tag{2.93}$$

with

$$\frac{\sigma_1(\omega)}{\sigma_N} = \frac{2}{\omega} \int_0^\infty dE (f(E) - f(E+\omega)) \rho(E) U^+(E, E+\omega)$$

$$+ \frac{1}{\omega} \int_0^\omega dE (1 - 2f(\omega - E)) \rho(E) U^-(E, \omega - E) \tag{2.94}$$

and

$$\frac{\sigma_2}{\sigma_N} = \frac{1}{\omega} \int_{-\infty}^\infty dE \left[1 - 2f(E)\right] \Re(g^R(E)) \left(\Im(g^R(E+\omega) + \Im\left(g^R(E-\omega)\right)\right) + \Big|_{g^R \to f^R} \tag{2.95}$$

with the shorthand notation

$$U^\pm(E, E') = \rho(E') K^\pm(E, E') \tag{2.96}$$

and $|_{g^R \to f^R}$ denotes the same terms when replacing $g^R$with f^R. Note that the second term in Eq. (2.94) only contributes for frequencies above the pair breaking threshold $\omega > 2E_g$, with gap in the density of states E_g.

2.4.1. BCS Limit

In the absence of magnetic impurities, Eq. (2.66) and the normalization condition (2.45) allow to solve for the Green's functions[12]

$$g^{R(A)} = -\frac{E}{\Delta} f^{R(A)} = \frac{E}{\xi_E^{R(A)}} \tag{2.97}$$

with

$$\xi_E^R = -(\xi_E^A)^* = \begin{cases} \sqrt{E^2 - \Delta^2}\,\mathrm{sign}(E) & \text{for} \quad |E| > \Delta \\ i\sqrt{\Delta^2 - E^2} & \text{for} \quad |E| < \Delta \end{cases} \tag{2.98}$$

This results in the BCS density of states (1.34), coherence factor (1.35) and complex conductivity (1.30) and (1.32).

The expression for the conductivity uses the local limit; in a clean superconductor the relation between current and field becomes non-local [MB58]. It is important to note that the assumption leading to the local relation for the current is more strict than the condition for the dirty limit $\xi \gg l$, as additionally the electromagnetic field was assumed to vary little over a mean free path. This especially requires a large penetration depth compared to the mean free path

$$\lambda \gg l \tag{2.99}$$

in addition to the dirty limit, i.e. electron motion must be diffusive on lengthscales relevant for the electromagnetic field in order for the Usadel equation to be applicable.[13] For general impurity concentrations it is still possible to derive the (generally non-local) current-field relation starting from the Eilenberger equation [Bel+99]; here only thin films (λ larger than the film thickness) are considered, for which (2.99) holds in general, as surface scattering limits the mean free path to the film thickness.

[12] Equations (2.66) and (2.45) only determine the quasiclassical functions up to a sign, we can choose the sign by requiring a positive real part of g^R corresponding to a positive density of states.

[13] Note that this is however a less strict requirement than $\lambda_L \gg l$

3. Quasiparticle energy distribution in resonators

Parts of this chapter were published in [FC23] and [FC24]. I did all the numerics and prepared all the figures, did parts of the analytical calculations and wrote parts of the manuscript.

In chapter 1, the quality factor and resonance frequency of a superconducting coplanar waveguide resonator was given. It was shown to depend on both the density of quasiparticles in the resonator and their distribution in energy. This property can be used in kinetic inductance detectors [Day+03] - incoming high energy radiation creates many quasiparticles. The corresponding change in quality factor and resonance frequency can be measured and used to estimate the energy deposited. Usually, this estimate assumes a narrow distribution (in energy) of width similar to the phonon temperature [Gao+08]. As quasiparticles absorb photons of the signal used to probe the resonator, their distribution becomes broadened in energy and such a crude modeling becomes inaccurate. Aside from this direct application, quality factors observed in experiments often show a dependence on the strength of the microwave field, raising the question whether this can be explained by the interaction of quasiparticles with the microwave photons. An especially relevant question is whether the microwave signal itself could be responsible for the creation of quasiparticles - although the energy of the microwave photons is usually chosen to be far below the pair breaking threshold, subsequent absorptions of low energy photons could drive quasiparticles to high energies $E > 3\Delta$. A quasiparticle of that energy could emit a phonon of energy above $\omega > 2\Delta$, which in turn creates new quasiparticles. Such a mechanism has been suggested by [Vis+14] to possibly provide a lower limit on quasiparticles encountered in experiments. However, as we show in this chapter, accurate modeling of the quasiparticle distribution shows this not to be a relevant process for typical parameter. Finally, we note that understanding the behaviour of quasiparticles is of great current interest for experiments with qubits in which quasiparticle tunneling leads to decoherence. Superconducting resonators provide a simple device that can be used to test our current theories on their dynamics without needing to consider additional complications from e.g. tunneling or interfaces with normal metals. Thus, an accurate modeling of quasiparticles in superconducting resonators is of great interest for both theory and application.

In chapter 2 rate equations were derived governing the quasiparticle distribution function in disordered superconductors under the influence of a time depended elec-

tromagnetic field and electron phonon scattering (2.70) , (2.66), (2.55), (2.82) (2.86) . In the following this system of equations is used to model the quasiparticle energy distribution function in superconducting resonators.

We calculate the re-distribution of quasiparticles in energy due to electromagnetic fields but neglect the direct effect of electromagnetic fields on the regular Green's functions (and thus density of states, order parameter and coherence factors). This is a valid approximation, as corrections introduced by the electromagnetic field to the retarded/advanced parts of the Usadel equation are of order $e^2\vec{A}^2 D\Delta^{-1}$ (2.65) while corrections to the distribution's shape are of order $e^2\vec{A}^2 D\tau_0$ (2.82, 2.86). As the characteristic time for phonon emission usually exceeds the inverse gap by several orders of magnitude (e.g. in aluminium $\tau_0 \sim 10^{-7}s$ and $\Delta^{-1} \sim 10^{-11}s$) corrections to the distribution are much stronger. Corrections to the quality factor are dominated by σ_1, in which corrections to the retarded/advanced Green's functions and distribution functions enter in a similar way. In the formula for the resonance frequency however, corrections to the distribution's shape enter only in the term in σ_2 that contains a factor $f(E)$, while corrections to the retarded Green's function (and to the order parameter) enter without this factor. Thus, in the calculation of the resonance frequency shift corrections from the non-equilibrium distribution contain an additional small parameter (the quasiparticle density) and it is not obvious if they provide the dominant contribution to its shift.[1] We disregard this possible complication and focus on the quality factor, and leave a more accurate discussion of the resonance frequency for future works.

3.1. Rate equations

The full system of equations can be significantly simplified by assuming spatial homogeneity. In a typical resonator this assumption is however likely violated: Typical diffusion coefficients in superconducting aluminium are on the order $100cm^2/s$ [HL68] , the electromagnetic field varies along the length of resonators, usually on the order of $1cm$, and typical energy relaxation times are on the order of $1\mu s$ [Kap+76]. Thus quasiparticles are more strongly heated through photon absorption in regions with larger field, and diffusion is not sufficiently fast to lead to a spatially homogeneous distribution, and one would in principle need to account for the fact that absorption rates depend on the position along the resonator's length. As the field distribution is non-negligible in most of the resonator's volume[2] we can however expect the correction introduced by the inhomogeneity to the electron photon coupling constant (E.4) to be of order one, and neglect it in the following, i.e. we replace the position dependent photon absorption rate by its value averaged over the resonator volume. Furthermore, as we focus on the description of capacitively coupled half-wavelength resonators, diffusion of quasiparticles out of the [central strip of the] resonator can

[1] Indeed, [Sem+16] claimed corrections to the retarded Green's function to provide a quantitative explanation to the shift in resonance frequency observed in experiments, see also Sec. 3.6.2.

[2] $|A|^2 \propto \sin^2(\frac{\pi z}{l})$ for half wavelength resonators

be neglected. The rate equation used to describe the quasiparticle distribution thus becomes

$$\frac{df(E)}{dt} = St^{Phon}\{f,n\} + St^{Phot}\{f,\bar{n}\} + St^{Phot}_{PB}\{f,\bar{n}_{PB}\}. \tag{3.1}$$

with E the energy measured from the Fermi level, number of photons with energy below the pair breaking threshold $\bar{n}$ and above the pair breaking threshold $\bar{n}_{PB}$. The collision integrals in the right-hand side account for the interaction between quasiparticles and phonons, $St^{Phon}\{f,n\}$, non-pair-breaking photons, $St^{Phot}\{f,\bar{n}\}$, and pair-breaking ones, $St^{Phot}_{PB}\{f,\bar{n}_{PB}\}$, respectively.

The self consistency equation (2.55) can be written as

$$\ln\left(\frac{\Delta_0}{\Delta}\right) = \int_{\Delta}^{\infty} dE\,\rho(E)\frac{2f(E)}{E}\,, \tag{3.2}$$

where Δ_0 is the zero-temperature gap (that is, in the absence of quasiparticles) .

3.1.0.1. Interaction with phonons

The phonon integral is given by $I^{Phon}/\rho(E)$ with I^{Phon} given in (2.86) using the BCS density of states (1.34) and coherence factors (1.35) i.e.

$$St^{Phon}\{f,n\} = St^{Phon}_{sp}\{f\} + St^{Phon}_{st}\{f,n\} + St^{Phon}_{r}\{f,n\} + St^{Phon}_{PB}\{f,n\}. \tag{3.3}$$

The first term on the right hand side describes spontaneous emission:

$$\begin{aligned} St^{Phon}_{sp}\{f\} = \frac{1}{\tau_0 T_c^3}\Bigg\{ &\int_0^{\infty} d\omega\,\omega^2 U^-(E,E+\omega) f(E+\omega)\left[1-f(E)\right] \\ &- \int_0^{E-\Delta} d\omega\,\omega^2 U^-(E,E-\omega) f(E)\left[1-f(E-\omega)\right]\Bigg\} \end{aligned} \tag{3.4}$$

The contribution of stimulated emission and absorption is

$$\begin{aligned} &St^{Phon}_{st}\{f,n\} = \\ &\frac{1}{\tau_0 T_c^3}\int_0^{\infty} d\omega\,\omega^2 U^-(E,E+\omega)\left\{f(E+\omega)\left[1-f(E)\right] - f(E)\left[1-f(E+\omega)\right]\right\} n(\omega) \\ &+ \frac{1}{\tau_0 T_c^3}\int_0^{E-\Delta} d\omega\,\omega^2 U^-(E,E-\omega)\left\{f(E-\omega)\left[1-f(E)\right] - f(E)\left[1-f(E-\omega)\right]\right\} n(\omega). \end{aligned} \tag{3.5}$$

Quasiparticle number conservation follows from the identities

$$\int_{\Delta}^{\infty} dE\,\rho(E) St^{Phon}_{sp} = \int_{\Delta}^{\infty} dE\,\rho(E) St^{Phon}_{st} = 0 \tag{3.6}$$

The recombination and pair-breaking terms are, respectively,

$$St_r^{Phon}\{f,n\} = -\frac{1}{\tau_0 T_c^3}\int_{E+\Delta}^{\infty} d\omega\,\omega^2 U^+(E,\omega-E)f(E)f(\omega-E)\left[1+n(\omega)\right] \tag{3.7}$$

and

$$St_{PB}^{Phon}\{f,n\} = \frac{1}{\tau_0 T_c^3}\int_{E+\Delta}^{\infty} d\omega\,\omega^2 U^+(E,\omega-E)[1-f(E)]\left[1-f(\omega-E)\right]n(\omega). \tag{3.8}$$

3.1.0.2. Interaction with photons

For the (non pair breaking) photon integral we use

$$\begin{aligned} &St^{Phot}\{f,\bar{n}\} = \\ &c_{Phot}^{QP}U^+(E,E+\omega_0)\Big\{f(E+\omega_0)\left[1-f(E)\right](\bar{n}+1) - f(E)\left[1-f(E+\omega_0)\right]\bar{n})\Big\} \\ &+ c_{Phot}^{QP}U^+(E,E-\omega_0)\Big\{f(E-\omega_0)\left[1-f(E)\right]\bar{n} - f(E)\left[1-f(E-\omega_0)\right](\bar{n}+1)\Big\} \end{aligned} \tag{3.9}$$

It differs from the photon integral in the first line of (2.82) by the inclusion of terms corresponding to spontaneous emission; these were absent in our derivation in chapter 2 because of the classical treatment of the electromagnetic field. Here, they are included for consistency with literature (e.g. [CB19; CS77; CS78]), but as shown below they do not give a relevant contribution to the quasiparticle dynamics for typical parameter, as phonon emission dominates over spontaneous emission and phonon assisted recombination over photon assisted recombination (see Sec. 3.5.1.1). The coupling constant is derived in appendix E.2. The collision integral for the pair breaking photons is

$$St_{PB}^{Phot}\{f,\bar{n}_{PB}\} = St^{Phot}\{f,\bar{n}_{PB}\} + St_{PB,g}^{Phot}\{f,\bar{n}_{PB}\} + St_{PB,r}^{Phot}\{f,\bar{n}_{PB}\} \tag{3.10}$$

Here, $St^{Phot}\{f,\bar{n}_{PB}\}$ is a number-conserving scattering term accounting for the redistribution of quasiparticles in energy due to the absorption of pair-breaking photons. It can be obtained from the photon integral St^{Phot} for non-pair-breaking photons of frequency ω_0 by replacing photon energy ω_0, photon number $\bar{n}$ and coupling constant c_{Phot}^{QP} by the respective values of the pair breaking photons ω_{PB}, $\bar{n}_{PB}$ and $c_{Phot,PB}^{QP}$ [the appearance of $\bar{n}$ or $\bar{n}_{PB}$ in the argument of the collision integral indicates which of these quantities should be used]. In addition to the scattering term, there is a term accounting for the generation of new quasiparticles, resulting from the second line in (2.82),

$$St_{PB,g}^{Phot} = c_{Phot,PB}^{QP}U^-(E,\omega_{PB}-E)\bar{n}_{PB}\left[1-f(E)\right]\left[1-f(\omega_{PB}-E)\right] \tag{3.11}$$

and a term describing recombination accompanied by the emission of a photon,

$$St_{PB,r}^{Phot}\{f,\bar{n}_{PB}\} = -c_{Phot,PB}^{QP}U^-(E,\omega_{PB}-E)(1+\bar{n}_{PB})f(\omega_{PB}-E)f(E) \tag{3.12}$$

We note that both for non- and pair-breaking photons we consider a single mode of definite frequency; this is justified for non-pair-breaking photons by the fact that in applications such as KIDs one high-quality factor mode of the resonator is probed. For pair-breaking photons this is in general a simplification; however, at least in some of the regimes we will consider, the extension to multiple modes is straightforward (see Sec. 3.5.1). Moreover, we will show that this simplification does not alter qualitatively our interpretation of experimental data for the quality factor in Sec. 3.6. Following Ref. [CB19], we define an effective photon temperature T_0 via $e^{\omega_0/T_0} \equiv (\bar{n}+1)/\bar{n}$.

3.1.1. Phonon rates

In the previous section the phonon distribution was assumed to be in equilibrium. Since the processes described by St^{Phon} involve the emission or absorption of a phonon, in a general non-equilibrium situation one must also consider the kinetic equation for the phonon distribution function [CS77; CS78],

$$\begin{aligned}\frac{dn(\omega)}{dt} &= \frac{2}{\pi\Delta_0\tau_0^{PB}}\int_{\Delta}^{\infty} dE\,\rho(E)U^{-}(E,E+\omega)\big\{f(E+\omega)\\ &\times\left[1-f(E)\right]\left[1+n(\omega)\right]-f(E)\left[1-f(E+\omega)\right]n(\omega)\big\}\\ &+\frac{1}{\pi\Delta_0\tau_0^{PB}}\int_{\Delta}^{\omega-\Delta} dE\,\rho(E)U^{+}(E,\omega-E)\big\{f(\omega-E)\\ &\times f(E)\left[1+n(\omega)\right]-\left[1-f(\omega-E)\right]\left[1-f(E)\right]n(\omega)\big\}\\ &-\frac{1}{\tau_l}\left[n(\omega)-n_T(\omega,T_B)\right]. \end{aligned} \tag{3.13}$$

The first integral on the right-hand side is the counterpart to the quasiparticle-conserving collision integrals St_{sp}^{Phon} and St_{st}^{Phon} of Eqs. (3.4) and (3.5), while the second integral to the recombination and pair-breaking terms of Eqs. (3.7) and (3.8), the factor of two in front of the first integral accounting for spin. For frequencies $\omega < 2\Delta$ the second integral must be replaced by zero. Within a phenomenological relaxation time approach, the last term in Eq. (3.13) accounts for phonon exchange with a thermal equilibrium bath of temperature T_B, $n_T(\omega,T_B) = (e^{\omega/T_B}-1)^{-1}$. Note that the lifetime of a phonon of energy $2\Delta_0$ against pair breaking at zero temperature τ_0^{PB} and the characteristic time τ_0 are related [GW12; Zeh95],

$$\frac{\tau_0}{\tau_0^{PB}} = \frac{2\Delta_0\pi\rho_F\omega_D^3}{9N_{\mathrm{ion}}T_c^3}, \tag{3.14}$$

where ρ_F is the single-spin electronic density of states at the Fermi energy, ω_D is the Debye frequency, and N_{ion} the ionic volume density. For Al, using the parameters reported in Ref. [Kap+76] this gives $\tau_0/\tau_0^{PB} \simeq 1.7\times10^3$, but this ratio is smaller for other materials considered there (for instance, it is about 36 for Nb). The system under investigation is shown schematically in figure 3.1.

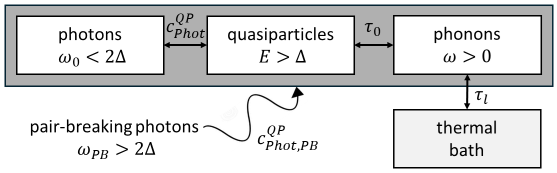

Figure 3.1.: A full model of a thin-film superconducting resonator (dark box) takes into account the resonant mode of frequency ω_0, quasiparticles, phonons, and their interactions (with coupling constants c^{QP}_{Phot} and τ_0). Additionally, quasiparticles can be generated by pair-breaking photons of frequency ω_{PB} and the phonons interact with the substrate, which act as a thermal bath (coupling constant τ_l).

3.2. Numerics

The equations (3.1) to (3.13) constitute a system of coupled non-linear integral equations whose solution, even in the steady state, is clearly non-trivial. Here we describe briefly how we solve the system numerically. To discretize the system in the steady state, we divide the energy axis in intervals $\Xi_i = [\psi_i, \psi_{i+1}]$ with $\psi_i = ih$ and average over each such intervals, so that the steady-state condition for Eq. (3.1) becomes

$$\frac{d}{dt} \int_{\Delta+\psi_i}^{\Delta+\psi_{i+1}} dE f(E) = 0 \tag{3.15}$$

We choose the discretization such that the gap is an integer multiple of h, and additionally round the photon energy to the nearest integer multiple of h. Furthermore, for $E_i \in \Xi_i + \Delta$ and $\omega_j \in \Xi_j$ we approximate $f(E_i) = f(\Delta + \psi_i)$, $n(\omega_j) = n(\psi_j)$, $K^{\pm}(E_i, E_i \pm \omega_j) = K^{\pm}(\Delta + \psi_i, \Delta + \psi_{i\pm j})$ to convert Eq. (3.1) to a system of ordinary equations. This procedure is equivalent to replacing the quasiparticle density of states by the density of states averaged over each interval Ξ_i and replacing the other quantities by their value on a grid as described above. A similar discretizetion procedure has been used in Ref. [Koz+04a]; the major differences to our work are that we discretize phonon and quasiparticle kinetic equations separately and neglect the variation of the coherence factors $K^{\pm}$ and the ω^2 factor over each interval, enabling us to calculate the weights analytically [3]. We use the same approach of replacing the quasiparticle density of states by the averaged one, and discretizing the other quantities as described above, to obtain the discretized version of Eq. (3.13).

[3] In contrast to our procedure, in which the BCS density of states Eq. (1.34) is kept unaltered, some authors introduce a broadened density of states and a cutoff using a Heaviside function [GW12; Gur18]. This approach can be problematic; for example, to our understanding the discretized version of the photon integral used in Ref. [Gur18] violates the conservation of the number of quasiparticles. With our approach, introducing a broadening and a cutoff is not necessary, and terms that conserve the number of quasiparticles in Eq. (3.1) also conserve the number of quasiparticles in the discretized version.

To arrive at the numerical solution of the full system, we proceed via intermediate steps that are similar to those we will employ to find approximate analytical results, see Secs. 3.4.1 and 3.4.2. To begin with, we take the phonon distribution to be the thermal equilibrium one, and approximately keeping only terms linear in $f \ll 1$, Eq. (3.1) reduces to a matrix equation

$$\mathbf{M} f^0 = 0\,, \tag{3.16}$$

where superscript 0 is used to denote the initial solution (that is, step zero) for the quasiparticle distribution function. This equation can be solved by diagonalizing $\mathbf{M}$ but it does not determine the distribution's normalization. The latter is fixed by the non-linear terms, and its approximate value can be found using the discretized version of the approach described in Sec. 3.4.2.

After obtaining the properly normalized f^0, non-linear terms in Eq. (3.1) as well as Eq. (3.13) can be taken into account using Newton's algorithm. To solve the two equations simultaneously, we follow Ref. [GW12] by forming the state vector $x = (f, n)^T$ and writing the system of equations determining the state vector in the steady state in the form $g(x) = 0$. Successive approximations x^i to the state vector are calculated using the recursive relation

$$x^{i+1} = x^i - J^{-1}(x^i) g(x^i) \tag{3.17}$$

with J^{-1} the inverse of the Jacobian matrix of g. The normalized f^0 is used as the initial guess for the quasiparticle distribution, while the initial guess for the phonon distribution can be obtained by inserting f^0 in Eq. (3.13), setting the temporal derivative to zero, and solving that linear equation for n. Calculations of the initial phonon distribution and of the Jacobian matrix can be carried out analytically, thus avoiding long computational times and rounding errors.

The discretized system of equation is not differentiable with respect to the gap Δ, so we do not include the self-consistency condition Eq. (3.2) in Newton's algorithm. To find deviations of the gap from its equilibrium value, we can solve Eq. (3.17) for a fixed gap. This gives the distribution f as function of the gap, and we can use the result in a bisection algorithm applied to Eq. (3.2) to calculate the non-equilibrium gap. While this method gives a fully self-consistently calculated gap, it is accurate only up to variations of the gap of order h, as both the gap and the photon energy have to be rounded to integer multiple of h in the calculation of the distribution function. For the small deviation $\delta = \Delta_0 - \Delta$ of the gap from its zero-temperature value encountered in this thesis, we instead proceed as follows: the left-hand side of Eq. (3.2) is approximately δ/Δ_0 at leading order; therefore, in an iterative approach to solving the equation, we calculate f with the gap fixed at its thermal equilibrium value, thus neglecting the deviation of the gap from equilibrium in the right-hand side. This gives an expression for δ in terms of an integral which depends only on the quasiparticle distribution obtained using the thermal equilibrium gap and that can be evaluated numerically. The numerical solution gives the quasiparticle distribution at points on an energy grid of spacing h; since we want to use a finer grid to numerically

evaluate the integral, between these points we linearly interpolate the distribution function (the interpolation can be used because the distribution function is smooth between two nearby peaks at multiples of ω_0 above the gap).

3.3. Relevant timescales

While a numerical solution to the system of coupled integral equations, Eqs. (3.1) and (3.13), can be found as just described, an exact analytical solution is likely impossible except in particular cases such as thermal equilibrium; it is therefore instructive to discuss the different timescales governing the dynamics of the quasiparticles and phonons and under which conditions approximate analytical solutions might be found. Throughout this work we assume the quasiparticles to be non-degenerate, $f(E) \ll 1$, so we always neglect Pauli Blocking factors by replacing $[1 - f(E)] \to 1$.

There are several characteristic times that can be read off from the kinetic equations, as detailed in Appendix C. These lifetimes in general depend on the energy E of the quasiparticle or ω of the phonon; we begin by discussing the phonon lifetimes. For phonons with energy above the pair-breaking threshold, $\omega > 2\Delta$, their pair-breaking lifetime $\tau_{PB}^{Phon}(\omega)$ depends weakly on energy near the threshold, so we take approximately $\tau_{PB}^{Phon}(\omega) \approx \tau_0^{PB}$; in Al, $\tau_0^{PB} \simeq 240\,\mathrm{ps}$ [Kap+76]. The lifetime due to the phonon being absorbed by a quasiparticle is in general much longer than this, $\tau_{abs}^{Phon}(\omega) \gg \tau_0^{PB}$, due to the assumed non-degeneracy (and hence low density) of the quasiparticles. In contrast, in aluminum films the thermalization time τ_l [last term in Eq. (3.13)] is comparable to the pair-breaking time, $\tau_l \sim \tau_0^{PB}$; for films of thickness 100 nm on a sapphire substrate, the thermalization time is estimated to be $\tau_l \simeq 500\,\mathrm{ps}$ [Kap79; Eis+76; CS78]. Since thermalization and pair-breaking times are comparable, we expect them to have both an impact on the above-threshold phonon distribution and hence on the quasiparticle number. Moreover, the absorption time being long means that the phonon distribution can significantly deviate from the equilibrium one; however, as we discuss below, generally this does not impact the shape of the quasiparticle distribution. We note that these consideration can be material-specific; for instance, for a 100 nm thick Nb film on sapphire we estimate $\tau_0^{PB} \simeq 4\,\mathrm{ps}$ and $\tau_l \simeq 1.5\,\mathrm{ns}$ [Kap+76; Kap79], so deviations from equilibrium can become more significant compared to aluminium.

Turning to the quasiparticle lifetimes, we can identify two scattering times, $\tau_{s,t}^{qp}(E)$ and $\tau_{s,n}^{qp}(E)$, involving photons and phonons respectively and accounting for all possible number-conserving processes (absorption as well as spontaneous and stimulated emission), and the recombination lifetime $\tau_r^{qp}(E)$, which is inversely proportional to the quasiparticle density. In this work we focus on quasiparticles of energies up to a few times the superconducting gap, as the energy dependence of the phonon scattering time implies that quasiparticles of higher energies typically relax very quickly towards the gap and therefore do not contribute directly to processes like photon absorption. When the recombination lifetime is longer than the scattering ones, $\tau_r^{qp} \gg \tau_{s,n}^{qp}, \tau_{s,t}^{qp}$, as is the case for low quasiparticle densities and sufficiently high

photon number, the shape of the quasiparticle distribution function is determined by the number-conserving processes, while generation and recombination affect its normalization (that is, the overall quasiparticle density). Moreover, for strong deviations from equilibrium to be possible, the photon scattering time should be the shortest time scale, $\tau_{s,t}^{qp} \lesssim \tau_{s,n}^{qp}$, a condition that can be met if the number of photons $\bar{n}$ is sufficiently large and/or the phonon bath temperature T_B sufficiently low; in particular, the phonon scattering time being longer than the photon one means that deviations of the phonon distribution from equilibrium have a small effect on the shape of the quasiparticle distribution (see also Sec. 3.4.1.3).

Above discussion allows to identify the main processes governing the distribution functions, they are shown schematically in figure 3.2.

3.4. Photons below the pair-breaking threshold

In this section, we assume the resonator to contain only photons of frequency below the pair breaking threshold $\omega_0 \ll 2\Delta$ to set the last term in (3.1) (and thus diagram e in figure 3.2) to zero.

3.4.1. Shape of the quasiparticle distribution function

Our goal in this section is to find the quasiparticle distribution function by approximately solving the system of coupled equations Eqs. (3.1), (3.2), and (3.13) in the steady state in the regime of low temperatures, and hence low quasiparticle density, and high number of photons, $\bar{n} \gg 1$, or equivalently $T_0 \gg \omega_0$. A sufficient condition for having low density is $f(E) \ll 1$, which enables us to approximate the Pauli-blocking factors as $[1 - f(E)] \approx 1$. Moreover, we neglect in this section the recombination and pair-breaking collision integrals, Eqs. (3.7) and (3.8) (diagrams f)-i) of figure 3.2), since they affect the normalization but not the shape of the quasiparticle distribution function, as argued in Sec. 3.3.

At low temperature $T_B \ll \omega_0$, the competition between absorption of photons and emission of phonons results in a quasiparticle distribution with peaks at energies $\Delta + m\omega_0$, $m = 0, 1, 2, \ldots$ [GW12; CB19]. Here we focus on the envelope function that determines the heights of these peaks. Then interpreting $f(E)$ as this envelope, the photon collision integral Eq. (3.9) can be approximately written as a generalized diffusion operator in energy space,

$$St^{Phot}\{f, \bar{n}\} \simeq c_{Phot}^{QP} \frac{\omega_0^2}{U^+(E,E)} \bar{n} \frac{\partial}{\partial E'} \left[U^+(E,E')^2 e^{-E'/T_0} \frac{\partial}{\partial E'} \left(f(E') e^{E'/T_0} \right) \right] \Bigg|_{E'=E} \tag{3.18}$$

as one can verify by Taylor expansion of Eq. (3.9) to second order in ω_0. Next, we consider explicitly three cases: A. phonons in equilibrium at zero temperature; B. phonons in equilibrium at finite temperature; C. nonequilibrium corrections to the

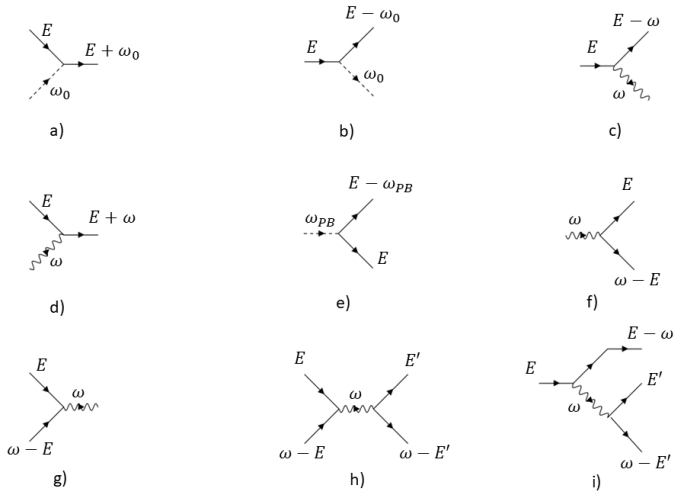

Figure 3.2.: Schematic depiction of the main processes entering the collision integrals in Eq. (3.1). Straight lines correspond to quasiparticles, wavy lines to phonons, and dashed lines to photons. Diagrams a) and b) represent the absorption and emission of non-pair-breaking photons [cf. Eq. (3.9)], c) the emission of a phonon [c.f. Eq (3.4) and first term in the first bracket and second term in the second bracket in Eq. (3.5)],d) Absorption of a phonon [second term in the first bracket and first term in the second bracket in Eq. (3.5)] e) quasiparticle generation by pair-breaking photons [Eq. (3.11)], Diagram f) depicts generation by a pair-breaking phonon (3.8), g) corresponds to (3.7) and provides the bare recombination rate $R_0 N_{qp}$, and h) renormalizes the bare recombination coefficient R_0 to R in Eq.(3.50) [see also Eq. (3.51)]. Diagram i) describes an additional pair-breaking mechanism due to phonon emitted by quasiparticles with energy $E > 3\Delta$; this process is only relevant for sufficiently large $\bar{n}$. We do not include the diagram corresponding to photon mediated recombination [similar in structure to f)], as its contribution is generally negligible compared to phonon mediated recombination (see Sec. 3.5.1.1)

phonon distribution function. Case A corresponds to diagrams a)-c), Case B additionally includes diagram d) assuming the phonon distribution to be in equilibrium. In case C. also non-equilibrium phonon distributions are included in diagram d).

3.4.1.1. Phonons in equilibrium at $T_B = 0$

The assumption that the phonons are in equilibrium corresponds to taking the limit $\tau_l \to 0$ in Eq. (3.13), so that $n(\omega) = n_T(\omega, T_B)$ is the (leading order) solution for the phonon distribution function. For $T_B = 0$, this implies $n(\omega) = 0$, and the steady-state equation for the quasiparticle distribution function reduces to

$$0 = St_{sp}^{Phon}\{f\} + St^{Phot}\{f, \bar{n}\} \tag{3.19}$$

with St_{sp}^{Phon} of Eq. (3.4) and St^{Phot} of Eq. (3.18). Even this much simplified equation cannot be solved exactly, so we consider separately three energy ranges – low, intermediate, and high – to be defined below. In all three ranges we assume the photon number to be so large that T_0 is the highest energy scale; then we can take the limit $T_0 \to \infty$ in Eq. (3.18) and replace the exponential factors with unity.

The low and intermediate energy ranges are sufficiently close to the gap, $E - \Delta \ll \Delta$, so that one can approximate

$$U^+(E_1, E_2) \simeq \sqrt{\frac{2\Delta}{E_2 - \Delta}} \tag{3.20}$$

for $E_2 > \Delta$, and $U_+ = 0$ otherwise, in Eq. (3.18) and

$$U^-(E_1, E_2) \simeq \frac{E_1 + E_2 - 2\Delta}{\sqrt{2\Delta(E_2 - \Delta)}} \tag{3.21}$$

in Eq. (3.4). Within this approximation, $St_{sp}^{Phon}\{f\}$ takes the form

$$\begin{aligned} St_{sp}^{Phon}\{f\} = &-\frac{128}{105\sqrt{2}}\left(\frac{\Delta}{T_c}\right)^3\left(\frac{E-\Delta}{\Delta}\right)^{7/2}\frac{f(E)}{\tau_0} \\ &+ \frac{1}{\tau_0 T_c^3}\int_0^\infty d\omega\, \omega^2 \frac{2E - 2\Delta + \omega}{\sqrt{2\Delta(E + \omega - \Delta)}} f(E + \omega) \end{aligned} \tag{3.22}$$

Introducing the temperature scale

$$T_* \equiv \left(\frac{105}{64} T_c^3 c_{Phot}^{QP} \bar{n} \tau_0 \omega_0^2 \Delta\right)^{1/6} \tag{3.23}$$

characterizing the width of the distribution function, and neglecting the first term on the right-hand side in Eq. (3.22) for $E - \Delta \lesssim T_*$ (low energy range) and the second one for $T_* \lesssim E - \Delta \lesssim \Delta$ (intermediate range) leads to the solution derived in Ref. [CB19]

$$f(x) \simeq \begin{cases} b_0\left(1 - 0.564x^{5/2} + 0.119x^{7/2}\right), \; x \lesssim 1 & (3.24) \\ 3b_0 \mathrm{Ai}\left(\dfrac{x^2}{4^{1/3}}\right), \; 1 \lesssim x \ll \Delta/T_* & (3.25) \end{cases}$$

with $x \equiv (E-\Delta)/T_*$, Ai the Airy function, and b_0 a normalization constant whose determination is the subject of Sec. 3.4.2. Note that depending on the parameters (and in particular by increasing $\bar{n}$) the intermediate regime could be absent; here we assume for simplicity that the condition $T_* < \Delta$ is satisfied (this is consistent with considering quasiparticles with energies up to few times the gap, cf. Sec. 3.3). Moreover, the initial assumptions that T_0 is large and that we can study the envelope concretely means $T_0 \gg T_* \gg \omega_0$.

In the high-energy range $E-\Delta \gtrsim \Delta$, we neglect terms of order $(\Delta/E)^2$ in Eq. (3.18), leading to

$$St^{Phot}\{f,\bar{n}\} = \bar{n} c_{Phot}^{QP} \omega_0^2 f''(E) \tag{3.26}$$

Since for $T_* < \Delta$ most quasiparticles are at energies below 2Δ, at energies $E > 2\Delta$ the first integral in Eq. (3.4) is much smaller than the second one and can be neglected. Therefore, we can further approximate

$$St_{sp}^{Phon} \simeq -\frac{f(E)}{\tau_0 T_c^3} \frac{(E-\Delta)^3}{3} \tag{3.27}$$

in the high-energy regime. Substituting $\tilde{x} \equiv (E-\Delta)/\tilde{T}_*$, with

$$\tilde{T}_* \equiv (3\bar{n} c_{Phot}^{QP} \omega_0^2 \tau_0 T_c^3)^{1/5} = \left(\frac{64}{35}\frac{T_*}{\Delta}\right)^{1/5} T_* \,, \tag{3.28}$$

into Eq. (3.19), that equation takes the form of a generalized Airy equation,

$$f''(\tilde{x}) - \tilde{x}^3 f(\tilde{x}) = 0 \,. \tag{3.29}$$

The solution to this equation can be written in terms of a modified Bessel function of the second kind,

$$f(\tilde{x}) = \tilde{b}_0 \sqrt{\tilde{x}} K_{1/5}\left(\frac{2}{5}\tilde{x}^{5/2}\right) \tag{3.30}$$

With our assumptions we are only interested in the limit of large $\tilde{x}$, so that we can approximate

$$f(\tilde{x}) \simeq \tilde{b}_0 \sqrt{\frac{5\pi}{4\tilde{x}^{3/2}}} e^{-\frac{2}{5}\tilde{x}^{5/2}} \tag{3.31}$$

This expression should match the similar approximation for Eq. (3.25) at an energy of order 2Δ. Indeed, the exponential factors are identical at $E = 143\Delta/80$ and the prefactors are then related by

$$\frac{\tilde{b}_0}{b_0} = \frac{3^{3/2}2^{2/3}}{5\pi}\left(\frac{64}{35}\frac{T_*}{\Delta}\right)^{-2/5} \tag{3.32}$$

Due to the faster than exponential decay of the distribution over the energy scale $T_* \lesssim \Delta$, it might seem irrelevant to calculate here and in the next subsection the behavior of its high-energy tail ($E \gtrsim 2\Delta$); however, quasiparticles with energy above 3Δ can relax by emitting a pair-breaking phonon, which in turn can generate two quasiparticles (diagram i) in figure 3.2). That is why knowledge of the tail will be needed to understand how the photons influence the quasiparticle density, see Sec. 3.4.2.

3.4.1.2. Equilibrium phonons, $T_B > 0$

We now consider in more detail the effect of thermal phonons. We aim to show that neglecting phonons is a good approximation up to a crossover energy E_*, above which the (envelope of the) quasiparticle distribution function takes the thermal equilibrium form. Using the expression in Eq. (3.5), we define the energy scale E_* as that energy at which the equation

$$St_{st}^{Phon}\{f, n_T\} + St^{Phot}\{f, \bar{n}\} = 0 \tag{3.33}$$

is satisfied with f as obtained in Sec. 3.4.1.1 and $n = n_T$ being the thermal distribution for phonons.

By the definition of E_*, up to that energy we can neglect the phonons and hence Eq. (3.19) holds; that equation enables us to express St^{Phot} in terms of St_{sp}^{Phon}. For the latter, at high energies $E - \Delta \gg \Delta$ we can use Eq.(3.27) to get:

$$St^{Phot}\{f, \bar{n}\} = -St_{sp}^{Phon}\{f\} \simeq \frac{(E-\Delta)^3}{3\tau_0 T_c^3} f(E) \tag{3.34}$$

with $f(E)$ decreasing faster than exponentially, cf. Eq. (3.31). To estimate E_* using Eq. (3.33) we need an approximate expression for St_{st}^{Phon}. It turns out that the main contribution to this collision integral originates from the term in Eq. (3.5) proportional to $f(E-\omega)$, since as function of ω that factor increases faster than exponentially (as long as $E - \omega$ remains sufficiently large). Thus, it dominates over the exponential suppression of $n(\omega, T_B)$ at $\omega \gg T_B$, leading to a sharply peaked maximum of the integrand at a certain energy ω_M, as detailed in Appendix D.1. Introducing the crossover temperature

$$T_B^* \equiv \left(\frac{T_*}{\Delta}\right)^3 \Delta = \omega_0 \sqrt{\frac{105}{64} c_{Phot}^{QP} \bar{n} \tau_0} \left(\frac{T_c}{\Delta}\right)^{3/2} \tag{3.35}$$

we can distinguish two regimes: for low phonon temperature/high photon number, $T_B \ll T_B^*$, we find

$$E_* \approx \Delta + \tilde{T}_* (\tilde{T}_*/T_B)^{2/3} \gtrsim 2\Delta\,, \tag{3.36}$$

while for high phonon temperature/low photon number, $T_B^* \lesssim T_B \ll T_*$, we get

$$E_* \approx \Delta + T_* (T_*/T_B)^{1/2} \lesssim 2\Delta\,. \tag{3.37}$$

In both cases, it turns out that for $E > E_*$ stimulated emission/absorption of phonons dominates over the interaction with photons, so that the distribution function is approximately of the Boltzmann form,

$$f(E) \simeq b_T e^{-E/T_B}, \tag{3.38}$$

where b_T can be found by requiring continuity of f at $E = E_*$. Note that while here the ratio between T_B and T_B^* being below or above unity has the apparently minor role of determining whether E_* is above or below 2Δ, we will later see that this ratio influences also the temperature dependence of both the quasiparticle density and the quality factor.

3.4.1.3. Finite thermalization time

So far, we have assumed that the phonon distribution has the equilibrium form, corresponding to the limit of zero thermalization time τ_l. If the thermalization time is non-zero, the phonon distribution can deviate from the equilibrium one, as discussed in Sec. 3.3. We can distinguish between phonons of energy ω below and above the pair-breaking threshold 2Δ. Above-threshold phonons can break Cooper pairs and thus influence the quasiparticle density – this is the subject of Sec. 3.4.2. These phonons can also affect the shape of the quasiparticle distribution by being absorbed, but these processes are far less frequent than pair breaking (since $\tau_{abs}^{Phon} \gg \tau_0^{PB}$) and the change would only take place at high energies $E > 3\Delta$ where the occupation is generically extremely small, so we neglect this effect.

Below-threshold phonons, in contrast, can affect the quasiparticle distribution at all energies. However, we now show that significant deviations from the equilibrium phonon distribution appear only at relatively high energy ω and have a negligible effect on the shape of the quasiparticle distribution. Indeed, for $\omega < 2\Delta$ we can approximately solve Eq. (3.13) in the steady state, writing $n(\omega) \simeq n_T(\omega, T_B) + n_1(\omega)$ with (see Appendix D.2 for details)

$$n_1(\omega) \simeq \frac{2\tau_l}{\pi\Delta_0\tau_0^{PB}} \int_{\Delta}^{\infty} dE\, \rho(E) U^-(E, E+\omega) f(E+\omega) \tag{3.39}$$

and the n_1 term becomes dominant above the crossover energy

$$\omega_c \approx T_B \ln\left(\frac{\Delta}{T_*}\frac{\tau_0^{PB}}{\tau_l} b_0^{-1}\right) \tag{3.40}$$

(this approximate expression is valid for $T_* \lesssim \omega_c \ll T_*\sqrt{3T_*/T_B}$ and $\omega_c \lesssim \Delta$, see Appendix D.2 for a more accurate determination of ω_c). The crossover energy depends on the quasiparticle density through $b_0 \ll 1$, which cannot be determined without considering the non-linear terms in the kinetic equations. However, for thermalization time τ_l short compared to τ_0^{PB}, we expect the density to be comparable to the one in thermal equilibrium and hence $b_0 \sim e^{-\Delta/T_B}$ (the quasiparticle density is discussed more in detail in Sec. 3.4.2); this implies that ω_c would become larger than Δ and grow with decreasing τ_l or T_*, as one would expect, since reducing these parameters means that the system is closer to thermal equilibrium. We will return to this point when comparing our results to numerical calculations in Sec. 3.4.4.

To determine if n_1 influences the shape of the distribution function f, one can proceed as in Sec. 3.4.1.2, by replacing $n_T \to n_T + n_1$ in Eq. (3.33). As mentioned there, the main n_T contribution to the collision integral St_{st}^{Phon} comes from the region around an energy ω_M; if this energy is smaller than ω_c, we expect negligible impact of n_1 on the shape of f. This is clearly the case in the limit of fast phonon thermalization $\tau_l \to 0$, since in this case, as discussed above, $\omega_c > \Delta$, while in general $\omega_M < \Delta$ (see Appendix D.1), so $\omega_M < \omega_c$. We do not investigate here more generally when the condition $\omega_M < \omega_c$ is satisfied, nor the effect of n_1 on f when it is violated, but we will

show numerically that for experimentally relevant parameters the shape of f derived in this section is valid at least up to energies of a few times Δ.

3.4.2. Quasiparticle density

The considerations in the previous section have been limited to the shape of the quasiparticle distribution function, including the effect of nonequilibrium phonons due to finite thermalization time, see Sec. 3.4.1.3. However, it follows from the pair-breaking phonon collision integral, Eq. (3.8), that nonequilibrium phonons can potentially affect the quasiparticle number as soon as the crossover frequency ω_c between equilibrium and nonequilibrium phonon population satisfies $\omega_c \lesssim 2\Delta$, a weaker condition than that required for them to affect the shape of the distribution function, $\omega_c < \omega_M$. Consequently, in this section we investigate the effect a non-zero thermalization time has on the number of quasiparticles in the regime $\omega_M < \omega_c \lesssim 2\Delta$, in which the influence of nonequilibrium phonons on the quasiparticle distribution shape can be neglected while their influence on the quasiparticle density must be established. Thus, we now include all diagrams of figure 3.2 except diagram e). Diagrams f)-i) directly affect the density of quasiparticles while diagrams a)-d) affect it only indirectly by determining the quasiparticle distribution's shape entering the other diagrams.

The quasiparticle density N_{qp} is given by

$$N_{\mathrm{qp}} \equiv 4\rho_F \int_{\Delta}^{\infty} dE\, \rho(E) f(E) \tag{3.41}$$

$$\simeq 4.2\rho_F \sqrt{2\Delta T_*} b_0 \tag{3.42}$$

where for f we used the distribution function of Sec. 3.4.1 and the numerical prefactor was determined in Ref. [CB19]. As remarked previously, to find the value of the normalization constant b_0, the recombination and pair-breaking collision integrals, Eqs. (3.7) and (3.8), must be taken into account. To do so, we multiply the kinetic equation Eq. (3.1) by the BSC density of states $\rho(E)$, integrate over energy E, and assume the steady-state condition $df/dt = 0$ to arrive at the equation

$$\int_{\Delta} dE\, \rho(E) \int_{E+\Delta} d\omega\, \omega^2 U^+(E, \omega - E) \left[n(\omega) - f(E) f(\omega - E) \right] = 0 \tag{3.43}$$

where, as before, we neglect Pauli-blocking factors and assume $n(\omega) \ll 1$ for $\omega > 2\Delta$. The two terms in square brackets originate from pair breaking and recombination, respectively. For the former, we can switch the integration order and realize that the resulting integral over E is the same as that determining the lifetime of phonons against pair breaking (cf. Appendix C); neglecting again the weak dependence of the result on ω, we rewrite the above equation as

$$\int_{2\Delta} d\omega\, \omega^2 \left[n(\omega) - \frac{1}{\pi\Delta} \int_{\Delta}^{\omega-\Delta} dE\, \rho(E) U^+(E, \omega - E) f(E) f(\omega - E) \right] = 0 \tag{3.44}$$

To proceed further, we need to know the phonon distribution function above the pair-breaking threshold, $\omega > 2\Delta$; as shown in Appendix D.2, it takes the form

$$n(\omega) \simeq \frac{\tau_0^{PB}}{\tau_l + \tau_0^{PB}} \left[n_T(\omega, T_B) + n_1(\omega) + n_2(\omega) \right] \tag{3.45}$$

with n_1 of Eq. (3.39) and n_2 being equal to the product of τ_l/τ_0^{PB} times the second term in square bracket in Eq. (3.44).

Equation (3.44) can now be recast as a quadratic equation for b_0 (see Appendix D.3)

$$I_2 b_0^2 - 2\frac{\tau_l}{\tau_0^{PB}} I_1 b_0 - I_0 = 0 \tag{3.46}$$

with the quadratic term arising from the pair-breaking contribution together with n_2, the linear term from n_1, and the constant term from n_T. Due to their origins, I_0 and I_2 are dimensionless functions of T_B/Δ and T_*/Δ respectively, while I_1 depends in general on both. We can distinguish two limiting cases: if $(\tau_l I_1/\tau_0^{PB})^2 \ll I_2 I_0$, then (cf. Appendix D.3)

$$b_0 \simeq \sqrt{\frac{I_0}{I_2}} \simeq \frac{1}{2.1}\sqrt{\frac{\pi T_B}{T_*}} e^{-\Delta/T_B} \tag{3.47}$$

and the quasiparticle density is approximately the same as in thermal equilibrium, even though the distribution function differs significantly from the equilibrium one.[4] In the opposite limit we find that $b_0 \simeq 2\tau_l I_1/\tau_0^{PB} I_2$ is larger than the thermal equilibrium value and is proportional to the ratio τ_l/τ_0^{PB}: the larger this ratio (that is, the longer τ_l), the easier it is to enter this limit and the larger the quasiparticle density.[5] We discuss further the corresponding nonequilibrium quasiparticle density in the framework of a generalized Rothwarf-Taylor model.

3.4.2.1. Generalized Rothwarf-Taylor model

Given the proportionality between b_0 and $N_{\rm qp}$, Eq. (3.42), the last and first terms in the left-hand side of Eq. (3.46) correspond exactly to the phonon generation and quasiparticle recombination terms in the steady-state version of the Rothwarf-Taylor model [RT67] (we do not consider here direct quasiparticle injection). In fact, we can relax the steady-state assumption and allow for variation in time of parameters such as bath temperature (T_B) and photon number (*i.e.*, T_*), as long as their change is slow on the scale over which the shape of the distribution function is established, namely the quasiparticle scattering times, see Sec. 3.3 (note that since τ_0^{PB} is shorter that τ_0, the phonon distribution quickly follows any change in the quasiparticle one). Then the shape of the distribution function is at all times the one we have calculated in Sec. 3.4.1 and integration over energy of the kinetic equation times $4\rho_F \rho(E)$ gives

$$\frac{dN_{\rm qp}}{dt} = G_{T_B} + G(T_*/\Delta) N_{\rm qp} - R N_{\rm qp}^2 \tag{3.48}$$

[4] This limit corresponds to diagram f) dominating over diagram i) in figure 3.2

[5] This limit corresponds to diagram i) dominating over diagram f) in figure 3.2

Here

$$G_{T_B} = \frac{16\pi\rho_F\Delta}{\bar{\tau}_0}\left(\frac{\Delta}{T_c}\right)^3 \frac{T_B}{\Delta} e^{-2\Delta/T_B} \tag{3.49}$$

is the rate of quasiparticle generation (per unit volume) due to thermal phonons for T_B small compared to 2Δ, and

$$R = \frac{2\Delta^2}{\rho_F \bar{\tau}_0 T_c^3} \tag{3.50}$$

is the quasiparticle recombination coefficient. Both quantities are renormalized by the finite phonon thermalization time, an effect known as "phonon trapping"[CS78],

$$\bar{\tau}_0 = \tau_0(1 + \tau_l/\tau_0^{PB}) \tag{3.51}$$

Note that as T_* approaches Δ, corrections to R and τ_0^{PB} resulting from the finite distribution's width $\sim T_*/\Delta$ can become relevant, as discussed in Appendix D.4.

The central term in the right-hand side of Eq. (3.48) is absent in the Rothwarf-Taylor model and represent an additional quasiparticle generation term proportional to the quasiparticle density itself. It originates from pair-breaking nonequilibrium phonons emitted by quasiparticles which have been excited to sufficiently high energies by the photons [diagram i) of Figure 3.2]. Indeed, the coefficient can be taken in the form (see end of Appendix D.3)

$$G(x) = \frac{\gamma}{\bar{\tau}_0}\frac{\tau_l}{\tau_0^{PB}}\left(\frac{\Delta}{T_c}\right)^3 x^{9/2} e^{-\sqrt{14/5}x^{-3}} \tag{3.52}$$

with $\gamma = 2^{13/6}3^{3/2}/(2.1 \times 5\sqrt{7}) \simeq 0.84$, and vanishes if the phonons are forced to be in thermal equilibrium ($\tau_l = 0$). At high phonon temperature/low photon number, $T_B \gtrsim T_B^*$, this term can be neglected and in the steady state the quasiparticle density takes the thermal equilibrium value; in the opposite regime, $T_B \ll T_B^*$, it leads to a quasiparticle density independent of the bath temperature T_B and larger than in thermal equilibrium. Although the linearity in $N_{\rm qp}$ of this additional generation term could be expected – the more quasiparticle there are, the more can be excited to high energy and emit phonons – we stress that the dependence on the photon number can be found only after solving the kinetic equation for the shape of the distribution function; therefore, it is beyond the reach of phenomenological treatments that consider just the quasiparticle density from the outset. In fact, in this regime the quasiparticle density is strongly dependent on the photon number; the strong dependence originates from the fact that only quasiparticles in the high-energy tail of the distribution function, $E > 3\Delta$, can emit pair-breaking photons, and a quasiparticle must absorb a large number of photons to reach that energy while also losing energy by emitting phonons. Note that in the extreme case $T_B = 0$, the solution $N_{\rm qp}$=0 is unstable: even a single quasiparticle can start the process of driving the phonons out of equilibrium and hence generate more quasiparticles. In Fig. 3.3 we provide an overview of the different regimes we have identified and of the parameter regions where our approach is applicable.

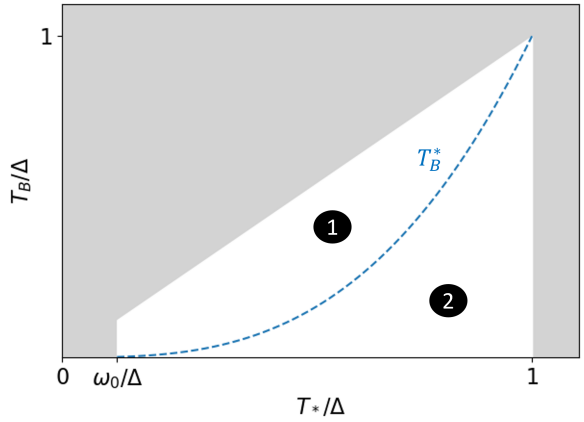

Figure 3.3.: Depending on the phonon temperature T_B and the photon number $\bar{n}$ [that is, T_* of Eq. (3.23)], there are two regimes for the quasiparticle density: in regime 1, thermal phonons dominate quasiparticle creation and the quasiparticle density is approximately as in equilibrium. In regime 2, the photons drive a sufficient number of quasiparticles to energies $E > 3\Delta$ such that quasiparticle creation from phonons emitted by these high-energy quasiparticles is dominant; in this regime, the quasiparticle density is larger than in equilibrium and depends on the photon number but not on the temperature of the phonon bath. The crossover between the two regimes takes places approximately when $T_B \sim T_*^3/\Delta^2$ [cf. Eq. (3.35)], as indicated by the dashed curve. The area shaded in gray ($T_* < \omega_0$, $T_* > \Delta$, $T_B > T_*$) identifies the parameter regions where approximations made in the analytical derivations are not valid.

3.4.3. Gap suppression

Once the normalization constant b_0 is found using Eq. (3.46) [or, equivalently, N_{qp} using Eq. (3.48)], we can perturbatively calculate the change in the gap $\delta\Delta = \Delta_0 - \Delta$. Indeed, substituting the distribution function of Sec. 3.4.1 into Eq. (3.2) we find

$$\frac{\delta\Delta}{\Delta_0} = 4.2 b_0 \sqrt{\frac{T_*}{2\Delta_0}} \left(1 - \frac{1}{4}\frac{0.88}{2.1}\frac{T_*}{\Delta_0}\right) \tag{3.53}$$

where we used the numerical estimate $\int_0 dx \sqrt{x} f(x) \simeq 0.88$ (in the perturbative calculation we neglect the deviation of Δ from Δ_0 in the right-hand side of Eq. (3.2); this is consistent if $T_*/\Delta_0 \gg b_0^2$). The leading order term is equal to the leading-order approximation for $N_{\mathrm{qp}}/(2\rho_F\Delta_0)$ [cf. Eq. (3.42)], which is the fraction of broken Cooper pairs; this result is generic to quasiparticles whose distribution function width above the gap (in our case, T_*) is small compared to the gap itself. Including corrections up to second order in T_*/Δ, we can rewrite Eq. (3.53) in the form

$$\frac{\delta\Delta}{\Delta_0} = \frac{N_{\mathrm{qp}}}{2\rho_F\Delta_0}\left[1 - 0.42\frac{T_*}{\Delta_0} + 0.22\left(\frac{T_*}{\Delta}\right)^2\right] \tag{3.54}$$

For comparison, in thermal equilibrium the terms in brackets read $1 - 0.5T_B/\Delta_0 + 3(T_B/\Delta_0)^2/8$; this shows that for a given quasiparticle density, the gap is less suppressed in the nonequilibrium case, since by assumption $T_* > T_B$. We can therefore find an enhancement of superconductivity, since for $T_B \gtrsim T_B^*$ the quasiparticle density takes roughly the same value as in equilibrium (more accurately, the quasiparticle density slightly decreases with increasing T_* in this regime, as discussed in Appendix D.4, and thus the enhancement is even stronger). In the opposite case, the density is much larger than in equilibrium and hence superconductivity is weakened. Note that the enhancement of the gap due to redistribution of quasiparticles has already been studied for temperatures close to T_c a long time ago [GM 72], in the regime $T_B \ll T_c$ studied here these effects are much weaker as the gap varies proportional to the quasiparticle density.

3.4.4. Comparison to numerics

As a validation of our approach, we now compare the analytical results to the numerical solution of the full system of kinetic equations, Eqs. (3.1)-(3.13). Unless otherwise stated, in this subsection we use the parameters listed in Table 3.1. Their values have been chosen to enable the comparison to experiments that will be discussed in section 3.6; that is, they should be typical for thin aluminum film resonators. The critical temperature is assumed to be connected to the gap via the BCS relation $\Delta_0 = 1.764 T_c$, resulting in $T_c \simeq 1.18\,\mathrm{K}$. Using Eq. (3.14) and the assumed τ_0, the phonon lifetime against pair breaking is $\tau_0^{PB} = 255\,\mathrm{ps}$. The parameters loosely satisfy the validity conditions for the analytical approximations, namely $\omega_0 \ll T_* \lesssim \Delta$, $b_0 \ll 1$, and $\omega_c > \omega_M$ (b_0 can be read off Fig. 3.4; using the results of Appendix D.1 we calculate

c_{Phot}^{QP}	τ_0	Δ_0	ω_0	$\bar{n}$	T_B	T_*	T_B^*
1 Hz	438 ns	180 μeV	$\Delta_0/9$	10^7	0.1 K	$\Delta_0/2$	0.26 K

Table 3.1.: Parameter used for the plots in Figs. 3.4 and 3.5. The quantities T_* and T_B^* are calculated from the other parameters using their respective definitions, Eqs. (3.23) and (3.35).

$\omega_M \simeq 0.57\Delta_0$, while ω_c can be estimated from Fig. 3.5). For the numerical calculations, we take $h = \Delta_0/180$ for the discretization step size and truncate the energy at $E_{\max} = 10\Delta_0$; note that $\omega_0 = 20h$, meaning the shape of the peaks is captured by the numerics.

In Fig. 3.4 we plot with solid lines the numerically calculated quasiparticle distribution function f as function of energy for different values of the thermalization time τ_l. In all cases, we find good agreement with the analytical predictions (dashed lines) of Sec. 3.4.1 spanning several orders of magnitude in occupation probability, whose large variation takes place over an energy range of a few times the gap. For $\tau_l = 0$, the phonons are at thermal equilibrium and the high-energy tail of f approaches the expected exponential decay, see Sec. 3.4.1.2. As τ_l increases, however, the high-energy tail deviates significantly from the $\tau_l = 0$ prediction; the reason for this deviation is the re-absorption of phonons emitted by recombination processes [cf. n_2 in Eq. (3.45)], which have energy $\omega > 2\Delta$. Consequently, the deviation takes place at energies above 3Δ. At those energies for $T_* \lesssim \Delta$ the occupation probability is so small that the deviation does not affect the quasiparticle density.

Figure 3.5 shows the phonon distribution function versus energy ω. There are no visible deviations from the thermal equilibrium behavior up to the τ_l-dependent energy ω_c, see Sec. 3.4.1.3, for all the values of τ_l considered. For ω between ω_c and 2Δ phonons spontaneously emitted by the non-equilibrium quasiparticles become relevant and the phonon distribution function is predominantly given by $n_1(\omega)$ of Eq. (3.39) (see also Appendix D.2). For $\omega > 2\Delta$ the recombination of non-equilibrium quasiparticles affects the phonon distribution. Since the quasiparticle density is larger than in equilibrium, this leads to a phonon occupation probability bigger than the equilibrium one, as captured by the term $n_2(\omega)$ in Eq. (3.45) (see also Appendix D.2, where we give an expression for n_2 valid up to $\omega \simeq 2\Delta + T_*$; the analytically calculated phonon distribution is in good agreement with the numerical results).

In Fig. 3.6 the quasiparticle density is shown as function of T_* for a few different bath temperatures T_B and as function of T_B for a few different phonon numbers (T_*). The analytical and numerical approaches give consistent results over a range of parameters relevant to experiments, with small deviations arising at low temperatures and photon numbers. These deviations are caused by the condition $\omega_0 \ll T_*$ holding only weakly and we have checked that there is a closer match between the two approaches when decreasing the photon energy. In fact, for $\bar{n} \gg 1$ Eq. (3.9) is a symmetric function of ω_0; therefore the leading corrections to Eq. (3.18) and hence to the density are of order $(\omega_0/T_*)^2$. As the magnitude of the deviations is beyond

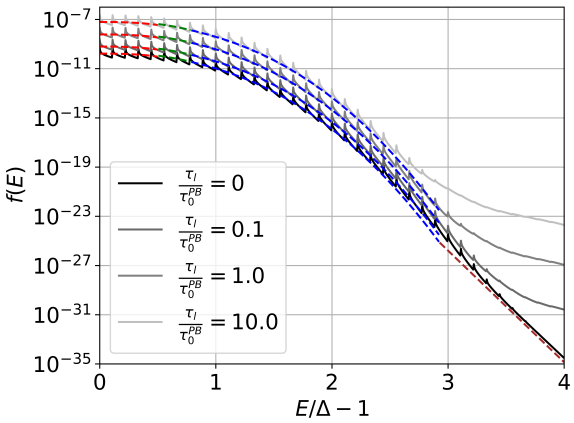

Figure 3.4.: Quasiparticle distribution function vs energy for the parameters in Table 3.1. Grey solid lines show the results of numerical calculations. The colored dashed lines are obtained using the analytical approximations in their respective regimes of applicability; from left to right: Eq. (3.24), Eq. (3.25), Eq. (3.31), and (for $\tau_l = 0$) Eq. (3.38). The normalization coefficient b_0 is calculated by using the steady-state solution to Eq. (3.48) in Eq. (3.42) (we have taken into account the corrections to recombination coefficient and quasiparticle density discussed in Appendix D.4).

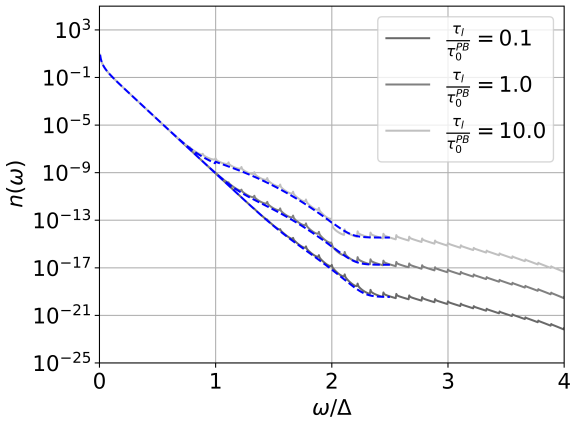

Figure 3.5.: Phonon distribution for the system simulated in figure 3.4. The blue dashed lines in the phonon distribution are the analytic results derived in Appendix D.2, solid grey lines are simulation results.

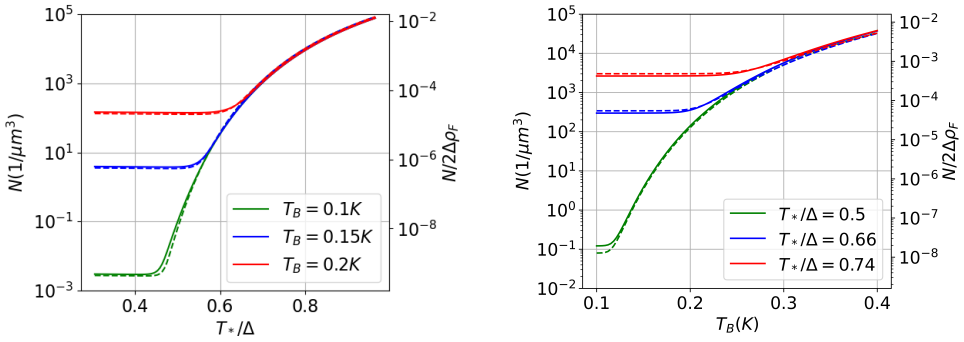

Figure 3.6.: Quasiparticle densities calculated from the simulation (full line) and from solving Eq. (3.48) in the steady state (dashed line). The upper plot is obtained by varying the photon number for three different bath temperatures, the lower plot by varying the bath temperature for $\bar{n} = 10^7, 5 \cdot 10^7, 10^8$ respectively. The thermalization time is fixed at $\tau_l = \tau_0^{PB}$, the other parameters as in Fig. 3.4 (given in Table 3.1). The corrections to the leading analytical results given in Appendix D.4 have been included.

the accuracy of the considerations in the next section, we do not pursue this further.

In Fig. 3.7 the nonequilibrium gap suppression $\delta\Delta$, Eq. (3.54), is compared to the equilibrium one $\delta\Delta_T$ for the same set of parameters as in Fig. 3.6. Superconductivity is enhanced relative to thermal equilibrium when the difference $\delta\Delta_T - \delta\Delta$ is positive. In fact, we focus on the region of low photon number (relatively small T_*/Δ) where the enhancement takes place; in this region the factor in brackets in Eq. (3.54) gives the main dependence of the gap on photon number, causing the gap to increase compared to thermal equilibrium. For larger photon numbers the quasiparticle density increases quickly (c.f. Fig. 3.6), leading to a strong suppression of the gap since $\delta\Delta \propto N_{qp}$. The analytical estimate (dashed lines) slightly overestimates the enhancement compared to the numerics (solid lines), but both set of curves display a maximum at the temperature-dependent value of T_* at which $G(T_*/\Delta)$ becomes the dominant term in Eq. (3.48); that is, above this value quasiparticle creation from re-absorption of pair-braking phonons becomes dominant.

3.5. Photons above the pair-breaking threshold

In this section, the effect of phonons above the pair breaking threshold $\omega_{PB} > 2\Delta$ (i.e. Eqs. (3.11), corresponding to diagram e) in figure 3.2, and (3.12)) is investigated. While different approximations will be employed in different regimes, some approximations are common to all cases we will consider: we generally assume small occupation probability at all energies, $f \ll 1$, so that we can replace Pauli blocking factors with unity, $(1 - f) \to 1$. The validity of this assumption, which limits our

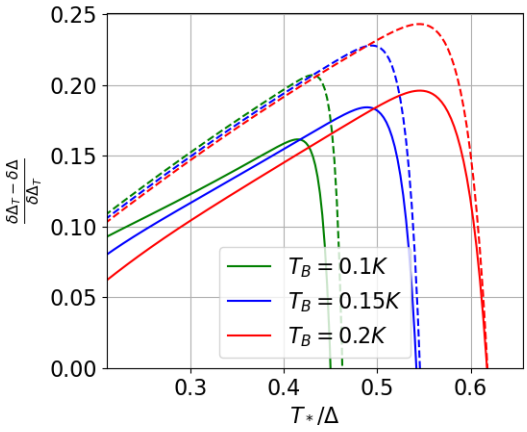

Figure 3.7.: Suppression $\delta\Delta$ of the gap as function of T_* for the same parameters used in the upper panel of Fig. 3.6. Full lines are numerical results, dashed lines correspond to the analytical formula in Eq. (3.54). The suppression is compared to that in thermal equilibrium, $\delta\Delta_T$; a positive difference $\delta\Delta_T - \delta\Delta$ corresponds to gap enhancement. The rapid change from positive to negative coincides with the onset of large nonequilibrium quasiparticle density (c.f. Fig. 3.6).

considerations to temperatures small compared to the critical one and small number of pair-breaking photons, can be checked once the solution to the kinetic equation is found; importantly, number-conserving contributions to the collision integrals [cf. Eq (3.9)] remain number conserving in this approximation. Also, except for section 3.5.4, in which we include the creation mechanism provided by diagram i) of figure 3.2, we focus on quasiparticles of low energy, $\Delta < E \lesssim 2\Delta$; assuming the phonon bath temperature T_B to be sufficiently low (at least compared to the gap, although more stringent conditions will be discussed), phonon absorption can be neglected and the phonon collision integral is approximately given by [cf. Ref. [CB19] and diagrams c), f), and g) in Fig. 3.2]

$$St^{Phon}\{f,n\} \simeq \frac{1}{\tau_0 T_c^3}\int_0^\infty d\omega\,\omega^2 \frac{2\epsilon+\omega}{\sqrt{2\Delta(\epsilon+\omega)}} f(\epsilon+\omega) - \left[\frac{128}{105\sqrt{2}}\left(\frac{\Delta}{T_c}\right)^3\left(\frac{\epsilon}{\Delta}\right)^{7/2}\frac{1}{\tau_0} + r x_{qp}\right] f(\epsilon) + St_g^{Phon} \tag{3.55}$$

where $\epsilon = E - \Delta$ is the energy measured from the gap [with a slight abuse of notation, we also substitute $f(E) = f(\Delta+\epsilon) \to f(\epsilon)$] and St_g^{Phon} is obtained from Eq. (3.11) following the steps given after Eq. (3.12). The last term inside square brackets accounts for quasiparticle recombination accompanied by phonon emission; here we have introduced the quasiparticle density normalized by the Cooper pair density,

$$x_{qp} = \frac{N_{qp}}{2\rho_F \Delta} \tag{3.56}$$

where the quasiparticle density is given by (3.41). The parameter $r = 4(\Delta/T_c)^3/\bar{\tau}_0$ is the (normalized) recombination coefficient, where $\bar{\tau}_0$ accounts for renormalization of the recombination coefficient by diagram h of figure 3.2 (c.f. (3.51)). The two terms inside square bracket in Eq. (3.55) define the energy-dependent spontaneous phonon emission rate [see eq. (C.11)]

$$\frac{1}{\tau^{qp}_{sp,n}(\epsilon)} = \frac{128}{105\sqrt{2}}\left(\frac{\Delta}{T_c}\right)^3\left(\frac{\epsilon}{\Delta}\right)^{7/2}\frac{1}{\tau_0} \tag{3.57}$$

and the density-dependent phonon-assisted recombination rate (C.14)

$$\frac{1}{\tau^{qp}_r} = r x_{qp} = R N_{qp} \tag{3.58}$$

with the recombination coefficient R (which, strictly speaking, depends weakly on energy and/or the width of the distribution function above the gap – that is, the "effective" quasiparticle temperature, – see appendix D.2, we neglect this factor-of-order-one correction in this section). The fact that the recombination time depends on the density represents the main non-linearity of the kinetic equation; as we will show, however, the density can be calculated without a detailed solution of the kinetic equation in an approach reminiscent of the phenomenological one pioneered by Rothwarf and Taylor [RT67], analogous to section 3.4.2.1. In fact, to use that approach one must also take into account the last term in the right-hand side of Eq. (3.55), namely the generation of quasiparticles by phonons; for $f \ll 1$, that term depends only on the phonon distribution function n and not on f. In this section we will not need the detailed form of St^{Phon}_g, rather the integral of its product time the quasiparticle density of states; for phonons in thermal equilibrium at temperature T_B we have

$$\int dE\, \rho(E) St^{Phon}_g = r_0 \pi T_B e^{-2\Delta/T_B} \equiv r_0 G_{T_B}/4r\rho_F \tag{3.59}$$

where r_0 is the recombination coefficient r for $\tau_l = 0$ and G_{T_B} defined in (3.49) . Two additional approximations can be introduced for the collision integral with pair-breaking photons, Eq. (3.10). First, for quasiparticles in the relevant energy range, in $St^{Phot}\{f, \bar{n}_{PB}\}$ the terms proportional to $U^+(E, E-\omega_{PB})$ [cf. Eq. (3.9)] vanish since $E - \omega_{PB} < \Delta$; we also assume that $f \ll 1$ at all energies and that the distribution function decays quickly with increasing energy, so that $f(E+\omega_{PB}) \ll f(E)\bar{n}_{PB}/(\bar{n}_{PB}+1)$, and arrive at

$$\begin{aligned} St^{Phot}\{f, \bar{n}_{PB}\} &\simeq -c^{QP}_{Phot,PB} U^+(E, E+\omega_{PB})\bar{n}_{PB} f(E) \\ &\simeq -c^{QP}_{Phot,PB}\bar{n}_{PB} f(E) = -\frac{1}{\tau^{qp}_{\mathrm{abs},PB}} f(E) \end{aligned} \tag{3.60}$$

where in the last equality we have introduced the quasiparticle lifetime against the absorption of pair-breaking photon. Second, we assume that photon-assisted recombination can be neglected in comparison to the phonon-assisted one, that is [see Eqs. (3.12) and (3.58)]

$$c^{QP}_{Phot,PB} U^-(E, \omega_{PB} - E)(1 + \bar{n}_{PB}) f(\omega_{PB} - E) \ll r x_{qp} \tag{3.61}$$

Clearly, this inequality is violated as $E \to \omega_{PB} - \Delta$ due to the divergence of the superconducting density of states; however, we will show that the violation happens so extremely close to that energy to have no impact on our results.

In closing this introductory section, we note that in all the formulas above the gap value Δ should be understood as given by the self-consistent equation for the order parameter. In the presence of a small density of quasiparticles, the gap is smaller than its no-quasiparticle value Δ_0; defining $\delta\Delta = \Delta_0 - \Delta$, at leading order we have $\delta\Delta/\Delta_0 \simeq x_{qp}$ (see Eq. (3.54)) and for most purposes the difference between Δ and Δ_0 can be ignored. One exception is the evaluation of the resonator's frequency shift, see Eq. (3.106). Another exception is when the width (in energy) of the source term is on the same order as the change in order parameter resulting from the quasiparticles - it can lead to a multivalued solution if the frequency of the source term $\omega_{PB} - 2\Delta_0 > -\delta\Delta$ is slightly below the pair breaking threshold at zero temperature, where $-\delta\Delta$ is the largest of the gap shifts forming a possible solution - in that case one solution is $\Delta = \Delta_0$ without quasiparticles, and another $\Delta = \Delta_0 - \delta\Delta$, where the pair breaking mode is above the non-equilibrium pair breaking threshold [Ele74]. Here this won't be relevant, as only the case of very low quasiparticle densities is considered, for which typical sources are expected to be much broader than $\delta\Delta$.

3.5.1. Generation by pair-breaking photons

As a first step, in this Section we study the steady-state quasiparticle distribution in the presence of pair-breaking photons only, a situation complementary to that analyzed in section 3.4 in which only non-pair-breaking photons were taken into account. Simple solutions for the quasiparticle distribution can be found in the limits of broad sources $\omega_{PB} - 2\Delta \gg \Delta$ and narrow sources $\omega_{PB} - 2\Delta \ll \Delta$ (see [GEK86] for a review). The narrow regime is characterized by a source sufficiently close to the gap such that the recombination rate greatly exceeds the rate for quasiparticle-number-conserving energy relaxation. In that regime, arising for low photon energies and not too low quasiparticle densities, quasiparticles recombine before emitting phonons, and the distribution function is determined by a balance of creation and recombination. The shape of the quasiparticle energy density in that limit is in good approximation the same as the shape of the source of excess quasiparticles. A broad source has a frequency $\omega_{PB} - 2\Delta \gg \Delta$. In that regime numerical solutions for the quasiparticle distribution function have been obtained by [Ima80] for $\omega_{PB} = 8\Delta$ and $\omega_{PB} = 20\Delta$. As quasiparticles in this regime typically relax their energy quickly for these parameter compared to recombination, the distribution shows only a weak dependence on the photon energy. Furthermore, good agreement with numerics has been obtained by phenomenological fitting the distribution to a Fermi distribution with effective temperature $\tilde{T}$ and effective chemical potential $\tilde{\mu}$ with $\tilde{\mu} < 0$ and $\tilde{T}$ exceeding the temperature corresponding to the same total quasiparticle density for a system in equilibrium, i.e. a broader distribution than would be expected when fitting a thermal distribution to the quasiparticle density. In the following, we investigate a system in between both limits $\omega_{PB} - 2\Delta \lesssim \Delta$. We will write a solution in this limit in terms

of a series successively taking a larger number of n emission processes before recombination into account. Comparing our findings to a numerical solution, we find that the series for $n = 2$, for which an analytic solution can be constructed, already gives a very good estimate to the numerical result for experimentally relevant quasiparticle densities in aluminium.

Concretely, we assume that there are no modes below the pair-breaking threshold and we set $St^{Phot}\{f, \bar{n}\} = 0$ (that is, $c^{QP}_{Phot} = 0$). We also assume that the phonons are at zero temperature, $n(\omega) = 0$, or in other words fast thermalization ($\tau_l \to 0$) with a $T_B = 0$ bath. Therefore, the kinetic equation reduces to

$$0 = St^{Phot}\{f, \bar{n}_{PB}\} + St^{Phot}_{PB,g}\{f, \bar{n}_{PB}\} + St^{Phon}\{f, n\} \tag{3.62}$$

with the pair-breaking photon collision integrals of Eqs. (3.9) [appropriately modified for pair-breaking photons] and (3.11) and the phonon collision integral of Eq. (3.55) [in which by assumption the last term accounting for generation by phonons vanishes].

Even in this simplified case, we can in principle distinguish two different regimes, depending on which process is dominant near the gap. Since at those energies phonon-assisted recombination is faster than phonon emission [$1/\tau^{qp}_{e,n}(\epsilon) \ll 1/\tau^{qp}_r$ as $\epsilon \to 0$], we should compare the rate for the former process, $1/\tau^{qp}_r$ [Eq. (3.58)], to the rate of absorption of photons, $1/\tau^{qp}_{\mathrm{abs},PB}$ [Eq. (3.60)]. We show below (Sec. 3.5.1.1) that the situation of experimental relevance for Al resonators is

$$\frac{1}{\tau^{qp}_{\mathrm{abs},PB}} \ll \frac{1}{\tau^{qp}_r} \tag{3.63}$$

In fact, to check when this inequality holds, we need to eliminate the dependence of the right-hand side on the quasiparticle density. To that end, we multiply Eq. (3.62) by $\rho(E)$, integrate over E, and use that St^{Phot} is number-conserving to find, for $f(\epsilon) \ll 1$,

$$r x^2_{qp} = \frac{2}{\Delta} \int_{\Delta}^{\omega_{PB}-\Delta} dE\, \rho(E) St^{Phot}_{PB,g} = 2 c^{QP}_{Phot,PB} \bar{n}_{PB} S_-(2 + \xi/\Delta) \tag{3.64}$$

where

$$\xi = \omega_{PB} - 2\Delta \tag{3.65}$$

and the structure factor $S_-(x)$ [Hou+19; GC21] has the approximate form $S_-(x) \simeq \pi(x-2)/2$ for $x - 2 \ll 2$. Using Eq. (3.64), the inequality in Eq. (3.63) can be rewritten as

$$c^{QP}_{Phot,PB} \bar{n}_{PB} \ll \pi r \xi/\Delta \tag{3.66}$$

where from now on we assume $\xi < \Delta$ ($\omega_{PB} < 3\Delta$). When the above condition is true, in most cases quasiparticles created by photon pair breaking relax towards the gap and/or recombine by phonon emission before they can absorb a photon; indeed, the condition can be satisfied if the number of photons is sufficiently small. If a photon is

absorbed before a recombination event, this will lead to a second peak in the quasiparticle distribution function at energies above 3Δ. At those energies, quasiparticle relaxation by phonon emission is much faster than near the gap, so assuming that to be the dominant process, one can treat the second peak in a perturbative way, similarly to the "cold" regime of Ref. [CB19]. We do not pursue this approach further in this section, since if the condition in Eq. (3.63), or equivalently Eq. (3.66), is satisfied, the effect of the second peak can be neglected and only energies $\epsilon < \xi$ are relevant (see, however, Sec. 3.5.3 for the expression for the second peak).

So long as Eq. (3.63) holds, we can further simplify Eq. (3.62) by ignoring the first term on the right-hand side to get

$$St^{Phot}_{PB,g}\{f, \bar{n}_{PB}\} = -St^{Phon}\{f, n\} \tag{3.67}$$

Next, we introduce the dimensionless energy variable

$$\gamma = \epsilon/\xi \tag{3.68}$$

and the function

$$\phi(\gamma) = \sqrt{\frac{2\Delta}{\xi}} \frac{r x_{qp}}{c^{Phot}_{QP,PB} \bar{n}_{PB}} \left[\left(\frac{\gamma}{\gamma'_*} \right)^{7/2} + 1 \right] f(\xi\gamma) \tag{3.69}$$

where the dimensionless parameter

$$\gamma'_* = \left(\frac{\tau^{qp}_{e,n}(\xi)}{\tau^{qp}_r} \right)^{2/7} = \left(\frac{105\sqrt{2}\, x_{qp}}{32} \right)^{2/7} \frac{\Delta}{\xi} \tag{3.70}$$

determines whether at the highest energy at which quasiparticles are generated (that is, $\epsilon = \xi$) recombination is faster, $\gamma'_* > 1$, or slower, $\gamma'_* < 1$, than relaxation by phonon emission. With this notation, the steady-state equation (3.67) takes the form of a Volterra integral equation of the second kind

$$\frac{1}{\sqrt{1-\gamma}} = \phi(\gamma) - \int_{\gamma}^{1} d\gamma' I(\gamma, \gamma') \phi(\gamma') \tag{3.71}$$

with the kernel

$$I(\gamma, \gamma') = \frac{105}{128} \frac{\gamma + \gamma'}{\sqrt{\gamma'}} \frac{(\gamma - \gamma')^2}{(\gamma'_*)^{7/2} + (\gamma')^{7/2}} \tag{3.72}$$

In Eq. (3.71) the first term on the right-hand side accounts for quasiparticle outscattering by spontaneous phonon emission and the second one for the corresponding in-scattering process; in that term the upper limit of integration is set to 1 consistently with ignoring absorption of pair-breaking photons and thus occupation at energies $\epsilon > \xi$, as discussed earlier in this section. The term on the left-hand sides originates from the quasiparticle generation by photons; its divergence as $\gamma \to 1$ originates from the diverging density of states and, as we will see, leads to a divergent distribution

function. This unphysical divergence is in fact cut off by the Pauli blocking factors that we have neglected by assuming $f \ll 1$; however, the divergence is integrable and to our knowledge it does not lead to unphysical behavior of any observable, so it is not further considered.

Depending on the value of γ'_* we can distinguish two cases. For $\gamma'_* \gtrsim 1$, the solution to Eq. (3.71) can be given in terms of a Neumann series [Bru17a]

$$\phi(\gamma) = \sum_{j=0}^{\infty} \phi^{(j)}(\gamma) \tag{3.73}$$

with $\phi^{(0)}(\gamma) = 1/\sqrt{1-\gamma}$ and

$$\phi^{(j)}(\gamma) = \int_{\gamma}^{1} d\gamma' I(\gamma,\gamma')\phi^{(j-1)}(\gamma') \tag{3.74}$$

over the whole range $\gamma \in [0,1]$. In fact, for $\gamma'_* \gg 1$ we can ignore $(\gamma')^{7/2}$ in the denominator of the kernel, Eq. (3.72), and readily see that the terms in the series are suppressed by $(\gamma'_*)^{-7j/2}$.

The second case, $\gamma'_* \ll 1$, is relevant to small quasiparticle density. In this case the solution has to be constructed differently. For $\gamma \gg \gamma'_*$, the kernel can be simplified to

$$I(\gamma,\gamma') \simeq \tilde{I}(\gamma,\gamma') \equiv \frac{105(\gamma'-\gamma)^2(\gamma+\gamma')}{128(\gamma')^4} \tag{3.75}$$

Using this simplified kernel, the solution to Eq. (3.71) can again be written as a Neumann series, Eq. (3.73), but using the approximate kernel $\tilde{I}$ in Eq. (3.74) instead of I. The first and second order terms can be calculated analytically and are given in Appendix F.1. In fact, such a solution is valid under a weaker assumption than $\gamma \gg \gamma'_*$: Using the simplified kernel is a good approximation if the dominant contribution to the integral in Eq. (3.71) comes from the interval $\gamma' \in [\gamma'_*, 1]$. This holds for $\gamma \gg \gamma_*$, with γ_* defined by

$$\int_{\gamma'_*}^{1} d\gamma' \phi(\gamma')\tilde{I}(\gamma_*,\gamma') = \int_{\gamma_*}^{\gamma'_*} d\gamma' \phi(\gamma')\tilde{I}(\gamma_*,\gamma') \tag{3.76}$$

(using the simplified kernel in the left-hand side is a reasonable approximation, while using it in the right-hand side overestimates the value of that integral, since the full kernel is smaller than the simplified one for small γ'; this leads to a conservative estimate for γ_*). While γ'_* determines whether out-scattering at energy γ is dominated by spontaneous phonon emission ($\gamma > \gamma'_*$) or recombination ($\gamma < \gamma'_*$), γ_* distinguish whether in-scattering mostly originates from states for which spontaneous phonon emission ($\gamma > \gamma_*$) or recombination dominates ($\gamma < \gamma_*$). Equation (3.76) can be solved numerically using a bisection algorithm, the solution is presented in Fig. 3.8. We see there that γ_* is at least an order of magnitude smaller than γ'_*; taking the

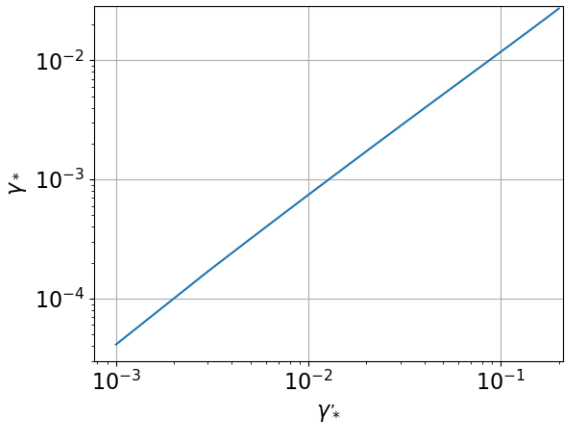

Figure 3.8.: Numerically calculated γ_* as function of γ'_*, determining the range of validity $\gamma > \gamma_*$ for the validity of the Neumann series constructed using the simplified kernel in Eq. (3.75).

geometrical average between the two quantities, we then estimate that the Neumann series constructed with the simplified kernel is a good approximation for $\gamma \gtrsim \gamma_c \equiv \gamma'_*/3$.

Except for the zeroth order, the terms in the "simplified" Neumann series diverge as $\gamma \to 0$; this is a result of the use of the simplified kernel, which has a non-integrable singularity for $\gamma = 0$ as $\gamma' \to 0$, while the exact kernel approaches zero in that limit. Thus, the solution for $\gamma \lesssim \gamma_c$ must be constructed differently. We proceed by considering a series expansion for ϕ up to third order in γ,

$$\phi(\gamma) = a_0 + a_1\gamma + a_2\gamma^2 + a_3\gamma^3. \tag{3.77}$$

Neglecting small factors of order $(\gamma_c/\gamma'_*)^{7/2}$ and higher, the lower integration limit in the right-hand side of Eq. (3.71) can be set to zero, and for consistency the left-hand side should be expanded also only up to third order in γ. Then the expansion coefficients for ϕ are given by

$$\begin{aligned} a_0 &= 1 + I_0\,, \\ a_1 &= \frac{1}{2} - I_1\,, \\ a_2 &= \frac{3}{8} - I_2\,, \\ a_3 &= \frac{5}{16} + I_3 \end{aligned} \tag{3.78}$$

with

$$I_l = \frac{105}{128}\int_0^1 d\gamma'\phi(\gamma')\frac{\gamma'^{5/2-l}}{\gamma'^{7/2}+\gamma'^{7/2}_*}\,. \tag{3.79}$$

In this expression ϕ should be understood as the exact solution, extending over the whole interval $[0, 1]$. The coefficients can be then calculated numerically, see the dots

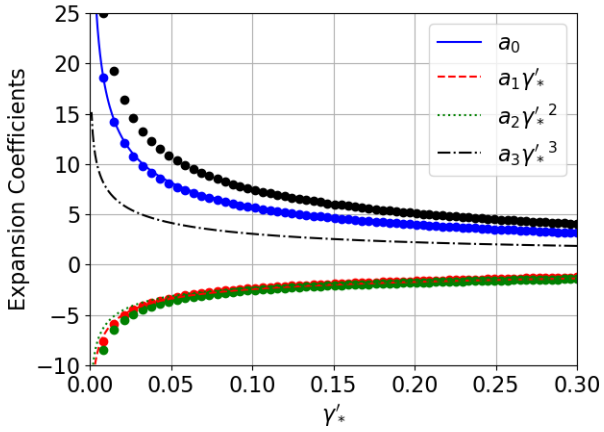

Figure 3.9.: Coefficients of the low-energy expansion for ϕ, Eq. (3.77). For better visibility, the products $a_l(\gamma'_*)^l$, $l = 0$ to 3, are plotted. Points are calculated using the numerical result for ϕ in Eq. (3.79), while lines using the approximate Neumann series as described in the text.

in Fig. 3.9. However, for an approximate estimate of the coefficients, we can set the lower integration limit in Eq. (3.79) to γ_c and use the "simplified" Neumann series solution for ϕ including terms up to $j = 2$ (see Appendix F.1). The approximate coefficients calculated in this way are shown as lines; except for a_3, we find good agreement between exact and approximate coefficients. For later use, we note that $a_0 \simeq 0.073\log^3(12/\gamma'_*) - 0.35\log^2(12/\gamma'_*) + 1.23\log(12/\gamma'_*)$ is a good approximation in the range covered by the dots in Fig. 3.9 (the dependence on powers of the logarithm originates from the behavior of $\phi^{(j)}$, $j = 0, 1, 2$, at small γ, while the numerical coefficients are obtained by comparison to the numerics.

We exemplify the results obtained in this section in Fig. 3.10. The black lines show the distribution function as obtained by numerical solution of the kinetic equation, while the colored lines are the analytical approximations. Both the "simplified" Neumann series [cf. Eq. (3.73)] and the low-energy expansion [Eq.(3.77)] are in excellent agreement with the numerical results in their respective regimes of validity.

The consideration of this Section can be straightforwardly generalized to account for multiple pair-breaking modes: to determine the quasiparticle density x_{qp}, it suffices to replace the right-hand side of Eq. (3.64) with its sum over all modes. Then, Eq. (3.67) [or equivalently Eq. (3.71)] being linear in the distribution function, it can be solved for the contribution $f_i(\xi_i\gamma_i)$ of each pair-breaking mode i as for a single mode. The distribution function f is finally given by the sum over all f_i.

3.5.1.1. Validity of assumptions

In obtaining the approximate solution for the distribution function, we made a number of assumptions whose validity depend on parameters such as the recombination rate r and the quasiparticle-phonon coupling constant $c^{QP}_{Phot,PB}$; for aluminum, as or-

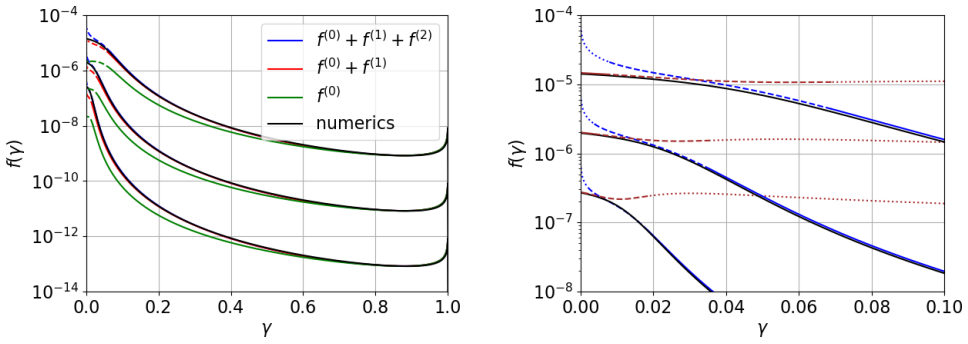

Figure 3.10.: Shape of the quasiparticle distribution for different pair-breaking photon numbers and $\omega_{PB} = 2.8\Delta$. Numerical results are displayed in black, different orders of the Neumann series [cf. Eq. (3.73)] in green ($j = 0$), red ($j \leq 1$) and blue ($j \leq 2$). The different photon numbers correspond to (top to bottom) $c^{QP}_{Phot,PB}\bar{n}_{PB} = 10^{-2}$, 10^{-4}, and 10^{-6} Hz; other parameters are $\tau_0 = 63\,\mathrm{ns}$, $\Delta = 189\,\mu\mathrm{eV}$, and $\tau_l = 0$, resulting in effective generation temperatures $\bar{T}_B \simeq 180\,\mathrm{mK}$, 150 mK, and 130 mK, respectively [c.f. Eq. (3.83)]. The bottom plot zooms into the low-energy region. Here, the Neumann series (up to second order) has been displayed with blue solid lines for $\gamma > \gamma'_*$, blue dashed lines for $\gamma'_* > \gamma > \gamma_*$ and blue dotted lines for $\gamma < \gamma_*$, while the low energy expansion [Eq. (3.77)] with solid brown lines for $\gamma < \gamma_c$, dashed lines for $\gamma_c < \gamma < \gamma'_*$, and dotted lines for $\gamma > \gamma'_*$.

der of magnitude we take $r \simeq 10^7\,\mathrm{Hz}$ [Wan+14], and we estimate in Appendix E.2 that for resonators of this material $c^{QP}_{Phot,PB} \simeq 10\,\mathrm{Hz}$. The condition in Eq. (3.66) can be interpreted as a bound on the number of pair-breaking photons, which with these parameters reads $\bar{n}_{PB} \ll 10^6 \xi/\Delta$. Even for pair-breaking photons near the threshold ($\xi \to 0$), this condition is in practice always satisfied for $\bar{n}_{PB} \lesssim 1$: while for sub-gap photons high quality factors of order 10^6-10^7 are possible [Vis+14; Val+19], the quality factor of above-gap modes is more than two orders of magnitude smaller, see Appendix E.2; this implies $\xi/\Delta > 10^{-5}$, since the frequency of the pair-breaking mode is known with relative precision given by the inverse quality factor. Alternatively, for pair-breaking photons of sufficient energy, $\xi/\Delta > 0.1$, the bound on the photon number becomes $\bar{n}_{PB} < 10^5$. We note that if Eq. (3.66) holds, then we also find from Eq. (3.64) that $x_{qp} \ll 1$; this ensures that the suppression of the gap $\delta\Delta/\Delta \simeq x_{qp}$ can also be neglected for the purposes of this section.

We now turn to the validity of Eq. (3.61), that is, negligibility of photon-mediated recombination. Setting $\varepsilon = \omega_{PB} - \Delta - E$, in the limit $\varepsilon \to 0$ (i.e., $\epsilon \to \xi$) we can rewrite that inequality in the form

$$\frac{\varepsilon}{\xi} \gg \left(\frac{a_0}{2\pi}\right)^2 \left[\frac{c^{QP}_{Phot,PB}(1+\bar{n}_{PB})}{r}\right]^2 \tag{3.80}$$

where we used Eqs. (3.69) and (3.77). For $\bar{n}_{PB} \gg 1$ and assuming $\gamma'_* \gtrsim 1$, we have $a_0 \simeq 1$ and, for the parameter discussed above we have $\varepsilon/\xi \gg 10^{-14}\bar{n}^2_{PB}$; even at the upper bound $\bar{n}_{PB} \simeq 10^5$ determined in the previous paragraph, the right-had side is small, of order 10^{-4}. In the opposite regime $\bar{n}_{PB}$, $\gamma'_* < 1$, the first factor on the right-hand side is of order unity (as can be verified by inspection of Fig. 3.9 or by using the approximate analytical expression for a_0 given previously) and the second factor is $\sim 10^{-12}$, meaning that the requirement becomes significantly less stringent. Therefore, recombination by photon emission can be ignored.

At the beginning of this section, we assumed that there are no other modes beside that of the pair-breaking photons by setting $c^{QP}_{Phot} = 0$. If such a mode is present ($c^{QP}_{Phot} > 0$), even if it is unpopulated ($\bar{n} = 0$) it can in principle affect the distribution function, since quasiparticles could relax by emitting a photon of energy ω_0. However, similarly to the process of photon-mediated recombination considered in the previous paragraph, we now show that we can ignore this relaxation mechanism. Indeed, this mechanism is accounted for by the last line of Eq. (3.9), and the corresponding relaxation rate diverges for $\epsilon \to \omega_0$. We compare this rate to that of relaxation by phonon emission, Eq. (3.57) (assuming that $1/\tau^{qp}_{e,n}(\omega_0) > 1/\tau^{qp}_r$, as we expect to be the case at low temperature and hence quasiparticle density); we find the condition

$$c^{QP}_{Phot}\sqrt{\frac{2\Delta}{\tilde{\varepsilon}}} \ll \frac{128}{105\sqrt{2}}\left(\frac{\Delta}{T_c}\right)^3\left(\frac{\omega_0}{\Delta}\right)^{7/2}\frac{1}{\tau_0} \tag{3.81}$$

where $\tilde{\varepsilon} = \omega_0 + \Delta - E \ll \omega_0$. This inequality is equivalent to

$$\tilde{\varepsilon}/\Delta \gg (\Delta/\omega_0)^7 (105 c^{QP}_{Phot}/16 r_0)^2 \tag{3.82}$$

and using $c_{Phot}^{QP} \simeq 1\,\mathrm{Hz}$ (see Appendix E.2), we estimate that the second factor on the right-hand side is small, of order 10^{-13}; while the first factor could in principle be large, since $\omega_0 \ll 2\Delta$, in practice the resonators are designed to have modes in the frequency range above at least a couple of GHz, in which case $(\Delta/\omega_0)^7 \lesssim 10^9$. Hence, we conclude that the above condition is violated only for energy so close to $\Delta + \omega_0$ as to not affect the quasiparticle distribution. In fact, the numerical solutions displayed in Fig. 3.10 were obtained with $c_{Phot}^{QP} = 1\,\mathrm{Hz}$ and $\omega_0/2\pi = 4.84\,\mathrm{GHz}$ and show no significant deviation from the analytical approximation derived assuming $c_{Phot}^{QP} = 0$.

Finally, we also assumed that we can ignore phonons by setting $T_B = 0$ and $\tau_l = 0$. Even within the assumption of fast thermalization ($\tau_l \ll \tau_0^{PB}$), thermal phonons with $T_B > 0$ can generate quasiparticles by breaking Cooper pairs; therefore, a necessary condition to ignore them is that this generation mechanism gives a negligible contribution to the quasiparticle density. By comparing the second equality in Eq. (3.64) (that is, the quasiparticle density generation rate due to pair-breaking photons) to the thermal phonon generation rate [Eq. (3.58)], we define the crossover (or effective generation) temperature

$$\bar{T}_B = \frac{2\Delta}{W\left(\frac{4r_0}{c_{Phot,PB}^{QP}\bar{n}_{PB}}\frac{\Delta}{\xi}\right)} \tag{3.83}$$

with W with the Lambert (product logarithm) function. For $T_B > \bar{T}_B$ thermal phonons are the main source of quasiparticles, while for $T_B < \bar{T}_B$, the dominant generation mechanism is photon pair breaking and $\bar{T}_B$ gives the temperature at which quasiparticles in thermal equilibrium would have the same density as those generated by the photons. For the typical parameters discussed above ($r_0 = 10^7$ Hz, $c_{Phot,PB}^{QP} = 10\,\mathrm{Hz}$), even for photons with frequencies close to the pair-breaking threshold, $\xi/\Delta = 10^{-3}$, and a low occupation probability, $\bar{n}_{PB} = 10^{-10}$, we estimate a relatively high crossover temperature $\bar{T}_B > 100\,\mathrm{mK}$. In fact, for the crossover temperature to go below e.g. 20 mK the photon occupation probability should be extremely small, $\bar{n}_{PB} < 10^{-84}$, so ignoring generation by thermal phonons should likely be a good approximation for typical low-temperature experiments; in our examples in the plots in Fig. 3.10 we have assumed $\bar{n}_{PB} \geq 10^{-7}$.

While the condition $T_B < \bar{T}_B$ implies that the density is not affected by thermal phonons, it is not sufficient to ensure that they do not alter the shape of the quasiparticle distribution. A more stringent condition is found by requiring that the rate of phonon absorption at the gap is small compared to the recombination rate [as defined in Appendix C, the former rate is approximately given by $3/\tau_{e,n}^{qp}(T_B)$], or equivalently by requiring that the typical energy gained by absorbing a phonon is small compared to the width of the distribution in the absence of phonons, $T_B < \gamma'_* \xi$. These requirements can be expressed as $x_{qp} > (T_B/\Delta)^{7/2}$. With the same parameters used above and assuming $\xi > 0.1\Delta$, for $T_B = 10\,\mathrm{mK}$ we estimate, using Eq. (3.64), that the condition is satisfied for $\bar{n}_{PB} > 10^{-8}$. The bound becomes more stringent as the phonon temperature increases; we do not explore this higher temperature regime further here, as we focus next on a competing mechanism affecting the distribution shape, namely

the absorption and emission of non-pair-breaking photons.

The results of this Section show that at low temperature a small number or photons above the pair-breaking threshold can lead to experimentally relevant quasiparticle densities. In fact, using Eqs. (3.64) and (3.69) one can show that if both ξ and γ'_* are not too small compared to unity, then $f(0)$ (cf. Fig 3.10) is of the same order of magnitude as the normalized density x_{qp}, which in various experiments has been estimated to range between 10^{-9} and 10^{-5} (see [CP22] and references therein). Even the width $\sim \gamma'_*\xi$ of the quasiparticle distribution can be determined by the interplay between pair breaking by photons and recombination, rather than by absorption of thermal phonons. This could happen in particular in superconducting qubits, for which pair-breaking photons can contribute directly to qubit transitions as well as to quasiparticle generation [Dia+22; MAC22], although the actual shape of the distribution function is likely affected by the fact that typically the films forming the qubit's junction have different gaps. While qubits are by necessity operated in a regime where at most a few non-pair-breaking photons are present, this is not the case for resonators, where the large number of non-pair breaking photons can determine the distribution's shape, as we discuss next.

Finally, we note that while this section assumed pair breaking due to photons, the fact that the balance of recombination and pair breaking provides a minimal width (in energy) for the quasiparticle distribution is valid for general generation mechanisms. This observation will be important in chapter 4.

3.5.2. Perturbative regime

We begin by investigating the effect of a small number of non-pair-breaking photons of frequency $\omega_0 < 2\Delta$ on the quasiparticle distribution function. We assume that the approximations employed in Sec. 3.5.1 are still applicable, so that the steady-state kinetic equation becomes [cf. Eq. (3.67)]

$$0 = St^{Phon}\{f,n\} + St^{Phot}_{PB,g}\{f,\bar{n}_{PB}\} + St^{Phot}\{f,\bar{n}\} \tag{3.84}$$

with $St^{Phot}\{f,\bar{n}\}$ given by Eq. (3.9). Simplifying that equation in the regime of low quasiparticle energies ($\epsilon < \Delta$) and densities ($f \ll 1$) we get

$$\begin{aligned} St^{Phot}\{f,\bar{n}\} \simeq\ & c^{QP}_{Phot}\sqrt{\frac{2\Delta}{\epsilon+\omega_0}}\left[f(\epsilon+\omega_0)(\bar{n}+1) - f(\epsilon)\bar{n}\right] \\ & + c^{QP}_{Phot}\sqrt{\frac{2\Delta}{\epsilon-\omega_0}}\left[f(\epsilon-\omega_0)\bar{n} - f(\epsilon)(\bar{n}+1)\right] \end{aligned} \tag{3.85}$$

where the last line vanishes for $\epsilon < \omega_0$.

In the previous subsection we have considered already when the effect of this term is negligible in the case $\bar{n} = 0$ by focusing on the decay rate associated with the last term on the right-hand side of Eq. (3.85) [a finite $\bar{n}$ adds the factor $(1+\bar{n})$ to the left-hand side of condition (3.81)]. For finite but small occupation, $\bar{n} \lesssim 1$, to find a necessary

condition enabling us to treat the non-pair-breaking photons as a perturbation we consider the absorption rate arising from the second term in the first square brackets, which is highest at the lowest energies $\epsilon < \omega_0$ at which the second line of Eq. (3.85) is zero [at higher energies, the photon absorption accounted for by the first term in the second square brackets should also be considered]; we then compare that rate to the recombination rate, Eq. (3.58), to find the condition

$$\bar{n} \ll \frac{r x_{qp}}{c_{Phot}^{QP}} \sqrt{\frac{\omega_0}{2\Delta}} \tag{3.86}$$

where x_{qp} depends on $\bar{n}_{PB}$ as follows from Eq. (3.64). Assuming the inequality holds, we write the quasiparticle distribution in the form

$$f(\epsilon) = f_0(\epsilon) + \delta f(\epsilon) \tag{3.87}$$

where f_0 is the steady-state distribution in the absence of low-energy photons, $\bar{n} = 0$, and the kinetic equation can be rewritten as

$$St^{Phot}\{f, \bar{n}\} + St^{Phon}\{\delta f\} = 0 \tag{3.88}$$

where in the phonon collision integral we dropped the explicit dependence on the phonon distribution as we assume zero temperature, $n = 0$ (this implies in particular $St_g^{Phon} = 0$). Although the photon collision integral in Eq. (3.9) accounts only for emission or absorption of a single photon at a time, consecutive absorption processes uninterrupted by phonon emission lead to peaks in the energy distribution function at multiples of the photon energy. Thus, we seek an expression for δf in form of an expansion $\delta f = f_1 + f_2 + ...$ using an iterative approach to find f_m once f_{m-1} is known:

$$St^{Phot}\{f_{m-1}, \bar{n}\} + St^{Phon}\{f_m\} = 0 \tag{3.89}$$

with $m = 1, 2, ...$

To find an explicit expression for f_m, $m \geq 1$, we ignore the in-scattering part of $St^{Phon}\{\delta f\}$ – that is, the first term on the right-hand side of Eq. (3.55); we will comment below on this step. We also assume $1/\tau_{e,n}^{qp}(\omega_0) > 1/\tau_r^{qp}$, so that for $\epsilon > \omega_0$ we can ignore the term proportional to x_{qp} in St^{Phon}. Furthermore, we note that in St^{Phot} there is at each iteration a term that diverge as $\epsilon \to m\omega_0$ originating from the last line in Eq. (3.85). Of the two terms in square brackets there, we expect the first one to be dominant; in other words, we assume

$$f_m(\epsilon) \gg f_m(\omega_0 + \epsilon)(\bar{n} + 1)/\bar{n}. \tag{3.90}$$

With these simplifications, we find peaks for $\epsilon > m\omega_0$ with approximate shape

$$\begin{aligned} f_m(\epsilon) \simeq & \left(\frac{T_*}{\omega_0}\right)^{6m} \sqrt{\frac{\omega_0}{\epsilon - m\omega_0}} f_0(\epsilon - m\omega_0) \\ & \times \left(\frac{\omega_0}{\epsilon}\right)^{7/2} \Pi_{j=1}^{m-1} \left(\frac{\omega_0}{\epsilon - j\omega_0}\right)^4 \end{aligned} \tag{3.91}$$

with T_* defined in (3.23). The value of T_* being larger than ω_0 means that the non-pair-breaking photons are effective at heating the quasiparticles [cf. [CB19] and section 3.4.1]; similarly, here it can counteract the fast suppression of the amplitude of the peaks caused by the terms in the second line in Eq. (3.91) being approximately $1/m^{7/2}[(m-1)!]^4$ for $\epsilon \simeq m\omega_0$.

The result for the peaks in Eq. (3.91) is compatible with Eq. (3.90) so long as $\bar{n} > 1/(m+1)^4$. We can also estimate if a given peak is visible by comparing its amplitude (which we estimate at $\epsilon = m\omega_0 + \gamma'_*\xi$) to the value of f_0 at the peak's position. We thus find the "visibility condition"

$$\left(\frac{T_*}{\omega_0}\right)^{6m} \frac{1}{[(m-1)!]^4} \gg \frac{105}{16}\sqrt{\frac{2\gamma'_*\xi}{\Delta}}\left(\frac{\Delta}{\omega_0}\right)^4 \frac{x_{qp}}{a_0} \tag{3.92}$$

where we assumed $\omega_0 > \gamma'_*\xi$. Using this expression, one can for instance check under which conditions the first peak is visible while at the same time Eq. (3.86) holds. More interestingly, for a given choice of parameters as m increases the left-hand side decreases, so there is a last visible peak which we denote with index m_l (we have implicitly assumed that $m_l < \xi/\omega_0$, so that it is consistent to ignore occupation at energies $\epsilon > \xi$ as in Sec. 3.5.1). For $m > m_l$, it is reasonable to set $f_m = 0$; in turn, this makes it possible to understand why Eq. (3.91) gives a good description of the last peak but not necessarily of lower-index peaks. Indeed, in our derivation we have ignored the first term on the right-hand side of Eq. (3.55); considering the contribution of that term to Eq. (3.88) for $\epsilon > m\omega_0$, one can check that the integral between ϵ and $(m+1)\omega_0$ can be ignored compared to the first term in square brackets in Eq. (3.55). At energies just above $(m+1)\omega_0$, the integral is dominated by the f_{m+1} term, which we ignore for $m = m_l$. On the other hand, taking for example $m = m_l - 1$, the m_l peak gives a non-negligible contribution to the integral, a contribution that accounts for quasiparticle relaxing to lower energies by emitting phonons; this mechanism then leads to the lower-index peaks to be broader than what Eq. (3.91) predicts. In Fig. 3.11 we show with points the results of numerical solutions of the kinetic equation simulation for different number of non-pair-breaking photons. Only for the smallest number Eq. (3.86) holds; nonetheless, in all cases the number of visible peaks agrees with the expectation from Eq. (3.92) and the last visible peak is well described by Eq. (3.91), see the solid lines.

3.5.3. Heating regime

We next consider the regime in which there are many non-pair-breaking photons, such that they can heat the quasiparticles, $T_* > \omega_0$. Even if this condition is met, the pair-breaking photons could affect the shape of the distribution function; therefore, we additionally require that the generation of quasiparticles can be ignored at lowest order, so that the results of section 3.4.1 can be used as a starting point. Near energy

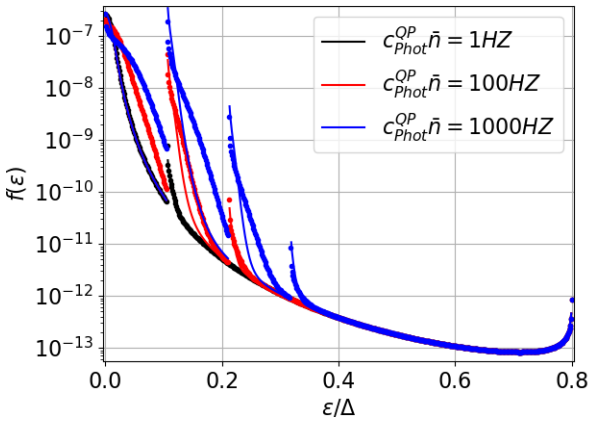

Figure 3.11.: Distribution function in the presence of non-pair-breaking photons in the perturbative regime. The dots are obtained by solving the kinetic equation numerically with parameters $\omega_{PB} = 2.8\Delta$, $\tau_l = 0$, $\tau_0 = 63\,\mathrm{ns}$, $\Delta = 189\,\mu\mathrm{eV}$, $c^{QP}_{Phot,PB}\bar{n}_{PB} = 10^{-6}\mathrm{Hz}$, and the values of $c^{QP}_{Phot}\bar{n}$ given in the inset. The solid lines are calculated using Eq. (3.91).

ξ we can approximate the photon generation collision integral, Eq. (3.11), as

$$St^{Phot}_{PB,g} \simeq c^{QP}_{Phot,PB}\bar{n}_{PB}\frac{\xi}{\sqrt{2\Delta(\xi-\epsilon)}} \tag{3.93}$$

which diverges as $\epsilon \to \xi$; however, since the width of the peaks in the distribution function is limited by the photon frequency ω_0, for our estimates we replace $\xi - \epsilon \to \omega_0$. If the shape is determined by the balance between phonon emission and the absorption/emission of non-pair-breaking photons, the above contribution from $St^{Phot}_{PB,g}$ should be small in comparison to, for instance, the phonon collision integral, or more precisely the term proportional to $(\epsilon/\Delta)^{7/2}$ in Eq. (3.55), where we can use equation (3.25)

$$f(\epsilon) \simeq \frac{3\times 2^{1/6}}{4.2\sqrt{2\pi}} x_{qp}\sqrt{\frac{\Delta}{\epsilon}}\, e^{-(\epsilon/T^*)^3/3} \tag{3.94}$$

for $\epsilon = \xi$. Assuming that the quasiparticle density is determined by the photon pair-breaking mechanism and hence given by Eq. (3.64), we arrive at the condition

$$\frac{T_*}{\xi} \gtrsim \left\{-3\ln\left[3.27 x_{qp}\left(\frac{\Delta}{\xi}\right)^3\sqrt{\frac{\Delta}{\omega_0}}\right]\right\}^{-1/3} \tag{3.95}$$

For the parameters of Fig. 3.11 this correspond to $T_*/\xi \gtrsim 0.29$, while for the highest photon number there we estimate $T_*/\xi \simeq 0.1$. Even doubling the value of T_* so that $T_*/\xi = 0.2$ (or $c^{QP}_{Phot}\bar{n} \simeq 8.2\times 10^4\,\mathrm{Hz}$), see Fig. 3.12, the considerations of the previous subsection are still valid with minor modifications. For example, according

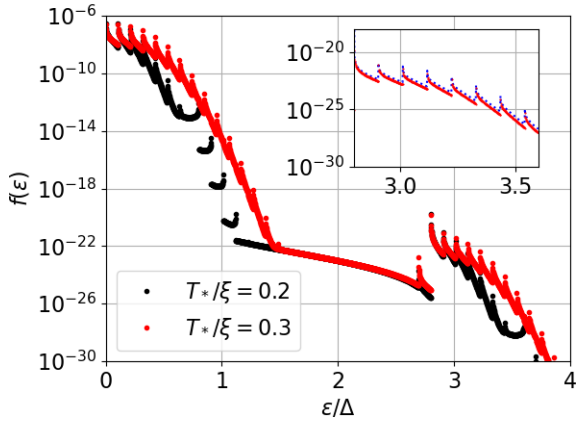

Figure 3.12.: Distribution function in the crossover from perturbative to heating regimes as identified by Eq. (3.95). We use the same parameters as in Fig. 3.11 except for the photon number $\bar{n}$, given in the bottom left inset in terms of the ratio between T_* of Eq. (3.23) and ξ of Eq. (3.65). The top right inset shows the second peak at energies $\epsilon > \omega_{PB}$, with the blue dashed curve corresponding to Eq. (3.96) where $f(\epsilon)$ is the numerically calculated distribution function at low energies.

to Eq. (3.92) the $m = 7$ peak should be the last visible one, but since that peak is close in energy to ξ, the right-hand side of that equation should be multiplied by a factor of order $\sqrt{\xi/\omega_0}$; including this factor, we find that the inequality holds only weakly. Further increasing T_* above the threshold value by setting $T_*/\xi = 0.3$ ($c^{QP}_{Phot}\bar{n} \simeq 9.3 \times 10^5\,\mathrm{Hz}$), the shape of the distribution function follows the predictions of section 3.4.1 up to energies beyond ξ.

In Fig. 3.12 it is evident that the distribution function changes qualitatively at a crossover energy $\epsilon_c > \xi$, becoming mostly smooth in the range $\epsilon_c \lesssim \epsilon \lesssim \omega_{PB}$. We ascribe this smooth part to "excess" quasiparticles relaxing by phonon emission (and/or scattering with non-pair-breaking photons), the excess being understood as the second broad peak at energies above ω_{PB}. As mentioned in Sec. 3.5.1, this second peak is due to the absorption of pair-breaking photons, and can be found by following the approach of Ref. [CB19] [cf. Eq. (8) there]:

$$f(\omega_{PB}+\epsilon) \simeq \frac{\bar{n}_{PB} f(\epsilon)/(1+\bar{n}_{PB})}{1+\frac{1}{12}\frac{r_0}{c^{QP}_{Phot,PB}}\left(\frac{\omega_{PB}}{\Delta}\right)^3\sqrt{\frac{2\epsilon}{\Delta}}\frac{\Delta+\omega_{PB}}{2\Delta+\omega_{PB}}}; \tag{3.96}$$

we compare this equation to numerical calculations in the top right inset of Fig. 3.12. These modifications affect the distribution only at the relatively large energies $\epsilon > \epsilon_c$ and, as explained in Sec. 3.5.1, do not contribute significantly to quasiparticle creation even when considering a finite phonon thermalization time (see also the next subsection). Furthermore, since usually $r_0 \gg c^{QP}_{Phot,PB}$, the second peak is much smaller than the first one and thus does not appreciably affect measurable properties

like the quality factor of a resonator.

3.5.4. Quasiparticle density and its fluctuations

So far, we have assumed that quasiparticle generation by phonons can be ignored. Once we enter the heating regime, however, the distribution function is not significantly affected by the pair-breaking photons, so that the latter can only influence the overall quasiparticle density. Therefore, in this regime we can extend the generalized Rothwarf-Taylor equation (3.48) determining the quasiparticle density by including contributions from both pair-breaking phonons and photons,

$$\frac{dN_{\rm qp}}{dt} = G_{T_B} + G_{\bar{T}_B} + G(T_*/\Delta)N_{\rm qp} - RN_{\rm qp}^2 \tag{3.97}$$

with G_{T_B} of Eq. (3.59) and $G_{\bar{T}_B}$, accounting for pair-breaking photons, obtained from G_{T_B} by replacing $r \to r_0$ and $T_B \to \bar{T}_B$, see Eq. (3.83); this is equivalent to

$$G_{\bar{T}_B} = 2\pi\rho_F c^{QP}_{Phot,PB}\bar{n}_{PB}\xi \tag{3.98}$$

The term linear in $N_{\rm qp}$ depends on T_* because it describes generation by nonequilibrium phonons emitted by quasiparticles heated by the non-pair-breaking photons to energies above 3Δ and is given in eq. (3.52), corresponding to diagram i) in figure 3.2. Equation (3.97) can be derived as in section 3.4.2 by multiplying Eq. (3.1) by $\rho(E)$ and integrating it over energy; the photon integral creating quasiparticles St_g^{phot} contributes $G_{\bar{T}_B}$ while the other terms remain unchanged compared to section 3.4.2.

Clearly, as far as the density is concerned, pair-breaking phonons and photons play the same role; for $r \sim r_0$, as discussed after Eq. (3.83) one of the two generation mechanisms is dominant, depending on which of the two temperatures, T_B or $\bar{T}_B$, is the largest. Then defining $T_G = \max\{T_B, \bar{T}_B\}$ and T_B^* as in Sec. 3.4.1.2, we can distinguish two steady-state regimes, in analogy to those discussed in Sec. 3.4.2.1 in the absence of pair-breaking photons. At high heating, $T_B^* > T_G$, we can neglect the first two terms on the right-hand side and find $N_{qp,0} \simeq G(T_*/\Delta)/R$, independent of phonon temperature and number of pair-breaking photons (we use subscript 0 to denote the steady state); for low heating, $T_B^* < T_G$, we can neglect the term linear in N_{qp} in Eq. (3.97) and the density is approximately $N_{qp,0} \simeq \sqrt{(G_{T_B} + G_{\bar{T}_B})/R}$, independent of the number of non-pair-breaking photons $\bar{n}$. In both regimes, the dependence of the density on bath temperature are similar: At low temperature – $T_B < \bar{T}_B$ for low heating and $T_B < T_B^*$ for high heating – the density is approximately constant, while above these crossover temperatures it increases exponentially, being approximately the same as in thermal equilibrium. As an example, in Fig. 3.13 we plot the density as function of temperature for a few values of $\bar{T}_B$ in the low-heating regime; the behavior resembles that in the high-heating regime, see Sec. 3.4.4

Interestingly, the two regimes display quantitatively different power spectral densities for quasiparticle number fluctuations. In general, as shown in Appendix F.2 the

spectral density (per unit volume) can be written in the form

$$S_N(\omega) = \frac{8RN_{qp,0}^2\bar{\tau}_r^2}{1+(\omega\bar{\tau}_r)^2} \tag{3.99}$$

where $\bar{\tau}_r = 1/[2RN_{qp,0} - G(T_*/\Delta)]$ is the relaxation time of quasiparticle number fluctuations and we assumed fast phonon dynamics, $\bar{\tau}_r \gg \tau_0^{PB},\ \tau_l$. At low heating, we have $\bar{\tau}_r \simeq 1/2RN_{qp,0}$ and we recover the result of Ref. [WP04]. At high heating $\bar{\tau}_r \simeq 1/RN_{qp,0}$, which modifies the relation between measurable quantities such as $\bar{\tau}_r$ and $S_N(0)$ and quantities than can be derived from them, such as the steady-state quasiparticle density.

It should be noted that in experiments the fluctuations measured are not directly those of the quasiparticle number, but those of phase and amplitude of the complex transmission. Therefore, comparison to experiments requires knowledge of the responsivities [Vis+11; Roo+21]

$$\frac{dA}{dN_{qp}} = -\frac{2\alpha Q}{\sigma_2}\frac{d\sigma_1}{dN_{qp}} \simeq -\frac{2Q}{N_{qp}Q_{i,qp}} \tag{3.100}$$

$$\frac{d\theta}{dN_{qp}} = \frac{4Q}{\omega_0}\frac{d\delta\omega_0}{dN_{qp}} \simeq 4Q\frac{\delta\omega_0}{N_{qp}\omega_0} \tag{3.101}$$

where Q is the loaded quality factor, α the kinetic inductance fraction, $\sigma_{1(2)}$ the real (imaginary) part of the ac conductivity, $Q_{i,qp}$ the contribution of quasiparticles to the internal quality factor, and $\delta\omega_0$ the frequency shift. For a coupling-limited quality factor, both responsivities are approximately independent of quasiparticle number. However, in the heating regime the responsivities depend on the photon number $\bar{n}$ via $Q_{i,qp}$ and $\delta\omega_0$– see also the next section.

In closing this section, we remark that the considerations presented in this work for the heating regime can be straightforwardly extended to the case of multiple pair-breaking modes (cf. Ref. [GGW16]) by introducing more sources like the term $G_{\bar{T}_B}$ in Eq. (3.97).

3.6. Comparison to experiments

The ac response of a superconductor depends on the quasiparticle distribution function and the dissipative part of the response can be strongly modified under non-equilibrium conditions. Indeed, in section 1.4.2 the quality factor of a resonator was expressed in terms of the real part of the conductivity σ_1. To estimate σ_1, we can use the low-energy approximation for coherence factors and density of states [cf. Eq. (3.20)], expand the integrand in Eq. (2.94) to lowest order in ω_0, and use the numerical result $\int_0 dx f'(x)/x \simeq -1.15b_0$, where $x = (E-\Delta)/T_*$, to find

$$\sigma_1 \simeq 2.3\sigma_N\frac{\Delta}{T_*}b_0 \approx 0.77\sigma_N\frac{N_{\mathrm{qp}}}{2\rho_F\Delta}\left(\frac{\Delta}{T_*}\right)^{3/2} \tag{3.102}$$

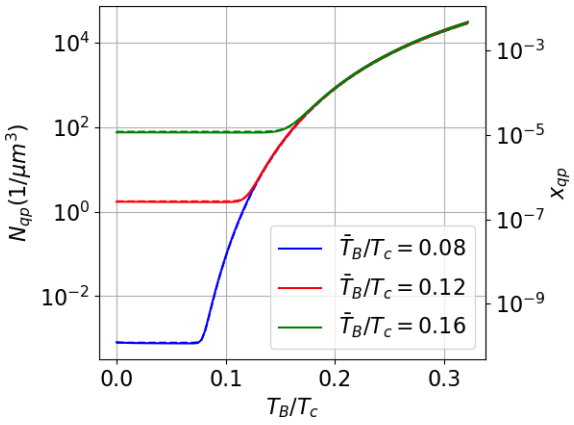

Figure 3.13.: Quasiparticle density for fixed numbers of pair-breaking photons (see parameter in the inset) as function of temperature in the low-heating regime in which non-pair-breaking photons have negligible influence on the density. Results calculated from numerical solutions to the kinetic equation are displayed with full lines and the corresponding analytical ones obtained by solving Eq. (3.97) in the steady state with dashed lines.

The form on the right shows that the dependence of σ_1 on the distribution function is not only via proportionality to the quasiparticle density, due to appearance of T_* in the last factor. Interestingly, as T_* increases (at fixed $N_{\rm qp}$), dissipation decreases; this effect is due to the redistribution of quasiparticles to higher energies, where the density of states is lower, similar to the decrease in relaxation of a superconducting qubit in which a residual quasiparticle is pushed on average to higher energy in the presence of a microwave drive [NCB17].

For $(\omega_0/4\Delta)^2 \ll 1$, the imaginary part σ_2 can be approximated as

$$\sigma_2 \simeq (\pi\sigma_N\Delta_0)/\omega_0 + \delta\sigma_2 \tag{3.103}$$

with

$$\begin{aligned} \delta\sigma_2 &= -\delta\sigma_{2,f} - \delta\sigma_{2,\Delta} \\ \delta\sigma_{2,f} &= \frac{2\sigma_N}{\omega_0}\int_{\Delta-\omega_0}^{\Delta} dE\, f(E+\omega_0)\frac{U^+(E,E+\omega_0)E}{\sqrt{\Delta^2-E^2}} \\ \delta\sigma_{2,\Delta} &= \frac{\pi\sigma_N\delta\Delta}{\omega_0} \end{aligned} \tag{3.104}$$

The contribution $\delta\sigma_2$ collects all the quasiparticle effects, with $\delta\sigma_{2,f}$ accounting directly for their distribution and $\delta\sigma_{2,\Delta}$ being due to the gap suppression of Eq. (3.53). Calculation of $\delta\sigma_{2,f}$ requires knowledge of the shape of distribution function within the first peak above the gap, and it is therefore beyond the description in terms of only the envelope that we have used in our analytical approach. For this reason, this

term will be evaluated numerically in what follows. Still, we can give an order-of-magnitude estimate assuming $f \sim b_0$, which gives $\delta\sigma_{2,f} \sim 2\pi\sigma_N\Delta_0 b_0/\omega_0$; this shows that the two contributions to $\delta\sigma_2$ can be of similar magnitude. Knowledge of the ac conductivity makes it possible to estimate the internal quality factor Q_i and resonant frequency shift $\delta\omega_0$ of superconducting resonators. For half-wavelength, open-ended resonators made of thin superconducting film, we have from Eq. (1.47)

$$Q_i \simeq \frac{\sigma_N \pi \Delta_0}{\omega_0 \alpha \sigma_1} \simeq \frac{\pi T_*}{2.3\alpha\omega_0 b_0} \simeq \frac{\pi}{0.77} \frac{T_*^{3/2}}{\alpha x_{qp}\omega_0\sqrt{\Delta}} \tag{3.105}$$

and from Eq. (1.50)

$$\frac{\delta\omega_0}{\omega_0} \simeq -\frac{\alpha\delta\Delta}{2\Delta_0} - \frac{\alpha\omega_0\delta\sigma_{2,f}}{2\pi\sigma_N\Delta_0} \tag{3.106}$$

Not surprisingly, this expression resembles that for the frequency shift in superconducting qubits, in which terms originating from gap suppression and virtual transitions mediated by quasiparticle tunneling have been identified [Cat+11]. Note that, in contrast to the frequency shift, the first peak's shape does not affect the calculation of Q_i, since $\delta\sigma_2/\sigma_2 \ll 1$. For an order of magnitude estimate we can use

$$\left|\frac{\delta\omega_0}{\omega_0}\right| \simeq -\frac{\alpha}{2} x_{qp} \left\{ \left[1 - 0.42\frac{T_*}{\Delta} + 0.22\left(\frac{T_*}{\Delta}\right)^2 \right] + \frac{1}{2.1}\sqrt{\frac{2\Delta}{T_*}} \right\} \tag{3.107}$$

The terms in square brackets originate from the suppression of the order parameter by the nonequilibrium quasiparticles, while the last term from the direct effect of the nonequilibrium distribution on the imaginary part of the ac conductivity. The latter term is in fact only a rough estimate, since for its actual calculation knowledge of the shape of the first peak (between energies Δ and $\Delta + \omega_0$) in the distribution function is needed. Both quality factor and frequency shift depend in general on the bath temperature T_B and the photon numbers $\bar{n}$ and $\bar{n}_{PB}$ through b_0 and T_* (in particular, the quality factor scales inversely with quasiparticle density [cf. Eq. (3.42)], but it also depends explicitly on T_*). For comparison to experiments, we henceforth assume that T_B corresponds to the reported base temperature of the fridge. To estimate $\bar{n}$, we relate it to power absorbed by the quasiparticles P_{abs},

$$\bar{n} = \frac{Q_i P_{\mathrm{abs}}}{\omega_0^2} \tag{3.108}$$

Using this relation in Eq. (3.105) we arrive at an implicit equation for Q_i in terms of P_{abs}. The latter is in general not a directly measurable quantity; however, for a half-wavelength resonator capacitively coupled to a transmission line we follow Ref. [Vis+14] and relate P_{abs} to the readout power P_{read},

$$P_{\mathrm{abs}} = 2P_{\mathrm{read}} \frac{Q^2}{Q_i Q_c} \tag{3.109}$$

where $Q = Q_i Q_c/(Q_i + Q_c)$ is the loaded quality factor and Q_c the coupling quality factor. The same expression for $\bar{n}$ in terms of $P_{\rm read}$ is obtained using the relation between internal power and photon number, $P_{\rm int} = \bar{n}\omega_0^2/2\pi$, together with that between internal and readout powers, $P_{\rm int} = P_{\rm read}Q^2/\pi Q_c$ [Gao08]. Equations (3.105), (3.108), and (3.109) make possible a self-consistent calculation of photon number and internal quality factor as a function of readout power. In the following we solve these equations explicitly in two regimes.

The approach just described simplifies considerably in the limit $Q_i \gg Q_c$, in which Eqs. (3.108) and (3.109) reduce to $\bar{n} = 2Q_c P_{\rm read}/\omega_0^2$, independent of Q_i. Then T_* can be calculated from its definition, Eq. (3.23), and b_0 by solving Eq. (3.46). In what follows, we denote with $T_{*,0}$ the value of T_* obtained under the assumption $Q_i \gg Q_c$, namely

$$\frac{T_{*,0}}{\Delta} \equiv \left[\frac{105}{64}\left(\frac{T_c}{\Delta}\right)^3 c_{Phot}^{QP}\tau_0\frac{2P_{\rm read}Q_c}{\Delta^2}\right]^{1/6} \tag{3.110}$$

If we further consider the regime in which non-pair breaking photons dominate quasiparticle creation, $T_G \ll T_B^*$, we find that the quality factor is given by

$$Q_{i,0} = \frac{\gamma_0\Delta}{\alpha\omega_0}\frac{\tau_0^{PB}}{\tau_l}\left(\frac{\Delta}{T_{*,0}}\right)^3 e^{\sqrt{14/5}(\Delta/T_{*,0})^3} \tag{3.111}$$

with $\gamma_0 = \pi 2^{1/3}5\sqrt{7}(2.1)^2/(2.3\times 3^{3/2}) \simeq 19.3$. Therefore, in this case the quality factor is a decreasing function of readout power and does not depend on T_B. The fast decrease of quality factor with increasing power is due to the large increase in the number of quasiparticles with photon number, as discussed in Sec. 3.4.2.1.

The high phonon temperature/low photon number regime $T_G \gtrsim T_B^*$ also offers significant simplification, since in that case we can relate b_0 to the (thermal) quasiparticle density using Eq. (3.42), and rewrite Eq. (3.105) as

$$Q_i = \frac{2.1\sqrt{2}\pi}{2.3\alpha}\frac{\Delta}{\omega_0}\left(\frac{T_*}{\Delta}\right)^{3/2}\left(\frac{N_{\rm qp}^{T_G}}{2\rho_F\Delta}\right)^{-1} \tag{3.112}$$

where the superscript T_G in $N_{\rm qp}^{T_G} = 2\rho_F\Delta\sqrt{2\pi T_G/\Delta}\times e^{-\Delta/T_G}$ denotes an effective temperature determined either by the pair breaking photons or phonons, c.f. section 3.5.4, which is independent of $\bar{n}$. This formula, using Eqs. (3.23), (3.108) and (3.109), leads to a quadratic equation for Q_i whose solution can be written in the form

$$Q_i = \tag{3.113}$$
$$\sqrt{\left(\frac{Q_c}{2}\right)^2 + \left(\frac{2.1\sqrt{2}\pi\Delta}{2.3\alpha\omega_0}\right)^2\left(\frac{T_{*,0}}{\Delta}\right)^3\left(\frac{N_{\rm qp}^{T_G}}{2\rho_F\Delta}\right)^{-2}} - \frac{Q_c}{2}$$

In this regime, Q_i is an increasing function of readout power (through $T_{*,0}$) and depends exponentially on T_G (through $N_{\rm qp}^{T_G}$). As remarked above, the increase of quality factor with readout power can be traced to the redistribution of the quasiparticles to

higher energies, where the density of states is lower. Note that if $Q_i \gg Q_c$ holds up to temperatures of order T_B^* or higher, Eqs. (3.111) and (3.113) together capture the temperature and power dependence of Q_i at all temperatures; we do not investigate here the case in which this condition is not satisfied.

So far, we have assumed that the internal quality factor is determined by the energy absorbed by quasiparticles. More generally, extrinsic (that is, non-quasiparticle) mechanisms such as dielectric losses can contribute to the total internal quality factor $Q_{i,\mathrm{tot}}$; collecting those contributions into $Q_{i,\mathrm{ext}}$ we have

$$1/Q_{i,\mathrm{tot}} = 1/Q_i + 1/Q_{i,\mathrm{ext}} \tag{3.114}$$

where, as before, Q_i denotes the quasiparticle part. For $T_B \gtrsim T_B^*$, Q_i is given by Eq. (3.113) with the replacement $1/Q_c \to 1/Q_c + 1/Q_{i,\mathrm{ext}}$ and is therefore unchanged (at leading order) if $Q_{i,\mathrm{ext}} \gg Q_c$.

3.6.1. No pair-breaking photons

We first consider the case without pair breaking photons $\bar{n}_{PB} = 0$ corresponding to $T_G = T_B$ and proceed to compare our theoretical findings to the measurements of the temperature dependencies of the quality factor and resonant frequency for different readout powers reported in Ref. [Vis+14]. In that work, a temperature-independent plateau in the quality factor at low temperatures is observed, which qualitatively agrees with the result in Eq. (3.111). In fact, by comparing experiments to numerical calculations the authors of Ref. [Vis+14] suggest the plateau to be explainable by the nonequilibrium steady-state solution to the kinetic equations. However, estimating the value of the plateau $Q_{i,0}$, Eq. (3.111), using the parameters in the first row of Table 3.2, we find much larger values than measured experimentally, see Table 3.2. The discrepancy cannot be due to approximations being used: while in particular the assumption $\omega_0 \ll T_*$ holds only weakly, for the highest readout power comparison with numerical results (see Fig. 3.6) shows that our analytical expression underestimates the quasiparticle density by a factor smaller than 2; then the quality factor could be overestimated by the same factor, but the estimated quality factor is 13 orders of magnitude larger than the measured one. [6] This indicates that the plateau is not due to the quasiparticles being driven out of equilibrium by the resonator's photons, but either to some other driving mechanism and/or to extrinsic relaxation channels. The measured power dependence of the quality factor is qualitatively opposite to that typically expected in the presence of two-level systems [Mac+10; MCL19], so they are unlikely to be the cause of the plateau. Moreover, the low temperature saturation of the quasiparticle lifetime reported in Ref. [Vis+14] (for a different sample and for a narrower range of power) point to the presence of a second driving mechanism, a situation that deserves further study. Nonetheless, assuming for simplicity an extrinsic

[6] We stress here that in discretizing the kinetic equations attention must be paid as to avoid introducing an unphysical quasiparticle source (cf. Sec. 3.2); in numerical calculations this would cause saturation of the quality factor to levels lower than our estimates provide.

$\frac{c_{Phot}^{QP}}{Hz}$	$\frac{\tau_0}{ns}$	$\frac{\Delta_0}{\mu eV}$	$\frac{\omega_0}{\Delta_T}$	$\frac{\tau_0^{PB}}{ps}$	$\frac{\tau_l}{ps}$	α	$c_{Phot,PB}^{QP}$	$\bar{n}_{PB,0}$	μ	ω_{PB}
0.06	63	189	$\frac{22}{189}$	40	170 ps	0.13	-	-	-	-
0.06	20	189	$\frac{22}{189}$	13	170 ps	0.13	1.6 Hz	2×10^{-4}	10^{-9}	2.8Δ

Table 3.2.: Parameters used for comparison between theory in this work and experiments of Ref. [Vis+14]. The estimation of c_{Phot}^{QP}, Δ_0, and α is discussed in Appendix E. For the phonon thermalization time τ_l and the coupling quality factor $Q_c = 20100$ we use the same values as in Ref. [Vis+14]. In the numerical calculations, the gap is fixed at its thermal equilibrium value Δ_T, the discretization step size is $h = \Delta_T/189$, and the energy is truncated at $E_{\max} = 10\Delta_T$. The time τ_0 is used as a free fit parameter, while τ_0^{PB} follows from it via Eq. (3.14).

mechanism, to fit the experimental data we use Eq. (3.114) and find the values of $Q_{i,\text{ext}}$ given in Table 3.2. Results from the analytic formula and the numerics are compared to experimental data for quality factor and resonance frequency in Fig. 3.14; in the numerical calculations, the experimentally measured (total) internal quality factor has been used in Eqs. (3.108)-(3.109) to obtain the photon number. At temperatures $T \gtrsim 0.25\,\text{K}$ we find good agreement between theory and experiment. The fitted value of τ_0 is shorter than an estimate derived from neutron scattering data [Kap+76] but consistent with other experimental estimates, see *e.g.* Ref. [CC79]. This further validates our approach, especially since from the analytical expressions it is evident that τ_0 enters into the quality factor via the product $c_{Phot}^{QP}\tau_0\bar{n}$, and therefore inaccuracies in the estimates of c_{Phot}^{QP} and/or $\bar{n}$ (equivalently, P_{read}) could affect the extracted value of τ_0.

Aside from the quality factor the predicted shift in resonance frequency differs from the theoretical prediction at low temperatures. In the next section we will see that the inclusion of a small number of pair breaking photons provides a quantitative explanation of the saturation of the quality factor at low temperatures while the shift in resonance frequency at low temperatures only agrees qualitatively.

3.6.2. Pair-breaking photons

To try and explain the low-temperature behavior of the quality factor, we now consider the effect of pair-breaking photons, assuming we remain in the low-heating regime. The quasiparticle density can be strongly affected by a small number of such photons, see the discussion after Eq. (3.83). In fact, in a series of works [BY09; Bas+12] radiation emitted by a higher temperature (3-4 K) stage of the refrigerator was identified as a source of quasiparticle generation, and at least partially mitigated by using a 'box in a box' design. Furthermore, to reduce the influence of pair-breaking photons propagating through coaxial cables, filters have been used at the cold stage that, extrapolating measurements below $\sim 10\,\text{GHz}$ to twice the gap, are expected to suppress the number of pair-breaking photons by almost 4 orders of magnitude. Despite such

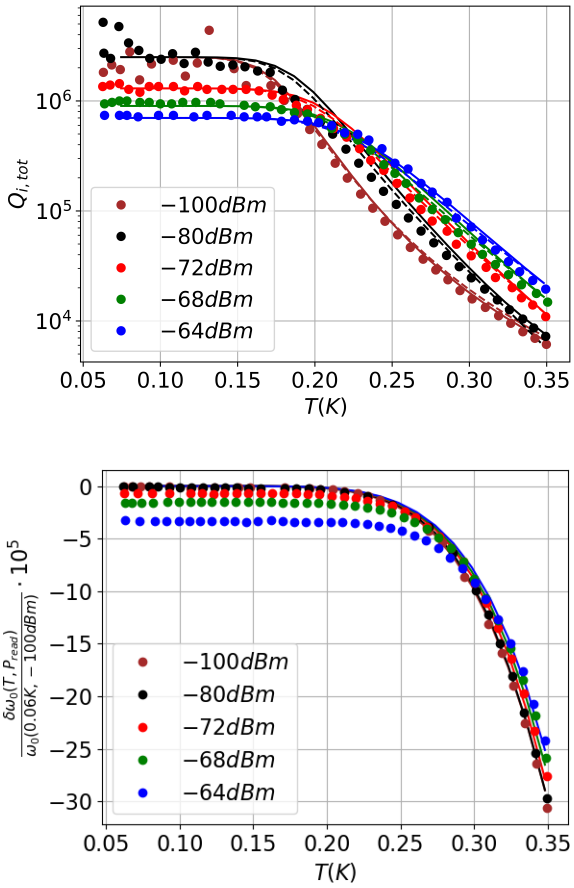

Figure 3.14.: Internal quality factor $Q_{i,\mathrm{tot}}$ vs temperature for different readout powers (left) and deviation of the resonance frequency from its experimentally determined low temperature and low readout power value $\delta\omega_0(T, P_{\mathrm{read}}) = \omega_0(T, P_{\mathrm{read}}) - \omega_0(T = 0.06\,\mathrm{K}, P_{\mathrm{read}} = -100\,\mathrm{dBm})$ in units of $10^{-5}\omega_0$ for different readout powers (right). Experimental data from [Vis+14] are displayed with circles (we omit the data for $P_{\mathrm{read}} = -90\,\mathrm{dBm}$ for clarity of presentation), results from the numerics described in Sec. 3.2 with full lines, and results from the analytical formulas [Eqs. (3.111)-(3.114)] with dashed lines. The analytical curve for the lowest readout power assume thermal equilibrium (see Appendix E).

P_{read} (dBm)	-100	-90	-80	-72	-68	-64
$T_{*,0}/\Delta$	0.09	0.13	0.19	0.26	0.3	0.36
$Q_{i,0}/10^6$	10^{997}	10^{330}	10^{105}	10^{40}	10^{25}	10^{14}
$Q_{i,\mathrm{ext}}/10^6$	2.5	2.5	2.5	1.3	0.9	0.7

Table 3.3.: For each readout power used in Ref. [Vis+14], we calculate $T_{*,0}$ using Eq. (3.110) and the (theoretical) low-temperature quality factors $Q_{i,0}$ using Eq. (3.111) (except for the lowest power, since in that case $T_{*,0} \approx \omega_0$, while the theory is valid for $T_{*,0} > \omega_0$). The experimental low-temperature quality factors $Q_{i,\mathrm{ext}}$ are assumed to be due to extrinsic (non-quasiparticle) mechanisms (see text). An error in the values of this table given in [FC23] was corrected here, that however does not affect any of the following results.

careful engineering, the "leakage" of pair-breaking photons from higher temperature stages is likely not completely eliminated. However, at low temperatures such leakage would result in a density of quasiparticles independent of $\bar{n}$ and of T_B (up to $\bar{T}_B$, see Fig. 3.13), and the quality factor should still increase with $\bar{n}$, in contrast with observation.

Since the assumption of a fixed number of pair-breaking photons is inconsistent with experiment, we are lead to amend it by setting

$$\bar{n}_{PB} = \bar{n}_{PB,0} + \mu\bar{n} \tag{3.115}$$

where the first term on the right-hand side accounts for the leakage from higher temperature stages discussed above. The second term introduces a dependence of $\bar{n}_{PB}$ on $\bar{n}$ and can originate from high-frequency noise produced by the source used to generate the signal probing the resonator. This dependence in turns implies that when $\bar{n} \gtrsim \bar{n}_{PB,0}/\mu$ the quasiparticle density increases with readout power even in the low-heating regime, because the second term on the right-hand side of Eq. (3.97) increases with $\bar{n}$. As shown in Fig. 3.15, with this assumption we can obtain a satisfactory fit to the measurements of Ref. [Vis+14] using reasonable parameters: the "leaked" photon number $n_{PB,0}$ is about one order of magnitude bigger than what one would expect assuming a higher-stage temperature of 3.5 K with a 10^{-4} attenuation factor for photons of energy $\omega_{PB} = 2.8\Delta$, but the discrepancy would drop to just a factor of 3 for photons at the pair-breaking threshold [7]. As for the value of $\mu = 10^{-9}$, it can be explained by a combination of 10^{-4} attenuation times a 10^{-5} ratio between power of the generated signal and of the high-frequency noise [8].

[7] We note that $n_{PB,0}$ could also originate from even higher-temperature stages with higher attenuation, so the independence of *e.g.* $\bar{\tau}_r$ on the temperature of the few Kelvin stage [Vis+11] does not exclude such leakage.

[8] Spectral purity of signal generators at few GHz frequencies can range between -30 dBc to -140 dBc, depending on whether harmonics, nonharmonics, or wideband noise are considered, indicating that power ratios up to 10^{-3} cannot be excluded.

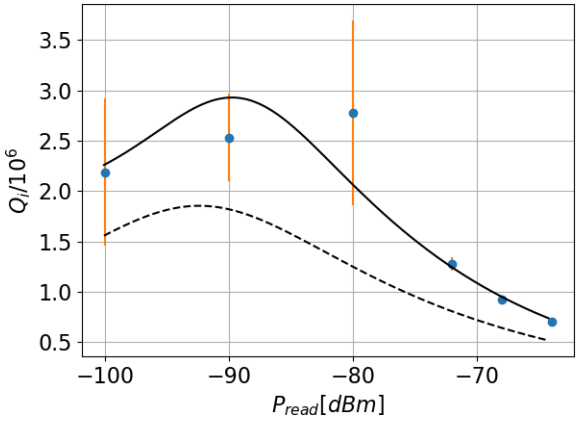

Figure 3.15.: Low-temperature Q-factor vs readout power. Experimental data points are obtained by averaging the low temperature ($T_B < 150\,\mathrm{mK}$) data in Ref. [Vis+14] and each error bar shows the corresponding standard deviation; the value of the data points coincide with those of $Q_{i,\mathrm{ext}}$ [cf. table 3.3] used in Fig. 3.14. The solid line is obtained from numerical solutions to the kinetic equation ignoring thermal phonons (that is, setting $T_B = 0$) and using parameters $\omega_{PB} = 2.8\Delta$, $c^{QP}_{Phot,PB} = 27 c^{QP}_{Phot}$, $\tau_0 = 20\,\mathrm{ns}$, $\bar{n}_{PB,0} = 2 \times 10^{-4}$, and $\mu = 10^{-9}$ [see Eq. (3.115)]; other parameters as in Fig. 3.14. The dashed line shows the analytical estimate, Eq. (3.105).

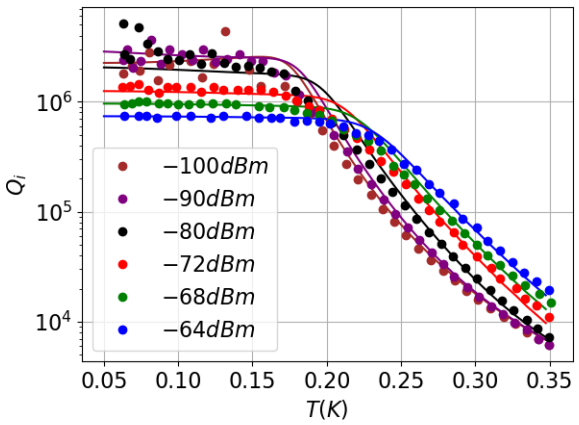

Figure 3.16.: Quality factor vs temperature for different readout powers. As in Fig. 3.14, the experimental points are from Ref. [Vis+14]. Here the solid lines include only the quasiparticle contribution, with no extrinsic loss mechanisms. The lines are calculated using the same parameters as in Fig. 3.15 but, in contrast to Fig. 3.14, here we take into account effect of a power-dependent number of pair-breaking photons, see Eq. (3.115) and the discussion that follows it.

The assumption in Eq. (3.115) is independent of temperature, so we can employ it also when evaluating the temperature dependence of the quality factor, as shown in Fig. 3.16. We stress that while in Fig. 3.14 the value of $Q_{i,\mathrm{ext}}$ is chosen independently for each of the six readout powers as to best fit the data, in Fig. 3.16 just the two parameters appearing in the right-hand side of Eq. (3.115) are used to fit all the data at the same time.[9] The agreement between theory and data in Figs. 3.15 and 3.16 thus support our proposed explanation for the physical mechanism responsible for the saturation of the quality factor in terms of excess pair-breaking photons.

We also remark that the way pair-breaking photons affect the quality factor is not equivalent to adding an extrinsic mechanism: the pair-breaking photons influence $Q_{i,qp}$ via the quasiparticle density N_{qp}, and in the low-heating regime we can write the latter in the form

$$N_{qp} = \sqrt{N_{T_B}^2 + N_{\bar{T}_B}^2} \tag{3.116}$$

with $N_{T_B} = \sqrt{G_{T_B}/R}$ and the analogous definition for $N_{\bar{T}_B}$. Defining $Q_{i,T_B(\bar{T}_B)}$ by the replacement $N_{qp} \to N_{T_B}(N_{\bar{T}_B})$ in Eq. (3.105), we find that

$$\frac{1}{Q_{i,qp}} = \sqrt{\frac{1}{Q_{i,T_B}^2} + \frac{1}{Q_{i,\bar{T}_B}^2}} \tag{3.117}$$

which should be contrasted with Eq. (3.114). Finally, we point out that the above analysis of the quality factor is not restricted to a single pair-breaking mode, but is valid in the heating regime if multiple pair-breaking modes (or even a broadband source) are present: the heating regime is by definition that in which the shape but not necessarily the normalization of the distribution function is determined by the interplay between non-pair-breaking photons and phonons, see Sec. 3.5.3; in this regime, the pair-breaking photons influence the quality factor only by contributing to the total quasiparticle density as in Eq. (3.116).

Equation (3.107) predicts at low temperature a non-monotonic dependence of the magnitude of the shift in resonance frequency on readout power: at low power, x_{qp} is independent of power as the quasiparticle generation is dominated by the leakage term $n_{PB,0}$ in Eq. (3.115), while the factor in curly brackets decreases slowly with power. As power increases and the last term in Eq. (3.115) becomes relevant, the magnitude of the shift increases with power as the increase in x_{qp} dominates on the decrease of the curly-bracket factor. In practice, however, one can measure the shift from the lowest readout power, not from zero power, so depending on the parameters the nonmonotonic behavior might not be measurable. In fact, for the parameters used to fit the quality factor data the difference in relative shift between the two lowest powers is about 10^{-6} which, given quality factors of order 10^6, is at the limit

[9] Strictly speaking, there are two additional parameters, $c_{Phot,PB}^{QP}$ and ξ; however, only the product $c_{Phot,PB}^{QP}\bar{n}_{PB}\xi$ is relevant, as it enters $G_{\bar{T}_B}$, see text following Eq. (3.97). To arrive at order-of-magnitude estimates for the parameters in Eq. (3.115), we choose $c_{Phot,PB}^{QP}$ based on the considerations in Appendix E.2 and the value of ξ based on Ref. [Hou+19].

of being measurable. For higher powers, the magnitude of the shift increases, in qualitative agreement with the experiment, see Fig. 3.17. In that figure, we plot both the analytical estimate above and the numerically calculated relative shift. Both curves deviate from the experimental data by less than a factor of 3.

We note that in Ref. [Sem+16] an alternative explanation for the shift was proposed: the authors argue that, in analogy with the case of a dc supercurrent, the non-pair-breaking photons cause a broadening of the peak in the superconducting density of states. This broadening effect can be characterized in terms of a depairing parameter $\tilde{\alpha}$ (not to be confused with the kinetic inductance fraction α) which is proportional to the readout power and which causes a change in the kinetic inductance: $\delta L_k/L_k \simeq 4.85\tilde{\alpha}/\Delta$ [Sem+16]. The relative shift is in turn proportional to the change in kinetic inductance, $\delta\omega_0/\omega_0 = -\alpha\delta L_k/2L_k$; implicitly assuming $\alpha = 1$, good agreement was found between the theory of Ref. [Sem+16] and the experiment of Ref. [Vis+14]. However, the kinetic inductance fraction in the experiment can be estimated as $\alpha \sim 0.1$, meaning that the theoretical result in fact underestimates the shift by approximately an order of magnitude compared to experiment. Interestingly, adding the contributions to the frequency shift of the two mechanisms improves agreement with the experimental data, but further investigation is needed to understand if in fact the two mechanisms coexist.

The inset in Fig. 3.17 displays the temperature dependence of the relative shift as extracted from the data of Ref. [Vis+14]. It is instructive to present the same data as function of normalized density x_{qp} instead, since Eq. (3.107) predicts a linear relationship with a slope dependent on readout power. For low readout power, the experimental data and the numerical estimates are in reasonable quantitative agreement with each other and with the expectation for thermal equilibrium, see Fig. 3.18. As power increases, the qualitative trend of decreasing magnitude of the slope in the frequency vs density plot is evident in both data and numerics; although there is quantitative discrepancy at the higher powers, we can conclude that a slope smaller in magnitude than the thermal equilibrium one is indicative of quasiparticle heating. Recently, such a reduced slope has been observed in a transmon qubit in which excess quasiparticles are generated due to the presence of an IR laser beam focused onto the qubit or the substrate next to it [Ben+24].

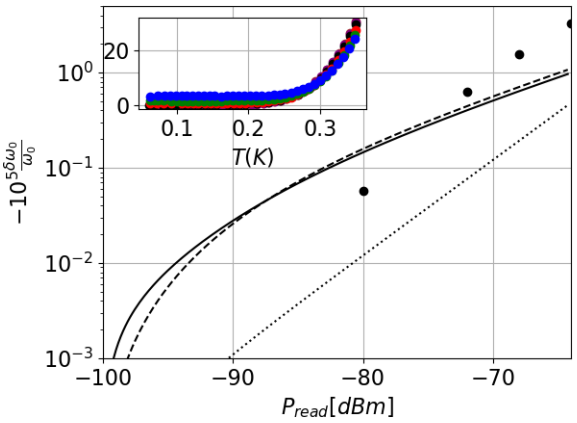

Figure 3.17.: Main panel: Dots: relative shift in resonance frequency from Ref. [Vis+14] at low temperature, $T_B < 150\,\mathrm{mK}$, relative to the lowest readout power, $P_{\mathrm{read}} = -100\,\mathrm{dBm}$. Solid line: numerical calculation of the shift for $T_B = 0$ and other parameters as in Fig. 3.15. Dashed line: order-of-magnitude estimate from Eq. (3.107); both lines calculated as deviations from the value for $P_{\mathrm{read}} = -100\,\mathrm{dBm}$. Dotted line: prediction from Ref. [Sem+16] (corrected for the finite kinetic inductance fraction, see text). Inset: temperature evolution of the shift in linear scale (the colors are the same as in Fig. 3.16).

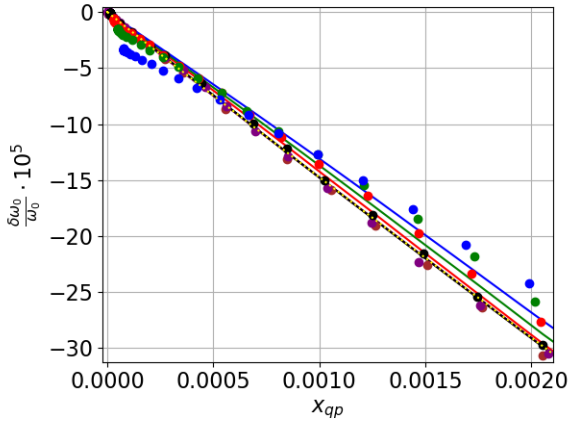

Figure 3.18.: Dots: Experimental shift of resonance frequency from Ref. [Vis+14] (see inset in Fig. 3.17) vs quasiparticle density; the latter is obtained from the numerical solution to the kinetic equation with the same parameters as in the fits in Figs. 3.15 and 3.16. Solid lines: numerical results for the frequency shift calculated using the same parameters as for the density; readout powers increases from bottom to top (colors as in Fig. 3.16). Yellow dotted line: frequency shift assuming a thermal equilibrium distribution; for reference, $x_{qp} = 0.002$ corresponds to $T_B = 350\,\mathrm{mK}$.

4. Quasiparticle dynamics in the presence of magnetic impurities

Parts of this chapter are currently under revision for publication. A preliminary version of the paper is available at [FC25]. I did parts of the calculations, wrote parts of the manuscript and prepared all figures.

4.1. Introduction

In chapter 3 we considered the quasiparticle dynamics in a system that was approximated to be spatial homogeneous. Recently it was suggested [Bes+16; Grü+18] that this assumption might fail in a system containing even a small number of magnetic impurities [or in the mathematically similar case of a fluctuating pairing constant [LO72]] - even a small number of impurities may lead to regions in space with a local gap in the excitation spectrum that is slightly reduced compared to the average gap. Such a region could thus host a quasiparticle at an energy below the average gap, and thereby trap it in space until it either recombines or increases its energy (e.g. by absorbing a phonon). If all quasiparticles are trapped within a different region they would remain separated in space for long timescales, and the recombination rate would greatly reduce below the simple Rothwarf-Taylor RN_{qp}^2 term used in chapter 3. So far, two different models have been proposed to account for such effects: [Bes+16] treated each quasiparticle as localized, with the shape of the quasiparticle states estimated from (microscopic) optimal fluctuation theory. This allowed to estimate the recombination rate without any fit parameter. This approach however disregards the presence of quasiparticles of energy above the average gap and thus neglects the finite width in the quasiparticle distribution in energy that can e.g. arise from phonon absorption or the balance of recombination and pair breaking processes [see section 3.5.1]. If the energy width of the distribution becomes large compared to the decrease in gap in the trapping regions, such a model clearly becomes inappropriate. In contrast, [Grü+18] used a purely phenomenological model based on rate equations for the density of localized (x_l) and mobile (x_m) quasiparticles

$$\begin{aligned} \frac{dx_l}{dt} &= \Gamma_{\mathrm{loc}} x_m - \Gamma_{\mathrm{ex}} x_l - \Gamma_{ml} x_m x_l - \Gamma_{ll} x_l^2 + g_l \\ \frac{dx_m}{dt} &= \Gamma_{\mathrm{ex}} x_l - \Gamma_{\mathrm{loc}} x_m - \Gamma_{ml} x_m x_l - \Gamma_{mm} x_m^2 + g_m \end{aligned} \tag{4.1}$$

Here, the densities x_α, $\alpha = l, m$, are normalized by that of the Cooper pairs, Γ_{ex} denotes the rate for excitation from a localized to a mobile state, Γ_{loc} the rate for the localization process, $\Gamma_{\alpha\beta}$, $\alpha, \beta = l, m$, the recombination coefficient between localized (l) and/or mobile (m) quasiparticles (see Fig. 4.1 right), and g_α the rate at which quasiparticles are generated by some pair-breaking mechanism. In the following we derive the rates entering (4.1) from microscopic theory. Doing so, we will show that trapping is not important for the quasiparticle dynamics for typical experimental parameter in aluminum devices.

4.2. Density of states and coherence factors

4.2.1. Abkrikosov-Gorkov theory of paramagnetic impurities

In section 2.2 the Keldysh-Usadel equation (2.65) for a dirty superconductor containing magnetic impurities was derived. We will not consider electromagnetic fields, and only consider the simpler case in which the retarded part of the Usadel equation is given by (2.66) and the Diffusion equation by (2.70) with $I^{pt} = 0$. In contrast to non-magnetic impurities, the presence of magnetic impurities affects the density of states by suppressing the energy gap in the excitation spectrum. In the following we parametrize the retarded/advanced Green's functions by

$$f^R = i\cosh(\psi) \tag{4.2}$$
$$g^R = i\sinh(\psi) \tag{4.3}$$

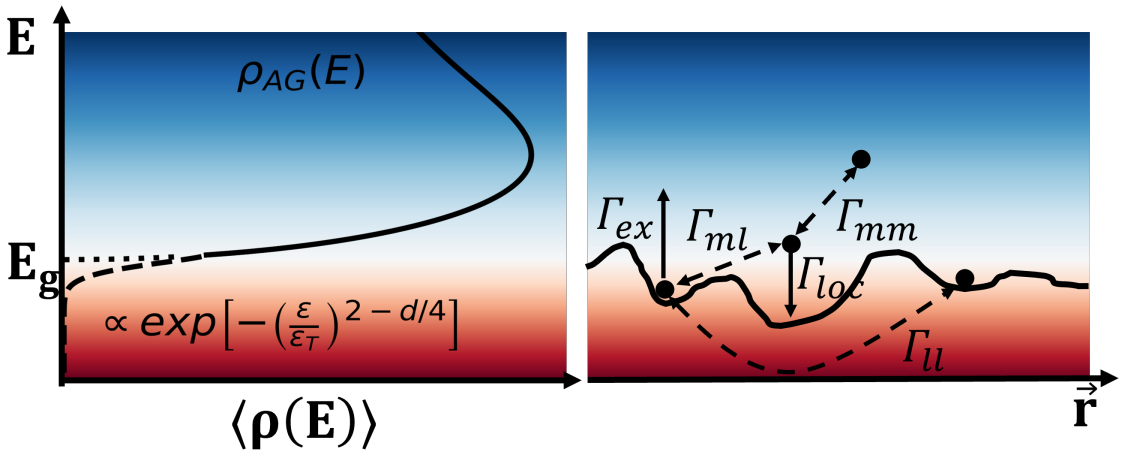

Figure 4.1.: Left: Average density of states as function of energy, showing the Abrikosov-Gorkov broadened peak above E_g and the subgap tail below it. Right: Local value of the gap as function of position; also depicted are the various processes affecting the quasiparticle densities, namely recombination between localized (red background) and/or mobile (blue background) quasiparticles, localization, and excitation.

with complex ψ. This parametrization automatically accounts for the normalization condition (2.45). The retarded quasiclassical Green's functions g^R, f^R can be obtained from the retarded part of the Usadel equation

$$0 = F(\psi)\Delta - \frac{D}{2}\nabla^2\psi - \cosh(\psi)\sinh(\psi)\Delta\delta\eta(\vec{R}) \tag{4.4}$$

with

$$F(\psi) = \sinh(\psi)(1 - \eta\cosh(\psi)) - \frac{E}{\Delta}\cosh(\psi) \tag{4.5}$$

depairing parameter $\eta = \tau_{sf}^{-1}\Delta^{-1}$ with (average) spin flip time τ_{sf}^{-1} and fluctuations in the depairing parameter

$$\langle\delta\eta(\vec{R})\delta\eta(\vec{R}')\rangle = \eta^{2/3}\sigma^2\xi^d\delta(\vec{R} - \vec{R}') \qquad \text{with} \qquad \sigma^2 = \frac{\eta^{4/3}}{n_{imp}\xi^d} \tag{4.6}$$

where d, the effective dimension of the film, is $d = 3$ for bulk systems and $d = 2$ for films thinner than the coherence length. Note that, due to the self consistency equation, fluctuations in η induce fluctuations in Δ which in principle must be included in equation (4.4). However, as discussed in appendix G.5, these fluctuations can be neglected in the limit $\eta \ll 1$ considered below.

4.2.1.1. Mean field theory

On mean field level we replace the position dependent spin flip time $\tau_{sf}(\vec{R})$ by its spatial average $\tau_{sf,0}$. In that case the system is spatial homogeneous and the retarded/advanced Green's functions are given by

$$F(\psi) = 0 \tag{4.7}$$

This corresponds to the well known Abrikosov-Gorkov (AG) theory [AG61]. While an analytic solution can be found [ST08] the resulting expressions are quite complicated and it is more instructive to discuss approximate solutions. Below the gap E_g in the excitation spectrum ψ becomes real, and we can write

$$\frac{E}{\Delta} = \tanh(\psi_0)(1 - \eta\cosh(\psi_0)) \tag{4.8}$$

with real ψ_0. The right-hand side has a maximum at $\cosh(\psi_0) = \eta^{-1/3}$ and, as the gap is defined as the maximum energy for which (4.8) has a solution, we get the well known result for the gap in the excitation spectrum $E_g = (1-\eta^{2/3})^{3/2}\Delta$ [AG61]. Close to the gap, we write $E = E_g(1 - \bar{\epsilon})$ and $\psi(\bar{\epsilon}) = \psi_0 + \delta\psi(\bar{\epsilon})$ and expand eq. (4.7) to second order in $\delta\psi(\bar{\epsilon})$, resulting in

$$\psi_0(\bar{\epsilon}) = \psi_0 \pm \sqrt{\frac{2\bar{\epsilon}}{3}}\eta^{-1/3}\sqrt{1 - \eta^{2/3}} \tag{4.9}$$

where the solution with the minus sign is the one used in the following. Above the gap (i.e. $\bar{\epsilon} < 0$) ψ obtains an imaginary part, corresponding to a finite density of states. Expanding F to third order, we can also obtain the next to leading order correction

$$\delta\psi_1(\bar{\epsilon}) = \frac{\bar{\epsilon}}{9}\eta^{-2/3}\sqrt{1-\eta^{2/3}}\left(1-2\eta^{2/3}\right) \tag{4.10}$$

We assume $\eta \ll 1$ in the following. From (4.9) and (4.10) we see that $\psi_0(\bar{\epsilon})$ provides a good approximation for the density of states if $|\bar{\epsilon}| \ll \eta^{2/3}$. At larger energies, the density of states approaches a maximum at $E_M = \Delta(1 + 3\eta^{4/3}/2^{5/3}) \simeq \Delta$[SBW64]. At even larger energies, the effect of the impurities becomes small and the Green's functions approach their BCS value.

The paramtrization (4.2) allows to express the coherence factors close to the gap in terms of $\Re(\delta\psi) = \Re(\psi - \psi_g)$: Expanding $\Re(f_R)/\Re(g_R)$ to linear order in $\delta\psi$ gives

$$\frac{\Re(f^R)}{\Re(g^R)} \simeq \sqrt{1-\eta^{2/3}} + \eta^{2/3}\Re(\delta\psi) \tag{4.11}$$

Inserting (4.9) and using $|\Re(\delta\psi)| \ll 1$ for $|\bar{\epsilon}| \ll \eta^{2/3}$ gives

$$K^-(E_g, E_g) \simeq \eta^{2/3} \tag{4.12}$$

Importantly, this remains a reasonable approximation for energies up to Δ as can be seen from the next to leading order correction ψ_1 calculated above. Furthermore, in the presence of fluctuations $\sigma \neq 0$ it remains valid for $\Re(\delta\psi) \ll 1$.

4.2.1.2. Perturbative regime

If corrections due to the fluctuations $\sigma \neq 0$ are small, it is possible to perturbatively calculate their effect on the disorder averaged Green's functions. Following [LO72] we expand (4.4) in $\delta\psi$ at ψ_0 to obtain

$$\eta^{1/3}\xi^2\nabla^2\delta\psi + \frac{3}{2}\eta^{2/3}\delta\psi^2 \simeq \bar{\epsilon} + \eta^{-1/3}\delta\eta \tag{4.13}$$

where for simplicity we set $\sqrt{1-\eta^{2/3}} \simeq 1$. Rescaling lengths as $\vec{R} \to |\bar{\epsilon}|^{1/4}\xi^{-1}\vec{R}$ and $\delta\psi \to \eta^{-1/3}\sqrt{|\bar{\epsilon}|}\delta\psi$ this becomes

$$\nabla^2\delta\psi + \frac{3}{2}\delta\psi^2 \simeq \mathrm{sgn}(\bar{\epsilon}) + \eta^{-1/3}\frac{\delta\eta}{|\bar{\epsilon}|} \tag{4.14}$$

For sufficiently small disorder one could now search for an expansion of $\delta\psi$ in orders of $\delta\eta$ (see [LO72] for the lowest order term for the three-dimensional system). Such a perturbative calculation however fails in the immediate vicinity of, and below, E_g: The last term on the RHS diverges upon approaching $\bar{\epsilon} \to 0$ and eventually fluctuations become dominant and a perturbative calculation even fails for small disorder. In the rescaled coordinate system $\langle\delta\eta(\vec{R})\delta\eta(\vec{R}')\rangle = \eta^{2/3}\sigma^2|\bar{\epsilon}|^{d/4}\delta(\vec{R}-\vec{R}')$, correspondingly the expansion in orders of $\delta\eta$ corresponds to an expansion in powers of $\sigma|\bar{\epsilon}|^{d/8-1}$. For $\sigma \gtrsim |\bar{\epsilon}|^{1-8/d}$ this eventually stops being a small parameter, and a perturbative solution becomes impossible.

4.2.1.3. Optimal fluctuations

While a perturbative treatment fails at energies close to and below the average gap E_g, an approximate solution for the averaged density of states can be obtained at energy far below E_g, where rare fluctuations of a specific shape, the 'optimal fluctuations', dominate contributions to the density of states. These optimal fluctuations corresponds to a saddle point in the functional integral over $\delta\eta$ that allows for a small imaginary part of $\delta\psi$ at an energy $\bar{\epsilon}$, corresponding to a non-zero density of states. We thus consider now energies below the average gap $\bar{\epsilon} > 0$. To get the optimal fluctuations, we follow the standard procedure used by [LO72; SI05; SF13]. Expanding (4.4) in $\delta\psi = \psi - \psi_0(\bar{\epsilon})$ with ψ_0 given by (4.9) results in

$$\delta\eta = \eta^{2/3}\left(\xi^2\nabla^2\delta\psi(\bar{\epsilon}) - \aleph(\bar{\epsilon})\delta\psi(\bar{\epsilon}) + \beth\delta\psi(\bar{\epsilon})^2\right) \tag{4.15}$$

with $\aleph(\bar{\epsilon}) = \sqrt{6\bar{\epsilon}}(1-\eta^{2/3})$ and $\beth = \frac{3}{2}\eta^{1/3}\sqrt{1-\eta^{2/3}}$. Transforming to $\vec{R}_{\bar{\epsilon}} = \sqrt{1-\eta^{2/3}}(6\bar{\epsilon})^{1/4}\vec{R}/\xi$ gives

$$\delta\eta(\bar{\epsilon}) = -\eta^{2/3}\frac{\aleph(\bar{\epsilon})^2}{\beth}\left[\phi(\bar{\epsilon},\vec{R}_{\bar{\epsilon}}) - \phi^2(\bar{\epsilon},\vec{R}_{\bar{\epsilon}}) - \nabla^2_{\vec{R}_{\bar{\epsilon}}}\phi(\bar{\epsilon},\vec{R}_{\bar{\epsilon}}) + \chi^2(\bar{\epsilon},\vec{R}_{\bar{\epsilon}})\right] \tag{4.16}$$

Here, we defined $\phi(\bar{\epsilon}) = \frac{\beth}{\aleph(\bar{\epsilon})}\Re\left(\delta\psi(\bar{\epsilon})\right)$ and $\chi(\epsilon) = \frac{\beth}{\aleph(\epsilon)}\Im\left(\delta\psi(\epsilon)\right)$. The equation for $\delta\eta$ is supplemented by the imaginary part of the Usadel equation

$$0 = \left[\nabla^2_{\vec{R}_{\bar{\epsilon}}} + 2\phi(\bar{\epsilon},\vec{R}_{\bar{\epsilon}}) - 1\right]\chi(\bar{\epsilon},\vec{R}_{\bar{\epsilon}}) \tag{4.17}$$

The main contribution to the disorder averaged density of states at energy $\bar{\epsilon}$ comes from traps that are just deep enough to accommodate quasiparticles at that energy. For these configurations, $\chi \ll \phi$, and we can set $\chi \sim 0$ in the calculation of the saddle point $\bar{\phi}$ of the functional integral via

$$\frac{\delta}{\delta\phi(\bar{\epsilon},r_{\bar{\epsilon}})}(\delta\eta[\phi])^2\Big|_{\phi=\bar{\phi}} = 0 \tag{4.18}$$

Using the chain rule for functional derivatives and $\frac{\delta}{\delta\phi}\nabla^2\phi = \nabla^2$ results in the saddle point equation

$$\hat{O}_d\left[\bar{\phi}(\bar{\epsilon},\vec{R}_{\bar{\epsilon}}) - \bar{\phi}(\bar{\epsilon},\vec{R}_{\bar{\epsilon}})^2 - \nabla^2_{\vec{R}_{\bar{\epsilon}}}\bar{\phi}(\vec{R}_{\bar{\epsilon}})\right] = 0 \tag{4.19}$$

with $\hat{O}_d = \left[1 - 2\bar{\phi}(\bar{\epsilon},\vec{R}_{\bar{\epsilon}}) - \frac{1}{R^{d-1}_{\bar{\epsilon}}}\partial_{R_{\bar{\epsilon}}}R^{d-1}_{\bar{\epsilon}}\partial_{R_{\bar{\epsilon}}}\right]$. Restricting the solution to spherically (for three dimensional fluctuations) or cylindrical (for two dimensional fluctuations) symmetric functions it can be rewritten to [SF13]

$$\tilde{O}_{d+2}\left[\bar{\phi}(\bar{\epsilon},R_{\bar{\epsilon}}) - \bar{\phi}(\bar{\epsilon},R_{\bar{\epsilon}})^2 - \frac{1}{R^{d-3}_{\bar{\epsilon}}}\partial_{R_{\bar{\epsilon}}}R^{d-3}_{\bar{\epsilon}}\partial_{R_{\bar{\epsilon}}}\bar{\phi}(\bar{\epsilon},R_{\bar{\epsilon}})\right] = 0 \tag{4.20}$$

where $d = 2,3$ is the effective dimension of the fluctuation. In three dimensions, the resulting saddle point is

$$\bar{\phi}(\bar{\epsilon},R_{\bar{\epsilon}}) = \frac{3}{2}\left[\cosh\left(\frac{R_{\bar{\epsilon}}}{2}\right)\right]^{-2} \tag{4.21}$$

as first obtained by [LO72]. In two dimensions, a good approximation to the saddle point is

$$\bar{\phi}(R_{\bar{\epsilon}};a) = (1+aR_{\bar{\epsilon}}^2)^{1/4}\left[\cosh\left(\frac{R_{\bar{\epsilon}}}{2}\right)\right]^{-2} \tag{4.22}$$

with $a = 0.26$ (c.f appendix G.1). Using (4.16) and (4.20) the resulting optimal fluctuation correponds to

$$\delta\bar{\eta}(\bar{\epsilon}) = \eta^{2/3}\frac{\Omega(\bar{\epsilon})^2}{\rho}\times\left[\frac{2\bar{\phi}'(R_{\bar{\epsilon}})}{R_{\bar{\epsilon}}}\right] \tag{4.23}$$

Furthermore, comparing eqs. (4.19) and (4.17) gives $\chi(\bar{\epsilon}) \propto \delta\bar{\eta}(\bar{\epsilon})$. Following [LO72] we determine the disorder averaged density of states using the method of [ZL66], the calculation is given in detail in appendix G.2.

The resulting disorder averaged sub-gap density of states is

$$\rho_l(\tilde{\epsilon}) \simeq \frac{a_d}{\eta^{2/3}}\left(\frac{\epsilon_T}{\Delta}\right)^{1/2}\tilde{\epsilon}^{\alpha_d}\exp[-\tilde{\epsilon}^{2-d/4}] \tag{4.24}$$

with $d = 2, 3$ the effective dimensionality of the system ($d = 2$ for films of thickness less than the coherence length), $\alpha_d = [d(10-d)-12]/8$, $a_2 \simeq 0.33$, $a_3 \simeq 0.53$, and $\tilde{\epsilon} = (E_g - E)/\epsilon_T$.[1] The energy scale is

$$\frac{\Delta}{\epsilon_T} \simeq \begin{cases} a_{\epsilon_T,3}\sigma^{-8/5} & \text{for } d=3 \\ a_{\epsilon_T,2}\sigma^{-4/3} & \text{for } d=2 \end{cases} \tag{4.25}$$

with $a_{\epsilon_T,2} \approx 5.7$ and $a_{\epsilon_T,3} \approx 27.5$. [2] Our result coincides with [LO72] but the pre-exponential factor disagrees with [SI05].[3] In the calculation $\eta \ll 1$ and $\bar{\epsilon}\Delta \gg \epsilon_T$ was assumed.

4.3. Quasiparticle rates

As shown in the previous section, fluctuations in the density of magnetic impurities change the gap in the excitation spectrum from a hard gap at energy E_g to an exponentially decreasing tail of sub gap states, localized on a lengthscale set by the coherence length, the energy scale of the tail ϵ_T is set by the amount of fluctuations σ. As discussed in the introduction, quasiparticles can localize in these tail states, in the following we calculate the corresponding rates entering the phenomenological model (4.1) from the Diffusion equation (2.70).

[1] More accurately, $a_{\rho,3} = \frac{10A}{\pi 21^{3/2}}$ and $a_{\rho,2} = \frac{A\Xi_1}{\pi\sqrt{6\Xi_0}}$ with the numerical constants given in (G.7) and (G.13)

[2] More precisely $a_{\epsilon_T,3} = 6\times(32\pi/15)^{4/5}$ and $a_{\epsilon_T,2} = 2^{7/3}\Xi_0^{2/3}/3^{1/3}$

[3] We note a mistake in the two dimensional result given by [SI05]: The factor $(2\pi\eta)^{3/2}$ [written in their notation, η used in that paper corresponds to σ used here] introduced in their equation B12 should be replaced by $2\pi\eta$ for the two dimensional system, as it arises from the contribution of one Gaussian integral per dimension to the denominator in the disorder averaging, each of which contributes a factor $\sqrt{2\pi\eta}$ to the denominator. Additionally the numerical factor differs, it is not completely clear to us how that disagreement arises.

4.3.1. Rates

We assume that diffusion over lengthscales ξ is the fastest process and set $\vec{\nabla} f \simeq 0$ for energies above the bulk gap: Quasiparticles diffuse over a distance of the coherence length in a typical time

$$\tau_{diff}(E) \simeq \left[2\Delta\rho^2(E)K^-(E,E)\right]^{-1} \tag{4.26}$$

For $-\bar{\epsilon} \sim \mathcal{O}(1)$ coherence factor and density of states are of order of unity and diffusion can be considered fast if $2\Delta\tau_0 \gg 1$, with typical time for phonon emission τ_0. In aluminium Δ exceeds τ_0 by four orders of magnitude (see chapter 3) and the condition holds. Close to E_g, phonon emission slows down and the phonon emission rate becomes much smaller than τ_0, as will be shown below. Even when estimating the phonon emission time with τ_0, diffusion would be a fast process up to very close to the gap[4] $-\bar{\epsilon} \gtrsim 10^{-4}$, and in practice diffusion over length scales set by the coherence length is always a fast process in aluminium. This allows to approximate the distribution of mobile quasiparticles as spatial homogeneous, which greatly simplifies the following calculations.

4.3.1.1. Zero temperature

We neglect Pauli blocking $1 - f(E) \simeq 1$ and start by considering zero phonon temperature $n(E) = 0$. Averaging (2.70) over the volume of the superconductor, integrating over energy, multiplying with $2/\Delta$ and splitting the normalized quasiparticle density in a mobile part x_m of energy above the gap $\omega > E_g$, and a localized part x_l of energy $\omega < E_g$ we obtain equation (4.1) with

$$\begin{aligned} \Gamma_{\mathrm{loc}} x_m &\simeq \frac{2}{\Delta} \int_{E_g}^{\infty} d\omega \rho_{AG}(\omega) f(\omega) \tau_{loc}^{-1}(\omega) \\ \Gamma_{mm} &\simeq \Gamma_{ml} \simeq r \end{aligned} \tag{4.27}$$

where we neglected the effect of fluctuations on the density of states above the average gap. The recombination coefficient $r = 4\Delta^3/\tau_0 T_c^3$ is (approximately) independent of energy and disorder and the same for both recombination processes involving mobile quasiparticles. The localization time becomes

$$\tau_{\mathrm{loc}}^{-1}(\tilde{\epsilon}) \approx r \frac{a_d}{8-d} \left(\frac{\epsilon_T}{\Delta}\right)^{7/2} \left[\Gamma\left(\frac{4(\alpha_d+1)}{8-d}\right)|\tilde{\epsilon}|^2 + 2\Gamma\left(\frac{4(\alpha_d+2)}{8-d}\right)|\tilde{\epsilon}| + \Gamma\left(\frac{4(\alpha_d+3)}{8-d}\right)\right] \tag{4.28}$$

where the symbols Γ within square brackets denote the gamma function. If the time τ_{loc} was independent of energy, we would simply have $\Gamma_{\mathrm{loc}} = 1/\tau_{\mathrm{loc}}$. Here for our

[4] Using density of states and coherence factors of section 4.2.1

purposes we establish an upper bound on Γ_{loc} by considering the competition between localization and relaxation of a mobile quasiparticle into mobile states. Considering again quasiparticles with energy close to E_g, the rate τ_m^{-1} for the latter process is

$$\tau_m^{-1}(\tilde{\epsilon}) \simeq r \frac{4}{105} \sqrt{\frac{2}{3}} \left(\frac{\epsilon_T}{\Delta}\right)^{7/2} |\tilde{\epsilon}|^{7/2} \tag{4.29}$$

We define the crossover (normalized) energy ϵ_c by the equation $\tau_{\text{loc}}(\epsilon_c) = \tau_m(\epsilon_c)$ [$|\epsilon_c| \simeq 3.55\,(2.32)$ for $d = 3\,(2)$]; quasiparticles with energy $|\tilde{\epsilon}| > |\epsilon_c|$ will more likely remain mobile after emitting a phonon, rather than localize, while the opposite holds for $\epsilon < \epsilon_c$. Therefore, the relevant energy range determining x_m can be taken between $\tilde{\epsilon} = 0$ ($E = E_g$) and $|\tilde{\epsilon}| \sim \epsilon_c$, and since τ_{loc}^{-1} is an increasing function of energy, we conclude that $\Gamma_{\text{loc}} \lesssim \tau_{\text{loc}}^{-1}(\epsilon_c)$; in what follows, we will take Γ_{loc} to be given by the upper bound,

$$\Gamma_{\text{loc}} \simeq b_d r (\epsilon_T/\Delta)^{7/2}, \tag{4.30}$$

with $b_3 \simeq 2.62$ and $b_2 \simeq 0.59$.

The recombination rate between two localized quasiparticles cannot be obtained using the approach employed here, as correlations between quasiparticle positions become important. However, the corresponding rate was calculated by [Bes+16] for three dimensional systems, we can qualitatively express the main insight of that paper by writing the recombination rate in the form

$$\Gamma_{ll} = g(\kappa)\Gamma_{mm} \tag{4.31}$$

Here, g is a function of the dimensionless parameter $\kappa = (n_{C_p} r_c^3)^2 g_m/\Gamma_{mm}$, where the radius of a localized state r_c is on the order of the coherence length and n_{C_p} the pair density, that is always smaller or equal unity, for $\kappa \gg \kappa_c$ it approaches unity while for $\kappa \ll \kappa_c$ it is smaller than unity. The crossover has been estimated from simulations to $\kappa_c \sim 10^{-4}$. In appendix G.3 we generalize the arguments developed in Ref. [Bes+16] to films thin compared to the coherence length.

4.3.1.2. Finite temperature

In the previous subsection delocalization processes were neglected as well as quasiparticle creation from phonons. The creation rate due to phonons results from the first term in the third integral in (2.86). We can distinguish three different contributions: Both quasiparticles are created as mobile quasiparticles, one is created as mobile and one as localized quasiparticle and both are created as localized quasiparticles. The latter process creates two quasiparticles within the same trap that quickly recombine, and should be excluded from our model. We give the other rates in appendix G.3, for not too low temperatures $T > \epsilon_T$ the generation rate for mobile quasiparticles by thermal phonons greatly exceeds that of the localized $g_m \gg g_l$. For sufficiently low temperatures $T \lesssim \epsilon_T$ this is not true when considering only quasiparticle generation from thermal phonons. However, at very low temperatures various non-equilibrium

processes dominate the creation of quasiparticles and the energy scale of quasiparticles created by the non-equilibrium process should be compared to ϵ_T instead. For instance, if the quasiparticle creation results from the absorption of radiation of energy far above the Debye energy followed by a cascade of phonon emission and pair breaking processes, the distribution of energies of pair breaking phonons (of energy above $2E_g$) created during the cascade decreases over an energy scale of several times the gap [5] such that the assumption $g_m \gg g_l$ holds for such processes.

As noted by [SI05], the excitation rate due to phonons is usually negligible for phonon temperature on the order of Milikelvin: For traps much deeper than the phonon temperature $\epsilon_T \gg T$, it is suppressed exponentially, and thus negligible. If instead the temperature is large compared to the depth of a trap $T \gg \epsilon_T$, we can estimate

$$\tau_{ex,pn}^{-1} \simeq a_T r \left(\frac{T}{\Delta}\right)^{7/2} \tag{4.32}$$

with $a_T = \sqrt{\frac{2\pi}{3}}\frac{15}{32}\zeta\left(\frac{7}{2}\right) \simeq 0.76$ for $T \ll \Delta\eta^{2/3}$ and the same absorption rate as for clean superconductors [Kap+76] $a_T = \zeta\left(\frac{7}{2}\right)\Gamma\left(\frac{7}{2}\right)/(4\sqrt{2}) \simeq 0.66$ for $T \gg \Delta\eta^{2/3}$. For temperatures sufficiently below the critical temperature, de-trapping by phonon absorption becomes very slow even for very shallow traps - for example for aluminium with $\tau_0 \sim 10^{-7}s$ the de-trapping time at milikelvin temperatures is of the order of seconds, and even very shallow traps can host a quasiparticle for long time. While absorption of phonons is not efficient at de-trapping quasiparticles, absorption of photons with energy $\omega_0 \gg \epsilon_T$ should be considered, as done in Ref. [Grü+18] for resonators. For such devices, one can set $\Gamma_{\mathrm{ex}} = \Gamma_0\bar{n}$, where $\bar{n}$ is the average number of photons stored in the resonator and Γ_0 is in general a material- and geometry-dependent parameter; it can be related to the coupling strength $c_{\mathrm{phot}}^{\mathrm{QP}}$ between the photons and the quasiparticles, $\Gamma_0 = c_{\mathrm{phot}}^{\mathrm{QP}}\sqrt{2\Delta/\omega_0}$; for aluminum resonators, we estimate $\Gamma_0 \approx 10^{-1}$-$10^{-2}\,\mathrm{s}^{-1}$. Finally, for $T \gg \epsilon_T$ the localization rate becomes modified due to stimulated phonon emission

$$\tau_{loc}^{-1}(E) = \frac{\epsilon_T^{5/2}T}{\Delta^{7/2}}\frac{a_d r}{8-d}\left(|\tilde{\epsilon}|\Gamma\left(\frac{4}{8-d}(\alpha_d - 1 + d/4)\right) + \Gamma\left(\frac{4}{8-d}(\alpha_d + d/4)\right)\right) \tag{4.33}$$

Compared to the excitation rate, the localization rate contains a small factor $(\epsilon_T/T)^{5/2}$ and we can use $\tau_{loc}^{-1} \ll \tau_{ex,pn}^{-1}$ for $T \gg \epsilon_T$.

4.4. Quasiparticle dynamics

Having estimated all relevant rates, we can turn to solving the rate equations (4.1), for simplicity we focus on the steady state $dx_l/dt = dx_m/dt = 0$ and assume quasiparticle

[5] The quasiparticle energy distribution during such a cascade is given in equation 26 of[Koz+00]. Calculating the total number of phonons emitted in a cascade as $N_{ph}(E) = \frac{4\rho_F}{\tau_0 T_c^3}\int_{E+\Delta}^{\infty} dE' \int_0^{\infty} dt E^2 K^-(E',E)\rho(E'-E)f(E',t)$ we obtain a phonon distribution in which only 18% of the phonons of energy $E > 2\Delta$ are in the interval $[2\Delta, 3\Delta]$.

creation as mobile quasiparticles $g_m \gg g_l$. First consider a small excitation rate, $\Gamma_{ex} \simeq 0$ and assume a sufficiently high quasiparticle density $\kappa \gg \kappa_c$ such that $\Gamma_{ll} \simeq r$. In that case the total quasiparticle density is the same as in the system without disorder $x = x_l + x_m = \sqrt{g_m/r}$ independent of the localization rate. The ratio of both components however does depend on the localization time

$$x_l = \sqrt{\frac{g_m}{r}}\frac{\beta}{1+\beta} \qquad x_m = \sqrt{\frac{g_m}{r}}\frac{1}{1+\beta} \tag{4.34}$$

with $\beta = \frac{\Gamma_{loc}}{\sqrt{r g_m}}$. Thus, in the limit of large $\beta \gg 1$ and $\kappa \gg \kappa_c$ the subgap states act as quasiparticle traps without increasing their density, which might be beneficial for qubits [Riw+16]. In the regime with large $\kappa \gg \kappa_c$ but small $\beta \ll 1$ the density of mobile quasiparticles greatly exceeds the density of localized quasiparticles and the subgap states have little influence on the quasiparticle's dynamics. Indeed, in that limit the rate for recombination of two localized quasiparticles $\tau_r^{-1} \simeq \sqrt{r g_m}$ is much larger than the rate for quasiparticle localization, hence most quasiparticles recombine before they have a chance to localize. Turning to the limit $\kappa \ll \kappa_c$ the localized-localized recombination rate decreases compared to the recombination rate between mobile quasiparticles. Still, if additionally $\beta \lesssim 1$, most of the quasiparticles are in a mobile state, and this reduction of the recombination rate cannot lead to an enhancement of the quasiparticle density. The mechanism suggested in Ref. [Bes+16] could thus only lead to an increase in quasiparticle density in the limit in which $\kappa \ll \kappa_c$ while $\beta \gg 1$. As the density is expected to monotonically decrease upon decreasing the generation rate, we can estimate an upper limit for the quasiparticle density in that regime by setting $\beta \sim 1$, leading to

$$x_l \lesssim \Gamma_{\mathrm{loc}}/r \tag{4.35}$$

We stress that only if the (total) density is below this upper limit, the mechanism considered in Ref. [Bes+16] could be relevant, since if the density is higher, x_l is determined by the competition between localization of mobile quasiparticles and localized-mobile recombination, while localized-localized recombination can be ignored. Now we consider the effect of a finite excitation rate $\Gamma_{ex} \neq 0$. As only the first term on the right-hand side of the first equation in (4.1) is positive [we keep the assumption $g_l \simeq 0$], a large excitation rate $\Gamma_{ex} \gg \Gamma_{loc}$ would imply $x_m \gg x_{loc}$ and the effect of localization would be negligible. Indeed, for $\kappa \gg \kappa_c$ equation (4.34) generalizes to

$$x_m = \sqrt{\frac{g_m}{r}}\frac{1+\tilde{\beta}}{1+\beta+\tilde{\beta}}, \quad x_l = \sqrt{\frac{g_m}{r}}\frac{\beta}{1+\beta+\tilde{\beta}} \tag{4.36}$$

where $\tilde{\beta} = \Gamma_{\mathrm{ex}}/\sqrt{g_m r}$. Thus, while the total density is unaffected by the finite excitation rate, a finite excitation rate increases the density of mobile quasiparticles on the expense of localized ones. A regime $\kappa \ll \kappa_c$ corresponding to $\Gamma_{ll} \ll r/\beta^2$ (with the further assumptions $\beta \gg 1$ and $\Gamma_{\mathrm{ex}} \ll \Gamma_{\mathrm{loc}}$) was considered in Ref. [Grü+18]; in this

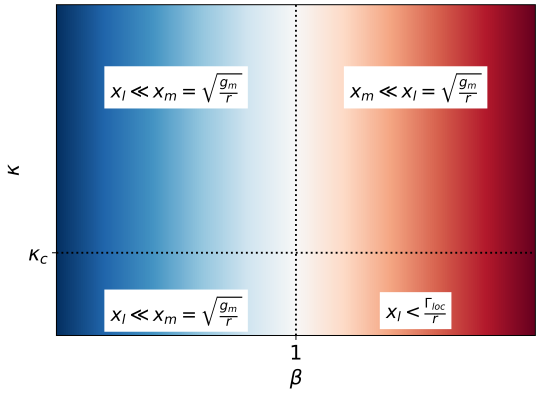

Figure 4.2.: Diagram representing the different regimes at zero excitation rate as a function of β and κ. The shades of red and blue represent regimes in which most quasiparticles are localized or mobile respectively. The increase in quasiparticle density proposed by [Bes+16] can only be relevant in the regime of $\kappa \ll \kappa_c$ and $\beta \gg 1$.

case, one can in fact ignore the effect of localized-localized recombination processes and the localized density is approximately

$$x_l \simeq \frac{\Gamma_{\text{loc}}}{r}\left[1+\frac{\bar{\gamma}}{1+\frac{1}{2}\left(\sqrt{1+4\bar{\gamma}}-1\right)}\right]^{-1} \tag{4.37}$$

with $\bar{\gamma} = 2\Gamma_{\text{loc}}\Gamma_{\text{ex}}/(g_m r) = 2\beta\tilde{\beta}$. Again, $x_l \sim \Gamma_{loc}/r$ provides an upper bound on the density of localized quasiparticles, a finite excitation rate can only further suppress the density below this limit.

4.5. Experimental consequences

Having discussed the relevant rates and dynamics, we turn to discussing the relevance of localization for experiments. For concreteness we focus on aluminum devices. The recombination coefficient and the localization rate depend on the material, while generation and excitation rates generally depend on experimental details such as temperature, device shielding and filtering. The recombination rate is rather well known, as in section 3.5.1.1 we estimate it to $r \sim 10^7 Hz$. The localization rate is sensitive to the energy scale ϵ_T which is generally not well known, to estimate it we note that - for our theory to apply - it must be small compared to the broadening of the peak $\epsilon_T \ll \eta^{2/3}\Delta$. In experiments usually the phenomenological Dynes parameter γ_D is used in fitting data sensitive to the peak shape using the formula $\rho_D(E) = \text{Re}[(E/\Delta + i\gamma_D)/\sqrt{(E/\Delta + i\gamma_D)^2 - 1}]$, we take the phenomenological broadening obtained in that way as an upper limit for the broadening $\Delta\eta^{2/3} \lesssim \gamma_D$. Although the Dynes formula predicts a finite DoS of order γ_D also at small energies $E \ll \Delta$, in

general the peak broadening and the deep subgap DoS are determined by different parameters; for example, if the broadening is due to the superconductor being in tunnel contact with a normal-metal film, the formula stops being valid below a so-called minigap energy whose value depends on the property of the normal layer [HC18]. For this reason, we do not estimate γ_D from measurements sensitive to deep subgap states. Current-voltage measurements in relatively thick (500 nm) Al SINIS structures found $\gamma_D \simeq 3 \times 10^{-4}$ [ONe+10]; experiments on thermal transport [For+15; For+17] and thermoelectric effect [Ger+22] in Josephson junctions with Al films of thicknesses between 14 and 40 nm report γ_D between 5×10^{-4} and 5×10^{-3}. As mentioned above, for the theoretical modeling of the subgap states that we use to be consistent, the condition $\epsilon_T \ll \gamma_D \Delta$ must be satisfied, so we conservatively assume $\epsilon_T/\Delta \sim 5 \times 10^{-4}$, a value an order of magnitude larger than estimated in Ref. [SI05]. Then according to Eq. (4.35) we have $x_l \lesssim \Gamma_{\rm loc}/r < 10^{-11}$. Since in Al we have $n_{\rm Cp} \simeq 5 \times 10^6\,\mu{\rm m}^3$, this normalized density corresponds to less than one quasiparticle even in large devices such as 3D transmons [Pai+11] or coplanar waveguide resonators [Vis+14] with volume of the order a few times $10^3\,\mu{\rm m}^3$. Therefore we must conclude that localization does not contribute to excess quasiparticles in typical aluminum devices.

Given our estimate above for ϵ_T, we additionally note that in typical experiments at $T \simeq 10\,{\rm mK}$, we have $T/\epsilon_T \sim 8$; even though the excitation rate in Eq. (4.32) is slow, $\Gamma_{\rm ex} \sim 0.03\,{\rm Hz}$, in rough agreement with the estimate in Ref. [SI05], the excitation rate exceeds the localization rate and the density of mobile quasiparticles thus exceeds the density of localized quasiparticles, again pointing to the conclusion that localization is not relevant in determining the quasiparticle density for typical aluminium devices.

In the discussion above we have considered typical Al-based devices. Even keeping aluminum as the main superconducting material, the value of γ_D and hence possibly the ratio ϵ_T/Δ can be increased in several ways, for example by Mn doping [ONe+10] and by proximity effect with a normal metal [HC18] such as Cu [Ger+22], methods that however suppress the gap Δ. Alternatively, oxygen doping can increase Δ [DG81; Val+19] (up to a point) as well as γ_D [Dyn+84]; in fact, the quasiparticle dynamics in granular aluminum resonators appears to be affected by localization [Grü+18]. Other materials, such as Nb ($\gamma_D \sim 5 \times 10^{-2}$ [Nev+12]), NbN ($\gamma_D \sim 2.4\text{-}4 \times 10^{-2}$ [CNM13]), or TaN ($\gamma_D \sim 7 \times 10^{-2}$ [CM14]), also have larger broadening (in units of Δ) than Al. Increasing ϵ_T/Δ by an order of magnitude would push up the bound on x_l by more than three orders of magnitude as well as make possible experiments in the regime $T \lesssim \epsilon_T$ in which excitation by thermal phonon is slower than localization. Moreover, materials with higher gap generally have faster recombination (larger r) than Al [Kap+76], making it easier to reach the regime $\beta > 1$ for a given generation rate g (since $\beta \simeq (\epsilon_T/\Delta)^{7/2}\sqrt{r/g_m}$. Therefore, exploring devices fabricated with properly chosen materials could shed further light on the role of subgap states in their performances. In a complementary direction, one could also consider the case of more strongly coupled magnetic impurities, such that an impurity band of localized states is formed with energy well below the gap [FS16]; then localization and mobile-localized quasiparticle recombination could be enhanced [Koz+08], effects that have been used

to interpret experiments in superconducting tunnel junction detectors [Hij+09].

Finally, we note that measurements of generation-recombination noise may provide an indication for the presence of subgap states. Neglecting recombination between mobile and localized quasiparticles, [WP04] already showed that (for small excitation rates) a measurement of generation-noise allows for a direct measurement of trapping rates. In appendix G.4 we extend these considerations to a non-zero Γ_{ml} and show that the noise power spectrum is also modified in the limit in which mobile-localized recombination dominates over excitation processes.

5. Conclusion

Quasiparticles affect a large variety of superconducting devices. At low temperatures, the quasiparticle density and energy distribution usually become non-thermal and are dominated by various non-equilibrium processes, depending on the device and experimental setup. In this thesis, we studied in detail the quasiparticle energy distribution in superconducting resonators in the regime of large photon numbers (of energy below the pair breaking threshold) and low phonon temperatures, as typically used in kinetic inductance detectors. To this end we use a (long known) set of rate equations [Eqs. (3.1,3.2,3.13)], which can be derived from quasiclassical theory, and obtain new approximate analytical solutions for the distribution in energy, that are valid if the distribution is broad compared to the photon energy [i.e. $T_* > \omega_0$]. These solutions are verified by comparison to numerical solutions. From these solutions we conclude that

- Interaction with photons leads to a width of the quasiparticle distribution in energy set by an energy scale T_* [or $\tilde{T}_*$ for energy $E > 2\Delta$] that increases with photon number [Eqs. (3.23,3.28)]. The polynomial decrease of the distribution function with energy for $E < T_*$ changes to a compressed exponential decrease for $E > T_*$[Eqs. (3.24,3.25,3.31)]. For energies $E > E_*$, the distribution function changes to a Boltzmann distribution due to phonon absorption, with crossover energy $E_* \sim \Delta + T_*\sqrt{T_*/T_B}$ [$E_* \sim \Delta + \tilde{T}_*(\tilde{T}_*/T_B)^{2/3}$ for $E > 2\Delta$ instead], increasing with photon number $\bar{n}$ and decreasing with phonon temperatures T_B.

- At sufficiently high T_B and sufficiently low $\bar{n}$, such that $T_B^* \sim \Delta(T_*/\Delta)^3 < T_B$, thermal phonons dominate quasiparticle creation and the quasiparticle density is the same as in equilibrium. Photon absorption broadens the distribution in energy, leading to an internal quality factor increasing with photon number and decreasing with phonon temperature T_B [Eq. (3.112)].

- At very high photon numbers/very low phonon temperatures, absorption of many low energy photons drives quasiparticles to energies above 3Δ, allowing them to create new quasiparticles. This becomes the dominant process for $T_B < T_B^*$, and the quality factor becomes independent of phonon temperature and (exponentially) decreasing with photon number [Eq. (3.111)].

The low photon number regime agrees with recently measured quality factors of superconducting aluminium resonators for temperatures $T_B \gtrsim 0.25K$. Reaching the high photon number regime requires several orders more photons than usually used in aluminium resonators, and does not provide a satisfying explanation for the saturation

of the quality factor observed at very low temperatures $T_B \lesssim 0.25K$. Instead, we propose that a small number $\bar{n}_{PB} = \bar{n}_{PB,0} + \mu\bar{n}$ of photons of energy above the pair breaking threshold $\omega_{PB} > 2\Delta$, with $\mu = 10^{-9}$ and $\bar{n}_{PB,0} = 2 \times 10^{-4}$, which we ascribe to higher harmonic noise of the microwave generator, may be responsible for the saturation. The resonators used in these experiments contain many non-pair breaking photons, that dominate the distribution's shape, while the pair breaking photons only contribute to the quasiparticle density. The pair breaking photon's contribution to the density has a similar form as the one from thermal phonons, when introducing an effective 'temperature' $\bar{T}_B$ [Eq. (3.83)] increasing with the number of pair breaking photons. In the opposite limit $\bar{n} = 0$, pair breaking photons can dominate both the quasiparticle density and the distribution's shape. We derive new analytic solutions for the quasiparticle energy distribution in the limit $\omega_{PB} < 3\Delta; \bar{n} = 0; T_B = 0$ [Eqs. (3.73, 3.77)] and investigate its crossover to the shape obtained for $\bar{n}_{PB} = 0$ upon increasing $\bar{n}$ or T_B [Eq. (3.91)]. The solutions at $\bar{n} = 0; T_B = 0$ depend on a dimensionless parameter $\gamma'_* = \left(\frac{\tau^{qp}_{e,n}(\xi)}{\tau^{qp}_r}\right)^{2/7}$, given by the lifetime of a quasiparticle against phonon emission $\tau^{qp}_{e,n}(\xi)$ at the highest energy above the gap at which quasiparticles are created, $\xi = \omega_{PB} - 2\Delta$, and the quasiparticle's lifetime against recombination τ^{qp}_r. If $\gamma'_* \gg 1$, phonon emission can be neglected at all energies, and the distribution's width is set by the energy range over which quasiparticles are created $\sim \xi$. If instead $\gamma'_* \lesssim 1$, the distribution's width is reduced by phonon emission to $\sim \gamma'_* \xi$.

In chapter 4 we investigate the influence of localized states on the dynamics of quasiparticles. To do this we generalize the phonon collision integral [Eq. (2.86)] to superconductors containing magnetic impurities of a (spatially) fluctuating density, described by a spatially inhomogeneous version of Abrikosov-Gorkov theory [Eq. (4.4)]. From this collision integral, we are able to obtain effective rates describing the system in terms of mobile and localized quasiparticles [see appendix G.3]. We introduce two dimensionless parameter $\kappa = (n_{C_p} r_c^3)^2 g_m / r$ and $\beta = \frac{\Gamma_{loc}}{\sqrt{r g_m}}$ to describe the dynamics of the quasiparticles, with pair density n_{C_p}, size of a localized state r_c of order of the coherence length, generation rate of mobile quasiparticles g_m, localization rate Γ_{loc} and recombination coefficient r [with all rates normalized by the pair density]: β controls the ratio of localized quasiparticles to mobile quasiparticles, κ determines whether recombination between localized quasiparticles is modified by the localization. We show that an increase in quasiparticle density due to localization only occurs if $\beta \gg 1$ and simultaneously $\kappa \ll \kappa_c \sim 10^{-4}$. The condition on β results from the competition of localization and recombination processes and implies the localized density to exceed the mobile one, while the condition on κ implies a regime in which correlations in positions of localized quasiparticles become important for their recombination rate. As the former condition does not hold in typical aluminium devices, we expect a negligible influence of localized state on the quasiparticle dynamics. This is in contrast to previous publications that only considered the condition on κ but ignored the condition on β. While trapping may be more important in devices with other materials, we emphasize that also in that case both mobile and localized quasiparticles must be considered to ensure the condition on β holds.

A. Thin film coplanar waveguides

In this appendix, we summarize the calculation of the impedance of a thin film coplanar waveguide, following [Cle13]. We choose our coordinate system with z along the length of the resonator, x along the resonator's width and y normal to the film's surface.

A.1. Transverse electromagnetic modes

A time harmonic field propagating along a waveguide in z-direction can generally be written as

$$\vec{E}(x,y,z) = (\vec{E}_t(x,y) + E_z(x,y)\vec{e}_z)e^{i\beta z}e^{i\omega_0 t} \tag{A.1}$$

$$\vec{H}(x,y,z) = (\vec{H}_t(x,y) + H_z(x,y)\vec{e}_z)e^{i\beta z}e^{i\omega_0 t} \tag{A.2}$$

In the following we look for a transverse electromagnetic mode with $E_z = H_z = 0$ propagating in the waveguide and assume a source free region outside the superconductor. Such a mode provides a solution to Maxwell's equation if [sec. 3.1 of [Poz12]]

$$\nabla_t^2 \vec{E}_t = \nabla_t^2 \vec{H}_t = 0 \tag{A.3}$$

with $\nabla_t^2 = \partial_x^2 + \partial_y^2$. Thus, the field distribution is the same as for a static problem with $\omega_0 = 0$. To solve the magneto-static problem, it is convenient to introduce the vector potential $\vec{A}$. Choosing the London gauge, the field outside the superconductor is given by $\vec{A} = (0, 0, A_z)$, where A_z is determined by Laplace's equation

$$\nabla_t^2 A_z = 0 \tag{A.4}$$

Strictly, a coplanar waveguide does not support a purely transverse electromagnetic mode due to the finite conductance of the superconductor and the presence of the substrate [Gao08]. Usually these effects are small and will be disregarded in the following.

A.2. Impedance

In the following we summarize the calculation of resistance and inductance for a thin film resonator $d \ll \lambda$ following [Cle13].

As an electromagnetic field penetrates a distance λ into a superconductor, the current density is approximately homogeneous over distances smaller than λ from

its surface. In thin films of thickness $d \ll \lambda$, we can thus approximate the current density as independent of y. Surface scattering limits the mean free path to $l \lesssim d \ll \lambda$ and in this regime the response of the superconductor is described by the complex conductivity in Eqs. (1.30) and (1.32). It is convenient to introduce the sheet current density $\vec{I}_s = \int_0^d dy \vec{j}(y) \approx \vec{j}d$ to approximately rewrite equation (1.28) in terms of the sheet current density

$$\vec{I}_s = -\frac{d}{\Lambda}\vec{P}\delta(y) \tag{A.5}$$

with Gauge invariant potential $\vec{P}$ for a thin film whose surface is in the $x-z$ plane. Correspondingly,

$$\nabla^2 \vec{A} = \vec{P}\delta(y)/\Lambda \tag{A.6}$$

where $\Lambda = 2\lambda^2/d$ is the two-dimensional screening length[1] that gives the length-scale on which fields penetrate the central strip of the CPW from the gaps. Generally, calculating the electromagnetic fields in the CPW requires a simultaneous solution of Maxwell's equation outside the superconductor, along with the London equation inside the superconductor, which can only be done numerically. However, in two different limits analytical solutions are possible: If both the slot width and the width of the central conductor are much larger than the two-dimensional screening length, penetration of flux into the superconductor adjacent to the slots can be neglected.[2] This allows treating the superconductor as perfect conductor with

$$A_z(x,y) = A_z \text{ on superconducting surface} \tag{A.7}$$

and one can first use conformal mapping techniques to calculate the field outside the superconductor and obtain the current response of the superconductor in that field in a second step. If instead the slot width approaches zero, an exact solution can be obtained simultaneously to the thin film London equation and Maxwell's equations [Cle13]. The latter is a good approximation provided the screening length is small compared to the slot width, as penetration of flux into the superconductor results in an 'effective' slot width on the order of Λ, even if the real slot width approaches zero. We only summarize the derivation of the first limit in the following as the waveguide investigated in chapter 3 is in that limit.

The goal is to solve the (two-dimensional) Laplace equation (A.4) with boundary condition (A.7) where the shape of the superconductor is given in figure A.1. Consider a complex function

$$f(z) = u(x,y) + iv(x,y) \tag{A.8}$$

with real u, v and $z = x + iy$. For any analytic f, its real part is a solution of the two dimensional Laplace equation. Thus, rather than solving the two dimensional Laplace equation, one can search for an analytic function whose real part obeys appropriate boundary conditions. This task can often be simplified by introducing a

[1] first introduced by [Pea64]

[2] We assume the film not to contain any vortices.

change in coordinate system by introducing a map $g : z \to a + ib$ with analytical g. As a composition of two analytic complex functions $f(g(z))$ defines a conformal map (i.e. a mapping that preserves angles), Laplace's equation can be solved in the new coordinate system where the boundary conditions $u(z_0) = const$ transform as $u(g(z_0)) = const$. For the (zero-thickness) coplanar waveguide shown in figure A.1 the upper half z-plane can be mapped to the interior of a parallel plate capacitor using the mapping[3] [Gao08]

$$a + ib \equiv g(z) = \int_0^z dz' \frac{1}{\sqrt{(1 - \left(\frac{2z'}{w}\right)^2)(1 - \frac{w^2}{(w+2s)^2}\left(\frac{2z'}{w}\right)^2)}} \tag{A.9}$$

shown in figure A.1. The magnetic field is given by $A_z = \mathcal{C}b$ with a real constant $\mathcal{C}$ given by the boundary conditions. The complex magnetic field $B = B_x + iB_y$ can be evaluated using the definition of the magnetic vector potential $\vec{B} = \nabla \times \vec{A}$ and the Cauchy-Riemann relationships

$$\frac{dg(z)}{dz} = 2(\partial_y A_z + i\partial_x A_z) = 2(B_x - iB_y) \tag{A.10}$$

Using Eqs. (A.5) and (A.6) the sheet current density is given by [Cle13]

$$I_s = -2\lim_{\epsilon\to 0} H_x(x,\epsilon) = \begin{cases} \frac{s+\frac{w}{2}}{2K(k)} \frac{I_z}{\sqrt{\left(\left(\frac{w}{2}\right)^2 - x^2\right)\left(\left(\frac{w}{2}+s\right)^2 - x^2\right)}} & \text{for } |x| < w/2 \\ -\frac{s+\frac{w}{2}}{2K(k)} \frac{I_z}{\sqrt{x^2 - \left(\left(\frac{w}{2}\right)^2\right)\left(x^2 - \left(\frac{w}{2}+s\right)^2\right)}} & \text{for } |x| > w/2 + s \end{cases} \tag{A.11}$$

with the magnetic field (A.10), $k = w/(w + 2s)$ and the Legendre elliptic integral K.Here, the constant $\mathcal{C}$ was fixed by demanding the total current through the central strip to be I_z. Using Faraday's law, the geometric inductance can also be calculated from the flux Φ through one of the slots of the waveguide

$$L_m = \frac{\Phi}{I_z} \tag{A.12}$$

instead of definition (1.40). Integrating

$$B_y = -\Im \frac{I_z \mu_0}{4K(k)\sqrt{1 - \left(\frac{2z}{w}\right)^2}\sqrt{1 - k^2\left(\frac{2z}{w}\right)^2}} \tag{A.13}$$

along the positive part of the x-axis to obtain the flux per unit length gives the well known result [WYK94; Cle13]

$$L_m = \frac{\mu_0 K(k')}{4K(k)} \tag{A.14}$$

[3] This mapping is a special case of the Schwarz-Chirstoffel mapping that maps the upper half plane to the interior of a polygon.

Near the slot edges, the sheet current (A.11) diverges. This is a consequence of the use of the perfect conductor boundary condition that does not allow for flux penetration, while in fact flux penetrates on a length scale $\Lambda \ll w, s$ from the slot edges. Thus, one should introduce cutoffs in the surface integral in Eq. (1.39) that are chosen such that the total current in the center strip equals the returning current through the ground plane. This leads to a kinetic inductance per unit length [Cle13]

$$L_k \approx \frac{\mu_0 \Lambda}{w} \frac{\ln\left(\frac{2(1-k)}{\epsilon(1+k)}\right)}{2(1-k)K^2(k)} \tag{A.15}$$

where the cutoff $\epsilon \sim \Lambda/w$ and the current was approximated constant over the thickness of the film.

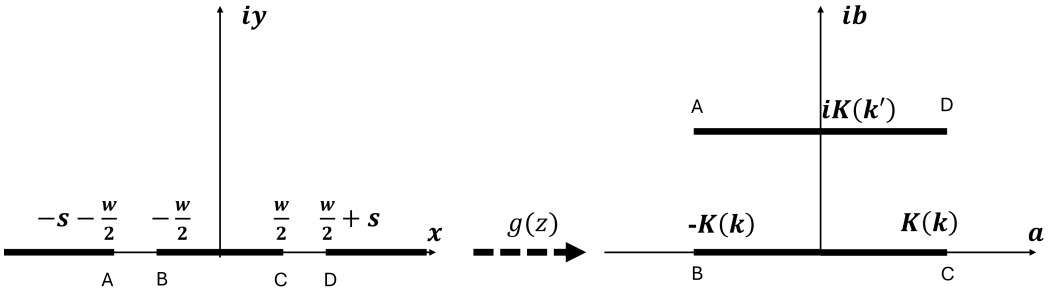

Figure A.1.: Thin film coplanar waveguide. The conformal map (A.9) maps the upper half plane of a coplanar waveguide to the interior of a parallel plate capacitor. Here, $k = w/(w + 2s)$ and $k' = \sqrt{1-k^2}$, K is the Legendre elliptic integral.

B. Feynman rules

In the main text the Feynman rules for the Nambu-Keldysh Green's function are given, here they are derived more in detail. The starting point is equation (2.10) with the contour c_2 replaced by the Keldysh contour c_K. As explained in the main text, the numerator can be set to unity, and we will only consider the full single particle Nambu Green's functions in the following. Expanding the interaction part of the exponential in a series, we can rewrite it as

$$\boldsymbol{G}_1(1,1') = -\boldsymbol{\tau}_3 \left(1 + \sum_{n=1}^{\infty} \frac{(-i)^n}{n!} \int_{c_K} dt_1 ... dt_n \right) \tag{B.1}$$

$$\times \mathrm{Tr} \mathcal{T}_{c_K} \left(\exp\left(-i \int_{c_K} dz H_0(z) \right) H_{int}(t_1) ... H_{int}(t_n) \boldsymbol{\psi}(1) \boldsymbol{\psi}^\dagger(1') \right) \tag{B.2}$$

The RHS can be rewritten in terms of the higher order bare Green's functions by rewriting the Hamiltonians as traces of products of Nambu spinors. For instance, we can write the Hamiltonian for interaction with an external potential

$$H_{int,V} = \sum_i \int d^3 r \boldsymbol{\psi}_i(\vec{r}) \boldsymbol{V}(\vec{r},t)_{i,i} \boldsymbol{\psi}_i^\dagger(\vec{r}) \tag{B.3}$$

where $\boldsymbol{V}(\vec{r}) = \boldsymbol{\tau}_3 V(\vec{r},t)$ for scattering preserving time reversal symmetry (e.g. non-magnetic impurities) and $\boldsymbol{V} = \mathbf{1} V(\vec{r},t)$ for interactions violating time reversal symmetry (e.g. the $\vec{p}\cdot\vec{A}$ term in the interaction with electromagnetic fields). The first order correction to the single particle Green's function $\boldsymbol{G}_1(1,1')_{j,k}$ becomes

$$\boldsymbol{G}_1^{(1),V}(1,1')_{j,k} = -i \int d1'' \sum_i \boldsymbol{G}^{(0)}_{2,i,j,i,k}(1'',1,1'',1') \boldsymbol{V}(1'')_{i,i} (\boldsymbol{\tau}_3)_{i,i} \tag{B.4}$$

where the integral includes spatial integration and integration along c_K. Applying Wicks theorem this becomes

$$\boldsymbol{G}_1^{(1),V}(1,1') = i \int d1'' \boldsymbol{G}^{(0)}(1,1'') \boldsymbol{V}(1'') \boldsymbol{\tau_3} \boldsymbol{G}^{(0)}(1'',1') \tag{B.5}$$

where the product is the matrix product, and the linked cluster theorem was used to drop vacuum diagrams. Higher order terms can be decomposed in the same way. Further simplification is possible by introducing the Green's function in Keldysh space $\hat{G}^{\pm}$ of Eq. (2.26) – the Green's functions in (B.5) are replaced by $\hat{G}^{\pm}$, the potential is a $\hat{\tau}_3$ matrix in Keldysh space, and the matrix multiplication also includes Keldysh indices.

For the interaction with phonons, we only include transitions that do not include interaction with an impurity [see [RS86b] for the opposite case]. These interactions can be obtained by replacing $V(1) \to g\boldsymbol{\tau}_3 u^l(1)$. The lowest order correction becomes

$$\boldsymbol{G}_1^{(2),ph}(1,1')_{k,l} = -ig^2 \int d1''d1''' \sum_{i,j} \boldsymbol{G}^{(0)}_{3,i,j,k,i,j,l}(1'',1''',1,1'',1''',1')D_0(1'',1''') \quad \text{(B.6)}$$

with phonon propagator $D_0(1,1') = -i\langle u_l(1)u_l(1')\rangle$. Decomposing into single particle Green's functions using Wick's theorem again results in the usual Feynman rules [BF04], when using the matrix Green's function and including a summation over internal matrix indices in the integral over the internal coordinates. Rewriting the Green's functions as matrices in the ± space, it becomes necessary to distinguish the position of the time arguments of the phonon Green's function on the Keldysh contour. The vertex describing phonon emission (absorption) thus acquires a tensor structure $\hat{\gamma}^k_{i,j} = \hat{\delta}_{i,j}(\hat{\tau}_3)_{j,k}$, where k is the index of the phonon function in ± space [L V65]. We thus get the following rules in ±-space

- The electron self energy consists of all topologically different, one-line irreducible, connected diagrams containing two external electron lines
- The electron Green's function $\hat{G}_0^{(0),\pm}$ is a matrix in Nambu and in Keldysh space, the phonon Green's function $\hat{D}_0$ is a matrix in Keldysh space. Phonon lines correspond to $i\hat{D}_0$.
- Interaction vertices with external fields are given by $\boldsymbol{V}(1)\boldsymbol{\tau}_3\hat{\tau}_3$, electron phonon interaction vertices by $g\hat{\gamma}$
- Each Fermion loop is multiplied by -1
- Integrate over internal variables and sum over internal indices, with the time integrals from $-\infty$ to ∞

Apart from the tensor structure of the vertices and the matrix structure of the Green's function, these are the standard Feynmann rules that can also be obtained from equilibrium theory.

C. Quasiparticle and phonon lifetimes

In Sec. 3.3 a number of lifetimes have been introduced to qualitatively discuss the behaviour of the quasiparticle distribution function out of equilibrium. In this appendix, we give their precise definitions in terms of the non-equilibrium quasiparticle and phonon distributions, as obtained by inspecting the structure of the kinetic equations. As in Sec. 3.3, we consider first the phonon lifetimes.

The lifetime of a phonon of energy ω against pair breaking is [cf. the last term in curly bracket in the second integral in Eq. (3.13)]

$$\frac{1}{\tau_{PB}^{Phon}(\omega)} = \frac{1}{\pi\Delta_0\tau_0^{PB}} \int_{\Delta}^{\omega-\Delta} dE\, \rho(E) U^{+}(E, \omega - E) \left[1 - f(\omega - E)\right] \left[1 - f(E)\right] \tag{C.1}$$

Approximating the Pauli-blocking factors as $[1 - f(E)] \simeq 1$, as done throughout this paper, the dependence of $1/\tau_{PB}^{Phon}$ on ω can be expressed in terms of the spectral density S_+ of Refs. [Hou+19; GC21] as

$$\frac{1}{\tau_{PB}^{Phon}(\omega)} = \frac{\Delta}{\pi\Delta_0\tau_0^{PB}} S_{+}(\omega/\Delta)\,, \tag{C.2}$$

where

$$S_{+}(x) = (x+2)E\left(\frac{x-2}{x+2}\right) - \frac{4x}{x+2}K\left(\frac{x-2}{x+2}\right) \tag{C.3}$$

with E and K the complete elliptic integrals of the second and first kind, respectively. Note that $S_+(x) = 0$ for $x < 2$, $S_+(x) \approx x$ for $x \gg 2$, and $S_+(x) \approx \pi\left[1 + (x-2)/4\right]$ for $x - 2 \ll 2$. The last expression shows that the pair-breaking lifetime approaches τ_0^{PB} at low temperature and only weakly depends on energy for $\omega \gtrsim 2\Delta$.

The lifetime of a phonon against being absorbed by a quasiparticle is [cf. the last term in curly bracket in the first integral in Eq. (3.13)]

$$\frac{1}{\tau_{abs}^{Phon}(\omega)} = \frac{2}{\pi\Delta_0\tau_0^{PB}} \int_{\Delta}^{\infty} dE\, \rho(E) U^{-}(E, E+\omega) f(E) \left[1 - f(E+\omega)\right]. \tag{C.4}$$

For $f \ll 1$, one can show that the right-hand side is bounded by $1/\pi\tau_0^{PB}$ times the normalized quasiparticle density $N_{\rm qp}/2\rho_F\Delta$. Since at low temperature the latter is much smaller than 1, we have $\tau_{abs}^{Phon} \gg \tau_0^{PB}$.

The last phonon lifetime we take into account is the thermalization time τ_l. For of a phonon of energy 2Δ whose mean free path against pair breaking $s\tau_0^{PB}$ (with s the

speed of sound) is of a similar order as the film thickness d, τ_l can be estimated to be [Kap79; Eis+76; CS78]

$$\tau_l \approx \frac{4d}{\eta s} \tag{C.5}$$

where η is the direction-averaged transmission coefficient between film and substrate. For aluminium on sapphire, the speed of sound and transmission coefficient are approximately $s \simeq 3.3\text{-}6.7\,\mathrm{km/s}$ and $\eta \simeq 0.2$ [Kap79]. For the resonator of Ref. [Vis+14] considered in Sec. 3.6, this expression gives $\tau_l \approx 180\text{-}360\,\mathrm{ps}$. In Ref. [Vis+14] the value $\tau_l = 170\,\mathrm{ps}$ was used, and to simplify comparison to their results we also use this latter value in our analysis. Our results do not depend on the exact value of the thermalization time at energies $\omega < 2\Delta$, if the condition $\tau_{abs}^{Phon} \gg \tau_l$ holds, as is the case for both choices of τ_l. We note that some authors [Koz+04a; Koz+04b] suggest the thermalization time of phonons with $\omega < 2\Delta$ to be limited by total internal reflection and, for sufficiently smooth interfaces, to be several orders of magnitude longer than the one at energies above 2Δ. We assume this not to be the case and use the thermalization time at energy $\omega = 2\Delta$ for all energies.

We now turn to the quasiparticle lifetimes. The scattering lifetime $\tau_{s,t}^{qp}$ of a quasiparticle due to interaction with photons has three contributions

$$\frac{1}{\tau_{s,t}^{qp}} = \frac{1}{\tau_{sp,t}^{qp}} + \frac{1}{\tau_{st,t}^{qp}} + \frac{1}{\tau_{abs,t}^{qp}} \tag{C.6}$$

originating respectively from spontaneous emission, stimulated emission, and absorption of a photon. They are given respectively by [cf. the second terms in curly brackets in Eq. (3.9)]

$$\frac{1}{\tau_{sp,t}^{qp}} = c_{Phot}^{QP} U^{+}(E, E-\omega_0)\,[1 - f(E-\omega_0)] \tag{C.7}$$

$$\frac{1}{\tau_{st,t}^{qp}} = c_{Phot}^{QP} \bar{n} U^{+}(E, E-\omega_0)\,[1 - f(E-\omega_0)] \tag{C.8}$$

$$\frac{1}{\tau_{abs,t}^{qp}} = c_{Phot}^{QP} \bar{n} U^{+}(E, E+\omega_0)\,[1 - f(E+\omega_0)] \tag{C.9}$$

The scattering lifetime $\tau_{s,n}^{qp}$ due to interaction with phonons has also three contributions

$$\frac{1}{\tau_{s,n}^{qp}} = \frac{1}{\tau_{sp,n}^{qp}} + \frac{1}{\tau_{st,n}^{qp}} + \frac{1}{\tau_{abs,n}^{qp}} \tag{C.10}$$

accounting for spontaneous phonon emission [cf. the last term in curly brackets in Eq. (3.4)]

$$\frac{1}{\tau_{sp,n}^{qp}} = \frac{1}{\tau_0 T_c^3} \int_0^{E-\Delta} d\omega\, \omega^2 U^{-}(E, E-\omega)\,[1 - f(E-\omega)] \tag{C.11}$$

stimulated phonon emission [cf. the last term in curly brackets in the second integral of Eq. (3.5)]

$$\frac{1}{\tau^{qp}_{st,n}} = \frac{1}{\tau_0 T_c^3} \int_0^{E-\Delta} d\omega\, \omega^2 U^-(E, E-\omega) n(\omega) \left[1 - f(E-\omega)\right] \tag{C.12}$$

and phonon absorption [cf. the last term in curly brackets in the first integral of Eq. (3.5)]

$$\frac{1}{\tau^{qp}_{abs,n}} = \frac{1}{\tau_0 T_c^3} \int_0^{\infty} d\omega\, \omega^2 U^-(E, E+\omega) n(\omega) \left[1 - f(E+\omega)\right] \tag{C.13}$$

In addition, the lifetime of a quasiparticle against recombination is [cf. Eq. (3.7)]

$$\frac{1}{\tau^{qp}_{r}} = \frac{1}{\tau_0 T_c^3} \int_{E+\Delta}^{\infty} d\omega\, \omega^2 U^+(E, \omega-E) f(\omega-E) \left[1 + n(\omega)\right] \tag{C.14}$$

For a system in equilibrium, these lifetimes (except those due to photons) are discussed in Ref. [Kap+76]. When $f \ll 1$, the only lifetimes with significant dependence on the quasiparticle distribution function are τ^{Phon}_{abs} and τ^{qp}_{r}: since the rates are proportional to f, the times are inversely proportional to the quasiparticle density. In fact, in Appendix D.4 we study the dependence of the recombination coefficient R [that is, the recombination rate for the quasiparticle density, see Eq. (3.48)] on T_*, while as discussed in Sec. 3.4.1.3 the effect of τ^{Phon}_{abs} on the quasiparticle distribution can be neglected.

D. Non-pair-breaking photons

D.1. Finite phonon temperature

In this appendix we present in some detail the derivation of the results discussed in Sec. 3.4.1.2. As mentioned there, we want to find the energy E_* below which neglecting the effect of thermal phonons is justified, in which case the formulas of Sec. 3.4.1.1 can be used, and to find E_* we need an estimate for St_{st}^{Phon}, Eq. (3.5), at $E = E_*$. In the integrands in that equation, we assume as usual $f \ll 1$ at all energies; then as long as factors other than $n(\omega) = n_T(\omega, T_B)$ grow with ω slower than exponentially, the integral is determined by the integration in the interval around $\omega \sim T_B$. This is the case for all terms except that proportional to $f(E_* - \omega)$, which increases faster than exponentially; for this term, the integral can be estimated as follow: we consider a frequency ω_* such that $\omega_* \gg T_B$ and $\omega_M - \omega_* \gg \tilde{T}_*$, with $\omega_M \gg T_B$ to be defined below (here we assume $E_* \gtrsim 2\Delta$; for $E_* \lesssim 2\Delta$ the condition reads $\omega_M - \omega_* \gg T_*$, with ω_M having different definitions in the two cases). The contribution to the integral from the interval $0 < \omega < \omega_*$ can be estimated together with the other terms in Eq. (3.5), while that from $\omega_* < \omega < E_* - \Delta$ is to be considered separately.

Let us start with the low-frequency contribution, $\omega < \omega_*$, which we denote with $St_{st,low}^{Phon}$. Then since n restricts ω to be of order $T_B \ll E_*$, while the (envelope of the) quasiparticle distribution function f varies at most over a scale $T_* \gg T_B$, we can approximate $U^-(E_*, E_* \pm \omega) \approx 1$, perform a series expansion for the distribution functions, and push the integration limit from ω_* to infinity to find

$$St_{st,low}^{Phon} \approx \frac{1}{\tau_0 T_c^3} \int_0^\infty d\omega\, \omega^4 \left.\frac{\partial^2 f}{\partial E^2}\right|_{E=E_*} n(\omega, T_B)\,. \tag{D.1}$$

According to Eq. (3.31), for $(E_* - \Delta)/\tilde{T}_* \gg 1$ we have

$$\left.\frac{\partial^2 f}{\partial E^2}\right|_{E=E_*} \approx \frac{1}{\tilde{T}_*^2} \left(\frac{E_* - \Delta}{\tilde{T}_*}\right)^3 f(E_*) \tag{D.2}$$

and therefore

$$St_{st,low}^{Phon} \approx \frac{24\zeta(5)}{\tau_0 T_c^3} \left(\frac{T_B}{\tilde{T}_*}\right)^5 (E_* - \Delta)^3\, f(E_*)\,, \tag{D.3}$$

with ζ denoting the Riemann Zeta function. Comparing this expression to Eq. (3.34), it is clear that the low-frequency contribution can be neglected for $T_B \ll \tilde{T}_*$. The

similar calculation for the case $E_* \lesssim 2\Delta$ is slightly more complex, as one needs to use the approximation in Eq. (3.21) for U^-; the resulting condition reads $(E_*-\Delta)T_B^5/T_*^6 \ll 1$.

We now turn to the high-frequency contribution

$$St^{Phon}_{st,hi} \approx \frac{1}{\tau_0 T_c^3} \int_{\omega_*}^{E_*-\Delta} d\omega\, \omega^2 f(E_* - \omega) e^{-\omega/T_B}\,, \tag{D.4}$$

where the approximations employed are $U^- \approx 1$ and $n(\omega, T_B) \approx e^{-\omega/T_B}$. For $E_* - \omega > 2\Delta$, we can use Eq. (3.31) for f and estimate the integral using Laplace's method; indeed, the argument of the exponential has a maximum at the frequency $\omega_M = E_* - \Delta - \tilde{T}_*(\tilde{T}_*/T_B)^{2/3}$, and $E_* - \omega_M > 2\Delta$ if $T_B/\Delta < (T_*/\Delta)^3$. Similarly, for $E_* - \omega < 2\Delta$ one can use the asymptotic approximation for the result in Eq. (3.25) to find $\omega_M = E_* - \Delta - T_*(T_*/T_B)^{1/2}$, and $E_* - \omega_M < 2\Delta$ if $(T_*/\Delta)^3 < T_B/\Delta \ll T_*/\Delta$ [we note that the algebraic prefactor is different in this case, as U^- takes approximately the form given in Eq. (3.21)]. The estimate of the integral in Eq. (D.4) is then obtained by evaluating the prefactor at $\omega = \omega_M$, expanding the argument of the exponential up to second order around ω_M, and finally performing the resulting Gaussian integral; here the integration limits can be extended to infinity, since the width of the Gaussian peak is of order $\tilde{T}_*(T_B/\tilde{T}_*)^{1/6}$ for $E_* > 2\Delta$ and $T_*(T_B/T_*)^{1/4}$ for $E_* < 2\Delta$.

We can now use the estimate thus found for St^{Phon}_{st} in Eq. (3.33) together with Eq. (3.34) to arrive at the following equation for $E_* > 2\Delta$:

$$4\sqrt{3\pi}(\tilde{x}_* - \tilde{\chi}^{2/3})^2 e^{\frac{3}{5}\tilde{\chi}^{5/3} + \frac{2}{5}\tilde{x}_*^{5/2} - \tilde{\chi}\tilde{x}_*} = \tilde{x}_*^{9/4}\tilde{\chi}^{2/3} \tag{D.5}$$

where $\tilde{x}_* = (E_* - \Delta)/\tilde{T}_*$ and $\tilde{\chi} = \tilde{T}_*/T_B$. For $E_* < 2\Delta$, the term St^{Phot} in Eq. (3.33) can be expressed as the opposite of the first term on the right-hand side of Eq. (3.22), and we similarly find the equation

$$105\sqrt{\pi}(x_* + \sqrt{\chi})(x_* - \sqrt{\chi})^2 e^{\frac{2}{3}\chi^{3/2} + \frac{1}{3}x_*^3 - x_*\chi} = 64 x_*^3 \chi^{3/4} \tag{D.6}$$

with $x_* = (E_* - \Delta)/T_*$ and $\chi = T_*/T_B$. These equations can be solved approximately by expanding up to second order, both in the prefactors and in the argument of the exponential, around $\tilde{x}_* = \tilde{\chi}^{2/3}$ ($x_* = \sqrt{\chi}$), to find for $T_B \ll T_B^*$

$$E_* \simeq \Delta + \tilde{T}_*(\tilde{T}_*/T_B)^{2/3} + \tilde{T}_* \sqrt{\frac{4}{3}\left(\frac{T_B}{\tilde{T}_*}\right)^{1/3} W\left[\frac{\sqrt{3}}{16\sqrt{\pi}}\left(\frac{\tilde{T}_*}{T_B}\right)^{5/2}\right]} \gtrsim 2\Delta \tag{D.7}$$

where W is the Lambert or product logarithm function with the asymptotic behavior $W(x) \approx \ln x - \ln\ln x$ for $x \gg 1$, while for $T_B^* \lesssim T_B \ll T_*$ we get

$$\begin{aligned} E_* &\simeq \Delta + T_*(T_*/T_B)^{1/2} \\ &+ T_* \sqrt{\left(\frac{T_B}{T_*}\right)^{1/2} W\left[\frac{32}{105\sqrt{\pi}}\left(\frac{T_*}{T_B}\right)^{9/4}\right]} \lesssim 2\Delta\,. \end{aligned} \tag{D.8}$$

In Sec. 3.4.1.2 we have reported for simplicity only the leading terms for E_*.

By construction, the energy E_* denotes that energy at which the effects of absorption and stimulated emission of phonons become comparable to that of photons, so that neglecting St_{st}^{Phon} is justified only below E_*. Conversely, we now show that for $E > E_*$ we can neglect the photons, and the quasiparticle distribution function takes the Boltzmann form,

$$f(E) \propto e^{-E/T_B} \,. \tag{D.9}$$

It is straightforward to check that (within the approximation of neglecting the Pauli blocking factors) this form satisfies the equation

$$St_{sp}^{Phon}\{f\} + St_{st}^{Phon}\{f, n_T\} = 0 \,. \tag{D.10}$$

Then using this equation and Eq. (3.27), which is valid irrespective of the exact form of f, we can write

$$St_{st}^{Phon} \simeq St_{sp}^{Phon}\Big|_{E=E_*} \left(\frac{E-\Delta}{E_*-\Delta}\right)^3 e^{-(E-E_*)/T_B} \tag{D.11}$$

Moreover, using Eq. (D.9) the photon collision integral can be written in the form

$$St^{Phot} = St^{Phot}\Big|_{E=E_*} e^{-(E-E_*)/T_B} \tag{D.12}$$

Since $St^{Phot}|_{E=E_*} = St_{sp}^{Phon}|_{E=E_*}$, comparing the last two equations we see that, in fact, $St^{Phot} < St_{st}^{Phon}$ for $E > E_*$. Note that to get the estimate in Eq. (D.11) we have assumed the validity of Eq. (D.9) at all energies, including $E < E_*$, and this assumption underestimates the contribution to St_{st}^{Phon} from the term in Eq. (3.5) proportional to $f(E-\omega)$ originating from the interval $E - E_* < \omega < E - \Delta$. However, this contribution is smaller than that coming from the interval $0 < \omega < E - E_*$ if $E - E_* \gtrsim E_* - \Delta - \tilde{T}_*(\tilde{T}/T_B)^{2/3}$ [with E_* of Eq. (D.7)], an inequality that identifies the width of the crossover region between the approximate expressions valid below and above E_*. These considerations are for the case $E_* > 2\Delta$, but they can be extended to the interval $E_* < E < 2\Delta$ in the remaining case.

D.2. Nonequilibrium phonon distribution

Here we study the nonequilibrium form of the phonon distribution function. We start by considering energies below the pair-breaking threshold, $\omega < 2\Delta$. Then writing $n = n_T + n_1$, in the steady state Eq. (3.13) takes the form (neglecting as usual Pauli-blocking factors)

$$n_1(\omega) = \frac{2\tau_l}{\pi\Delta_0\tau_0^{PB}} \int_\Delta^\infty dE\, \rho(E) U^-(E, E+\omega) \tag{D.13}$$
$$\left\{ f(E+\omega)\left[1 + n_T(\omega) + n_1(\omega)\right] - f(E)\left[n_T(\omega) + n_1(\omega)\right] \right\}$$

To solve this equation approximately, we consider two limiting cases. First, we consider energies such that $n_1 \ll n_T$; then we can neglect n_1 in the right-hand side, and the resulting expression amounts to the first iterative solution. To this case belongs in particular the low-energy regime $\omega \ll T_B$, in which case we can approximate $n_T(\omega) \simeq T_B/\omega$, $f(E+\omega) \simeq f(E) + \omega f'(E)$, $U^-(E, E+\omega) \simeq U^-(E,E) = 1/\rho(E)$ and therefore find $n_1 \simeq (2\tau_l/\pi\tau_0^{PB})(T_B/\Delta_0)b_0$. Then typically $n_1 \ll n_T$ unless τ_l is several orders of magnitude longer than τ_0^{PB}.

A second limiting case is when $n_T \ll n_1 \ll f(E+\omega)/f(E)$ (since f is in general monotonically decreasing, the latter inequality also implies $n_1 \ll 1$). In this case n_1 is approximately as in Eq. (3.39) and using Eq. (3.25) we have, for $T_* \lesssim \omega \lesssim \Delta$,

$$f(E+\omega) \simeq \frac{3b_0}{2^{5/6}\sqrt{\pi}} \left(\frac{E+\omega-\Delta}{T_*}\right)^{-\frac{1}{2}} e^{-[(E+\omega-\Delta)/T_*]^3/3} \tag{D.14}$$

In the argument of the exponential function, we can keep terms linear in $(E-\Delta)/T_*$ while disregarding higher powers, and for $\omega \gtrsim T_*$ we can approximate $U^-(E, E+\omega) \simeq \omega/\sqrt{\omega^2 + 2\omega\Delta}$. In integrating over energy E, we can also approximate $\rho(E) \simeq \sqrt{\Delta/(2(E-\Delta))}$ to arrive at

$$n_1(\omega) \simeq \frac{3}{2^{1/3}\pi} b_0 \frac{\tau_l}{\tau_0^{PB}} \left(\frac{T_*}{\Delta}\right)^2 \frac{\Delta}{\omega} \sqrt{\frac{\Delta}{2\Delta+\omega}}\, e^{-(\omega/T_*)^3/3}. \tag{D.15}$$

For $\omega \gtrsim \Delta$ we can proceed as for $\omega \lesssim \Delta$, but using Eq. (3.31) instead of Eq. (3.25); this way we obtain

$$n_1(\omega) \simeq \frac{2^{1/6}3^{3/2}}{\sqrt{5}\pi} b_0 \frac{\tau_l}{\tau_0^{PB}} \left(\frac{T_*}{\Delta}\right)^2 \frac{\Delta}{\omega} \sqrt{\frac{\Delta}{2\Delta+\omega}} \exp\left[-\frac{2}{5}\sqrt{\frac{35}{64}} \left(\frac{\omega}{T_*}\right)^{5/2} \sqrt{\frac{\Delta}{T_*}}\right] \tag{D.16}$$

Note that the two exponents in Eqs. (D.15) and (D.16) match at $\omega = 63\Delta/80$, which as expected is of order Δ.

To find the crossover frequency ω_c between thermal distribution at $\omega < \omega_c$ and nonequilibrium distribution at higher energies, assuming $\omega_c \lesssim \Delta$ we equate Eq. (D.15) for n_1 to $n_T(\omega) \simeq e^{-\omega/T_B}$, which leads to the equation

$$\frac{1}{3}y^3 - \frac{T_*}{T_B}y + \ln y + \frac{1}{2}\ln\left(1 + \frac{T_*}{2\Delta}y\right) + \ln\left(\frac{2^{5/6}\pi}{3}\frac{\Delta}{T_*}\frac{\tau_0^{PB}}{\tau_l}b_0^{-1}\right) = 0 \tag{D.17}$$

where $y = \omega_c/T_*$. For $y \ll \sqrt{3T_*/T_B}$, we can neglect the first term in this equation, and up to small corrections we arrive at Eq. (3.40). More accurate estimates for ω_c can be found by solving Eq. (D.17) numerically. For $\omega_c \gtrsim \Delta$ the same approach can be employed, but using Eq. (D.16) for n_1.

We now turn to energies above the pair-breaking threshold, $\omega > 2\Delta$. Based on the considerations made thus far, so long as $\omega_c \lesssim 2\Delta$ we expect the inequalities $n_T \ll n_1 \ll 1$ to hold, meaning that we could discard n_T in Eq. (3.13); however, to allow for $\omega_c > 2\Delta$ we keep the n_T term. In both cases, in the second integral in Eq. (3.13) we can neglect $n(\omega) \ll 1$ in the first term in curly brackets and, using the approximate energy-independence of $1/\tau_{PB}^{Phon}$ (cf. Appendix C), rewrite the second term as $-n(\omega)/\tau_0^{PB}$. Furthermore, we assume the quasiparticle density to be sufficiently low for $\tau_{abs}^{Phon} \gg \tau_{PB}^0$ to hold, so we can neglect the second term in curly brackets in the first integral of Eq. (3.13) (cf. Sec. 3.3). Then the approximate solution for the phonon distribution reads

$$\begin{aligned} n(\omega) &\simeq \frac{1}{\zeta}\left[n_1(\omega) + n_2(\omega) + n_T(\omega)\right] = \\ &\frac{\tau_l}{\pi\Delta_0\tau_0^{PB}\zeta}\Bigg[2\int_\Delta^\infty dE\,\rho(E)U^-(E,E+\omega)f(E+\omega) \\ &+ \int_\Delta^{\omega-\Delta} dE\,\rho(E)U^+(E,\omega-E)f(\omega-E)f(E)\Bigg] \\ &+ \frac{1}{\zeta}n_T(\omega) \end{aligned} \tag{D.18}$$

where

$$\zeta = 1 + \tau_l/\tau_0^{PB} \tag{D.19}$$

is the phonon trapping factor [cf. Eq. (3.51)]. The first term in the square brackets coincides with n_1 of Eq. (3.39), but here the prefactor $1/\zeta$ is smaller than unity, since in addition to scattering a new relaxation channel for phonons (that is, pair breaking) is now available. The second term in square brackets, $n_2(\omega)$, takes into account phonon generation by quasiparticle recombination. Assuming the (envelope of the) quasiparticle distribution to be monotonically decreasing, we can bound this term by $b_0^2\Delta S_+(\omega/\Delta)$ [with S_+ of Eq. (C.3)], which near $\omega = 2\Delta$ is approximately $b_0^2\Delta\pi$; then, using Eq. (D.16) (with the appropriate prefactor) we find that the first term always dominates over the second one at the threshold $\omega = 2\Delta$ if

$$b_0 < (3\times 2^{1/6}/\sqrt{5}\pi)\zeta(T_*/2\Delta)^2 e^{-\sqrt{35/32}(2\Delta/T_*)^3/5} \tag{D.20}$$

Even if n_2 dominates, as discussed in Sec. 3.4.1.3, these nonequilibrium phonons due to quasiparticle recombination could affect the shape of the quasiparticle distribution only at energies $E > 3\Delta$ by contributing to the collision integral St_{st}^{Phon}, Eq. (3.5). For $\omega - 2\Delta \lesssim T_*$, one can apply the low energy approximation to the product of density of

states times coherence factor and use Eq. (3.24) to evaluate approximately the second term in the square brackets of Eq. (D.18) to find

$$n_2(\omega) \approx \frac{b_0^2 \tau_l}{\pi(\tau_0^{PB} + \tau_l)} \left[\pi - 1.20(\omega - 2\Delta)^{5/2}\right] \tag{D.21}$$

We do not consider here the behavior of n_2 for frequencies $\omega > 2\Delta + T_*$.

D.3. Normalization equation

We derive here explicit expression for the coefficients I_i ($i = 0, 1, 2$) entering Eq. (3.46) for the normalization constant b_0. To find those coefficient, we substitute Eq. (3.45) into Eq. (3.44) and divide the result by $(2\Delta)^3/(1+\tau_l/\tau_0^{PB})$. From the term containing n_T we find

$$I_0 = \frac{1}{(2\Delta)^3}\int_{2\Delta} d\omega\,\omega^2 n_T(\omega, T_B) \simeq \frac{T_B}{2\Delta}e^{-2\Delta/T_B} \tag{D.22}$$

To find I_2, we collect together the terms quadratic in f, switch the integration order between ω and E, and change variable from ω to $E' = \omega - E$; we obtain

$$I_2 = \frac{1}{b_0^2\pi\Delta(2\Delta)^3}\int_{\Delta} dE \int_{\Delta} dE'\,(E+E')^2\rho(E)U^+(E,E')f(E)f(E') \tag{D.23}$$

The presence of the two distribution functions implies that the main contributions to the integrals come from regions close to Δ, and employing similar approximations as those used in Eq. (3.42) we arrive at

$$I_2 \simeq \frac{(2.1)^2}{\pi}\frac{T_*}{2\Delta} \tag{D.24}$$

Finally, considering the n_1 term we get

$$I_1 = \frac{1}{b_0\pi\Delta(2\Delta)^3}\int_{\Delta} dE \int_{2\Delta} d\omega\,\omega^2\rho(E)U^-(E,E+\omega)f(E+\omega) \tag{D.25}$$

Here we have to consider separately various regimes. For high phonon temperature/low photon number, $T_B^* \lesssim T_B \ll T_*$, the distribution function takes the Boltzmann form $f(E) = b_T e^{-E/T_B}$ above the energy $E_* \lesssim 2\Delta < 3\Delta$, see Sec. 3.4.1.2, and we have

$$I_1 \simeq \frac{1}{\sqrt{2\pi}}\frac{b_T}{b_0}\left(\frac{T_B}{2\Delta}\right)^{3/2} e^{-3\Delta/T_B} \tag{D.26}$$

where

$$\frac{b_T}{b_0} \approx \frac{3}{2^{5/6}\sqrt{\pi}}\left(\frac{T_B}{T_*}\right)^{1/4} e^{\Delta/T_B} e^{(2/3)(T_*/T_B)^{3/2}} \tag{D.27}$$

With these expression, using that

$$(T_*/\Delta)^3 \lesssim T_B/\Delta \tag{D.28}$$

the condition for the normalization constant b_0 to give the thermal equilibrium density can be written as

$$0.16(\tau_l/\tau_0^{PB})^2(T_B/\Delta)^2 e^{-2\Delta/3T_B} < 1 \tag{D.29}$$

even at the relatively high temperature $T_B = 0.3T_c$, this condition becomes

$$10^{-4}(\tau_l/\tau_0^{PB})^2 < 1 \tag{D.30}$$

showing that in this regime deviations from the thermal equilibrium density are possible only if τ_l exceeds τ_0^{PB} by at least a few orders of magnitude. We do not pursue the analysis of this long-τ_l limit here, as we focus on the experimentally relevant case of aluminum films in which τ_l is comparable to τ_0^{PB}. However, the long-τ_l regime could be relevant for other materials, such as niobium.

For low phonon temperature/high photon number, $T_B \ll T_B^*$, we have $E_* \gtrsim 2\Delta$, so we need to distinguish between $E_* < 3\Delta$ and $E_* > 3\Delta$. In the former case, Eq. (D.26) still holds, but now

$$\frac{b_T}{b_0} \approx \frac{3^{3/2}}{2^{1/3}\sqrt{5\pi}} \sqrt{\frac{35}{64}} \left(\frac{T_B}{\Delta}\right)^{1/2} \left(\frac{T_*}{\Delta}\right)^{-1} e^{\frac{\Delta}{T_B}} e^{\frac{3}{5}\left(\frac{\tilde{T}_*}{T_B}\right)^{5/3}} \tag{D.31}$$

Using this expression, one can check that the condition for b_0 to give the thermal equilibrium density is easily violated, due to the last exponential factor in Eq. (D.31) being dominant and large in the regime $T_B/\Delta \ll (T_*/\Delta)^3$ (the violation takes place unless τ_l/τ_0 is small compared to the inverse of that exponential factor). Similarly, in the case $E_* > 3\Delta$ we find again that the density generically deviates from the thermal equilibrium one. In this case we have

$$I_1 = \frac{3^{3/2}}{2^{7/3}5\pi\sqrt{7}} \left(\frac{T_*}{\Delta}\right)^5 \exp\left[-\sqrt{\frac{14}{5}} \left(\frac{\Delta}{T_*}\right)^3\right] \tag{D.32}$$

and in the ratio $I_1^2/(I_0 I_2)$ the exponential factor $e^{2\Delta/T_B}$ from I_0 dominates over the exponential in I_1. Note that despite the similarity, the coefficient I_1 and hence the value of b_0 in the two cases are different. Also, although we have included the case $E_* < 3\Delta$ for completeness, it has limited relevance, since the inequality holds if $(T_*/\Delta)^3 < 2^{3/2}\sqrt{35/64}\,(T_B/\Delta)$, and at the same time we require $T_B/\Delta \ll (T_*/\Delta)^3$.

To summarize, we have found that for high phonon temperature/low photon number the quasiparticle density is the same as in thermal equilibrium and the term linear in b_0 in Eq. (3.46) can be neglected. Conversely, at low phonon temperature/high photon number the constant term can be neglected. The relationship to the generalized Rothwarf-Taylor equation can be found by restoring all prefactors; in practice, this amounts to expressing b_0 in terms of $N_{\rm qp}$ using Eq. (3.42), multiplying the left-hand side of Eq. (3.46) by $4\rho_F(2\Delta/T_c)^3\pi\Delta/\bar{\tau}_0$, and equating the result to $dN_{\rm qp}/dt$. In this procedure, we can use for I_1 the formula in Eq. (D.32); in this way, the crossover between the two regimes is correctly identified up to numerical factors of order unity.

D.4. Photon-number dependent corrections in the generalized RT model

In the discussion of the generalized RT model in Sec. 3.4.2.1 we limited our considerations to the leading order in the parameter $T_*/\Delta \lesssim 1$. However, corrections in powers of $\varepsilon \equiv T_*/\Delta$ can be taken into account, as we now show. We begin by evaluating corrections to the expression for the quasiparticle density, Eq. (3.42). In the integral there, we make the change of variables $E = \Delta(1+\varepsilon x)$ and express the density of states as $\rho(E) \simeq \sqrt{\Delta/2T_* x}\,(1 + 3\varepsilon x/4 - 5(\varepsilon x)^2/32)$. Defining $a_\beta = \int_0 dx\, x^\beta f(x)/b_0$, we find

$$N_{\rm qp} \simeq 2\rho_F \sqrt{2T_*\Delta}\, b_0 \left(a_{-1/2} + \frac{3}{4} a_{1/2}\varepsilon - \frac{5}{32} a_{3/2}\varepsilon^2 \right) \tag{D.33}$$

The a_β factors can be estimated numerically; they have the approximate values $a_{-1/2} \simeq 2.1$, $a_{1/2} \simeq 0.88$, and $a_{3/2} \simeq 0.77$.

The same procedure can be applied to the evaluation of I_2 of Eq. (D.23) by expanding in the integral the energy-dependent factors multiplying the two distribution functions. By comparing the result to the square of Eq. (D.33), we find that the recombination term in Eq. (3.48) can be written as $\bar{R} N_{\rm qp}^2$ with

$$\frac{\bar{R}}{R} = 1 + \frac{a_{1/2}}{a_{-1/2}}\varepsilon + \left[\frac{5}{4}\frac{a_{3/2}}{a_{-1/2}} - \frac{3}{4}\left(\frac{a_{1/2}}{a_{-1/2}}\right)^2 \right] \varepsilon^2 \tag{D.34}$$

and R defined in Eq. (3.50). In Fig. D.1 we show that this second-order-in-ε expression gives a reasonable approximation for the recombination coefficient even for T_* close to Δ.

Additional corrections originate from taking into account the dependence on ω of the phonon pair-breaking lifetime $\tau_{PB}^{Phon}(\omega)$, Eq. (C.2), which we have previously neglected. In the expression for the phonon distribution function Eq. (D.18), this amounts to the substitution $\zeta \to \zeta(\omega)$, where the energy-dependent phonon trapping factor is

$$\zeta(\omega) = 1 + \tau_l/\tau_{PB}^{Phon}(\omega)\,. \tag{D.35}$$

We also need to modify Eq. (3.44) by multiplying the distribution function $n(\omega)$ by $\tau_0^{PB}/\tau_{PB}^{Phon}(\omega)$. Inserting the thus corrected Eq. (D.18) into the modified Eq. (3.44), we find that the two integrals I_0 and I_1 for the generation terms are modified by inserting in the integrands of Eqs. (D.22) and (D.25) a factor $\tau_0^{PB}\zeta/\tau_{PB}^{Phon}(\omega)\zeta(\omega)$, while in the integrand for the generation term I_2, Eq. (D.23), we must include the factor $\zeta/\zeta(E+E')$. Since in the relevant regime ($T_B \ll T_B^*$) I_1 has stronger than exponential dependence on T_*/Δ, see Eq. (D.32), we do not pursue the calculation of weak corrections proportional to $\varepsilon^{9/5}$ [in fact, the main correction to the function $G(x)$ originates from the linear term in Eq. (D.33) for $N_{\rm qp}$, so that the right-hand side of Eq. (3.52) should be multiplied by $1-(3a_{1/2}/4a_{-1/2})\varepsilon$]. Similarly, we neglect the small corrections in T_B/Δ that would be introduced to the leftmost expression in Eq. (D.22). For I_2, we limit ourselves to terms linear in ε; at this order we find that the coefficient

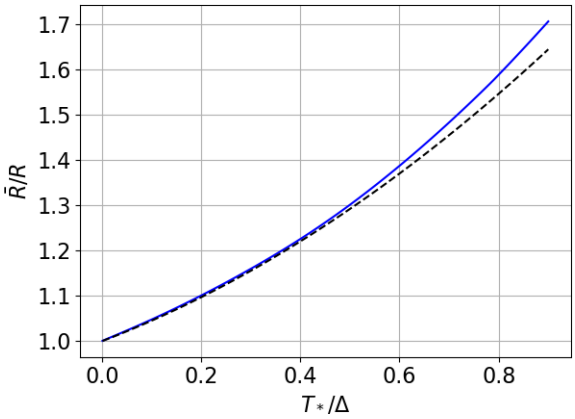

Figure D.1.: Blue (solid): numerically calculated recombination coefficient for the distributions derived in Sec. 3.4.1 (for $T_B = 0$), in units of the (zeroth-order) recombination coefficient R defined in Eq. (3.50). Black (dashed): analytical approximation Eq. (D.34).

of the linear term in Eq. (D.34) should be multiplied by $(1 + \tau_l/2\tau_0^{PB})/(1 + \tau_l/\tau_0^{PB})$. As function of τ_l, this factor varies between 1 and 1/2, so the finite thermalization time can weaken the dependence of the recombination coefficient $\bar{R}$ on T_*/Δ, but it does not change its increase with this parameter. Therefore, in the high phonon temperature regime $T_B \gtrsim T_B^*$ in which the I_1 term can be neglected, this increase implies a decrease of quasiparticle number with increasing photon number.

E. Parameters for comparison to experiment

E.1. Kinetic inductance fraction and order parameter

We discuss here our estimates for the parameters used in the comparison to the experiment of Ref. [Vis+14], see Table 3.2 in Sec. 3.6. The kinetic inductance fraction α and the zero-temperature gap Δ_0 are obtained by fitting the measured internal quality factor for temperatures $T > 0.25\,\mathrm{K}$ and the lowest readout power, $P_{\mathrm{read}} = -100\,\mathrm{dBm}$, to the thermal equilibrium expression [Gao08]

$$Q_i = \frac{\pi}{4\alpha \sinh(x) K_0(x)} \exp\left(\frac{\Delta_T}{T}\right) \tag{E.1}$$

where $x = \omega_0/(2T)$ and K_0 is the 0-th order modified Bessel function. A least square fit gives $\alpha \simeq 0.13$ and $\Delta_0 \simeq 189\,\mu\mathrm{eV}$. The assumption of the thermal equilibrium for the quasiparticles is justified, since the estimated T_* is comparable to ω_0, see Table 3.3.

The kinetic inductance fraction can be estimated to be $\alpha \simeq 0.08$ based on equation (1.48), which is of the same order as the value obtained from the fit. In Ref. [Vis+14] a smaller value for Δ_0 is given, estimated by measuring the critical temperature and using the BCS relation for the ratio Δ_0/T_c; our estimate agrees with previous findings of a higher ratio in thin aluminum films [CEP69].

E.2. Coupling constant

In this Appendix, we estimate the coupling constant for the non-pair breaking and pair breaking photons c^{QP}_{Phot} and $c^{QP}_{Phot,PB}$. Following Ref. [Vis+14] we assume the volume occupied by the quasiparticles to be twice the central strip volume, $V = 2 \cdot 1770\,\mu\mathrm{m}^3$, to account for quasiparticles in the ground plane, and take $\rho_F = 1.74 \times 10^4/\mu\mathrm{eV}\mu\mathrm{m}^3$. To obtain c^{QP}_{Phot}, we average Eq. (2.82) over the resonator's cross section S and define the coupling constant as

$$\bar{n} c^{QP}_{Phot} = \frac{1}{4S}\frac{\sigma_N}{\rho_F}\int dS |A_{\omega_0}|^2 = \frac{\sigma_N}{4S\omega_0^2|\sigma|^2\rho_F}\int dS \vec{j}^2_{\omega_0} = \frac{L_k \vec{I}^2_{\omega_0}\sigma_N}{4S\omega_0\sigma_2\rho_F} \tag{E.2}$$

with amplitude of the magnetic field [current] A_{ω_0} [I_{ω_0}], where the London equation was used in the first step and the kinetic inductance per unit length

$$\frac{1}{2}L_k\vec{I}^2 = \frac{1}{2\omega}\frac{\sigma_2}{|\sigma|^2}\int dS \vec{j}^2 \tag{E.3}$$

in the second step.[1] The average energy per unit length stored in the current is $\tilde{E} = \frac{1}{4} L_k \vec{I}^2_{\omega_0}$ and thus the total energy stored in the resonator per unit length is $E = \frac{1}{2\alpha} L_k \vec{I}^2_{\omega_0}$, with kinetic inductance fraction α. Replacing E integrated over the resonator's length by $\bar{n}\omega_0$ the coupling constant becomes

$$c^{QP}_{Phot} = \frac{\sigma_N \alpha}{2V\rho_F \sigma_2} \simeq \frac{\omega_0 \alpha}{2V\rho_F \pi \Delta} \tag{E.4}$$

where the last expression is valid for $(\omega_0/4\Delta)^2 \ll 1$. For the resonator investigated in the main text this leads to $c^{QP}_{Phot} \approx 60\,\mathrm{mHz}$. Note that the coupling constant (E.4) together with the conductance, Eqs. (2.94) and (2.95), ensures energy conservation when treating the field classically (i.e. neglecting the spontaneous emission terms). In [FC23], we used this property in an alternative derivation of Eq. (E.4) that did not require a calculation of the pre-factors in Eq. (2.82).

To find $c^{QP}_{Phot,PB}$ we can start from the first equality sign in equation (E.4). At small quasiparticle densities ($f \ll 1$), at leading order σ_2 is [MB58]

$$\frac{\sigma_2(\omega)}{\sigma_N} = \frac{1}{2}\left[\left(\frac{2\Delta}{\omega} + 1\right) E(k') + \left(\frac{2\Delta}{\omega} - 1\right) K(k')\right] \tag{E.5}$$

with E and K the complete elliptic integrals of the second and first kind, respectively, $k' = \sqrt{1-k^2}$, $k = |2\Delta - \omega|/|2\Delta + \omega|$; the left-hand side has the limiting forms $\pi\Delta/\omega$ for $\omega \ll 2\Delta$ and $\pi(\Delta/\omega)^2$ for $\omega \gg 2\Delta$. Assuming the kinetic inductance fraction to be small leads to $\alpha(\omega) \propto L_k$. Moreover, using $L_k \propto \frac{\sigma_2}{\omega|\sigma|^2}$ we calculate the ratio between coupling strengths at different frequencies as

$$\frac{c^{QP}_{Phot,PB}}{c^{QP}_{Phot}} = \frac{|\sigma(\omega_0)|^2\omega_0}{|\sigma(\omega_{PB})|^2\omega_{PB}} \simeq \frac{\pi^2\Delta^2}{\omega_{PB}\omega_0}\frac{\sigma_N^2}{|\sigma(\omega_{PB})|^2} \tag{E.6}$$

where in the second equation we have used that for $\omega_0 \ll 2\Delta$ we have $\sigma_1 \ll \sigma_2$ and the approximate value for σ_2 discussed after Eq. (E.5). In the limit $\omega_{PB} \gg 2\Delta$, the conductivity approaches its normal state value and hence $c^{QP}_{Phot,PB}/c^{QP}_{Phot} \simeq \pi^2\Delta^2/\omega_0\omega_{PB}$. Here we are interested into moderate frequencies, $\omega \lesssim 3.6\Delta$; in this range the kinetic inductance varies by less than a factor 2, and we can approximate the kinetic inductance fraction as frequency independent. Then we get $c^{QP}_{Phot,PB}/c^{QP}_{Phot} \sim \sigma_2(\omega_0)/\sigma_2(\omega_{PB}) \sim \omega^2_{PB}/\omega_0\Delta$. For a typical aluminium resonator with $\omega_0 \simeq 0.1\Delta$, this gives $c^{QP}_{Phot,PB} \sim (10^1 - 10^2) c^{QP}_{Phot}$ in this regime. Accordingly, for order-of-magnitude estimates we use a conservative value for the coupling constant for pair-breaking photons of order $c^{QP}_{Phot,PB} \sim 10\,\mathrm{Hz}$.

With the assumptions made in this Appendix, we also find that the ratio between the quality factors for above- and below-threshold frequencies is

$$\frac{Q(\omega_{PB})}{Q(\omega_0)} \simeq \frac{c^{QP}_{Phot}}{c^{QP}_{Phot,PB}}\frac{Q'(\omega_0)}{Q(\omega_0)} \tag{E.7}$$

[1] The factor 1/4 arises as the field used in the derivation of Eq. (2.82) has amplitude $2A_{\omega_0}$

where Q' is the quality factor if the resistivity were as in the normal state. Since for our parameters the first factor on the right-hand side is of order $10^{-2} - 10^{-1}$ and the second factor is typically less than 1, this shows that the quality factor of pair-breaking modes is smaller than that of non-pair-breaking ones, as expected.

F. Pair breaking photons

F.1. Neumann series

We give in this Appendix the $j = 1, 2$ terms in the Neumann series, Eq. (3.73), discussed in Sec. 3.5.1. For the $j = 1$ contribution, performing the integral in Eq. (3.74) using the simplified kernel in Eq. (3.75) we find

$$\phi^{(1)}(\gamma) = \frac{105}{128}\frac{5\gamma^3 - 6\gamma^2 - 8\gamma + 16}{8}\text{arctanh}(\sqrt{1-\gamma}) + \frac{105}{128}\frac{\sqrt{1-\gamma}}{24}\left[15\gamma^2 - 8\gamma - 28\right] \tag{F.1}$$

The similar calculation for the second order term gives

$$\begin{aligned}\phi^{(2)}(\gamma) = &\left[B(\gamma) - 4A(\gamma)\ln\left(\frac{\gamma}{2}\right)\right]\ln\left(1-\sqrt{1-\gamma}\right) \\ &+ 2A(\gamma)\ln^2\left(1-\sqrt{1-\gamma}\right) + A(\gamma)\ln^2(\gamma) - \frac{B(\gamma)}{2}\ln(\gamma) \\ &- 4A(\gamma)\text{Li}_2\left(\frac{1}{2} + \frac{\sqrt{1-\gamma}}{2}\right) - 2A(\gamma)\ln^2(2) + \frac{\pi^2}{3}A(\gamma) \\ &+ C(\gamma)\end{aligned} \tag{F.2}$$

with

$$A(\gamma) = -\left(\frac{105}{128}\right)^2\frac{1}{32}\left(5\gamma^3 + 6\gamma^2 + 8\gamma + 16\right) \tag{F.3}$$

$$B(\gamma) = -\left(\frac{105}{128}\right)^2\frac{1}{48}\left(33\gamma^3 - 150\gamma^2 + 96\gamma - 224\right) \tag{F.4}$$

$$C(\gamma) = \left(\frac{105}{128}\right)^2\frac{1}{144}\sqrt{1-\gamma}\left(279\gamma^2 - 68\gamma + 524\right) \tag{F.5}$$

and the dilogarithm defined as $\text{Li}_2(x) = \int_1^x dt\frac{\ln(t)}{1-t}$ [note that sometimes a different convention is used, in which the integral is defined as giving $\text{Li}_2(1-x)$ instead].

In the limit $\gamma \to 0$, the above results reduce at leading order to $\phi^{(1)} \simeq -(105/128)\ln(\gamma)$ and $\phi^{(2)} \simeq (105/128)^2\ln^2(\gamma)/2$, respectively. These expressions that can be obtained simply by keeping the leading contribution $\tilde{I}(0,\gamma')$ in the simplified kernel and taking $\phi^{(0)} = 1$ as the first term in the series.

F.2. Power spectral density

To calculate the power spectrum of quasiparticle number fluctuations, we follow the approach of Ref. [WP04]; we summarize here the necessary steps solely to make our work self-contained, with no claim of novelty. We assume short phonon lifetimes compared to the quasiparticle lifetimes to neglect fluctuations in the phonon number; the applicability of this assumption to aluminum resonators is discussed also in section C. Using that each recombination/generation process involves two quasiparticles, we can identify their respective rates in Eq. (3.97), which we then use to set up a master equation for the probability $P(N,t|k,0)$ of finding N quasiparticles at time t if there were k quasiparticles at time 0,

$$\begin{aligned}\frac{dP(N,t|k,0)}{dt} = &-[g(N)+r(N)]P(N,t|k,0)\\ &+g(N-2)P(N-2,t|k,0)\\ &+r(N+2)P(N+2|k,0)\end{aligned} \tag{F.6}$$

The recombination rate – renormalized by phonon trapping – is

$$r(N) = \frac{1}{2}\tilde{R}N^2 \tag{F.7}$$

where $\tilde{R} = R/\mathcal{V}$ with $\mathcal{V}$ the resonator volume and $N = N_{qp}\mathcal{V}$ the quasiparticle number, and the generation rate is

$$g(N) = \frac{1}{2}\left(\tilde{G}_{T_B} + \tilde{G}_{\bar{T}_B} + G(T_*/\Delta)N\right) \tag{F.8}$$

with $\tilde{G} = G\mathcal{V}$. To check the identification of the rates, we multiply both sides of the master equation by N and sum over N to find

$$\frac{d}{dt}\langle N(t)\rangle_k = 2\langle g(N(t))\rangle_k - 2\langle r(N(t))\rangle_k \tag{F.9}$$

where the expectation value of a function of quasiparticle number $A(N)$ at time u under the assumption of k quasiparticles at 0 defined by

$$\langle A(N(u))\rangle_k = \sum_{l=0}^{\infty} A(l)P(l,u|k,0). \tag{F.10}$$

One can verify that Eq. (F.9) agrees with Eq. (3.97) if fluctuations are small compared to the average quasiparticle number. In the steady state, the system approaches a probability distribution for which $\langle g(N)\rangle = \langle r(N)\rangle$; for small deviations from the steady-state expectation value $N_0 = \langle N\rangle$ we can write $N = N_0 + \Delta N$ and expand the generation/recombination rates up to second order in ΔN to find

$$g(N_0) + \frac{1}{2}g''(N_0)\langle\Delta N^2\rangle = r(N_0) + \frac{1}{2}r''(N_0)\langle\Delta N^2\rangle \tag{F.11}$$

The autocorrelation function for the number can be written in the form

$$\phi(u) = \langle N(u)N(0)\rangle = \sum_{k=0}^{\infty} kP(k,0)\langle N(u)\rangle_k \tag{F.12}$$

with $P(k,0)$ the probability of k quasiparticles at time $t = 0$. Expanding Eq. (F.9) to linear order in the (time-dependent) fluctuation $\Delta N(t)$, solving the resulting differential equation for $\langle \Delta N(t)\rangle_k$, and inserting the result into the autocorrelation function of the fluctuations we find

$$\Delta\phi(u) \equiv \langle \Delta N(u)\Delta N(0)\rangle = \langle \Delta N(0)^2\rangle e^{-t/\bar{\tau}_r} \tag{F.13}$$

with $1/\bar{\tau}_r = 2\tilde{R}N_0 - G(T_*/\Delta)$. To calculate the variance, we multiply both sides of the master equation by N^2 and sum over N to get

$$\frac{d}{dt}\langle N(t)^2\rangle_k = 4\langle g(N)(N+1)\rangle_k(t) - 4\langle r(N)(N-1)\rangle_k(t) \tag{F.14}$$

Considering the steady state, expanding to second order in ΔN, and using Eq. (F.11) one finds the variance

$$\langle \Delta N^2\rangle = \frac{2\langle r(N)\rangle}{\tilde{R}N_0 - \frac{1}{2}G(T_*/\Delta)} \simeq 4\tilde{R}N_0^2\bar{\tau}_r \tag{F.15}$$

If quasiparticle creation is dominated by photons or thermal phonons, one can neglect G, and the variance of the quasiparticle number is equal to its expectation value. In the regime in which phonon trapping dominates, we instead have $G(T_*/\Delta) = RN_0$, and the variance is twice the quasiparticle number. Fourier transforming the autocorrelation function (F.13) leads to equation (3.99) for the number spectral density.

G. Fluctuations

G.1. Two dimensional fluctuations

If the superconductor consists of a thin film of thickness t much smaller than the coherence length $t \ll \xi$, optimal fluctuations become effectively two dimensional. In that case, the saddle point equation reads

$$\left[\bar{\phi}(R_{\bar{\epsilon}},\bar{\epsilon}) - \bar{\phi}(R_{\bar{\epsilon}},\bar{\epsilon})^2 - \partial^2_{R_{\bar{\epsilon}}}\bar{\phi}(R_{\bar{\epsilon}},\bar{\epsilon}) + \frac{1}{R_{\bar{\epsilon}}}\partial_{R_{\bar{\epsilon}}}\bar{\phi}(R_{\bar{\epsilon}},\bar{\epsilon})\right] = 0$$

As an exact analytic solution to this equation is not available, we seek for a numeric solution leading to a saddle point of the action

$$\begin{aligned} S[\bar{\phi}] &= \frac{1}{2\sigma^2\xi^2\eta^{2/3}}\int d^2R\delta\eta^2[\bar{\phi}(R_{\bar{\epsilon}})] \\ &= \frac{\eta^{2/3}}{\sigma^2\xi^2}\frac{\Omega^4(\bar{\epsilon})}{\rho^2}\left[\frac{dR}{dR_{\bar{\epsilon}}}\right]^2 \times \Xi_0[\bar{\phi}] = \frac{c_0^{-2}}{2\sigma^2\xi^2\eta^{2/3}} \end{aligned} \tag{G.1}$$

with

$$\begin{aligned} \Xi_0[\bar{\phi}] &= \pi\int dR_{\bar{\epsilon}}R_{\bar{\epsilon}}\left[\bar{\phi}(R_{\bar{\epsilon}}) - \bar{\phi}^2(R_{\bar{\epsilon}}) - \nabla^2_{R_{\bar{\epsilon}}}\bar{\phi}(R_{\bar{\epsilon}})\right]^2 \\ &= \pi\int dR_{\bar{\epsilon}}R_{\bar{\epsilon}}\left[\frac{2}{R_{\bar{\epsilon}}}\bar{\phi}'(R_{\bar{\epsilon}})\right]^2 \end{aligned} \tag{G.2}$$

We seek a solution that has

- a finite action
- a smooth, non-diverging $\bar{\phi}(R_\epsilon)$
- a negative, non-diverging fluctuation, i.e. $0 < \bar{\phi}'(R_{\bar{\epsilon}})/R_{\bar{\epsilon}} < \infty$

In the vicinity of $R \to 0$ we can seek a solution in form of a Taylor series $\phi = \sum a_i R^i_{\bar{\epsilon}}$. The term linear in $R_{\bar{\epsilon}}$ must be zero for a non-diverging gap. Thus, the terms containing derivatives cancel to lowest order in R, and we get the limit $\bar{\phi} \to 1$. Writing $\bar{\phi} = 1 - \delta\phi$ we find the solution $\bar{\phi}(R_{\bar{\epsilon}}) = 1 - a_1 R_{\bar{\epsilon}} J_1(R_{\bar{\epsilon}})$ in the limit $\delta\phi \ll 1$, where J_1 is the Bessel Function of first kind, and a_1 is an arbitrary constant. In the opposite limit $\bar{\phi} \ll 1$ (corresponding to $R \to \infty$), the equation reduces to $\left[\bar{\phi}(R_{\bar{\epsilon}},\bar{\epsilon}) - \partial^2_{R_{\bar{\epsilon}}}\bar{\phi}(R_{\bar{\epsilon}},\bar{\epsilon}) + \frac{1}{R_{\bar{\epsilon}}}\bar{\phi}(R_{\bar{\epsilon}},\epsilon)\right] = 0$, corresponding to $\bar{\phi}(r_{\bar{\epsilon}}) = const \times R_{\bar{\epsilon}} \times K_1(R_{\bar{\epsilon}}) \to a_2 \times \sqrt{R_{\bar{\epsilon}}}e^{-R_{\bar{\epsilon}}}$. Here, we discarded the solution involving the other modified

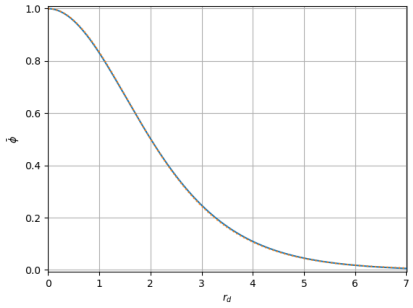

Figure G.1.: Dotted line: analytic estimate for $\bar{\phi}$. Full line: numeric result

Bessel function, as it does not lead to a finite action. We can construct an approximate solution using a variational Ansatz $\bar{\phi}(R_{\bar{\epsilon}}; a) = (1 + aR_{\bar{\epsilon}}^2)^{1/4} \cosh^{-2}(R_{\bar{\epsilon}}/2)$ that has the correct form in the limits of small and large R. Minimizing the action, the variational Ansatz gives $a = 0.26$. In order to find a numerical solution, the differential equation can be discretized using finite differences and $\bar{\phi}(0) = 1, \bar{\phi}'(0) = 0$ and arbitrary second derivative at the boundary. Varying the second derivative at the boundary, we find a solution with the required asymptotic behaviour at $r_{\bar{\epsilon}} \to \infty$ for $\bar{\phi}''(0) = 0.382$. The solution is plotted in figure G.1, agreement between approximate and numerical solution is excellent. Integrating the numerically obtained gap reproduces $\Xi_0 = 2.09$ from [SF13].

G.2. Disorder averaging

Here, we outline how the method of [ZL66] can be used to find the disorder averaged localization time, as already used by [LO72; SI05]: For each disorder configuration, we introduce a single optimal fluctuation of depth [the lowest energy state it can accommodate] d_0 centered at $\vec{R}_0$ and choose both d_0 and $\vec{R}_0$ such that it minimizes the distance between the disorder realization $\delta\eta$ and the optimal fluctuation, i.e. minimizes

$$D(\vec{R}_0, d_0) = \int d^d R (\delta\eta(\vec{R}) - \delta\bar{\eta}(d_0, \vec{R}, \vec{R} - \vec{R}_0))^2 \tag{G.3}$$

with respect to $\vec{R}_0$ and d_0. We assumed the fluctuations to be effectively d-dimensional.

We can thus introduce the disorder averaged density of states

$$\left\langle \rho(\vec{R}, \epsilon) \right\rangle = \left\langle \int_\sigma d^d R' \rho(d_0, \epsilon, \vec{R}, \vec{R}_0) \delta(\vec{R}' - \vec{R}_0) \right\rangle \tag{G.4}$$

i.e. we approximate the density of states of a given disorder configuration by the one with the optimal fluctuation that gives the best approximation to the disorder configuration. By definition, $D(R')$ has a minimum at $\vec{R}' = \vec{R}_0$, and we can transform the coordinates to $\nabla D(\vec{R}')$

$$\left\langle \rho(\epsilon) \right\rangle = \left\langle \int_\sigma d^d R' \rho(d_0, \epsilon, \vec{R}, \vec{R}_0) \delta(\nabla D(\vec{R}')) |\det \nabla\nabla D(\vec{R}')| \right\rangle \tag{G.5}$$

To get an explicit equation for the Dirac delta and the Jacobian, it is useful to expand $\delta\bar{\eta}$ in the basis of orthonormal functions ϕ_l to $\delta\bar{\eta}(\vec{R}) = \sum_{j=0}^{\infty} \xi_l \phi_l(\vec{R}, d_0)$ and to choose $\phi_0(\vec{R}, d_0) = -c_0 \delta\bar{\eta}(\vec{R}, d_0)$ and $\phi_{1+i}(\vec{R}, d_0) = c_1 \frac{\partial}{\partial \vec{R}_i} \delta\bar{\eta}(\vec{R}, d_0)$ where $i = 0, 1, .., d-1$. [1] The coefficients are

$$c_j^{-2}(\epsilon) = 2\eta^{4/3} \frac{\Omega^{4+j-d/2}(\epsilon)}{\rho^2 \xi^{2j-d}} \Xi_j \tag{G.6}$$

for $j = 0, 1$ and $d = 2, 3$ with

$$\Xi_0 = 2 \int d^d R_\epsilon \left[\frac{\bar{\phi}'(R_\epsilon)}{R_\epsilon} \right]^2 = \begin{cases} 2.09 \text{ for } d = 2 \\ \frac{24\pi}{5} \text{ for } d = 3 \end{cases} \tag{G.7}$$

$$\Xi_1 = \frac{2}{d} \int d^d R_\epsilon \left[\frac{\bar{\phi}''(R_\epsilon)}{R_\epsilon} - \frac{\bar{\phi}'(R_\epsilon)}{R_\epsilon^2} \right]^2 = \frac{1}{d} \begin{cases} 0.82 \text{ for } d = 2 \\ \frac{24\pi}{7} \text{ for } d = 3 \end{cases} \tag{G.8}$$

The action is

$$S[\bar{\phi}] = \frac{1}{2\sigma^2 \xi^3 \eta^{2/3}} \int d^3 R \delta\eta^2[\bar{\phi}(R_\epsilon)] = \frac{c_0^{-2}}{2\sigma^2 \xi^3 \eta^{2/3}} \tag{G.9}$$

[1] To avoid confusion, we note that the expansion coefficients ξ_i denoted with an index are not related to the coherence length denoted by ξ

with c_0 given in (G.6). By construction the value of d_0 that minimizes D for disorder configuration $\delta\bar{\eta}$ is given implicitly by $\xi_0 = c_0^{-1}(d_0)$ relating ξ_0, determining the probability for a configuration, to the best approximation for a corresponding trap depth d_0. Correspondingly, we get

$$(\nabla D)_i(R') = -2c_1^{-1}\xi_{1+i} \tag{G.10}$$

where we used the orthonormality of the ϕ_i and the expansion of $\delta\bar{\eta}$. Furthermore, the Jacobian is evaluated using

$$(\nabla\nabla D)_{i,j} = \frac{\partial^2}{\partial\vec{R}'_i\partial\vec{R}'_j}D(\vec{R}', d_0) = 2c_1^{-2}\delta_{i,j} \tag{G.11}$$

to $|\det\nabla\nabla D(\vec{R}_d)| = 2^d c_1^{-2d}$. In the preceding sections, the proportionality constant entering χ was left unspecified. To determine it, we can approximate the shape of χ and ϕ as independent of energy, and rewrite (4.16) as $\chi^2 = \sum_{j=0}^{\infty}\xi_l\phi_l(\vec{R}, d_0) - c_0^{-1}\phi_0$. Multiplying with ϕ_0, integrating over space and using the orthonormality of the ϕ_l results in

$$\int d^dR\rho(R,\epsilon) = \frac{\eta^{-1/3}\Omega(\epsilon)}{\rho}\int d^dR\chi(R) = \sqrt{\xi_0 - c_0^{-1}}\frac{\xi^{d/2}}{\Omega^{1+\frac{d}{4}}\eta}Ac_0^{-1/2} \tag{G.12}$$

with

$$A = \frac{\int d^dR_{\bar{\epsilon}}\frac{2\bar{\phi}'(R_{\bar{\epsilon}})}{R_{\bar{\epsilon}}}}{\sqrt{\int d^dR_{\bar{\epsilon}}\left[\frac{2\bar{\phi}'(R_{\bar{\epsilon}})}{R_{\epsilon}}\right]^3}} \simeq \begin{cases} 8.84 & \text{for} \quad d=2 \\ 15.91 & \text{for} \quad d=3 \end{cases} \tag{G.13}$$

(G.5) becomes

$$\begin{aligned}
\langle\rho(\epsilon)\rangle &= \frac{c_1^{-d}\int d^dR'\int_{-\infty}^{\infty}\prod_{n=0}^{\infty}\left[d\xi_n e^{-\frac{\xi_n^2}{2\sigma^2\xi^d\eta^{2/3}}}\right]\delta(\xi_1)...\delta(\xi_d)\rho(\vec{R}-\vec{R}',\epsilon)}{\int_{-\infty}^{\infty}\prod_{n=0}^{\infty}(d\xi_n)e^{-\frac{1}{2\sigma^2\xi^d\eta^{2/3}}(\sum_{n=0}^{\infty}\xi_n^2)}} \\
&= \frac{c_1^{-d}Ac_0^{-1/2}}{\sqrt{2\pi\sigma^2}(2\pi\sigma^2\xi^d)^{d/2}\Omega^{1+d/4}\eta^{\frac{4+d}{3}}}\int d\xi_0\sqrt{\xi_0 - c_0^{-1}}\exp\left(-\frac{\xi_0^2}{2\sigma^2\xi^d\eta^{2/3}}\right) \\
&\simeq \frac{c_1^{-d}Ac_0^{-1/2}\Gamma(\frac{3}{2})e^{-S}}{\pi^{d/2+1/2}\sigma 2^{d/2+5/4}\left[\sigma^2\xi^d\right]^{d/2-3/4}\Omega^{1+d/4}\eta^{\frac{5+2d}{6}}S^{3/4}} \\
&= \frac{c_1^{-d}A\Gamma(\frac{3}{2})e^{-S}}{c_0^{-1}\pi^{d/2+1/2}\sigma 2^{d/2+1/2}\left[\sigma^2\xi^d\right]^{d/2-3/2}\Omega^{1+d/4}\eta^{\frac{1+d}{3}}} \\
&\simeq \begin{cases} 0.33\sqrt{\epsilon}\eta^{-2/3}e^{-S} & \text{for} \quad d=2 \\ 4.18\sqrt{\epsilon}\eta^{-2/3}\sigma^{-1}e^{-S} & \text{for} \quad d=3 \end{cases}
\end{aligned} \tag{G.14}$$

where the second step is valid for $S \gg 1$ [SI05].

G.3. Rates

In this appendix we give the calculation of the various rates entering the rate equations (4.1). In the main text we used equation (2.86) for the phonon collision integral. In this appendix, we keep the discussion slightly more general by replacing $\omega^2 \to \omega^\mu$ with $\mu = 1, 2, 3$ in the collision integral. The cases $\mu = 1$ and $\mu = 3$ can be relevant if the (non-magnetic) disorder is very strong, and are included for completeness [Gia+06].

G.3.1. Localization rate

We start by noting that for an optimal fluctuation $\Re(\delta\psi) \sim \mathcal{O}\left(\sqrt{\bar{\epsilon}\eta^{-2/3}}\right)$. As the density of states decreases over an energy scale $\epsilon_T \ll \Delta\eta^{2/3}$, this is much smaller than one, and we can replace the coherence factor for localization processes originating from an energy $E_1 < \Delta$ by $K^-(E_1, E_2) \sim \eta^{2/3}$. This decouples the integrals over E and ω and allows to write the localization rate in the form (4.27), where the (inverse) localization lifetime is given by

$$\tau_{\mathrm{loc}}^{-1}(E) = \frac{\eta^{2/3}}{\tau_0 T_c^3} \int_0^{E_g} dE' \, (E - E')^\mu \rho(E') \left[n(E - E') + 1 \right] \tag{G.15}$$

We approximate the sub gap density of states by its asymptotic form (4.24). At very low temperatures $T \ll \epsilon_T$, localization is dominated by spontaneous emission and we can set the phonon distribution to zero. The localization rate becomes

$$\tau_{loc}^{-1}(\tilde{\epsilon}) = 2^{2-\mu} r \frac{a_d}{8-d} \left(\frac{\epsilon_T}{\Delta} \right)^{\frac{3}{2}+\mu} \sum_{k=0}^{\mu} \binom{\mu}{k} |\tilde{\epsilon}|^k \Gamma\left(\frac{4\left[\alpha_d + 3 - k\right]}{8-d} \right) \tag{G.16}$$

with Binomial coefficient $\binom{n}{k}$ and Gamma function Γ. For high temperatures $T \gg \epsilon_T$ and $\epsilon\epsilon_T \ll T$ we can replace $n(E - E') + 1 \simeq T/(E - E')$ and get from (G.15)

$$\tau_{loc}^{-1}(\tilde{\epsilon})\Big|_{T,\mu} = \tau_{loc}^{-1}(\tilde{\epsilon})\Big|_{T=0,\mu-1} \frac{T}{T_c} \tag{G.17}$$

where the zero temperature result is given by (G.16).

G.3.2. Excitation rates

The rates for excitations due to phonon absorption are given by

$$\begin{aligned} \Gamma_{ex} x_l &= \frac{2}{\Delta} \int_0^{E_g} dE \rho(E) f(E) \int_{E_g - E}^{\infty} d\omega \omega^\mu \rho_{AG}(E + \omega) n(\omega) K^-(E, E + \omega) \\ &\equiv \frac{2}{\Delta} \int_0^{E_g} dE \rho(E) f(E) \tau_{ex}^{-1}(E) \end{aligned} \tag{G.18}$$

For $T \gg \epsilon_T$ we can set $E \approx E_g$ in $\tau_{ex}^{-1}(E)$. If additionally $T \ll \eta^{2/3}\Delta$ we can replace the density of states in τ_{ex}^{-1} by the Abrikosov-Gorkov one and $K^-(E, E') = \eta^{2/3}$ to obtain

$$\tau_{ex}^{-1} \simeq \sqrt{\frac{2}{3}} \frac{T^{\mu+\frac{1}{2}}}{\sqrt{\Delta}\tau_0 T_c^\mu} \Gamma\left(\mu + \frac{3}{2}\right) \zeta\left(\mu + \frac{3}{2}\right) \tag{G.19}$$

If instead $T \gg \eta^{2/3}\Delta$ the excitation rate becomes the same as for a BCS superconductor and we can use (3.21) to approximate density of states and coherence factor, leading to

$$\tau_{ex}^{-1} \simeq \sqrt{\frac{1}{2}} \frac{T^{\mu+\frac{1}{2}}}{\sqrt{\Delta}\tau_0 T_c^\mu} \Gamma\left(\mu + \frac{3}{2}\right) \zeta\left(\mu + \frac{3}{2}\right) \tag{G.20}$$

If excitation occurs due to absorption of photons in a resonator, one can distinguish cases with $\omega_0 \ll \epsilon_T, \epsilon_T \ll \omega_0 \ll \eta^{2/3}\Delta$ and $\omega_0 \gg \eta^{2/3}\Delta$. For $\omega_0 \gg \eta^{2/3}\Delta$ coherence factor and density of states can be replaced by its BCS values, the resulting excitation rate is[CB19]

$$\Gamma_0 = \sqrt{\frac{1}{2}} \left(\frac{\Delta}{\omega_0}\right)^{3/2} \frac{\pi}{\alpha} \tag{G.21}$$

Transition rates in the limit $\epsilon_T \ll \omega_0 \ll \eta^{2/3}\Delta$ can be found in [FHG11], we do not discuss them here as we usually expect the photon energy to be large compared to the broadening.

G.3.3. Mobile-mobile transitions

The inverse lifetime of a quasiparticle towards relaxation from a mobile state of energy E into another mobile state of lower energy is defined as

$$\tau_m^{-1}(E) = \frac{1}{\tau_0 T_c^{\mu+1}} \int_0^{E_g - E} d\omega \omega^\mu K^-(E, E-\omega) \rho(E-\omega) \left[1 + n(\omega)\right] \tag{G.22}$$

First consider the case $T = 0$ and $E < \Delta$. In that case the coherence factor can be replaced by $\eta^{2/3}$ and the density of states by the Abrikosov-Gorkov density of states, leading to

$$\tau_{m,sp}^{-1}(E) = \frac{2^{3/2-\mu} |\bar{\epsilon}|^{\mu+3/2}}{\sqrt{3}} r \sum_{k=0}^{\mu} \binom{\mu}{k} \frac{(-1)^k}{(2k+3)} \tag{G.23}$$

At $E \gg \Delta$ the spontaneous emission rate becomes the same as in the BCS case

$$\tau_{m,sp}^{-1}(E) = 2^{1-\mu} |\bar{\epsilon}|^{\mu+3/2} r \sum_{k=0}^{\mu} \binom{\mu}{k} \frac{(-1)^k}{(2k+3)} \tag{G.24}$$

where for simplicity we assumed $E < 2\Delta$ to use the approximate density of states and coherence factor (3.21).

G.3.4. Recombination rates

The recombination rate is given by

$$\begin{aligned}\Gamma_r &= \frac{1}{\tau_0 T_c^{\mu+1}} \frac{2}{V\Delta} \int d^3r \int_0^\infty dE dE' \rho(E) f(E) \rho(E') f(E') (E'+E)^\mu K^+(E,E') \\ &\equiv \Gamma_{ll} + \Gamma_{ml} + \Gamma_{mm} \end{aligned} \tag{G.25}$$

Here, all quantities are to be understood to be position dependent, we assumed a sufficiently large superconducting volume V to replace disorder averaging by spatial averaging. In the following we split it in three parts, the recombination between two localized quasiparticles Γ_{ll} (with $E < E_g, E' < E_g$), recombination of two mobile quasiparticles Γ_{mm} (with $E > E_g, E' > E_g$) and recombination of a localized and a mobile quasiparticle Γ_{ml} (with $E > E_g, E' < E_g$ or $E' > E_g, E < E_g$) . Neglecting the position dependence of f and ρ for energies above E_g, approximating $K^+(E,E') \simeq 2$ and $E + E' \simeq 2\Delta$ we obtain

$$\Gamma_{ml} = r x_l x_m; \quad \Gamma_{mm} = r x_m^2 \tag{G.26}$$

with recombination coefficient

$$r = \frac{2^\mu}{\tau_0} \left(\frac{\Delta}{T_c}\right)^{\mu+1} \tag{G.27}$$

To estimate the recombination between localized quasiparticles we can not in general neglect the position dependence, instead we refer to [Bes+16] for an estimate and write their result in the form of equation (4.31). Using the expression in Eq. (4.22), it is in principle possible to adapt the arguments of Ref. [Bes+16] to the $d = 2$ case. In particular, one needs to calculate the function $g_2(\tilde{\vec{R}}) = \int d^2\tilde{r} \bar{\phi}_2(\tilde{\vec{r}}) \bar{\phi}_2(\tilde{\vec{r}} + \tilde{\vec{R}})$; its asymptotic behavior at large $\tilde{R}$ is $g_2(\tilde{R}) \simeq 2\pi\sqrt{\pi a}[\Gamma(7/4)/\Gamma(9/4)]\tilde{R}^{5/2} e^{-\tilde{R}}$. The latter expression shows that the overlap between trapped quasiparticles states decays more slowly in $d = 2$ compared to the $d = 3$ result $g_3(\tilde{R}) \propto e^{-\tilde{R}}$ [Bes+16]; therefore, the suppression of the recombination rate Γ_{ll} below Γ_{mm} as κ (that is, the generation rate) decreases is weaker in $d = 2$, implying that the recombination suppression is less efficient in thin superconducting films. We note that despite this reduced efficiency, if the regime in which the considerations of Ref. [Bes+16] apply were reached (implying $\kappa \ll 1$), the estimated density in films (n_f) would be higher than that in the bulk (n_b): the reference shows that in the bulk the density can be expressed as $n_b \sim 1/[r_c^3 \ln(1/\kappa)]$; the corresponding expression for thin films is $n_f \sim 1/[r_c^2 t \ln(t^2/\kappa r_c^2)]$, with thickness $t \ll \xi \lesssim r_c$. Using the latter condition, we find $n_b \ll n_f$.

G.3.5. Pair-breaking rates

Various non-equilibrium processes can create new quasiparticles, in the following we discuss some of them regarding the creation of local and mobile quasiparticles. We disregard processes that create two localized quasiparticles; as quasiparticles created

from these processes are trapped within the same region in space they recombine quickly and have negligible influence on the rate equations. Neglecting these processes, the generation rate for localized quasiparticles due to thermal phonons becomes

$$g_l = \frac{1}{\tau_0 T_c^\mu} \frac{2}{\Delta} \int_0^{E_g} dE \int_{E_g}^{\infty} dE' \rho(E)\rho(E') K^+(E,E')(E+E')^\mu n(E+E') \tag{G.28}$$

Assuming $T \ll \Delta$ we set $K^+(E,E') \simeq 2$, $E+E' \simeq 2\Delta$ and $n(E+E') \simeq \exp\left(-(E+E')/T\right)$. We replace $\rho(E)$ with the disorder averaged subgap density of states and $\rho(E')$ with the Abrikosov Gorkov density of states. Further assuming $T \gg \epsilon_T$ leads to

$$g_l \simeq \frac{16}{8-d} \sqrt{\frac{\pi}{6}} a_d \eta^{-4/3} r \frac{(T\epsilon_T)^{3/2}}{\Delta^3} \Gamma\left[\frac{4}{8-d}(\alpha_d+1)\right] e^{-2E_g/T} \tag{G.29}$$

The rate for creation of two localized quasiparticles g_m is defined similarly, with the integral over E extending from $[E_g, \infty]$ instead of $[0, \infty]$. Using the Abrikosov Gorkov density of states and assuming $T \gg \epsilon_T$ results in

$$g_m \simeq \frac{2\pi}{3} r \eta^{-4/3} \left(\frac{T}{\Delta}\right)^3 e^{-2E_g/T} \tag{G.30}$$

Thus, $g_m \gg g_l$ is valid for $T \gg \epsilon_T$. In the opposite limit the exponential tail in the density of states decreases more slowly with energy than the increase in the Boltzmann factor, and in principle one could get $g_l \gg g_m$ [2]. At the very low temperatures required to reach this limit, usually other creation mechanisms dominate, and should be used instead of the thermal creation rates.

G.4. Generation-recombination Noise

In section III.C of Ref. [WP04] generation-recombination noise for a system containing mobile and localized quasiparticles was considered. There, quasiparticles were assumed to recombine only if they are mobile, i.e. compared to our considerations of chapter 4 the rate Γ_{ml} was neglected. In the following we extend their calculations to a non-zero Γ_{ml}. We form the state vector as $\vec{N} = (N_m, N_l)$ with number of mobile quasiparticles N_m and localized quasiparticles N_l and write a rate equation for small deviations $\Delta\vec{N}$ from steady state as

$$\frac{d\langle\Delta\vec{N}\rangle}{dt} = -\mathbf{\Lambda}\langle\Delta\vec{N}\rangle \tag{G.31}$$

with linearized transition rate (see Eqs. 5.5 and 5.13 of Ref. [Lax60])

$$\mathbf{\Lambda} = \begin{pmatrix} 2\Gamma_{mm}N_m + \Gamma_{ml}N_l + \Gamma_l & \Gamma_{ml}N_m - \Gamma_{ex} \\ -\Gamma_l + \Gamma_{ml}N_l & \Gamma_{ml}N_m + \Gamma_{ex} \end{pmatrix} \tag{G.32}$$

[2] Note however that the process described in (G.28) also creates a mobile quasiparticle which we did not include in g_m

Note that in this appendix we do not normalize quasiparticle densities by the Cooper pair densities, hence the recombination rates contain an additional factor $1/2\Delta\rho_F$ compared to ones used in the main text. Here, and in the following, we neglect recombination between localized quasiparticles, corresponding to traps that are sparsely populated. N_m and N_l are to be understood as steady state values and we only include quasiparticle creation as mobile quasiparticles. We can use the steady state condition

$$0 = G_m - \Gamma_{mm} N_m^2 - \Gamma_{ml} N_m N_l + \Gamma_{ex} N_l - \Gamma_l N_m \tag{G.33}$$

$$0 = -\Gamma_{ml} N_m N_l - \Gamma_{ex} N_l + \Gamma_l N_m \tag{G.34}$$

to write the diffusion matrix (see Eq. 5.6 of Ref, [Lax60])

$$\boldsymbol{D} = \begin{pmatrix} 2\Gamma_{mm} N_m^2 + 3\Gamma_l N_m - 2\Gamma_{ex} N_l & -\Gamma_{ex} N_l \\ -\Gamma_{ex} N_l & \Gamma_l N_m \end{pmatrix} \tag{G.35}$$

In the limit with negligible Γ_{ml} we have $\Gamma_l N_m = \Gamma_{ex} N_l$ and thus reproduce $\boldsymbol{M} \equiv \boldsymbol{\Lambda}$ and $\boldsymbol{B} \equiv 2\boldsymbol{D}(\vec{N}_0)$ of [WP04].

Let us instead consider the opposite limit $\Gamma_{ex} = 0$. In steady state, the covariance matrix $\boldsymbol{C} = \langle \Delta\vec{N}(t) \Delta\vec{N}(t) \rangle$ can be obtained by solving [Lax60]

$$\boldsymbol{B} = \boldsymbol{M}\boldsymbol{C} + \boldsymbol{C}\boldsymbol{M}^\dagger \tag{G.36}$$

For simplicity we set $\Gamma_{ml} = \Gamma_{mm} = R$, resulting in the covariance matrix

$$\boldsymbol{C} = \begin{pmatrix} N_m \frac{3R^2 N_m^2 + 7RN_m\Gamma_l + 3\Gamma_l^2}{(RN_m+\Gamma_l)(3RN_m+2\Gamma_l)} & -\frac{\Gamma_l N_m}{3RN_m+2\Gamma_l} \\ -\frac{\Gamma_l N_m}{3RN_m+2\Gamma_l} & \frac{\Gamma_l}{R} \end{pmatrix} \tag{G.37}$$

In the limit of slow localization $\Gamma_l \ll RN_m$ the variance of the mobile quasiparticles is $C_{11} \to N_m$ as for the case without any traps. In the opposite limit $C_{11} \to \frac{3}{2} N_m$ and the mobile quasiparticles exhibit super-poissonian noise. To estimate the relevance of trapping for noise measurements, we require the responsivities of localized and mobile quasiparticles. If the depth of the traps is much smaller than the frequency of the signal used to probe the resonator, we can expect both responsivities to have a similar value to write

$$\delta A = \frac{dA}{dN_{qp}} (\delta N_m + \delta N_l) \tag{G.38}$$

where δA is the amplitude shift of the probing signal due to a fluctuation $\delta N_{m/l}$, and $\frac{dA}{dN_{qp}}$ approximately constant. Then

$$\langle \delta A^2 \rangle = \left(\frac{dA}{dN_{qp}} \right)^2 \sum_{i,j} \boldsymbol{C}_{i,j} = \left(\frac{dA}{dN_{qp}} \right)^2 \left(N_m + N_l - \frac{N_m \Gamma_l^2}{(RN_m + \Gamma_l)(3RN_m + 2\Gamma_l)} \right) \tag{G.39}$$

The last term always gives a small contribution compared to that of the total density, and the variance of the fluctuations is approximately the same as for the model

without traps, when replacing the density of mobile quasiparticles by the total quasiparticle density.

The cross power spectrum is [WP04]

$$\boldsymbol{G}(\omega) = 2\Re\left[(\boldsymbol{M} + i\omega\mathbf{1})^{-1}\,\boldsymbol{B}\left(\boldsymbol{M}^T - i\omega\mathbf{1}\right)^{-1}\right] \tag{G.40}$$

resulting in

$$\begin{aligned}
\boldsymbol{G}_{11} &= \frac{4}{R}\frac{1}{1+v^2}\left[\frac{2+4u+v^2(2+3u)}{4(1+u)^2+v^2}\right] \\
\boldsymbol{G}_{22} &= \frac{4u}{R}\frac{1}{1+v^2} \\
\boldsymbol{G}_{12} &= \boldsymbol{G}_{21} = -\frac{8u^2}{R(1+v^2)\left[v^2+4(1+u)^2\right]}
\end{aligned} \tag{G.41}$$

with $v = \omega/RN_m$ and $u = \Gamma_l/RN_m = N_l/N_m$. In the limit of slow trapping or large quasiparticle generation $N_l \ll N_m$ fluctuations in the mobile quasiparticle density are unaffected by the traps and one recovers G_{11} of [WP04].[3] In the opposite limit $u \gg 1$ the noise spectral density is modified

$$\boldsymbol{G}_{11} \simeq \frac{4}{R}\frac{u}{1+v^2}\left[\frac{4+3v^2}{v^2+4u^2}\right] \tag{G.42}$$

Integrating over frequency reproduces $C_{11} \simeq \frac{3}{2}N_m$ obtained above. The roll-off frequency is shifted to $\omega \sim \Gamma_l$ which in principle allows for a direct measurement of the trapping time. However, as the limit $u \gg 1$ was assumed, fluctuations in the localized density $\boldsymbol{G}_{22}$ and mobile density $\boldsymbol{G}_{11}$ are on the same order only for $v \sim u \gg 1$ and $\boldsymbol{G}_{11}$ becomes relevant only for very large frequencies at which the noise spectral density is very small. For small frequencies and slow recombination/fast trapping, $v, 1 \ll u$, G_{22} dominates the power spectral density. In that limit, (G.41) predicts both the roll-off frequency and the amplitude of the power spectral density to depend on N_m, while for a system containing only mobile quasiparticles the amplitude of the power spectral density is independent of quasiparticle density. Moreover, as the recombination time for localized quasiparticles is given by $RN_m \ll R(N_m + N_l)$, the roll-off frequency measures the number of mobile quasiparticles, while loss measurements and measurements of the fluctuation's variance take into account both localized and mobile quasiparticles. Therefore, disagreement between the quasiparticle density estimated from the roll-off frequency and the quasiparticle density estimated from the fluctuation's variance may indicate trapping.

[3] Here we disregard phonon trapping

G.5. Self consistency equation

In the main text we disregarded fluctuations in the order parameter induced by fluctuation in the depairing parameter. In this appendix we discuss the validity of this assumption. The following calculation has already been done by [FS16] using a non-linear sigma model, we repeat it here using Green's functions to make it more accessible to readers unfamiliar with non-linear sigma models, without claim of novelty. The calculation is easiest by assuming thermal equilibrium and using the residue theorem to rewrite the self consistency equation in its Matsubara form

$$\Delta = \lambda T \sum_{n>0} f_{i\omega_n} \tag{G.43}$$

with $f_{i\omega_n} = \sin(\theta_n)$ where the spectral angle $\theta_{\omega_n} = i\left(\frac{\pi}{2} + \psi(iE)\right)$ is given by the Matsubara version of the Usadel equation obtained by replacing $iE \to \omega_n$

$$0 = \Delta F(\theta_n) - \Delta\xi^2\nabla^2\theta_n - \sin(\theta_n)\cos(\theta_n)\Delta\delta\eta(\vec{R}) \tag{G.44}$$

with

$$\Delta F(\theta_n) = -\omega_n \sin(\theta_n) + \Delta\cos(\theta_n)\left(1 - \eta\sin(\theta_n)\right) \tag{G.45}$$

where the Matsubara frequency is $\omega_n = T\pi(2n+1)$. The advantage of considering the Matsubara Usadel equation rather than the retarded/advanced one is that the spectral angle θ_n is real for the homogeneous system with $F(\theta_n) = 0$. We now expand (G.43) to linear order in $\Delta = \Delta_0 + \delta\Delta$ and $\theta = \theta_0 + \delta\theta$, where Δ_0, θ_0 are the solutions to the homogeneous system [we do not write the Matsubara index explicitly in the following], to get

$$\delta\Delta = \lambda T \sum_{n>0} \cos(\theta_0)\delta\theta \tag{G.46}$$

Expanding also (G.44) in $\delta\Delta, \delta\theta$ allows to solve for [Note that $\Delta\eta = \tau_{sf}^{-1}$ is independent of the order parameter and should not be expanded in $\delta\Delta$]

$$\delta\theta(\vec{q}) = \Pi[\vec{q}, \omega_n] \times \left(-\sin(\theta_0)\cos(\theta_0)\Delta\delta\eta(\vec{q}) + \cos(\theta_0)\delta\Delta(\vec{q})\right) \tag{G.47}$$

where $\vec{q}$ is the fourier transform of $\vec{R}$ and

$$\Pi[\vec{q}, \omega_n] = \left(\Delta_0\xi^2\vec{q}^2 + \Delta_0\sin(\theta_0) + \omega_n\cos(\theta_0) + \Delta_0\eta\cos(2\theta_0)\right)^{-1} \tag{G.48}$$

Inserting in the self consistency equation allows to solve for

$$\frac{\delta\Delta(\vec{q})}{\Delta_0} = -\delta\eta(\vec{q})\left[\frac{1}{\lambda} - T\sum_{n>0}\cos^2(\theta_0)\Pi[\vec{q}, \omega_n]\right]^{-1} T\sum_{n>0}\Pi[\vec{q}, \omega_n]\cos^2(\theta_0)\sin(\theta_0) \tag{G.49}$$

At zero temperature, we can convert the sums to integrals and use

$$\frac{d\omega_n}{d\theta_0} = -\frac{1}{\sin(\theta_0)\Pi[\vec{q} = 0, \omega_n]} \tag{G.50}$$

following from equation (G.45) to change the integration from ω_n to θ. The boundaries of the integral become $\theta(\omega_n = 0) = \pi/2$ and $\theta(\omega_n = \infty) = \theta_c$, where the cutoff θ_c is introduced to remove divergences arising from high energies. The zeroth order term of the self consistency equation allows to replace

$$\frac{1}{\lambda} = \left[\eta \frac{\pi}{4} - \int_{\theta_c}^{\pi/2} d\theta \frac{1}{\sin(\theta)} \right] \tag{G.51}$$

The integral over $1/\sin(\theta)$ cancels with the same term arising in the integral in the denominator of (G.49) and the cutoff can be set to zero, leading to

$$\frac{\delta\Delta(0)}{\Delta_0} = \frac{\pi\delta\eta(0)}{4 - \pi\eta} \tag{G.52}$$

In the limit $\eta \ll 1$ fluctuations in $\delta\eta$ enter the Usadel equation with an additional factor $\cosh(\psi) \simeq \eta^{-1/3} \gg 1$, thus $\delta\eta$ dominates over the induced fluctuations in the order parameter, and we can set $\delta\Delta \simeq 0$. This is assumed to be the case in the main text.

H. List of symbols

Symbol	Name	Comments and relations
$\vec{P}$	Gauge invariant potential	$\left(\vec{A} - \frac{1}{2e}\vec{\nabla}\chi\right)$
$\vec{A}$	Magnetic vector potential	Maxwell equations
$\vec{E}$	Electric field	$-\vec{\nabla}\phi_{el} - \frac{\partial}{\partial t}\vec{A}$
$\vec{B}$	Magnetic flux density	$\nabla \times \vec{A}$
$\vec{H}$	Magnetic field	$\mu_0\vec{B}$, relative permeability μ = 1 is assumed everywhere
$\vec{j}$	Current density	Current field relation (1.28)
ϕ_{el}	Electric potential	Maxwell equations

Table H.1.: Electromagnetic Symbols

Symbol	Name	Comments and relations
$L^{(,)}$	Inductance	per unit length (effective)
$L^{(,)}_{kin}$	Kinetic inductance	per unit length (effective)
$L^{(,)}_{m}$	Geometric inductance	per unit length (effective)
$R^{(,)}$	Resistance per unit length	per unit length (effective)
$C^{(,)}$	Capacitance per unit length	per unit length (effective)
α	Kinetic inductance fraction	L_{kin}/L
Q_i	Quality factor	Internal
Q_c	Quality factor	Coupling
Q	Quality factor	Total
ω_0	Resonance frequency	Lowest, $\omega_0 \ll 2\Delta$
c^{QP}_{Phot}	Quasiparticle photon coupling	Eqs. (E.4) and (E.6)
d	Film Thickness	
w	Central strip width	
s	Gap width	
l	Resonator length	Same symbol for mean free path

Table H.2.: Resonator properties

e	Electron charge	
μ	Chemical potential	
V_{BCS}	BCS pairing interaction	
n_s	Superfluid Density	
ρ_F	Density of states at Fermi level per spin	
σ_N	Normal state conductivity	
l	Electron mean free path	Same symbol for resonator length
v_F	Fermi velocity	
D	Diffusion coefficient	$\frac{1}{3}v_F l$
ω_D	Debye frequency	
N_{ion}	Ion density	per volume
$\epsilon_{\vec{k}}$	Single electron energy	Measured from Fermi surface

Table H.3.: Material properties

Symbol	Name	Comments and relations
$\|\Psi_\phi\rangle$	BCS ground state	
$\|\Psi_N\rangle$	BCS electron number basis state	
$\|0\rangle$ and $\|1\rangle$	Qubit states	
$c^{(\dagger)}/\psi^{(\dagger)}$	Electron annihilation (creation) operator	Momentum/Position
$\gamma^{(\dagger)}$	Quasiparticle annihilation (creation) operator	
H	Hamiltonian	
N_c	Cooper pair number operator	
$\boldsymbol{O}$	Matrix with two nambu indices	All bold operators
$\hat{O}$	Matrix with two nambu and two Keldysh indices	All operators with hat
τ_i	i-th Pauli matrix	

Table H.4.: States and operators

Symbol	Name	Comments and relations
σ	Complex conductivity **or** magenetic disorder strength	$\sigma_1 + i\sigma_2$ **or** Eq. (4.6)
$\lambda_{(L)}$	(London) penetration depth **or** Dimensionless BCS coupling constant	Eq. (1.37) **or** $g^2\rho_F$
Λ	Two dimensional screening length	
ξ	(dirty limit) coherence length **or** shifted pair breaking photon energy	$\sqrt{D/2\Delta}$ **or** $\omega_{PB} - 2\Delta$
ξ_0	clean limit coherence length	v_F/Δ
$u_{\vec{k}}/v_{\vec{k}}$	Bogoliubov amplitudes	
$K^{\pm}$	Coherence factors	Eqs.(2.72), (1.35),(4.12)
ρ	Quasiparticle density of states	Normalized by $4\rho_F$, Eqs. (2.71) ,(1.35)
$U^{\pm}(E_1, E_2)$		$\rho(E_2)K^{\pm}(E_1, E_2)$
$E_{\vec{k}}$	Quasiparticle energy	
$\Delta_{(0)}$	Order parameter	finite (zero) temperature
E_g	Energy gap	
γ_D	Dynes Parameter	
η	Depairing Parameter	Eq. (4.4)

Table H.5.: Superconducting symbols

Symbol	Name	Comments and relations
$G/F/D$	Normal/ Anomalous/ Phonon Green's function	
g/f	Quasiclassical Green's functions	
$\cdot^{R/A/K}$	Retarded/Advanced/ Keldysh Component	
$(A \otimes B)(x, x''t, t'')$		$\int d1' A(1,1')B(1',1'')$ including spatial and temporal components
$(A \circ B)(x, x''t, t'')$		$\int d\vec{r}' A(1,1')B(1',1'')$
$\mathcal{T}_{(c)}$	(Contour) time ordering operator	
$\vec{X}/\vec{x}$	Average/relative coordinates	
$g\hat{\tilde{\gamma}}/g\hat{\gamma}$	Phonon emission/absorption vertex	

Table H.6.: Green's functions

Symbol	Name	Comments and relations
$E/\omega/\omega_0/\omega_{PB}$	Electron/phonon/photon/ pair breaking photon energy	
T_0	Photon temperature	$e^{\omega_0/T_0} \equiv (\bar{n}+1)/\bar{n}$
$T_*, \tilde{T}_*$	Quasiparticle distribution width	Eqs. (3.23), (3.28)
T_B	Phonon bath temperature	
E_*	Quasiparticle nonequilibrium crossover	Eqs. (3.36),(3.37)
T_B^*	Crossover temperature	Eq. (3.35)
ω_c	Phonon nonequilibrium crossover	Eq. (3.40)
$\bar{T}_B$	Pair breaking photon generation temperature	Eq. (3.83)
$x[\tilde{x}]$		$(E-\Delta)/T_*[(E-\Delta)/\tilde{T}_*]$
ϵ		$E-E_g$
$\bar{\epsilon}$		$(E_g-E)/E_g$
$\tilde{\epsilon}$		$(E_g-E)/\epsilon_T$
ε		$\omega_{PB}-\Delta-E$
$\tilde{\varepsilon}$		$\omega_0+\Delta-E$
ϵ_T	Tail witdh	Eq.(4.25)
ξ	Shifted pair breaking photon energy **or** (dirty limit) coherence length	$\omega_{PB}-2\Delta$ **or** $\sqrt{D/2\Delta}$
γ		ϵ/ξ
γ'_*, γ_*, γ_c	Crossover energy	Eqs. (3.70),(3.76), Fig. 3.8

Table H.7.: Energies and Temperatures

Symbol	Name	Comments and relations
N_{qp} (x_{qp})	(normalized) quasiparticle density	Eqs. (3.41), (3.56)
$R(r)$	(normalized) recombination coefficient	Eqs. (3.50), (3.58)
$G_{\bar{T}_B}, G(T_*/\Delta)$	Generation rates	Eqs. (3.49), (3.52),(3.98)
g_α	normalized generation rates	Eq. (4.1)
$\Gamma_{\alpha,\beta}$	Normalized Recombination rates	Eq. (4.1)
$\Gamma_{ex/loc}$	normalized excitation/localization rates	Eq. (4.1)

Table H.8.: Rothwarf-Taylor paramter

Bibliography

[AG61] A.A. Abrikosov and L.P. Gorkov. "Contribution to the theory of superconducting alloys with paramagnetic impurities". In: *Soviet Physics JETP* 12.6 (1961), pp. 1243–1253.

[And59] P. W. Anderson. "Theory of dirty superconductors". In: *Journal of Physics and Chemistry of Solids* 11.1 (1959), pp. 26–30. ISSN: 0022-3697. DOI: 10.1016/0022-3697(59)90036-8.

[AS10] Alexander Altland and Ben Simons. *Condensed Matter Field Theory*. 2nd ed. Cambridge University Press, 2010.

[Bar+10] H. Bartolf et al. "Current-assisted thermally activated flux liberation in ultrathin nanopatterned NbN superconducting meander structures". In: *Phys. Rev. B* 81.2 (2010), p. 024502. DOI: 10.1103/PhysRevB.81.024502.

[Bas+12] Jochem Baselmans et al. "Ultra Low Background Cryogenic Test Facility for Far-Infrared Radiation Detectors". In: *Journal of Low Temperature Physics* 167.3-4 (2012), pp. 360–366. ISSN: 1573-7357. DOI: 10.1007/s10909-012-0511-0.

[BCS57] J. Bardeen, L. N. Cooper, and J. R. Schrieffer. "Theory of Superconductivity". In: *Phys. Rev.* 108.5 (1957), pp. 1175–1204. DOI: 10.1103/PhysRev.108.1175.

[Bel+99] Wolfgang Belzig et al. "Quasiclassical Green's function approach to mesoscopic superconductivity". In: *Superlattices and Microstructures* 25.5 (1999), pp. 1251–1288. ISSN: 0749-6036. DOI: 10.1006/spmi.1999.0710.

[Ben+24] R. Benevides et al. "Quasiparticle Dynamics in a Superconducting Qubit Irradiated by a Localized Infrared Source". In: *Phys. Rev. Lett.* 133 (6 Aug. 2024), p. 060602. DOI: 10.1103/PhysRevLett.133.060602.

[Bes+16] Anton Bespalov et al. "Theoretical Model to Explain Excess of Quasiparticles in Superconductors". In: *Phys. Rev. Lett.* 117.11 (2016), p. 117002. DOI: 10.1103/PhysRevLett.117.117002.

[BF04] H. Bruus and K. Flensberg. *Many-Body Quantum Theory in Condensed Matter Physics: An Introduction*. Oxford Graduate Texts. OUP Oxford, 2004. ISBN: 9780191057472.

[Bog58] N. N. Bogoljubov. "On a new method in the theory of superconductivity". In: *Il Nuovo Cimento (1955-1965)* 7.6 (1958), pp. 794–805. ISSN: 1827-6121. DOI: 10.1007/BF02745585.

[Bru17a] "Linear Volterra Integral Equations". In: *Volterra integral equations*. Ed. by Hermann Brunner. Cambridge monographs on applied and computational mathematics. Cambridge, New York, NY, and Port Melbourne: Cambridge University Press, 2017, pp. 1–56. ISBN: 9781107098725. DOI: 10.1017/9781316162491.002.

[Bru17b] Hermann Brunner, ed. *Volterra integral equations: An introduction to theory and applications*. Vol. 30. Cambridge monographs on applied and computational mathematics. Cambridge, New York, NY, and Port Melbourne: Cambridge University Press, 2017. ISBN: 9781107098725. DOI: 10.1017/9781316162491.

[BT97] A. V. Balatsky and S. A. Trugman. "Lifshitz Tail in the Density of States of a Superconductor with Magnetic Impurities". In: *Phys. Rev. Lett.* 79.19 (1997), pp. 3767–3770. DOI: 10.1103/PhysRevLett.79.3767.

[Bul+11] L. N. Bulaevskii et al. "Vortex-induced dissipation in narrow current-biased thin-film superconducting strips". In: *Physical Review B* 83.14 (2011), p. 144526. DOI: 10.1103/PhysRevB.83.144526.

[BY09] J. J. A. Baselmans and S. J. C. Yates. "Long quasiparticle lifetime in Aluminum Microwave Kinetic Inductance Detectors using coaxial stray light filters". In: *AIP Conference Proceedings* 1185.1 (Dec. 2009), pp. 160–163. DOI: 10.1063/1.3292305.

[Car+21] L. Cardani et al. "Reducing the impact of radioactivity on quantum circuits in a deep-underground facility". In: *Nature Communications* 12.1 (2021), p. 2733. ISSN: 2041-1723. DOI: 10.1038/s41467-021-23032-z.

[Cat+11] G. Catelani et al. "Relaxation and frequency shifts induced by quasiparticles in superconducting qubits". In: *Phys. Rev. B* 84 (6 Aug. 2011), p. 064517. DOI: 10.1103/PhysRevB.84.064517.

[Cat14] G. Catelani. "Parity switching and decoherence by quasiparticles in single-junction transmons". In: *Phys. Rev. B* 89.9 (2014), p. 094522. DOI: 10.1103/PhysRevB.89.094522.

[CB19] Catelani, G. and Basko, D.M. "Non-equilibrium quasiparticles in superconducting circuits: photons vs. phonons". In: *SciPost Phys* 6.1 (2019), p. 13. DOI: 10.21468/SciPostPhys.6.1.013.

[CC79] C. C. Chi and John Clarke. "Quasiparticle branch mixing rates in superconducting aluminum". In: *Phys. Rev. B* 19.9 (1979), pp. 4495–4509. DOI: 10.1103/PhysRevB.19.4495.

[CEP69] P. Chubov, V. Eremenko, and Y. A. Pilipenko. "Dependence of the critical temperature and energy gap on the thickness of superconducting aluminum films". In: *Sov. Phys. JETP* 28 (1969), p. 389.

[Cla72] John Clarke. "Experimental Observation of Pair-Quasiparticle Potential Difference in Nonequilibrium Superconductors". In: *Physical Review Letters* 28.21 (1972), pp. 1363–1366. ISSN: 0031-9007. DOI: 10.1103/physrevlett.28.1363.

[Cle13] John R. Clem. "Inductances and attenuation constant for a thin-film superconducting coplanar waveguide resonator". In: *Journal of Applied Physics* 113.1 (2013), p. 013910. DOI: 10.1063/1.4773070.

[CM14] S. Chaudhuri and I. J. Maasilta. "Superconducting tantalum nitride-based normal metal-insulator-superconductor tunnel junctions". In: *Applied Physics Letters* 104.12 (Mar. 2014), p. 122601. ISSN: 0003-6951. DOI: 10.1063/1.4869563.

[CNM13] S. Chaudhuri, M. R. Nevala, and I. J. Maasilta. "Niobium nitride-based normal metal-insulator-superconductor tunnel junction microthermometer". In: *Applied Physics Letters* 102.13 (Apr. 2013), p. 132601. ISSN: 0003-6951. DOI: 10.1063/1.4800440.

[CP22] G. Catelani and J. P. Pekola. "Using materials for quasiparticle engineering". In: *Mater. Quantum. Technol.* 2 (2022), p. 013001. DOI: 10.1088/2633-4356/ac4a75.

[CS77] Jhy-Jiun Chang and D. J. Scalapino. "Kinetic-equation approach to nonequilibrium superconductivity". In: *Phys. Rev. B* 15 (1977).

[CS78] Jhy-Jiun Chang and D. J. Scalapino. "Nonequilibrium superconductivity". In: *Journal of Low Temperature Physics* 31.1 (1978), pp. 1–32. ISSN: 1573-7357. DOI: 10.1007/BF00116228.

[Day+03] Peter K. Day et al. "A broadband superconducting detector suitable for use in large arrays". In: *Nature* 425.6960 (2003), pp. 817–821. ISSN: 1476-4687. DOI: 10.1038/nature02037.

[DG81] R. C. Dynes and J. P. Garno. "Metal-Insulator Transition in Granular Aluminum". In: *Phys. Rev. Lett.* 46 (2 Jan. 1981), pp. 137–140. DOI: 10.1103/PhysRevLett.46.137.

[Dia+22] S. Diamond et al. "Distinguishing Parity-Switching Mechanisms in a Superconducting Qubit". In: *PRX Quantum* 3 (4 Oct. 2022), p. 040304. DOI: 10.1103/PRXQuantum.3.040304.

[Dyn+84] R. C. Dynes et al. "Tunneling Study of Superconductivity near the Metal-Insulator Transition". In: *Phys. Rev. Lett.* 53 (25 Dec. 1984), pp. 2437–2440. DOI: 10.1103/PhysRevLett.53.2437.

[Eil68] Gert Eilenberger. "Transformation of Gorkov's equation for type II superconductors into transport-like equations". In: *Zeitschrift für Physik A Hadrons and nuclei* 214.2 (1968), pp. 195–213. ISSN: 0939-7922. DOI: 10.1007/BF01379803.

[Eis+76] W. Eisenmenger et al. "Quasiparticle recombination and 2Δ-phonon-trapping in superconducting tunneling junctions". In: *Applied physics* 11.4 (1976), pp. 307–320. ISSN: 1432-0630. DOI: 10.1007/BF00919359.

[Ele74] V. F. Elesin. "Nonequilibrium state of superconductors with optical excitation of quasiparticles". In: *Journal of Experimental and Theoretical Physics* 39.5 (1974), p. 862.

[Eli60] G. M. Eliashberg. "INTERACTIONS BETWEEN ELECTRONS AND LATTICE VIBRATIONS IN A SUPERCONDUCTOR". In: *Journal of Experimental and Theoretical Physics* 11 (1960), pp. 696–702.

[ES81] Ulrich Eckern and Albert Schmid. "Quasiclassical Green's function in the BCS pairing theory". In: *Journal of Low Temperature Physics* 45.1 (1981), pp. 137–166. ISSN: 0022-2291. DOI: 10.1007/BF00661147.

[FC23] P.B. Fischer and G. Catelani. "Nonequilibrium Quasiparticle Distribution in Superconducting Resonators: An Analytical Approach". In: *Phys. Rev. Appl.* 19 (5 May 2023), p. 054087. DOI: 10.1103/PhysRevApplied.19.054087.

[FC24] Paul B. Fischer and Gianluigi Catelani. "Nonequilibrium quasiparticle distribution in superconducting resonators: Effect of pair-breaking photons". In: *SciPost Phys.* 17 (2024), p. 070. DOI: 10.21468/SciPostPhys.17.3.070.

[FC25] Paul B. Fischer and Gianluigi Catelani. "Excess quasiparticles and their dynamics in the presence of subgap states". In: *arXiv:2507.06902* (2025). DOI: https://doi.org/10.48550/arXiv.2507.06902.

[FHG11] Ya. V. Fominov, M. Houzet, and L. I. Glazman. "Surface impedance of superconductors with weak magnetic impurities". In: *Phys. Rev. B* 84.22 (2011), p. 224517. DOI: 10.1103/PhysRevB.84.224517.

[For+15] Antonio Fornieri et al. "Nanoscale phase engineering of thermal transport with a Josephson heat modulator". In: *Nat. Nanotechnol.* 11 (2015), p. 258. DOI: 10.1038/nnano.2015.281.

[For+17] Antonio Fornieri et al. "0–π phase-controllable thermal Josephson junction". In: *Nat. Nanotechnol.* 12 (2017), p. 425. DOI: 10.1038/nnano.2017.25.

[FS16] Yakov V. Fominov and Mikhail A. Skvortsov. "Subgap states in disordered superconductors with strong magnetic impurities". In: *Phys. Rev. B* 93 (14 Apr. 2016), p. 144511. DOI: 10.1103/PhysRevB.93.144511.

[Gao+08] J. Gao et al. "Equivalence of the Effects on the Complex Conductivity of Superconductor due to Temperature Change and External Pair Breaking". In: *Journal of Low Temperature Physics* 151.1 (2008), pp. 557–563. ISSN: 1573-7357. DOI: 10.1007/s10909-007-9688-z.

[Gao08] Jiansong Gao. "The Physics of Superconducting Microwave Resonators". PhD thesis. California Institute of Technology, 2008. DOI: 10.7907/RAT0-VM75.

[GC21] Leonid I. Glazman and Gianluigi Catelani. "Bogoliubov quasiparticles in superconducting qubits". In: *SciPost Phys. Lect. Notes* (2021), p. 31. DOI: 10.21468/SciPostPhysLectNotes.31.

[GEK86] V. M. Galitskii, V. F. Elesin, and Yu.V. Kopaev. "The Kinetic Theory of superconductors with excess quasiparticles". In: *Nonequilibrium Superconductivity*. Ed. by D.N Langenberg and A. I. Larkin. Modern Problems in condensed matter science. 1986.

[Ger+22] G. Germanese et al. "Bipolar thermoelectric Josephson engine". In: *Nat. Nanotechnol.* 17 (2022), p. 1084. DOI: 10.1038/s41565-022-01208-y.

[GGW16] T. Guruswamy, D. J. Goldie, and S. Withington. "Broadband illumination of superconducting pair breaking photon detectors". In: *Superconductor Science and Technology* 29.4 (2016), p. 045011. DOI: 10.1088/0953-2048/29/4/045011.

[Gia+06] Francesco Giazotto et al. "Opportunities for mesoscopics in thermometry and refrigeration: Physics and applications". In: *Reviews of Modern Physics* 78.1 (2006), pp. 217–274. ISSN: 0034-6861. DOI: 10.1103/RevModPhys.78.217.

[Gin09] V. L. Ginzburg. *On Superconductivity and Superfluidity: A Scientific Autobiography*. Heidelberg: Springer, 2009.

[GL50] V. L. Ginzburg and L. D. Landau. "On the Theory of Superconductivity". In: *Zh. Eksp. Teor. Fiz. (ZhETF)* 20 (1950), p. 1064.

[GM 72] G.M Eliashberg. "Inelastic Electron collisions and nonequillibrium states in superconductors". In: *Soviet Physics JETP* 34 (1972).

[Gol+01] G. N. Gol'tsman et al. "Picosecond superconducting single-photon optical detector". In: *Applied Physics Letters* 79.6 (2001), pp. 705–707. DOI: 10.1063/1.1388868.

[Grü+18] Lukas Grünhaupt et al. "Loss Mechanisms and Quasiparticle Dynamics in Superconducting Microwave Resonators Made of Thin-Film Granular Aluminum". In: *Phys. Rev. Lett.* 121.11 (2018), p. 117001. DOI: 10.1103/PhysRevLett.121.117001.

[Grü19] Lukas Grünhaupt. "Granular aluminium superinductors". PhD thesis. Karlsruher Institut fuer Technologie, 2019. DOI: 10.5445/KSP/1000097320.

[GS74] Günter Grünewald and Kurt Scharnberg. "Lifetimes of long wavelength longitudinal phonons in impure metals". In: *Zeitschrift für Physik* 268.2 (1974), pp. 197–205. ISSN: 0044-3328. DOI: 10.1007/BF01669880.

[Gur18] Tejas Guruswamy. "Nonequilibrium behaviour and quasiparticle heating in thin film superconducting microwave resonators". PhD thesis. Apollo - University of Cambridge Repository, 2018. DOI: 10.17863/CAM.24510.

[Gv95] A. M. Gulian and D. van Vechten. "Nonequilibrium dynamic conductivity of superconductors: An exploitable basis for high–energy resolution x–ray detectors". In: *Applied Physics Letters* 67.17 (1995), pp. 2560–2562. ISSN: 0003-6951. DOI: 10.1063/1.114432.

[GW12] D. J. Goldie and S. Withington. "Non-equilibrium superconductivity in quantum-sensing superconducting resonators". In: *Superconductor Science and Technology* 26.1 (2012), p. 015004.

[HC18] A. Hosseinkhani and G. Catelani. "Proximity effect in normal-metal quasiparticle traps". In: *Phys. Rev. B* 97 (5 Feb. 2018), p. 054513. DOI: 10.1103/PhysRevB.97.054513.

[Hij+09] Richard A. Hijmering et al. "Modeling of Local Trapping States in Superconductor Tunnel Junctions With Kondo Impurities". In: *IEEE Trans. Appl. Supercond.* 19.3 (2009), p. 423. DOI: 10.1109/TASC.2009.2018506.

[HL68] S. Y. Hsieh and James L. Levine. "Diffusion of Quasiparticles in Superconducting Aluminum Films". In: *Phys. Rev. Lett.* 20.26 (1968), pp. 1502–1504. DOI: 10.1103/PhysRevLett.20.1502.

[Hol+94] T. Holst et al. "Effect of a Transmission Line Resonator on a Small Capacitance Tunnel Junction". In: *Phys. Rev. Lett.* 73 (25 Dec. 1994), pp. 3455–3458. DOI: 10.1103/PhysRevLett.73.3455.

[Hou+19] M. Houzet et al. "Photon-Assisted Charge-Parity Jumps in a Superconducting Qubit". In: *Phys. Rev. Lett.* 123.10 (2019), p. 107704. DOI: 10.1103/PhysRevLett.123.107704.

[IGE94] Gert-Ludwig Ingold, Hermann Grabert, and Udo Eberhardt. "Cooper-pair current through ultrasmall Josephson junctions". In: *Phys. Rev. B* 50 (1 July 1994), pp. 395–402. DOI: 10.1103/PhysRevB.50.395.

[Ima80] Syozo Imay. "Stability of the Nonequilibrium State of a Superconductor Irradiated by an Electromagnetic Field". In: *Journal of Low Temperature Physics* 40 (1980). ISSN: 1573-7357.

[Ish+98] K. Ishida et al. "Spin-triplet superconductivity in Sr2RuO4 identified by 17O Knight shift". In: *Nature* 396.6712 (1998), pp. 658–660. ISSN: 1476-4687. DOI: 10.1038/25315.

[JD83] J.W Serene and D Rainer. "The quasiclassical approach to superfluid 3He". In: *Physics Reports* 101.4 (1983), pp. 221–311. ISSN: 0370-1573. DOI: 10.1016/0370-1573(83)90051-0.

[K H+12] K. Hattori et al. “Development of Superconducting Detectors for Measurements of Cosmic Microwave Background”. In: *Physics Procedia* 37 (2012), pp. 1406–1412. ISSN: 1875-3892. DOI: 10.1016/j.phpro.2012.02.478.

[Kap+76] S. B. Kaplan et al. “Quasiparticle and phonon lifetimes in superconductors”. In: *Phys. Rev. B* 14.11 (1976), pp. 4854–4873. DOI: 10.1103/PhysRevB.14.4854.

[Kap79] Steven B. Kaplan. “Acoustic matching of superconducting films to substrates”. In: *Journal of Low Temperature Physics* 37.3 (1979), pp. 343–365. ISSN: 1573-7357. DOI: 10.1007/BF00119193.

[Kar+19] K. Karatsu et al. “Mitigation of cosmic ray effect on microwave kinetic inductance detector arrays”. In: *Applied Physics Letters* 114.3 (2019), p. 032601. DOI: 10.1063/1.5052419.

[KI68] I. O. Kulik and O. Yu Itskovich. “EFFECT OF CONCENTRATION NON-UNIFORMITY ON THE PROPERTIES OF SUPERCONDUCTORS WITH PARAMAGNETIC IMPURITIES”. In: *Journal of Experimental and Theoretical Physics* 28.1 (1968), p. 102.

[KL57] W. Kohn and J. M. Luttinger. “Quantum Theory of Electrical Transport Phenomena”. In: *Phys. Rev.* 108.3 (1957), pp. 590–611. DOI: 10.1103/PhysRev.108.590.

[KM61] Leo P. Kadanoff and Paul C. Martin. “Theory of Many-Particle Systems. II. Superconductivity”. In: *Phys. Rev.* 124 (3 Nov. 1961), pp. 670–697. DOI: 10.1103/PhysRev.124.670.

[Koc+07] Jens Koch et al. “Charge-insensitive qubit design derived from the Cooper pair box”. In: *Phys. Rev. A* 76.4 (2007), p. 042319. DOI: 10.1103/PhysRevA.76.042319.

[Kop01] N. B. Kopnin. *Theory of Nonequilibrium Superconductivity*. Clarendon Press, 2001.

[Koz+00] A. G. Kozorezov et al. “Quasiparticle-phonon downconversion in nonequilibrium superconductors”. In: *Phys. Rev. B* 61.17 (2000), pp. 11807–11819. DOI: 10.1103/PhysRevB.61.11807.

[Koz+04a] A. G. Kozorezov et al. “Evidence for an excited nonequilibrium quasiparticle distribution in superconducting tunnel junctions resulting from energy accumulation via sequential tunneling”. In: *Phys. Rev. B* 69.18 (2004), p. 184506. DOI: 10.1103/PhysRevB.69.184506.

[Koz+04b] A. G. Kozorezov et al. “The role of phonons in establishing a nonequilibrium quasiparticle state in small gap multiple tunnelling superconducting tunnel junctions”. In: *physica status solidi (c)* 1.11 (2004), pp. 2816–2819. DOI: 10.1002/pssc.200405399.

[Koz+08] A. G. Kozorezov et al. “Inelastic scattering of quasiparticles in a superconductor with magnetic impurities”. In: *Phys. Rev. B* 78 (17 Nov. 2008), p. 174501. DOI: 10.1103/PhysRevB.78.174501.

[KP61] O. V. Konstantinov and V. I. Perel. “A diagram technique for evaluating transport quantities”. In: *Journal of Experimental and Theoretical Physics* 12.1 (1961), pp. 142–149. ISSN: 1063-7761.

[Kur00] Masahiko Kurakado. “An introduction to superconducting tunnel junction detectors”. In: *X-Ray Spectrometry* 29.2 (2000), pp. 137–146.

[L P08] L. Pitaevskii. “Phenomenology and Microscopic Theory: Theoretical Foundations”. In: *Superconductivity*. Ed. by K.H. Bennemann and J.B. Ketterson. Springer, 2008.

[L V65] L. V. Keldysh. “DIAGRAM TECHNIQUE FOR NONEQUILIBRIUM PROCESSES”. In: *Journal of Experimental and Theoretical Physics* 20.4 (1965), pp. 1018–1026. ISSN: 1063-7761.

[Lax60] Melvin Lax. “Fluctuations from the Nonequilibrium Steady State”. In: *Rev. Mod. Phys.* 32.1 (1960), pp. 25–64. DOI: 10.1103/RevModPhys.32.25.

[LL35a] F. London and H. London. “Supraleitung und diamagnetismus”. In: *Physica* 2.1 (1935), pp. 341–354. ISSN: 0031-8914. DOI: 10.1016/S0031-8914(35)90097-0.

[LL35b] F. London and H. London. “The electromagnetic equations of the supraconductor”. In: *Proceedings of the Royal Society of London. Series A - Mathematical and Physical Sciences* 149.866 (1935), pp. 71–88. ISSN: 0080-4630. DOI: 10.1098/rspa.1935.0048.

[LO69] A. I. Larkin and Yu N. Ovchinnikov. “QUASICLASSICAL METHOD IN THE THEORY OF SUPERCONDUCTIVITY”. In: *Journal of Experimental and Theoretical Physics* 28 (1969), pp. 1200–1205. ISSN: 1063-7761.

[LO72] A. I. Larkin and Yu. N. Ovchinnikov. “DENSITY OF STATES IN INHOMOGENEOUS SUPERCONDUCTORS”. In: *Journal of Experimental and Theoretical Physics* 34 (1972), pp. 1144–1150.

[LO75] A. I. Larkin and Yu N. Ovchinnikov. “Nonlinear conductivity of superconductors in the mixed state”. In: *Journal of Experimental and Theoretical Physics* 46 (1975).

[LO77] A. I. Larkin and Yu N. Ovchinnikov. “Non-linear effects during the motion of vortices in superconductors”. In: *Zh. Eksp. Teor. Fiz.* 73.1 (1977), p. 7.

[LO86] A. I. Larkin and Yu N. Ovchinnikov. “Vortex Motion in superconductors”. In: *Nonequilibrium Superconductivity*. Ed. by D.N Langenberg and A. I. Larkin. Modern Problems in condensed matter science. 1986.

[Low+14] Amy Lowitz et al. "A Comparison of Fundamental Noise in Kinetic Inductance Detectors and Transition Edge Sensors for Millimeter-Wave Applications". In: *Journal of Low Temperature Physics* 176 (2014). ISSN: 1573-7357. DOI: 10.1007/s10909-014-1133-5.

[Mac+10] P. Macha et al. "Losses in coplanar waveguide resonators at millikelvin temperatures". In: *Applied Physics Letters* 96.6 (2010), p. 062503. DOI: 10.1063/1.3309754.

[MAC22] Giampiero Marchegiani, Luigi Amico, and Gianluigi Catelani. "Quasiparticles in Superconducting Qubits with Asymmetric Junctions". In: *PRX Quantum* 3 (4 Dec. 2022), p. 040338. DOI: 10.1103/PRXQuantum.3.040338.

[Mau18] P. D. Mauskopf. "Transition Edge Sensors and Kinetic Inductance Detectors in Astronomical Instruments". In: *Publications of the Astronomical Society of the Pacific* 130.990 (2018), p. 082001. ISSN: 0004-6280. DOI: 10.1088/1538-3873/aabaf0.

[Maz05] Benjamin A. Mazin. "Microwave kinetic inductance detectors". PhD thesis. California Institute of Technology, 2005. DOI: 10.7907/GZ72-V784.

[MB58] D. C. Mattis and J. Bardeen. "Theory of the Anomalous Skin Effect in Normal and Superconducting Metals". In: *Phys. Rev.* 111.2 (1958), pp. 412–417. DOI: 10.1103/PhysRev.111.412.

[MCL19] Clemens Müller, Jared H Cole, and Jürgen Lisenfeld. "Towards understanding two-level-systems in amorphous solids: insights from quantum circuits". In: *Reports on Progress in Physics* 82.12 (Oct. 2019), p. 124501. DOI: 10.1088/1361-6633/ab3a7e.

[Mig58] D. Migdal A. "INTERACTION BETWEEN ELECTRONS AND LATTICE VIBRATIONS IN A NORMAL METAL". In: *Soviet Physics JETP* 34.6 (1958), pp. 996–1001.

[MO33] W. Meissner and R. Ochsenfeld. "Ein neuer Effekt bei Eintritt der Supraleitfähigkeit". In: *Naturwissenschaften* 21.44 (1933), pp. 787–788. ISSN: 1432-1904. DOI: 10.1007/BF01504252.

[MS59] Paul C. Martin and Julian Schwinger. "Theory of Many-Particle Systems. I". In: *Phys. Rev.* 115 (6 Sept. 1959), pp. 1342–1373. DOI: 10.1103/PhysRev.115.1342.

[Nam60] Yoichiro Nambu. "Quasi-Particles and Gauge Invariance in the Theory of Superconductivity". In: *Phys. Rev.* 117 (3 Feb. 1960), pp. 648–663. DOI: 10.1103/PhysRev.117.648.

[NCB17] D. V. Nguyen, G. Catelani, and D. M. Basko. "Dissipation in a superconducting artificial atom due to a single nonequilibrium quasiparticle". In: *Phys. Rev. B* 96 (21 Dec. 2017), p. 214508. DOI: 10.1103/PhysRevB.96.214508.

[Nev+12] M. R. Nevala et al. "Sub-micron normal-metal/insulator/superconductor tunnel junction thermometer and cooler using Nb". In: *Applied Physics Letters* 101.11 (Sept. 2012), p. 112601. ISSN: 0003-6951. DOI: 10.1063/1.4751355.

[NTH12] Chandra M. Natarajan, Michael G. Tanner, and Robert H. Hadfield. "Superconducting nanowire single-photon detectors: physics and applications". In: *Superconductor Science and Technology* 25.6 (2012), p. 063001. ISSN: 0953-2048. DOI: 10.1088/0953-2048/25/6/063001.

[ONe+10] G. C. O'Neil et al. "Quasiparticle density of states measurements in clean superconducting AlMn alloys". In: *J. Appl. Phys.* 107.9 (May 2010), p. 093903. ISSN: 0021-8979. DOI: 10.1063/1.3369280.

[Onn11] H. Kamerlingh Onnes. In: *Commun. Phys. Lab. Univ. Leiden* 120b, 122b, 124c (1911).

[Pai+11] Hanhee Paik et al. "Observation of High Coherence in Josephson Junction Qubits Measured in a Three-Dimensional Circuit QED Architecture". In: *Phys. Rev. Lett.* 107 (24 Dec. 2011), p. 240501. DOI: 10.1103/PhysRevLett.107.240501.

[Pea64] J. Pearl. "CURRENT DISTRIBUTION IN SUPERCONDUCTING FILMS CARRYING QUANTIZED FLUXOIDS". In: *Applied Physics Letters* 5.4 (1964), pp. 65–66. ISSN: 0003-6951. DOI: 10.1063/1.1754056.

[Pip53] Alfred Brian Pippard. "An experimental and theoretical study of the relation between magnetic field and current in a superconductor". In: *Proceedings of the Royal Society of London. Series A - Mathematical and Physical Sciences* (1953). ISSN: 0080-4630.

[Poz12] David M. Pozar. *Microwave engineering*. Fourth edition. Hoboken, NJ: John Wiley & Sons Inc, 2012. ISBN: 9781118213636.

[RCP09] Sukumar Rajauria, Hervé Courtois, and Bernard Pannetier. "Quasiparticle-diffusion-based heating in superconductor tunneling microcoolers". In: *Phys. Rev. B* 80 (21 Dec. 2009), p. 214521. DOI: 10.1103/PhysRevB.80.214521.

[Ric69] G. Rickayzen. In: *Superconductivity*. Ed. by Parks. New York, 1969, pp. 51–115.

[Ris+13] D. Ristè et al. "Millisecond charge-parity fluctuations and induced decoherence in a superconducting transmon qubit". In: *Nature Communications* 4.1 (2013), p. 1913. ISSN: 2041-1723. DOI: 10.1038/ncomms2936.

[Riw+16] R.-P. Riwar et al. "Normal-metal quasiparticle traps for superconducting qubits". In: *Phys. Rev. B* 94 (10 Sept. 2016), p. 104516. DOI: 10.1103/PhysRevB.94.104516.

[Roo+21] Steven A. H. de Rooij et al. "Strong reduction of quasiparticle fluctuations in a superconductor due to decoupling of the quasiparticle number and lifetime". In: *Phys. Rev. B* 104 (18 Nov. 2021), p. L180506. DOI: 10.1103/PhysRevB.104.L180506.

[Roo+24] Steven A. H. de Rooij et al. "Recombination of localized quasiparticles in disordered superconductors". In: *arXiv:2410.18802* (2024).

[RS86a] J. Rammer and H. Smith. "Quantum field-theoretical methods in transport theory of metals". In: *Rev. Mod. Phys.* 58 (2 Apr. 1986), pp. 323–359. DOI: 10.1103/RevModPhys.58.323.

[RS86b] M. Yu Reizer and A. V. Sergeyev. "Electron–Phonon Interaction in Impure Metals and Superconductors". In: *Journal of Experimental and Theoretical Physics* 63 (1986), pp. 616–624. ISSN: 1063-7761.

[RT67] Allen Rothwarf and B. N. Taylor. "Measurement of Recombination Lifetimes in Superconductors". In: *Phys. Rev. Lett.* 19.1 (1967), pp. 27–30. DOI: 10.1103/PhysRevLett.19.27.

[SBW64] S. Skalski, O. Betbeder-Matibet, and P. R. Weiss. "Properties of Superconducting Alloys Containing Paramagnetic Impurities". In: *Phys. Rev.* 136 (6A Dec. 1964), A1500–A1518. DOI: 10.1103/PhysRev.136.A1500.

[Sch80] Schmid, Albert. "Kinetic equations for dirty superconductors". In: *Nonequilibrium Superconductivity, Phonons and Kapitza Boundaries*. Ed. by Kenneth E. Gray. Nato Advanced Study Institutes Series B. 1980.

[Sem+16] A. V. Semenov et al. "Coherent Excited States in Superconductors due to a Microwave Field". In: *Phys. Rev. Lett.* 117.4 (2016), p. 047002. DOI: 10.1103/PhysRevLett.117.047002.

[Ser+18] K. Serniak et al. "Hot Nonequilibrium Quasiparticles in Transmon Qubits". In: *Phys. Rev. Lett.* 121.15 (2018), p. 157701. DOI: 10.1103/PhysRevLett.121.157701.

[SF13] M. A. Skvortsov and M. V. Feigel'man. "Subgap states in disordered superconductors". In: *Journal of Experimental and Theoretical Physics* 117.3 (2013), pp. 487–498. ISSN: 1063-7761. DOI: 10.1134/S106377611311006X.

[She85] A. L. Shelankov. "On the derivation of quasiclassical equations for superconductors". In: *Journal of Low Temperature Physics* 60.1-2 (1985), pp. 29–44. ISSN: 0022-2291. DOI: 10.1007/BF00681651.

[SI05] Alessandro Silva and Lev B. Ioffe. "Subgap states in dirty superconductors and their effect on dephasing in Josephson qubits". In: *Phys. Rev. B* 71 (10 Mar. 2005), p. 104502. DOI: 10.1103/PhysRevB.71.104502.

[SM00] A. Sergeev and V. Mitin. "Electron-phonon interaction in disordered conductors: Static and vibrating scattering potentials". In: *Phys. Rev. B* 61.9 (2000), pp. 6041–6047. DOI: 10.1103/PhysRevB.61.6041.

[SSW66] D. J. Scalapino, J. R. Schrieffer, and J. W. Wilkins. "Strong-Coupling Superconductivity. I". In: *Phys. Rev.* 148 (1 Aug. 1966), pp. 263–279. DOI: 10.1103/PhysRev.148.263.

[ST08] R.V.A. Srivastava and W. Teizer. "Analytical density of states in the Abrikosov–Gorkov theory". In: *Solid State Communications* 145.9 (2008), pp. 512–513. ISSN: 0038-1098. DOI: https://doi.org/10.1016/j.ssc.2007.11.030.

[Tau+16] M. Taupin et al. "Tunable quasiparticle trapping in Meissner and vortex states of mesoscopic superconductors". In: *Nature Communications* 7.1 (2016), p. 10977. ISSN: 2041-1723. DOI: 10.1038/ncomms10977.

[TC72] M. Tinkham and John Clarke. "Theory of Pair-Quasiparticle Potential Difference in Nonequilibrium Superconductors". In: *Phys. Rev. Lett.* 28.21 (1972), pp. 1366–1369. DOI: 10.1103/PhysRevLett.28.1366.

[Teu08] John Daniel Teufel. "Superconducting Tunnel Junctions as Direct Detectors for Submillimeter Astronomy". PhD thesis. Yale University, 2008.

[Tin96] Michael Tinkham. *Introduction to superconductivity.* 2nd ed. 1996.

[Twe88] Damian Twerenbold. "Superconducting tunneling junctions as X-ray detectors and their possible applications in astrophysics". In: *Nuclear Instruments and Methods in Physics Research Section A: Accelerators, Spectrometers, Detectors and Associated Equipment* 273.2 (1988), pp. 575–582. ISSN: 0168-9002. DOI: 10.1016/0168-9002(88)90059-9.

[UFN98] J. N. Ullom, P. A. Fisher, and M. Nahum. "Magnetic field dependence of quasiparticle losses in a superconductor". In: *Applied Physics Letters* 73.17 (1998), pp. 2494–2496. DOI: 10.1063/1.122493.

[Usa70] Klaus D. Usadel. "Generalized Diffusion Equation for Superconducting Alloys". In: *Physical Review Letters* 25.8 (1970), pp. 507–509. ISSN: 0031-9007. DOI: 10.1103/PhysRevLett.25.507.

[Val+19] Francesco Valenti et al. "Interplay Between Kinetic Inductance, Nonlinearity, and Quasiparticle Dynamics in Granular Aluminum Microwave Kinetic Inductance Detectors". In: *Phys. Rev. Appl.* 11.5 (2019), p. 054087. DOI: 10.1103/PhysRevApplied.11.054087.

[Vis+11] P. J. de Visser et al. "Number Fluctuations of Sparse Quasiparticles in a Superconductor". In: *Phys. Rev. Lett.* 106.16 (2011), p. 167004. DOI: 10.1103/PhysRevLett.106.167004.

[Vis+14] P. J. de Visser et al. "Evidence of a Nonequilibrium Distribution of Quasiparticles in the Microwave Response of a Superconducting Aluminum Resonator". In: *Phys. Rev. Lett.* 112.4 (2014), p. 047004. DOI: 10.1103/PhysRevLett.112.047004.

[vS13] Robert van Leeuwen and Gianluca Stefanucci. "Equilibrium and nonequilibrium many-body perturbation theory: a unified framework based on the Martin-Schwinger hierarchy". In: *Journal of Physics: Conference Series* 427 (2013), p. 012001. ISSN: 1742-6588. DOI: 10.1088/1742-6596/427/1/012001.

[Wan+14] C. Wang et al. "Measurement and control of quasiparticle dynamics in a superconducting qubit". In: *Nature Communications* 5.1 (2014), p. 5836. ISSN: 2041-1723. DOI: 10.1038/ncomms6836.

[WP04] C. M. Wilson and D. E. Prober. "Quasiparticle number fluctuations in superconductors". In: *Phys. Rev. B* 69.9 (2004), p. 094524. DOI: 10.1103/physrevb.69.094524.

[WYK94] Koki Watanabe, Keiji Yoshida, and Takeshi Aoki Kohjiro. "Kinetic Inductance of Superconducting Coplanar Waveguides". In: *Japanese Journal of Applied Physics* 33.10R (1994), p. 5708. ISSN: 0021-4922. DOI: 10.1143/JJAP.33.5708.

[Zeh95] A. Zehnder. "Response of superconductive films to localized energy deposition". In: *Phys. Rev. B* 52.17 (1995), pp. 12858–12866. DOI: 10.1103/PhysRevB.52.12858.

[ZL66] J. Zittartz and J. S. Langer. "Theory of Bound States in a Random Potential". In: *Phys. Rev.* 148 (2 Aug. 1966), pp. 741–747. DOI: 10.1103/PhysRev.148.741.